Numerical techniques for analytical high-multiplicity scattering amplitudes

Giuseppe De Laurentis

A Thesis presented for the degree of
Doctor of Philosophy

Institute for Particle Physics Phenomenology
Department of Physics
Durham University
United Kingdom

July 2020

Numerical techniques for analytical high-multiplicity scattering amplitudes

Giuseppe De Laurentis

Submitted for the degree of Doctor of Philosophy

July 2020

ABSTRACT

In this thesis we employ generalised unitarity methods to compute high-multiplicity one-loop scattering amplitudes in quantum chromodynamics, and leverage the scattering equations to obtain high-multiplicity tree-level amplitudes in higher-derivative theories. We develop a set of numerical strategies, based on the study of singular limits in complex phase space and on the reconstruction of generic ansatze, to obtain compact analytical spinor expressions from numerical evaluations only. The advantages of analytical expressions for scattering amplitudes include faster evaluation and increased numerical stability in soft and collinear limits. Thus, they provide a solid foundation for phenomenological studies. The amplitudes we present include the first full set of analytical expressions for 1) six-gluon scattering at one-loop with a gluon in the loop, 2) Higgs + four-parton amplitudes with a top-quark loop retaining full mass effects, and 3) tree-level amplitudes in a $(DF)^2$ theory and in conformal gravity.

Contents

Declaration

This thesis is based on research carried out at the Institute for Particle Physics Phenomenology within the University of Durham. No part of this thesis has been submitted elsewhere for any degree or qualification. This thesis is partly based on joint research as noted below.

[1] G. De Laurentis and D. Maître, *Extracting analytical one-loop amplitudes from numerical evaluations*, *JHEP* **07** (2019) 123 [1904.04067].

[2] G. De Laurentis, *Analytical amplitudes from numerical solutions of the scattering equations*, *JHEP* **02** (2020) 194 [1910.11355].

[3] L. Budge, J. M. Campbell, G. De Laurentis, R. Keith Ellis and S. Seth, *The one-loop amplitudes for Higgs + 4 partons with full mass effects*, [2002.04018].

More specifically, Chapters 1 to 4 are reviews of the literature, Chapters 5 to 7 are based on Ref. [1], Chapter 8 is based on Ref. [3], Chapter 9 is based on Ref. [2].

Acknowledgements

First and foremost, I would like to thank my supervisor Daniel Maître for providing me with interesting and challenging projects, as well as for his patience and continuous guidance during my PhD. I would also like to thank Adriano Lo Presti, Keith Ellis, John Campbell, Simon Badger and Arthur Lipstein for many insightful discussions.

My gratitude goes to all my course mates and members of the IPPP for creating such a friendly and stimulating work environment. In particular, I would like to thank Joey Reiness, James Whitehead, Ryan Moodie, Francesco Sarandrea, Wendy Gray, Lucy Budge and Joseph Farrow for proofreading chapters of this thesis.

Last but not least, I would like to thank my parents, Giacomo and Daniela, for supporting and encouraging me throughout my studies.

In memoria dei miei nonni

Introduction

This thesis builds on what is currently our best understanding of the fundamental short-distance interactions of nature, which comes from the union of two of the greatest achievements of the past century in the field of particle physics, namely the theories of special relativity and quantum mechanics. A consistent treatment of both of these theories naturally led to the development of the concept of quantum fields. In this introductory chapter we will review the framework of quantum field theories and its application in the Standard Model of particle physics. We will also introduce the complications that arise in perturbative calculations, and how some of them are tackled by the research presented in this thesis regarding the reconstruction of compact analytical expressions from numerical routines.

1.1 Interacting Quantum Fields

Classical mechanics can be formulated in terms of the action, S, which is defined as the integral of the Lagrangian, L, or of the Lagrangian density, $\mathcal{L}$, as

$$S = \int L(t)\, dt = \int \mathcal{L}(t, \vec{x})\, d^4x\,. \tag{1.1}$$

The extrema of the action, $\delta S = 0$, give the Euler-Lagrange equations of motion, whose solutions correspond to the classically-favoured paths.

Classical field theory is formulated in a similar fashion, by letting the Lagrangian density depend on the space time variables through the fields

$$\mathcal{L}(t, \vec{x}) \longrightarrow \mathcal{L}(\phi, \partial_\mu \phi) \,, \quad \phi = \phi(t, \vec{x}) \,. \tag{1.2}$$

Quantum mechanics, in Feynman's interpretation, is based on the idea that all paths are possible, albeit with different probability amplitudes given by the exponential of the action. More formally, it can be shown that the matrix element between two position eigenstates is given by

$$\langle t_f, \vec{x}_f | t_i, \vec{x}_i \rangle = \langle \vec{x}_f | e^{-\frac{i}{\hbar} H (t_i - t_f)} | \vec{x}_i \rangle \propto \int \mathcal{D}x \exp\left(\frac{i}{\hbar} \int_{t_i}^{t_f} dt \, \mathcal{L}(x, \dot{x})\right). \tag{1.3}$$

where H is the Hamiltonian, and the last equality follows from identity insertions and square completion, which results in a sign flip for the kinetic term. In analogy with statistical mechanics, this quantity is sometimes called the partition function, $\mathcal{Z}$. More involved expectation values are then obtained by time-ordered operator insertions

$$\langle t_f, \vec{x}_f | \mathcal{T}\big(\hat{x}(t_1) \dots \hat{x}(t_n)\big) | t_i, \vec{x}_i \rangle \propto \int \mathcal{D}x \, \hat{x}(t_1) \dots \hat{x}(t_n) \, e^{\frac{i}{\hbar} \int_{t_i}^{t_f} dt \, \mathcal{L}(x, \dot{x})} \,. \tag{1.4}$$

An alternative way to obtain Eq 1.4 is to promote the partition function $\mathcal{Z}$ to a generating functional $\mathcal{Z}[J]$, where J is the source, and act with functional derivatives. Classical physics is recovered by taking the $\hbar \to 0$ limit[1], or, in other words, the limit where all quantities are much bigger than the unit of quantisation.

Quantum field theory, in analogy to the classical case, is obtained by letting all space-time dependencies appear through field operators. For instance, in the case of a theory with a single scalar field, we can write the generating functional $\mathcal{Z}[J]$ as

$$\mathcal{Z}[J] \propto \int \mathcal{D}\phi \, e^{i \int d^4 x [\mathcal{L}(\phi, \partial_\mu \phi) + J\phi]} \,. \tag{1.5}$$

Matrix elements can be computed by differentiating the generating functional and then setting the source to zero (this corresponds to connected Feynman diagrams)

$$\langle 0 | \mathcal{T}\big(\phi(x_1) \dots \phi(x_n)\big) | 0 \rangle = \frac{i^{-n} \, \delta^n \ln Z[J]}{\delta J(x_1) \dots \delta J(x_n)} \bigg|_{J=0} \,. \tag{1.6}$$

These functions are also known as Green's functions, since they yield a delta function when acted upon with the correct operator. For instance, the scalar propagator satisfies

$$D_F(x - y) = \langle 0 | \mathcal{T}\big(\phi(x)\phi(y)\big) | 0 \rangle \quad \text{and} \quad (\Box_x + m^2) \, D_F(x - y) = -i\delta(x - y) \,. \tag{1.7}$$

---

[1] From now on we will use natural units, i.e. $\hbar = c = 1$.

In general, a field theory Lagrangian will contain several covariant fields, organised according to the representation of the Lorentz group they transform under (see Section 2.2.1). The three lowest-lying fields are the scalar field ϕ, the Dirac field ψ, and the vector field A, respectively given by

$$\phi(\mathbf{x}) = \int \frac{d^3p}{(2\pi)^3} \frac{1}{2E_{\mathbf{p}}} \left(a_{\mathbf{p}} e^{i\mathbf{p}\cdot\mathbf{x}} + a_{\mathbf{p}}^{\dagger} e^{-i\mathbf{p}\cdot\mathbf{x}} \right), \tag{1.8}$$

$$\psi(\mathbf{x}) = \int \frac{d^3p}{(2\pi)^3} \frac{1}{2E_{\mathbf{p}}} \sum_s \left(a_{\mathbf{p}}^s u_{\mathbf{p}}^s e^{-i\mathbf{p}\cdot\mathbf{x}} + b_{\mathbf{p}}^{s\dagger} v_{\mathbf{p}}^s e^{i\mathbf{p}\cdot\mathbf{x}} \right), \tag{1.9}$$

$$A_\mu(\mathbf{x}) = \int \frac{d^3p}{(2\pi)^3} \frac{1}{2E_{\mathbf{p}}} \sum_\alpha \left(a_{\mathbf{p}}^\alpha \epsilon_{\mu,\mathbf{p}}^\alpha e^{-i\mathbf{p}\cdot\mathbf{x}} + a_{\mathbf{p}}^{\alpha\dagger} \epsilon_{\mu,\mathbf{p}}^{\alpha*} e^{i\mathbf{p}\cdot\mathbf{x}} \right). \tag{1.10}$$

Note that they are all given as the Fourier transform of momentum space creation and annihilation operators. In analogy to the quantisation of the energy levels in a harmonic oscillator, these operators satisfy canonical (anti-) commutation relations

$$\left[a_{\mathbf{p}}, a_{\mathbf{q}}^{\dagger} \right] = (2\pi)^3 \, 2E_{\mathbf{p}} \, \delta^3(\mathbf{p} - \mathbf{q}), \tag{1.11}$$

$$\left\{ a_{\mathbf{p}}^r, a_{\mathbf{q}}^{s\dagger} \right\} = \left\{ b_{\mathbf{p}}^r, b_{\mathbf{q}}^{s\dagger} \right\} = (2\pi)^3 \, 2E_{\mathbf{p}} \, \delta^3(\mathbf{p} - \mathbf{q}) \, \delta^{rs}, \tag{1.12}$$

$$\left[a_{\mathbf{p}}^\alpha, a_{\mathbf{q}}^{\beta\dagger} \right] = -(2\pi)^3 \, 2E_{\mathbf{p}} \, \delta^3(\mathbf{p} - \mathbf{q}) \, \eta^{\alpha\beta}. \tag{1.13}$$

These (anti-) commutation relations impose the correct statistics on the wavefunctions, i.e. Bose-Einstein for integer spin representations and Fermi-Dirac for half-integer spin representations. A consequence of the field quantisation is that the number of particles is no longer conserved: new particles can be created (a) if there is sufficient energy, or (b) for short periods of time even without enough energy, as long as Heisenberg's uncertainty principle $\Delta E \Delta t \geq \hbar/2$ is respected. Case (a) corresponds to on-mass-shell particles, case (b) to off-mass-shell ones.

In order to be able to easily generalise the result of Eq. 1.7 to the cases containing more fields, we would like to move all annihilation operators to the right to have them vanish on the vacuum. Operators satisfying this structure are said to be *normal ordered* (denoted by pairs of colons), and the relation between normal and time ordering is given in Wick's Theorem as the sum of all possible field *contractions*

$$\mathcal{T}\big(\phi(x_1)\ldots\phi(x_n)\big) = \, : \phi(x_1)\ldots\phi(x_n) + \text{all possible contractions} : \tag{1.14}$$

Since normal ordered field strings vanish when acting on the vacuum, by sandwiching Eq. 1.14 between vacua only fully-contracted field strings survive. Finally, by graphically interpreting field contractions in Wick's theorem we obtain Feynman rules and diagrams.

1.2   The Standard Model

Currently, the best working theory of the fundamental interactions of nature, with the exception of gravity, is the quantum field theory known as the Standard Model. It is based on the following local, or gauge, symmetry groups[2]

$$U(1)_Y \times SU(2)_L \times SU(3)_C \longrightarrow U(1)_{EM} \times SU(3)_C \,. \tag{1.15}$$

The arrow indicates the electroweak spontaneous symmetry breaking (EWSB), which is realised through the Higgs mechanism and happens at a temperature of about 160 GeV [4]. The subscripts in the unbroken phase refer to colour, left-handedness, and hypercharge, whereas on the right-hand side we have colour and electromagnetism.

A popular way of writing the Standard Model Lagrangian is

$$
\begin{aligned}
\mathcal{L} = \ & -\ \frac{1}{4} F_{\mu\nu} F^{\mu\nu} \\
& +\ i \overline{\Psi} \slashed{D} \Psi \\
& +\ D_\mu \Phi^\dagger D^\mu \Phi - V(\Phi) \\
& +\ \overline{\Psi}_L \hat{Y} \Phi \Psi_R + h.c. \,.
\end{aligned}
\tag{1.16}
$$

We could summarise each line respectively as pure gauge, matter, Higgs and Yukawa. More specifically, in the first line $F^{\mu\nu}$ is the field strength tensor, which contains both gauge-field kinetic terms and interactions. In the second line, Ψ denotes the fermionic fields and D is the gauge covariant derivative; this describes the propagation of matter fields and their interactions with gauge fields. In the third line, with Φ representing the Higgs field (as a complex doublet), we have the Higgs kinetic term, its interactions with the gauge fields and with itself (i.e. its potential). Lastly, in the fourth line, $\hat{Y}$ is the Yukawa matrix, which is diagonal in the mass basis. This combination of operators describes the Higgs-field interactions with the matter fields, from which their masses arise after EWSB.

In the standard model we can write the covariant derivative as

$$D_\mu = \partial_\mu - i \frac{g_1}{2} Y B_\mu - i g_2 \frac{\sigma_j}{2} W_\mu^j - i g_s \frac{\lambda_a}{2} G_\mu^a \,, \tag{1.17}$$

where g_1 is the $U(1)_Y$ coupling, Y is the appropriate hypercharge, B_μ is the $U(1)_Y$ gauge field, g_2 is the $SU(2)_L$ coupling, σ_j are the Pauli matrices, i.e. the $SU(2)_L$ generators, W_μ^j are the $SU(2)_L$ gauge fields, g_s is the $SU(3)_C$ (strong) coupling, λ_a are the Gell-Mann

---

[2]Ignoring a $\mathcal{Z}_6$ central charge.

Gauge Field	$U(1)_Y$	$SU(2)_L$	$SU(3)_C$
B	**1**	0	0
W	0	**3**	0
g	0	0	**8**

Table 1.1: Gauge fields and corresponding gauge groups.

matrices, i.e. the $SU(3)_C$ generators, and, finally, G_μ^a are the $SU(3)_C$ gauge fields, i.e. the eight gluons. The gauge fields live in the adjoint representation of their $SU(N)$ gauge group, and therefore there are $N^2 - 1$ of them, as shown in Table 1.1. Special unitary groups will play an important role in the discussion of both dynamics and kinematics in Chapter 2 of this thesis. They are treated in more detail in that context.

The field strength tensor is defined as the commutator of two covariant derivatives as

$$F_{\mu\nu} = -\frac{1}{ig}\big[D_\mu, D_\nu\big] = \partial_\mu A_\nu - \partial_\nu A_\mu - ig\big[A_\mu, A_\nu\big] \, , \tag{1.18}$$

where A_μ is a generic gauge field, defined by a sum over appropriate generators $A_\mu = t^a A_\mu^a$. The commutator is the defining property of the Lie algebra associated with a particular gauge group. In the $U(1)$ case the commutator simply vanishes, meaning it is an abelian group; in the $SU(2)$ case the commutator gives rise to the Levi-Civita fully anti-symmetric tensor ϵ^{ijk} from the commutation of the Pauli matrices; similarly, in the $SU(3)$ case the commutation of the Gell-Mann matrices gives rise to a structure constant f^{abc}. In general, we can write the field strength tensor as

$$F_{\mu\nu}^a = \partial_\mu A_\nu^a - \partial_\nu A_\mu^a + g f^{abc} A_\mu^b A_\nu^c \, , \tag{1.19}$$

where it is understood that the appropriate coupling and structure constant has to be picked. In the standard model, the pure gauge part of the Lagrangian, partially expanded, out will read

$$\frac{1}{4}F_{\mu\nu}F^{\mu\nu} = \frac{1}{4}B_{\mu\nu}B^{\mu\nu} + \frac{1}{4}W_{\mu\nu}^a W^{a,\mu\nu} + \frac{1}{4}G_{\mu\nu}^b G^{b,\mu\nu} \, , \tag{1.20}$$

and it is now clear that $B_{\mu\nu}B^{\mu\nu}$ is purely kinetic, whereas $W_{\mu\nu}^a W^{a,\mu\nu}$ and $G_{\mu\nu}^b G^{b,\mu\nu}$ contain also gauge-gauge interactions.

The next part to address is the matter fields. In Eq. 1.16 they are denoted just as Ψ, but they actually have a fairly complicated structure, which is summarised in Table 1.2. The $SU(2)_L$ gauge fields break parity by coupling exclusively to left-handed particles and right-handed anti-particles. This is mathematically enforced by the doublet/singlet

Matter Field	Y	I	I_3	$Q = I_3 + Y/2$	$SU(3)_C$
(l_L^0, l_L^-)	-1	$1/2$	$(1/2, -1/2)$	$(0, -1)$	0
l_R^-	-2	0	0	-1	0
(q_L^u, q_L^d)	$1/3$	$1/2$	$(1/2, -1/2)$	$(2/3, -1/3)$	$\mathbf{3}$
q_R^u	$4/3$	0	0	$2/3$	$\mathbf{3}$
q_R^d	$-2/3$	0	0	$-1/3$	$\mathbf{3}$

Table 1.2: Matter fields and their charges.

Scalar Fields	Y	I	I_3	$SU(3)_C$
(ϕ^+, ϕ^0)	1	$1/2$	$(1/2, -1/2)$	0

Table 1.3: Higgs field and its charges.

structure of the left/right handed fields respectively. The $SU(2)_L$ charge is called *weak isospin* and is denoted by I, in analogy to the spin quantum number J. Its third component is denoted by I_3, which is analogous to the projection of spin onto the z-axis J_z. A further distinction in the representation of the $SU(3)_C$ group is between leptons, that are trivial singlets, and quarks, that are fundamental triplets. The hypercharge Y is chosen such that the electric charge Q reproduces the experimentally-observed value. The relation between hypercharge, isospin and charge will be partially derived in Section 1.2.2. The anti-quark charges follow from the action of CP symmetry on the quark ones.

Finally, we have the Higgs field Φ, whose charges are summarised in Table 1.3. It is a complex scalar doublet under $SU(2)_L$ with a quartic potential

$$\Phi = \begin{pmatrix} \phi^+ \\ \phi^0 \end{pmatrix} = \frac{1}{\sqrt{2}} \begin{pmatrix} \phi_1 + i\phi_2 \\ \phi_3 + i\phi_4 \end{pmatrix} , \quad V(\Phi) = \mu^2 \Phi^\dagger \Phi + \lambda (\Phi^\dagger \Phi)^2 . \tag{1.21}$$

1.2.1   Quantum Chromodynamics

Quantum chromodynamics (QCD) is the theory of the strong interaction, which, at low energies, is responsible for holding quarks in bound states called hadrons. At higher energies, such as in collider collisions, QCD is the main source of radiation, with every subsequent emission costing only a factor of $\alpha_s(m_Z) \sim 0.1178$ [5]. By comparison, electroweak radiation is suppressed by more than one order of magnitude.

The relevant part of the Lagrangian for QCD interactions is

$$\mathcal{L}_{QCD} = -\frac{1}{2}\mathrm{tr}\big(G_{\mu\nu}G^{\mu\nu}\big) + i\overline{\Psi}(\slashed{D} - m)\Psi \ . \tag{1.22}$$

The mass term arises from the Yukawa interaction and in calculations for high energy collision it is usually neglected for all quark flavours, with the exception of the top quark. By expanding out the product of field strengths in the pure gauge term $\mathrm{tr}\big(G_{\mu\nu}G^{\mu\nu}\big)$, we obtain the following three structures

$$\mathcal{L}_{gauge-kinetic} \;=\; \frac{\delta^{ab}}{4}\big(\partial_\mu G_\nu^a - \partial_\nu G_\mu^a\big)\big(\partial^\mu G^{b,\nu} - \partial^\nu G^{b,\mu}\big) \ , \tag{1.23}$$

$$\mathcal{L}_{triple-gauge} \;=\; \frac{1}{2}gf^{abc}\big(\partial_\mu G_\nu^a - \partial_\nu G_\mu^a\big)G^{b,\mu}G^{c,\nu} \ , \tag{1.24}$$

$$\mathcal{L}_{quadruple-gauge} \;=\; \frac{1}{4}g^2 f^{abc}f^{ade}G_\mu^b G_\nu^c G^{d,\mu}G^{e,\nu} \ , \tag{1.25}$$

which correspond respectively to gluon kinetic term, gluon 3-point vertex and gluon 4-point vertex. The corresponding Feynman rules are given in Appendix A.

Similarly, by expanding the matter-gauge term $i\overline{\Psi}(\slashed{D} - m)\Psi$, we obtain

$$\mathcal{L}_{matter-kinetic} \;=\; i\overline{\Psi}(\slashed{\partial} - m)\Psi \ , \tag{1.26}$$

$$\mathcal{L}_{matter-gauge} \;=\; -gt^a\overline{\Psi}\slashed{G}^a\Psi \ , \tag{1.27}$$

which correspond respectively to quark kinetic term and quark-gluon interaction.

1.2.2 Electroweak Sector & Symmetry Breaking

For the sake of completeness, in this section we are going to briefly review the electroweak sector. In the broken phase, the physically-propagating degrees of freedom are a mixture of the B, W and Φ fields, which we will now determine.

Spontaneous symmetry breaking happens when the Higgs field acquires a vacuum expectation value, which can be found by locating the minimum of its potential

$$\frac{\partial V(\Phi)}{\partial \Phi} = \Phi^\dagger\big(\mu^2 + 2\lambda(\Phi^\dagger\Phi)\big) = 0 \ , \tag{1.28}$$

$$\implies \Phi^\dagger\Phi = v^2/2 = -\mu^2/(2\lambda) \ . \tag{1.29}$$

Figure 1.1: Higgs potential in the broken phase.[3]

Massive oscillations around this minimum are the physical Higgs field h (radial direction in Figure 1.1), whereas the massless Goldstone modes

---

[3]Image courtesy of Ref. [6].

Field	Y	I	I_3	$Q = I_3 + Y/2$	$SU(3)_C$
(W^+, W^3, W^-)	0	1	$(1, 0, -1)$	$(1, 0, -1)$	0

Table 1.4: W bosons as a $SU(2)_L$ triplet.

(azimuthal direction) can be removed by choosing the unitary gauge. One says that they are *eaten* by the $SU(2)_L$ gauge bosons. Thus, after EWSB, Φ can be taken to be

$$\Phi = \frac{1}{\sqrt{2}} \begin{pmatrix} 0 \\ v + h \end{pmatrix} . \tag{1.30}$$

This means that the loss of three degrees of freedom from the field Φ is compensated by three new degrees of freedom in the electroweak bosons. These come in the form of longitudinal polarisations, now allowed by their non-zero mass, which is derived by expanding the Higgs kinetic term retaining only the part dependant on the v.e.v.

$$
\begin{aligned}
D_\mu \Phi^\dagger D^\mu \Phi \quad &\supset \quad \left|\left(-i\frac{g_1}{2}B_\mu\Phi - ig_2\frac{\sigma_j}{2}W_\mu^j\Phi\right)\right|^2 \\
&\supset \quad \left|\frac{-i}{2\sqrt{2}}\begin{pmatrix} g_1 B_\mu + g_2 W_\mu^3 & g_2 W_\mu^1 - ig_2 W_\mu^2 \\ g_2 W_\mu^1 + ig_2 W_\mu^2 & g_1 B_\mu - g_2 W_\mu^3 \end{pmatrix}\begin{pmatrix} 0 \\ v \end{pmatrix}\right|^2 \\
&= \quad \frac{1}{2}\frac{v^2}{4}\left(g_2^2(W_\mu^1)^2 + g_2^2(W_\mu^2)^2 + g_1^2(B_\mu)^2 + g_2^2(W_\mu^3)^2 - 2g_1 g_2 B^\mu W_\mu^3\right) .
\end{aligned}
\tag{1.31}
$$

The last line can be written as a mass matrix for the W^i and B bosons, which once diagonalised yields the physically-propagating states. In particular, the eigenvalues and eigenvectors of the 2×2 block involving W^3 and B give the masses and mixing of the photon and of the Z boson, respectively

$$m_\gamma = 0 , \quad m_Z = \frac{v}{2}\sqrt{g_1^2 + g_2^2} , \tag{1.32}$$

$$A_\mu = \sin\theta_W \, W_\mu^3 + \cos\theta_W B_\mu , \quad Z_\mu = \cos\theta_W W_\mu^3 - \sin\theta_W B_\mu . \tag{1.33}$$

The weak mixing angle θ_W is defined in terms of the couplings as

$$\cos\theta_W = \frac{g_2}{\sqrt{g_1^2 + g_2^2}} , \quad \sin\theta_W = \frac{g_1}{\sqrt{g_1^2 + g_2^2}} . \tag{1.34}$$

The electroweak unification condition $e = g_2 \sin\theta_W = g_1 \cos\theta_W$ can be read off Eq. 1.33. Furthermore, from Eq. 1.31 we see that the physical $W^\pm$ bosons and their masses are

$$W_\mu^\pm = \left(W_\mu^1 \mp iW_\mu^2\right)/\sqrt{2} \quad \text{and} \quad m_W = \frac{v}{2}g_2 = m_Z \cos\theta_W . \tag{1.35}$$

The generators associated with the $W^\pm$ bosons are the $SU(2)$ raising and lowering operators $\tau^\pm = \left(\sigma^1 \pm i\sigma^2\right)$ and, together with W^3, they form a $SU(2)_L$ triplet (see Table 1.4).

1.3 Regularisation & Renormalisation

Perturbative quantum field theory computations are notoriously plagued by a proliferation of infinities, which need to be suitably accounted for in order to obtain sensible predictions for physical observables.

A procedure by which infinities are quantified and made treatable is called a *regularisation* procedure. For instance, infinities may appear when massless particles acquire vanishing four-momenta (soft limit). One possible way to regulate such a divergence is by associating a fictitious mass to the massless particle. This allows to sensibly perform cancellations between would-be divergent terms at non-zero mass values and, after all divergences have been cancelled, take the physical zero-mass limit. The same philosophy applies to an array of regularisation strategies, each of which has its own regularisation parameter.

The most common framework is surely that of dimensional regularisation (dim-reg). In this case the computation is performed in $4 - 2\epsilon$ dimensions, where ϵ is the regularisation parameter. For instance, the one-loop integral measure in dim-reg becomes

$$d^4l \longrightarrow \mu_R^{4-D} d^D l \quad \text{with} \quad D = 4 - 2\epsilon \,, \tag{1.36}$$

where μ_R is an arbitrary scale needed to maintain the correct dimensions of the loop integral. Loop integrals can then be expressed as a Laurent series in ϵ, thus regularising their divergences. A complete set of one-loop scalar integrals and their analytical expansions can be found in Ref. [7].

The types of divergences that arise and need to be regularised fall into two separate categories: ultra-violet (UV) and infra-red (IR).

UV divergences are a consequence of the high-energy (i.e. short-distance) interacting nature of the quantum fields. For instance, there is no such thing as an electron by itself without a cloud of (virtual) photons. We refer to the idealised standalone quantities as *bare*, and to the physical ones as *renormalised*. In QCD the gluon field G, the quark field Ψ and the coupling constant g_s need to be renormalised. Renormalised and bare quantities[4] are related by the renormalisation constants Z_1, Z_2 and Z_3

$$G_0 = \sqrt{Z_3} G \,, \quad \Psi_0 = \sqrt{Z_2} \Psi \,, \quad Z_1 g_s \overline{\Psi} \slashed{G} \Psi = g_{s,0} Z_2 \sqrt{Z_3} \overline{\Psi} \slashed{G} \Psi \,. \tag{1.37}$$

The divergent part of a renormalisation constant is called the counter term δ, and the

---

[4]Bare quantities are denoted by a 0 subscript.

relation is $Z = 1 + \delta$. By computing the relevant one-loop diagrams, the QCD counter terms are obtained to leading order in α_s

$$\delta_1 = -(C_A + C_F)\frac{\alpha_s}{4\pi}\frac{1}{\epsilon}\,, \quad \delta_2 = -C_F\frac{\alpha_s}{4\pi}\frac{1}{\epsilon}\,, \quad \delta_3 = \left(\frac{5}{3}C_A - \frac{4}{3}n_f T_R\right)\frac{\alpha_s}{4\pi}\frac{1}{\epsilon}\,. \qquad (1.38)$$

where n_f is number of quark flavours, $T_R = 1/2$, and C_A and C_F are the $SU(3)$ Casimir operators (see Section 2.1.1). In the case of gravity, the infinite tower of n-point vertices requires a infinite number of counter terms. In turn, this implies that an infinite number of experimental observations are required to fix an infinite number of parameters, making the theory lose all predictive power. We say that the theory is not renormalisable.

IR divergences have a completely different physical interpretation and mathematical resolution (although in a calculation they will still appear as divergences in the regularisation parameter). They arise both in loop calculations and in phase space integrals when a real radiation is integrated over a soft and/or collinear region of phase space (hence IR for the low-energy). In the Standard Model, by the KLN theorem [8], these two types of IR divergences have to match and cancel for any physical IR-safe measurable quantity. The physical interpretation is that a n-point process is not distinguishable from an $(n+1)$-point process if the extra radiation cannot be resolved.

In the following section we will see how this cancellation of IR divergences finds a natural resolution in the structure of perturbative calculations.

1.4   Anatomy of a Perturbative Calculation

The aim of phenomenological calculations in perturbative QFT (pQFT) is to obtain predictions for physical observables. Usually these are either decay rates or cross sections, σ. In the case of hadron colliders, the latter can be expressed as a convolution between parton distribution functions (PDFs), $f_{a/h}$, and partonic cross sections $\hat{\sigma}$, formally

$$\sigma_{2 \to n-2} = \sum_{a,b} \int dx_a dx_b f_{a/h_1}(x_a, \mu_F)\, f_{b/h_2}(x_b, \mu_F)\, \hat{\sigma}_{ab \to n-2}(\mu_F, \mu_R)\,, \qquad (1.39)$$

where a and b refer to the partons in the hadrons h_1 and h_2 respectively, and x represent momentum fractions (see Bjorken x [9]). The factorisation scale μ_F separates the high-energy physics of the partonic cross section from the lower-energy physics of the PDFs. The renormalisation scale μ_R is a leftover of the renormalisation procedure, and the cross section should depend on it only through higher orders of the expansion parameter compared to the precision of the calculation.

$\mathcal{A}^{loops}_{multi.} \propto g_s^n$		Multiplicity			
		4	5	6	7
Loops	0	2	3	4	5
	1	4	5	6	7
	2	6	7	8	9

Table 1.5: Powers of coupling in pure gluon scattering
as function of number of loops and multiplicity.

The (differential) partonic cross section itself is given by the product of the Lorentz invariant measure $d\Pi$, a delta function to enforce four-momentum conservation and, lastly, the amplitude (or matrix element) squared, over a flux factor $2\hat{s}$

$$d\hat{\sigma}_n = \frac{1}{2\hat{s}} d\Pi_{n-2} \, (2\pi)^4 \delta^4\big(\Sigma^n_{i=1} p_i\big) \, |\mathcal{A}_n(p_i, \mu_F, \mu_R)|^2 \, . \tag{1.40}$$

In this work we will focus on the high-energy physics described by the amplitude $\mathcal{A}$. Since at high energies the coupling constants are small, we can perform a Taylor expansion. For instance, Table 1.5 shows the powers of the coupling as a function of number of loops and multiplicity for pure gluon scattering. When taking the modulus square of the amplitude, different components may contribute at the same power of the coupling, for instance

$$|\mathcal{A}_{4g}|^2 = \alpha_s^2 |\mathcal{A}^{(0)}_{4g}|^2 + \alpha_s^3 \Big(2Re[\mathcal{A}^{(0)}_{4g} \mathcal{A}^{(1)}_{4g}] + |\mathcal{A}^{(0)}_{5g}|^2 \Big) + \mathcal{O}(\alpha_s^4) \, . \tag{1.41}$$

This structure reflects exactly the discussion in the previous section about the cancellation of IR divergences between loops and real radiation, which more concretely in the above equation means cancellations between $2Re[\mathcal{A}^{(0)}_{4g} \mathcal{A}^{(1)}_{4g}]$ and $|\mathcal{A}^{(0)}_{5g}|^2$. In truth, Eq. 1.41 is a slight abuse of notation, since the amplitude with the extra radiation in the final state needs to be integrated over the soft and/or collinear region of phase space before divergences can be cancelled with the virtual contribution. Since all phase space integration is done numerically, it is crucial to have fast and stable routines for the evaluation of the amplitudes.

Two types of complexities arise in the expansion of Eq. 1.41, and are usually referred to as *analytic* and *algebraic*. The former refers to the more complicated functions that arise at higher loop orders (logarithms, polylogarithms, etc...), the latter refers to the increase in the number of variables (or scales) for processes with higher multiplicity.

This work focuses on understanding and taming this second type of complexity, which will be estimated in the following subsection.

multiplicity	3	4	5	6	7	...
# diagrams	1	4	25	220	34300	...
# ind. hel. conf.	2	4	4	8	9	...

Table 1.6: Number of tree level gluon diagrams
and independent helicity configurations as a function of multiplicity.

1.4.1   Estimate of the Algebraic Complexity of a Calculation

A first naive estimate of the algebraic complexity of a calculation could be the number of Feynman diagrams contributing to a specific amplitude. Carrying on with the pure gluon scattering example, we can calculate the number of tree diagrams with a simple recursion relation[5]. Every 3-point vertex is labelled by a t, and every gluon by a g. The 3-point amplitude is then given by tg^3. To increase by one the multiplicity of the process, we can either add a 3-point vertex to a gluon line, that is act with the operator $tg^3\frac{\partial}{\partial g}$, or turn a 3-point vertex into a 4-point one, with the operator $g\frac{\partial}{\partial t}$. The recursion relation is then

$$N_m(t,g) = (tg^3\frac{\partial}{\partial g} + g\frac{\partial}{\partial g})N_{m-1}(t,g)\,, \quad N_m = N_m(t,g)\big|_{t=g=1}\,, \quad N_3(t,g) = tg^3. \quad (1.42)$$

This yields the series displayed in the first row of Table 1.6, which show a worse than factorial growth. Thankfully, this turns out to be a huge overestimate of the number of independent quantities to compute and arguably also of the complexity of the results. A famous example is the Parke-Taylor formula for n-gluon maximally-helicity-violating (MHV) tree amplitudes[6] [10]

$$A_n^{(0)}\big(1_g^+,\ldots,i_g^-,\ldots,j_g^-,\ldots,n_g^+\big) = \frac{i\,\langle ij\rangle^4}{\langle 12\rangle\langle 23\rangle\ldots\langle n1\rangle}\,, \quad (1.43)$$

which clearly shows only a very modest increase in complexity[7] as a function of the multiplicity n. Next-to-maximally-helicity-violating ($N^{k\geq 1}MHV$) amplitudes are more complicated, but not terribly so, at least at tree level. In Chapter 3 we will review modern techniques to compute scattering amplitudes, which rely on the existence of Feynman diagrams but use on-shell tree amplitudes as building blocks. Thus, instead of thinking about the number of Feynman diagrams, we could think about the number of independent tree amplitudes, or helicity configurations, whose growth is much more modest than that of Feynman diagrams, as shown in the second row of Table 1.6.

---

[5]From a lecture by Simon Badger.

[6]Spinors and the spinor-helicity notation is introduced in Chapter 2 Section 2.2.

[7]We could define it more rigorously as the *leaf count* of an expression.

Lorentz invariant structures	Mass dimension (d)			
	2	4	6	8
Multiplicity (n) 4	2	3	4	5
5	5	16	40	85
6	9	50	205	675
7	14	120	735	3486

Table 1.7: Linearly independent Lorentz invariant structures, as function of multiplicity and mass dimension.

However, this does not really address how complicated the individual tree amplitudes or, at loop level, integral coefficients are. Since these are Lorentz invariant quantities we should count the number of Lorentz invariant variables. There are two possible linearly-independent momenta contractions: the Mandelstam invariants s_{ij}, and traces involving γ^5 denoted as tr_5. Assuming massless momenta, we can define them as

$$s_{ij} = 2P_i \cdot P_j \,, \quad \mathrm{tr}_5(ijkl) = 4\,i\,\epsilon^{\alpha\beta\gamma\delta}P_\alpha^{(i)}P_\beta^{(j)}P_\gamma^{(k)}P_\delta^{(l)} \tag{1.44}$$

and count how many linearly-independent ones there are

$$n_s = \frac{n(n-3)}{2} \,, \quad n_t = \binom{(n-1)}{4} \,. \tag{1.45}$$

In natural units they have mass dimension of 2 and 4 respectively, and, in fact, the expression for n_s reproduces the first column in Table 1.7. We can now write an approximate formula for the content of Table 1.7 (which was obtained by Gaussian elimination and is thus exact)

$$\left(\!\binom{n_s}{d/2}\!\right) \leq \begin{array}{c} \text{\# lin. independent} \\ \text{Lorentz inv. structures} \end{array} \leq \left(\!\binom{n_s}{d/2}\!\right) + n_t\left(\!\binom{n_s}{(d-4)/2}\!\right) \tag{1.46}$$

where the double parentheses denotes combinations with replacement. The upper bound is saturated for ($\forall n$, $d \leq 4$) and ($\forall d$, $n \leq 5$), otherwise it is an over-counting due to a Schouten identity for four-momenta[8]

$$\mathrm{tr}_5(2345)1^\mu - \mathrm{tr}_5(1345)2^\mu + \mathrm{tr}_5(1245)3^\mu - \mathrm{tr}_5(1235)4^\mu + \mathrm{tr}_5(1234)5^\mu = 0 \,. \tag{1.47}$$

Table 1.7 shows a steep increase towards higher multiplicities and higher mass dimensions (think about the latter as a consequence of more complicated pole structures). Although clearly not all possible structures will appear in final expressions, many of them often do appear in intermediate stages of the calculation, before simplifications take place.

---

[8]This follows from the simple observation that the momenta live in a four-dimensional vector space.

1.5   Reconstructing Analytics from Numerics

Numerical methods are used in the calculation of scattering amplitudes when analytical calculations become intractable. A common bottleneck that makes conventional analytical computations unfeasible in practice is in intermediary steps, rather than in the complexity of the final answer. We have shown a notable example of this is in the Parke-Taylor formula for MHV amplitudes, that is significantly simpler than the intermediate expressions needed to calculate it. We develop a method to recover the analytical form of expressions when only a numerical program is available for their evaluation. For example, this is often the case for high-multiplicity one-loop amplitudes. Alternatively, this method can be used to explore the structure of already available analytical expressions and further simplify them when possible.

Analytical expressions are often preferable to numerical solutions when they are to be used in extreme phase space configurations, such as for integration in soft or collinear regions of the phase space. Analytical expressions can be expanded in the relevant limit to provide numerically-stable results. Furthermore, compact analytical expressions evaluate often faster and with a smaller memory footprint than numerical procedures, and can be more amenable to parallelisation.

The use of numerical samples to reconstruct analytical expressions is beginning to find direct applications to scattering amplitude calculations as a means of taming the complexity of the problem. In particular, computations over finite fields are used to perform integral reduction [11–14], to reconstruct polynomials in kinematic variables in the calculation of two-loop QCD [15–27] and $\mathcal{N} = 8$ [28, 29] amplitudes, as well as in higher loop calculations [30, 31]. The method described in this thesis differs from the above in that it uses large-precision floating-point arithmetic, rather than exact integer arithmetic modulo a prime number. This approach offers an easy interface to existing code as many programs already make use of high precision floating-point arithmetic to deal with numerical instabilities. As we will see later, using large scale differences allows us to restrict the calculation to specific parts of the answer rather than solving for the full answer at once. This targeted approach decreases the size of the fitting problem significantly.

To illustrate the usefulness of our method, in Ref. [1] we presented analytical expressions for colour-ordered six-gluon one-loop amplitudes with a gluon in the loop for all helicity configurations. These amplitudes were already calculated in the literature [32–44] and

summarised in Ref. [45], but to the best of our knowledge they were never presented in a single place using a single framework. Furthermore, the expressions we provided are explicitly rational (no square roots of spinors), gauge invariant (no arbitrary reference momenta), and in most cases fairly compact.

Subsequently, in Ref. [3] we presented the first full set of compact publishable analytical expression for the Higgs + 4 partons process at one-loop in all helicity configurations with full mass effects. Also in this case our reconstruction method proved to be very useful in analysing and simplifying the spinor-helicity expressions. Previously available results for this process were the analytical all-plus Higgs + 4-gluon amplitude [46], and a mix of numerical and analytical results [47–49].

Finally, we applied the reconstruction method in a slightly different setting, namely in the study of amplitudes obtained from the CHY formalism [2] (see Section 1.6). We obtained the first full set of five-point amplitude in the $(DF)^2$ theory, and partial expressions for six-point NMHV amplitudes in both $(DF)^2$ and conformal gravity.

1.6 Beyond Lagrangians and Feynman Diagrams

There exist relations among amplitudes in different theories known as KLT [50] or double-copy relations, which are completely obscured in a standard Lagrangian formulation. The most famous example must be that of QCD, which double copies into Einstein gravity. The CHY formalism for massless scattering provides a cohesive framework that elucidates these interconnections. However, even at tree level, it entails operations that are highly non-trivial to perform analytically, most notably solving the scattering equations (SE).

The SE are a set of theory independent equations which form the backbone of the CHY formalism. They first appeared in the literature in the context of string theory in the '70s [51–53] and '80s [54]. They were more recently rediscovered by Cachazo, He and Yuan (CHY) in a series of pioneering papers [55–57] demonstrating that the SE provide a set of algebraic equations that are key to an alternative formulation of scattering amplitudes at tree level in d dimensions. Shortly afterwards, this framework was proven to reproduce the correct results for ϕ^3 and Yang-Mills [58], to generalise to loop level [59, 60], and to arise naturally from a worldsheet theory called ambitwistor string [61].

In this alternative QFT formulation, the kinematic information of the scattering process is encoded in a set of variables describing the location of punctures on the Riemann sphere.

The locations of the punctures are related to the external momenta by the SE. Tree-level amplitudes are obtained by integrating over the position of the punctures on the Riemann sphere, while removing a redundancy coming from Möbius transformations, and imposing the solution of the SE. Alternatively, this integral can be recast as a contour integral around the punctures of the Riemann sphere. The rest of the integrand (called the CHY-integrand) depends on the chosen theory and it has the nice feature of making manifest the double-copy relations. For instance, the CHY-integrands for Yang-Mills, Einstein gravity and biadjoint scalar theory closely match the KLT relations [62].

The main bottleneck for the study of QFTs following this approach is the factorial growth of the number of solutions to the SE. In general, the CHY formulae are supported on $(n-3)!$ solutions of the SE. More specifically, at three-point there are no free punctures, at four-point the SE have a single rational solution, and at five-point there are two irrational solutions. At six-point there are six irrational solutions which have been shown to be still algebraic in $d=4$ [63]. Starting at seven-point in $d=4$ and at six-point for general d dimensions the solutions cannot be expressed in terms of radicals. At the same time, tree-level amplitudes are rational functions of the external kinematics for any phase space multiplicity. Clearly some non-trivial simplification has to occur.

An intriguing solution found in the literature [64,65] to this factorial growth is to obtain the sum of residues without explicitly finding the position of the poles. This powerful approach makes the rationality of the amplitude manifest even when the punctures are irrational. However, as the analytical complexity grows with the multiplicity of the scattering process, even this approach seems to require some form of numerical or semi-numerical reconstruction.

We develop a purely numerical approach, followed by an analytical reconstruction with the strategy of Ref. [1]. To perform this reconstruction, we need an implementation of the CHY formulae that is both sufficiently stable in singular limits and that yields amplitudes with enough numerical precision. We provide code that satisfies these criteria in a `Python` package called seampy ("Scattering equations and amplitudes with Python").

A publicly-available package to compute amplitudes within the CHY framework in $d=4$ had already been presented in Ref. [66]. However, it was not designed to provide amplitudes with the high precision needed by our reconstruction strategy. Furthermore, although the reconstructed analytical expressions we obtained are specific to $d=4$, our package provides numerical solutions to the SE in general d dimensions.

1.7 Structure of this Thesis

The rest of this thesis is organised as follows. The first three chapters are introductory. They review topics in particle physics which are instrumental for the rest of the thesis.

- Chapter 2 introduces both dynamics and kinematics in QFTs by taking a group theory approach. This allows for a very natural introduction of all major concepts and mathematical tools necessary throughout this thesis.

- Chapter 3 discusses modern methods for the computation of scattering amplitudes at tree and loop level, mainly BCFW recursion and generalised unitarity. It is through these methods that the amplitudes reconstructed in Chapter 7 and 8 were obtained.

- Chapter 4 reviews the CHY formalism, which was qualitatively introduced in the previous section, and is essential for the discussion in Chapter 9.

All subsequent chapters present new research. Two chapters review the method developed in [1] for the reconstruction of analytical expressions from numerical evaluations.

- Chapter 5 considers how to numerically probe the structure of poles and zeros of tree amplitudes or loop integral coefficients. This will ultimately yield important information that will aid our analytical reconstruction.

- Chapter 6 reviews the parametrisation of the remaining numerator information and its reconstruction by means of Gaussian elimination. Different reconstruction strategies are discussed, which allow us to tackle increasingly complex structures.

The next three chapters make use of the reconstruction method to obtain analytical scattering amplitudes in different sectors of the SM and in other theories.

- Chapter 7 presents results for six-gluon scattering at one loop.

- Chapter 8 presents the Higgs + 4 partons one-loop amplitude, with full mass effects.

- Chapter 9 presents tree amplitudes in the $(DF)^2$ theory and conformal gravity.

Lastly, Chapter 10 presents the conclusion. Additional resources and details are given in the Appendices A-G.

Dynamics & Kinematics

In this chapter we take a group theory approach to review both dynamic and kinematic aspects of a perturbative calculation, described respectively by the interaction gauge groups and the Lorentz group. This distinction is reflected in the organisation of pQFT calculations, and especially QCD ones. In fact, dynamics and kinematics factorise, allowing us to treat them separately. In the case of QCD, we talk about colour factors for the dynamic part and colour-ordered amplitudes for the kinematic one (see colour decomposition in Section 2.1.2). The true complexity of the calculation lies in the kinematic part, for which we will make use of the spinor helicity formalism (see Section 2.2.3). Through the following discussion, similarities between the QCD and Lorentz algebras will become apparent. This is the basis of what is known as colour-kinematics duality [67–69].

2.1 Dynamics

Fundamental interactions among fields arise from their transformation properties under different gauge symmetries. The mediators of the forces are associated with the generators of the Lie algebras of these symmetries. Because of the structure of the gauge groups in the Standard Model, the most important symmetry for us to discuss is the special unitary group $SU(N)$. This covers both non Abelian SM gauge groups $SU(2)_L$ and $SU(3)_C$, as well as potential extensions to the Standard Model, and even the Lorentz group.

2.1.1   Special Unitary Group

The special unitary group $SU(N)$ is the Lie group of $N \times N$ unitary matrices with unit determinant. Its Lie algebra, denoted as $\mathfrak{su}(N)$, is obtained by considering an infinitesimal exponential map. Following the physics convention, we have[1]

$$U(\vec{\epsilon}) = e^{i\epsilon^a T^a} \, , \tag{2.1}$$

where ϵ^a are infinitesimal real parameters, T^a are the generators, and $U \in SU(N)$. The unitarity and unit-determinant conditions translate into hermiticity and tracelessness conditions for the generators

$$UU^\dagger = e^{i\epsilon^a T^a} e^{-i\epsilon^a T^{a,\dagger}} \approx \mathbb{1} + i\epsilon^a T^a - i\epsilon^a T^{a,\dagger} = \mathbb{1} \quad \Longrightarrow \quad T^a = T^{a,\dagger} \, , \tag{2.2}$$

$$\det(U) = \det(e^{i\epsilon^a T^a}) = e^{i\epsilon^a \operatorname{tr}(T^a)} = 1 \quad \forall \epsilon \quad \Longrightarrow \quad \operatorname{tr}(T^a) = 0 \, . \tag{2.3}$$

The generators T^a have to form a basis for a vector space of traceless Hermitian matrices, so there must be $N^2 - 1$ of them. As anticipated in the previous chapter, the generators for $N = 2$ are proportional to the Pauli matrices σ^i and those for $N = 3$ are proportional to the Gell-Mann matrices. The proportionality factor of $1/2$ is convention. To keep track of the convention used, one can use the trace of two generators

$$\operatorname{tr}(T^a T^b) = T_R \, \delta^{ab} \, , \tag{2.4}$$

where in our case $T_R = 1/2$. Note that this factor is equal to the proportionality constant between the generators and the Pauli/Gell-Mann matrices only by coincidence. For example, choosing the proportionality factor to be $1/\sqrt{2}$ results in $T_R = 1$.

The defining property of a Lie algebra is the commutator

$$[T^a, T^b] = if^{abc}T^c \, , \tag{2.5}$$

where f^{abc} are called structure constants. This means that if two sets of generators share the same structure constant then they are merely two representations of the same group. By multiplying the above by another generator and taking the trace we obtain

$$iT_R f^{abc} = \operatorname{tr}(T^c[T^a, T^b]) = \operatorname{tr}(T^a T^b T^c) - \operatorname{tr}(T^a T^c T^b) \, , \tag{2.6}$$

which can be used to show that the structure constants are fully anti-symmetric. Furthermore, by considering matrices defined by the structure constants as $(F^a)_{bc} = if^{abc}$ it can be

---

[1]In mathematics usually the imaginary unit is omitted from the exponent.

shown[2] that the structure constants themselves obey the $SU(N)$ Lie algebra

$$\left[F^a,\, F^b\right] = i f^{abc} F^c \ . \tag{2.7}$$

In fact, the $(T^a)_{ij}$'s are the generators of the fundamental representation of $SU(N)$, and the f^{abc}'s are the generators of the adjoint representation.

It is useful to introduce a diagrammatic notation for the colour algebra. For example, Eq. 2.6 for the structure constants can be visualised as follows.
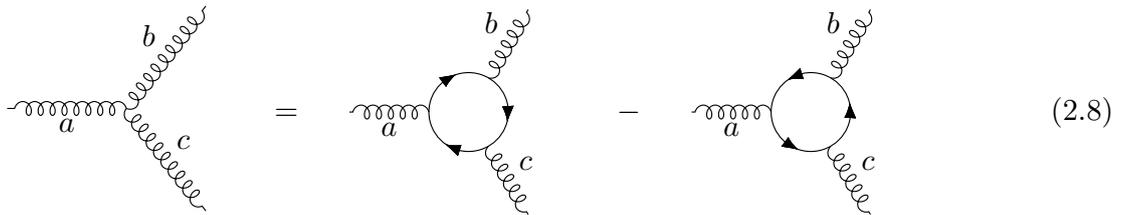
$$\tag{2.8}$$

With the addition of the unit matrix, the generators span the complex space of $N \times N$ matrices. That is, any $N \times N$ matrix M can be written as

$$M = M_0 \mathbb{1} + M_a T^a \;=\; \frac{1}{N}\mathrm{tr}(M)\,\mathbb{1} + \frac{1}{T_R}\mathrm{tr}(MT^a)\,T^a. \tag{2.9}$$

The complex coefficients M_0 and M_a can be projected out by multiplying by generators and taking the trace. By writing the above in index notation and factoring out the matrix M, one obtains the following important Fierz completeness relation

$$T^a_{ij}T^a_{kl} = T_R\left[\delta_{il}\delta_{jk} - \frac{1}{N}\delta_{ij}\delta_{kl}\right] \ . \tag{2.10}$$

The sub-leading $1/N$ term comes from the tracelessness condition, and can be thought of as originating from a $U(1)$ *photon*. In some cases[3] its presence does not affect the result of a calculation, and can therefore be neglected. This is equivalent to introducing an identity generator, with vanishing structure constants, which decouples from the gluons. The resulting identities are called *photon decoupling* identities.

Eq. 2.10 can also be interpreted graphically as follows.

$$\tag{2.11}$$

Eq. 2.6 and Eq. 2.10 together with their graphical formulations allow to simplify colour factors from Feynman diagrams and to derive colour decomposition relations.

---

[2]Consider the Jacobi identity for the generators.

[3]For instance, in the case of tree level pure gluon amplitudes.

We have seen that groups can have different representations, including, but not limited to, the fundamental and the adjoint representation. Representations of groups are categorised based on quantities that are invariant under the action of the symmetry. These quantities are called Casimirs, and are constructed in such a way to commute with all generators of the Lie group. The $SU(N)$ fundamental and adjoint quadratic Casimir operators are defined as

$$T_{ij}^a T_{jk}^a = C_F \delta_{ik} \,, \quad C_F = T_R \frac{N^2 - 1}{N} \,; \qquad f^{abc} f^{abd} = C_A \delta^{cd} \,, \quad C_A = N \,. \qquad (2.12)$$

They arise, for example, in the computation of self energy diagrams in QCD, which is why we have already encountered them in the counter terms of Eq. 1.38. Roughly speaking, they can be thought of as the QCD charges of quarks and gluons respectively.

The fundamental quadratic Casimir will be familiar from the representations of $SU(2)$. In that case it is the squared total spin operator[4]

$$S^2 = S_x^2 + S_y^2 + S_z^2 \,. \qquad (2.13)$$

This will be important to classify the representations of the Lorentz group in Section 2.2.1. Lastly, let us mention that for $N > 2$ more Casimirs exist, beyond the quadratic one. For instance, there is a cubic Casimir defined as

$$d^{abc} T^a T^b T^c = C_{3F} \mathbb{1} \,, \quad \text{where} \quad T_R \, d^{abc} = \text{tr}\big(T^c \{T^a, T^b\}\big) \,. \qquad (2.14)$$

2.1.2 Colour Decomposition

As anticipated, it is possible to factorise dynamics from kinematics by means of colour decompositions. For instance, if we drew all diagrams contributing to an n-point tree-level gluon amplitude and made use of the diagrammatic relations from Eq. 2.8 and Eq. 2.11 we would see that all sub-leading colour terms cancel, leaving only single trace structures. Mathematically, this leads to the following colour decomposition

$$\mathcal{A}_n^{(0)}(p_i, \lambda_i, a_i) = g^{n-2} \sum_{\sigma \in S_n/Z_n} \text{Tr}(T^{a_{\sigma(1)}} \dots T^{a_{\sigma(n)}}) A_n^{(0)}(\sigma(1^{\lambda_1}), \dots, \sigma(n^{\lambda_n})) \,, \qquad (2.15)$$

where the sum runs over all $(n-1)!$ non-cyclically-equivalent permutations, and $A_n^{(0)}$ is a tree-level colour-ordered amplitude, which is a rational function of the momenta. Other names used in the literature for the colour-ordered amplitudes are primitive or

---

[4]A quick sanity check: $(N^2 - 1)/(2N) = s(s+1)$ for $N = 2$ and $s = 1/2$.

sub-amplitudes[5]. It should be noted, that not all $(n-1)!$ sub-amplitudes from Eq. 2.15 are independent. Kleiss-Kuijf relations bring the number down to $(n-2)!$ [70], and Bern-Carrasco-Johansson relations further lower it $(n-3)!$ [67]. Alternative colour decompositions that make use of some of these relations exist [71]. Colour-ordering significantly simplifies the structure of amplitudes, for instance in the case of QCD by restricting the possible singularities to those involving cyclically-adjacent momenta.

As an example of a one loop colour decomposition, in the following we reproduce that for the n-point one-loop gluon amplitude [72]

$$\mathcal{A}_n^{(1)}(p_i, \lambda_i, a_i) = g^n \Big[\sum_{\sigma \in S_n/Z_n} N_c \text{Tr}(T^{a_{\sigma}(1)} \dots T^{a_{\sigma}(n)}) A_{n;1}^{(1)}(\sigma(1^{\lambda_1}), \dots, \sigma(n^{\lambda_n}))$$

$$+ \sum_{c=2}^{\lfloor n/2 \rfloor + 1} \sum_{\sigma \in S_n/Z_{n;c}} \text{Tr}(T^{a_{\sigma}(1)} \dots T^{a_{\sigma}(c-1)}) \text{Tr}(T^{a_{\sigma}(c)} \dots T^{a_{\sigma}(n)}) A_{n;c}^{(1)}(\sigma(1^{\lambda_1}), \dots, \sigma(n^{\lambda_n}))$$

$$+ n_f \sum_{\sigma \in S_n/Z_n} \text{Tr}(T^{a_{\sigma}(1)} \dots T^{a_{\sigma}(n)}) A_{n;1}^{(1/2)}(\sigma(1^{\lambda_1}), \dots, \sigma(n^{\lambda_n})) \Big] . \tag{2.16}$$

The first two lines originate from gluon-loop diagrams, and the last line from quark-loop ones. Note that now there exist non vanishing sub-leading colour contributions, but the corresponding $A_{n;c}^{(1)}$ amplitudes can be obtained by summing over permutations of the leading colour ones $A_{n;1}^{(1)}$.

Loop amplitudes can be decomposed as sums over master integrals (I^i) multiplied by rational coefficients $(a_i, b_i, \dots)$ with a rational remainder term (R). At one-loop a general decomposition in terms of scalar integrals is known and reads [73]

$$A_{n;1}^{1-\text{loop}} = \sum_i d_i I_{\text{Box}}^i + \sum_i c_i I_{\text{Triangle}}^i + \sum_i b_i I_{\text{Bubble}}^i + \sum_i a_i I_{\text{Tadpoles}}^i + R . \tag{2.17}$$

In the case of massless particles running in the loop the tadpoles contributions are scaleless, and so vanish in dim-reg. Furthermore, pentagons should be included in the set of master integrals if the loop momentum is treated in a generic number of dimensions. The integral coefficients are usually referred to as the *cut constructible* part of the amplitude, since they can be obtained from generalised unitarity cuts in four dimensions. In Ref. [1] we obtained a complete set for the integral coefficients and rational parts of $A_{6;1}^{(1)}$.

Finally, the colour decomposition for the $0 \to ggggh$ amplitudes presented in Ref. [3] is

$$\mathcal{H}_n(p_i, \lambda_i, a_i) \propto g_s^n \frac{m_{\text{top}}^2}{v} \sum_{\sigma \in S_n/Z_n} \text{Tr}(T^{a_{\sigma}(1)} \dots T^{a_{\sigma}(n)}) H_n(\sigma(1^{\lambda_1}), \dots, \sigma(n^{\lambda_n}); h) \tag{2.18}$$

where the semicolon is used to separate colour-ordered particles from colour singlets.

---

[5]Slight distinctions exit between these at loop level, but not at tree level.

2.2   Kinematics

Particle physics kinematics is solely determined by the symmetries of Minkowski spacetime: translations, rotations and boosts. This section reviews the consequences that these symmetries have for the particle content of physical theories, such as the Standard Model, as well as for the building blocks of physical observables, such as scattering cross-section and decay rates. The concepts of spin, mass, chirality and helicity, all naturally arise from the representations of the groups underlying the symmetries of spacetime.

The three transformations, or isometries, mentioned above form what is known as the Poincaré group $R^{1,3} \rtimes SO(1,3)$, while its subgroup composed of rotations and boosts only is the Lorentz group $SO(1,3)$. The two coincide for finite dimensional representations, such as *field operators*, since they transform trivially under translations. In other words, asking for Poincaré invariance of a field Lagrangian is not more general than asking for Lorentz invariance. However, these representations are not unitary. In fact, non-compact groups do not admit finite dimensional unitary representation. This is not an issue since there is no well-defined inner product in the space of field operators. It is in the case of particle states that unitarity is crucial, since transition probabilities are given by their expectation values. However, these are not finite, because they are labelled by their momentum.

We will now discuss the representations of the Lorentz group, and then briefly those of the Poincaré group. This topic was first treated in 1939 by Wigner [74].

2.2.1   Representations of the Lorentz Group

The defining property of isometries is that they preserve "distances", i.e. inner products in Minkowski spacetime are left unchanged. A spacetime distance is also known as *interval*. Let Λ be a Lorentz transformation and η the Minkowski metric in the mostly negative convention $\eta = \mathrm{diag}(1, -1, -1, -1)$, preservation of distances implies that

$$\Lambda^T \eta \Lambda = \eta \quad \text{or} \quad \Lambda^\sigma{}_\mu \Lambda^\rho{}_\nu \eta_{\sigma\rho} = \eta_{\mu\nu}. \tag{2.19}$$

In order to establish the representations of $SO(1,3)$ we look at its Lie algebra $so(1,3)$, which can be obtained by considering the exponential map

$$\Lambda = e^{i\vec{\alpha}\cdot\vec{\omega}}, \tag{2.20}$$

where $\vec{\omega}$ are the generators and $\vec{\alpha}$ are some parameters. In doing so, we are actually

restricting ourselves to the *proper orthochronous* Lorentz group $SO_+^\uparrow(1,3)$, that is the part of the Lorentz group connected to the identity. In total, there are 4 disconnected parts in the Lorentz group: the first separation is between *proper* and *improper* transformations, having $\det(\Lambda) = \pm 1$ respectively; the second one is between *orthochronous* and *non-orthochronous* transformations, having $\text{sign}(\Lambda^0{}_0) = \pm 1$ respectively. The parity operator $\hat{P} = \text{diag}(+1, -1, -1, -1)$, the time reversal operator $\hat{T} = \text{diag}(-1, +1, +1, +1)$ and their product $\hat{P}\hat{T}$ are all examples of Lorentz transformations not connected to the identity. Inserting Eq. 2.20 in Eq. 2.19 and keeping the leading order in $\vec{\alpha}$, we obtain

$$\vec{\alpha} \cdot (\vec{\omega}^T \eta + \eta \vec{\omega}) = 0 \quad \forall \, \vec{\alpha}, \tag{2.21}$$

that is $\omega_{\mu\nu} = -\omega_{\nu\mu}$ in index notation, meaning $\omega_{\mu\nu}$ is fully anti-symmetric. The more conventional form involves one raised and one lowered index $\omega^\mu{}_\nu$, which will therefore be symmetric in the spacetime components and anti-symmetric in the space-space ones. Explicitly, we can write the six $\vec{\omega}$ generators as

$$K_x = \begin{bmatrix} 0 & i & 0 & 0 \\ i & 0 & 0 & 0 \\ 0 & 0 & 0 & 0 \\ 0 & 0 & 0 & 0 \end{bmatrix}, \quad K_y = \begin{bmatrix} 0 & 0 & i & 0 \\ 0 & 0 & 0 & 0 \\ i & 0 & 0 & 0 \\ 0 & 0 & 0 & 0 \end{bmatrix}, \quad K_z = \begin{bmatrix} 0 & 0 & 0 & i \\ 0 & 0 & 0 & 0 \\ 0 & 0 & 0 & 0 \\ i & 0 & 0 & 0 \end{bmatrix}, \tag{2.22}$$

$$J_x = \begin{bmatrix} 0 & 0 & 0 & 0 \\ 0 & 0 & 0 & 0 \\ 0 & 0 & 0 & -i \\ 0 & 0 & i & 0 \end{bmatrix}, \quad J_y = \begin{bmatrix} 0 & 0 & 0 & 0 \\ 0 & 0 & 0 & i \\ 0 & 0 & 0 & 0 \\ 0 & -i & 0 & 0 \end{bmatrix}, \quad J_z = \begin{bmatrix} 0 & 0 & 0 & 0 \\ 0 & 0 & -i & 0 \\ 0 & i & 0 & 0 \\ 0 & 0 & 0 & 0 \end{bmatrix}, \tag{2.23}$$

where the K_i's generate boosts and the J_i's generate rotations. They satisfy the following commutation relations

$$[J_i, J_j] = i\epsilon_{ijk}J_k, \qquad [K_i, K_j] = -i\epsilon_{ijk}J_k, \qquad [J_i, K_j] = i\epsilon_{ijk}K_k. \tag{2.24}$$

Consider now the following linear combinations of the generators

$$N_i = \frac{1}{2}(J_i - iK_i) \quad \& \quad \bar{N}_i = \frac{1}{2}(J_i + iK_i), \tag{2.25}$$

and their respective commutation relations

$$[N_i, N_j] = i\epsilon_{ijk}N_k, \qquad [\bar{N}_i, \bar{N}_j] = i\epsilon_{ijk}\bar{N}_k, \qquad [N_i, \bar{N}_j] = 0. \tag{2.26}$$

Clearly, N_i and $\bar{N}_i$ form two independent copies of the $\mathfrak{su}(2)$ Lie algebra. Therefore, we

(j_-, j_+)	dimension	name	field	variable
$(0,0)$	1	scalar	h	mass
$(0, 1/2)$	2	right-handed Weyl spinor	$\chi_{R\alpha}$	λ_α
$(1/2, 0)$	2	left-handed Weyl spinor	$\chi_L^{\dot\alpha}$	$\bar\lambda^{\dot\alpha}$
$(1/2, 1/2)$	4	rank-two spinor/four vector	$A^\mu / A^{\dot\alpha\alpha}$	$P^\mu / P^{\dot\alpha\alpha}$
$(1/2, 0) \oplus (0, 1/2)$	4	bispinor (Dirac spinor)	Ψ	u, v

Table 2.1: List of low dimensional representations of the Lorentz group.

classify the representations of the Lorentz group in terms of the eigenvalues $n(n+1)$ and $\bar{n}(\bar{n}+1)$ of the two $\mathfrak{su}(2)$ Casimir operators N^2 and $\bar{N}^2$, or more simply by the pair of (half-) integer numbers $(n, \bar{n})$. These correspond to two *spins*, one for each $\mathfrak{su}(2)$ copy. The lowest lying representations of the Lorentz group are given in Table 2.1.

Chirality is the intrinsic property of a field or particle that refers to which representation of the Lorentz group it transforms under. It is not to be confused with *helicity*, which is defined as the projection of spin onto the direction of the momentum. The two properties are related in the massless limit, and in order for a right (left) chiral massless particle to be a positive (negative) helicity eigenstate, we must choose N ($\bar{N}$) as the generator for the j_+ (j_-) representation.

An important distinction that has to be stressed is between two target spaces of the Lorentz group: the field operators and the kinematic variables. Although the two may behave in the same way under Lorentz transformations, they are also fundamentally different. For example, spin-1/2 field operators χ and spinors λ carry the same index ($\alpha/\dot{\alpha}$), but the former is an abstract Grassmann-odd object thanks to the anti-commuting creation and annihilation operators that form it, whereas the latter is Grassmann-even two-component object that solves the Weyl equation and can be assigned a numerical value.

The conventions we adopt are as follow. Right-handed spinors will carry undotted indices, whereas left-handed spinors will carry dotted indices. The former will be contracted "downwards" ($^\alpha_{\ \alpha}$), whereas the latter will be contracted "upwards" ($_{\dot\alpha}^{\ \dot\alpha}$). Since contracted indices can be omitted, we are also going to use a bar over all left-handed spinors. Finally, let us introduce the Infeld-van der Waerden symbols, which form a basis for 2×2 Hermitian matrices. They are: $(\sigma^\mu)^{\dot\alpha\alpha} = (\mathbf{1}, \sigma^i)$ and $(\bar\sigma^\mu)_{\alpha\dot\alpha} = (\mathbf{1}, -\sigma^i)$.

What follows is a review of the lowest-lying representations of the Lorentz group.

Trivial Representation (0, 0)

Both left and right generators are trivial

$$d_{(0,0)}(\bar{N}_i) = 0 \;\&\; d_{(0,0)}(N_i) = 0 \;\implies\; d_{(0,0)}(K_i) = 0 \;\&\; d_{(0,0)}(J_i) = 0$$

$$\implies\; d_{(0,0)}(\Lambda) = 1. \tag{2.27}$$

A field operator (eg. the Higgs field h) or a kinematic variable (eg. the rest mass m) living in this representation will transform trivially to itself under any Lorentz transformation.

Right-Handed Spinor Representation (0, 1/2)

The left generator is trivial, the right ones are given by the fundamental $\mathfrak{su}(2)$ generators

$$d_{(0,1/2)}(\bar{N}_i) = 0 \;\&\; d_{(0,1/2)}(N_i) = \sigma_i/2 \;\implies\; d_{(0,1/2)}(K_i) = i\sigma_i/2 \;\&\; d_{(0,1/2)}(J_i) = \sigma_i/2$$

$$\implies\; d_{(0,1/2)}(\Lambda) = \Lambda_\alpha{}^\beta = e^{(i\vec{\theta} - \vec{\rho})\vec{\sigma}/2}. \tag{2.28}$$

In the above we have replaced the $\vec{\alpha}$ parameters from Eq. 2.20 with physical ones: $\vec{\theta}$ are the rotation angles, and $\vec{\rho}$ are the rapidities. The index choice is made to match the "downwards" convention for undotted indices, so that the expression $\lambda \to \Lambda\lambda$ is unambiguous. It is easy to show that, in the case of 2×2 Lorentz transformations, the role of the metric η in Eq. 2.19 is fulfilled by the 2×2 fully anti-symmetric Levi-Civita tensor[6]. Therefore, we can define the metric to be $\epsilon^{\alpha\beta} = \epsilon^{\dot\alpha\dot\beta} = \epsilon$ and its inverse $\epsilon_{\alpha\beta} = \epsilon_{\dot\alpha\dot\beta} = \epsilon^T$.

The transformation law for the raised-index spinor $\lambda^\alpha = \epsilon^{\alpha\beta}\lambda_\beta$ in index notation is $\lambda^\alpha \to \Lambda^\alpha{}_\beta \lambda^\beta = \lambda^\beta (\Lambda_\beta{}^\alpha)^T$. In order to write this in index-free notation let us consider again Eq. 2.19 and rearranged it as

$$\Lambda^T \epsilon \Lambda = \epsilon \;\implies\; \epsilon \Lambda \epsilon^T = (\Lambda^T)^{-1} \quad \text{i.e.} \quad \Lambda^\alpha{}_\beta = ((\Lambda_\alpha{}^\beta)^T)^{-1}. \tag{2.29}$$

Thus, we have $(\epsilon\lambda) \to (\epsilon\lambda)(\Lambda)^{-1}$. This also proves that $(\epsilon\lambda)\lambda$ is a Lorentz scalar.

To show that λ is indeed a right-handed spinor we write down Weyl equation in momentum space and perform some straightforward manipulation to expose the helicity operator

$$(\sigma^\mu)^{\dot\alpha\alpha} P_\mu \lambda_\alpha = 0 \implies (\mathbf{1} \cdot p^0 - \vec{\sigma} \cdot \vec{p})\lambda = 0 \implies \frac{1}{2}\frac{\vec{\sigma} \cdot \vec{p}}{p^0}\lambda = +\frac{1}{2}\lambda. \tag{2.30}$$

Note that this describes massless particles only (helicity is not a good quantum number for massive particles).

---

[6]Simply take Eq. 2.19 and substiture ω with the Pauli matrices and η with the Levi-Civita simbol.

We can also solve the above to obtain an explicit expression for the spinor λ

$$P^{\dot{\alpha}\alpha}\lambda_\alpha = 0 \implies (\mathbf{1} \cdot p^0 - \vec{\sigma} \cdot \vec{p})\lambda = 0 \implies \begin{pmatrix} p^0 - p^3 & -p^1 + ip^2 \\ -p^1 - ip^2 & p^0 + p^3 \end{pmatrix} \begin{pmatrix} \lambda_1 \\ \lambda_2 \end{pmatrix} = 0. \quad (2.31)$$

These two linear equations for λ_1 and λ_2 are not independent due to the on-shell massless condition $(p^0)^2 - (p^1)^2 - (p^2)^2 - (p^3)^2 = 0$. Therefore, we need some form of normalisation to fully constrain the system. The most sensible choice is to use a covariant normalisation. In particular, for reasons that will become clearer when we discuss the vector representation, $\lambda^\dagger \lambda$ should be equal to twice the zeroth component of the corresponding four vector, i.e. $\lambda^\dagger \lambda = 2p^0$. The two equations are then

$$|\lambda_1|^2 + |\lambda_2|^2 = 2p^0 \quad \& \quad \lambda_2 = \frac{p^0 - p^3}{p^1 - ip^2}\lambda_1. \quad (2.32)$$

Therefore, up to a conventional phase, we may write

$$\lambda_\alpha = \begin{pmatrix} \sqrt{p^0 + p^3} \\ \frac{p^1 + ip^2}{\sqrt{p^0 + p^3}} \end{pmatrix} \quad \& \quad \lambda^\alpha = \epsilon^{\alpha\beta}\lambda_\beta = \begin{pmatrix} \frac{p^1 + ip^2}{\sqrt{p^0 + p^3}}, & -\sqrt{p^0 + p^3} \end{pmatrix}. \quad (2.33)$$

Left-Handed Spinor Representation $(1/2, 0)$

In analogy with the right-handed representation, we have

$$d_{(1/2,0)}(\bar{N}_i) = \sigma_i/2 \ \& \ d_{(1/2,0)}(N_i) = 0 \implies d_{(1/2,0)}(K_i) = -i\sigma_i/2 \ \& \ d_{(1/2,0)}(J_i) = \sigma_i/2$$

$$\implies d_{(1/2,0)}(\Lambda) = \Lambda^{\dot{\alpha}}_{\dot{\beta}} = e^{(i\vec{\theta} + \vec{\rho})\vec{\sigma}/2}. \quad (2.34)$$

By comparing Eq. 2.34 with Eq. 2.28 becomes apparent that the former is the inverse of the Hermitian conjugate of the latter. Therefore, the transformation law in index-free notation is $\bar{\lambda} \to (\Lambda^\dagger)^{-1}\bar{\lambda}$. For the lower index left-handed spinor we may then write: $(\epsilon^T \bar{\lambda}) \to (\epsilon^T \bar{\lambda})\Lambda^\dagger$. The relevant momentum space Weyl equation now reads:

$$(\bar{\sigma}^\mu)_{\alpha\dot{\alpha}} P_\mu \bar{\lambda}^{\dot{\alpha}} = 0 \implies (\mathbf{1} \cdot p^0 + \vec{\sigma} \cdot \vec{p})\bar{\lambda} = 0 \implies \frac{1}{2}\frac{\vec{\sigma} \cdot \vec{p}}{p^0}\bar{\lambda} = -\frac{1}{2}\bar{\lambda}. \quad (2.35)$$

Applying the same procedure that we saw for the $(0, 1/2)$ representation, we can obtain an explicit expression for the spinor $\bar{\lambda}$, which now reads:

$$\bar{\lambda}_{\dot{\alpha}} = \begin{pmatrix} \sqrt{p^0 + p^3}, & \frac{p^1 - ip^2}{\sqrt{p^0 + p^3}} \end{pmatrix} \quad \& \quad \bar{\lambda}^{\dot{\alpha}} = \epsilon^{\dot{\alpha}\dot{\beta}}\bar{\lambda}_{\dot{\beta}} = \begin{pmatrix} \frac{p^1 - ip^2}{\sqrt{p^0 + p^3}} \\ -\sqrt{p^0 + p^3} \end{pmatrix}. \quad (2.36)$$

For real momenta with positive energy, λ_α and $\bar{\lambda}_{\dot{\alpha}}$ are related by complex conjugation.

Four-vector Representation (1/2, 1/2)

The reason for the name of this representation may not be obvious at a first glance, since the classification implies that this is the vector space of the tensor product between the left-handed and the right-handed spinor vector spaces. Therefore, objects in this representation carry one undotted and one dotted index, and we call them *rank-two* spinors. However, four-vectors are essentially just a reformulation of 2×2 spinors as 4×1 objects. As such, the two are closely related. The transformation law reads

$$\bar{P}_{\alpha\dot{\alpha}} \to \Lambda_\alpha{}^\beta \Lambda_{\dot{\alpha}}{}^{\dot{\beta}} \bar{P}_{\beta\dot{\beta}} = \Lambda_\alpha{}^\beta \bar{P}_{\beta\dot{\beta}} (\Lambda^\dagger)^{\dot{\beta}}{}_{\dot{\alpha}} = (\Lambda \bar{P} \Lambda^\dagger)_{\alpha\dot{\alpha}} \tag{2.37}$$

$$\text{or} \quad P^\mu \to \Lambda^\mu{}_\nu P^\nu = (\Lambda P)^\mu. \tag{2.38}$$

In order to understand the relation between the two, we need an object which carries left-handed, right-handed and vector indices. We have already seen such an object: it is the Infeld-van der Waerden symbol $(\sigma^\mu)^{\dot{\alpha}\alpha}$ (or, equivalently, $(\bar{\sigma}^\mu)_{\alpha\dot{\alpha}}$). Then, we have[7]

$$\bar{P}_{\alpha\dot{\alpha}} = (\bar{\sigma}^\mu)_{\alpha\dot{\alpha}} P_\mu \quad \text{and} \quad P_\mu = \frac{1}{2} (\sigma^\mu)^{\dot{\alpha}\alpha} \bar{P}_{\alpha\dot{\alpha}} . \tag{2.39}$$

The factor of a half comes from the relation $(\sigma^\mu)^{\dot{\alpha}\alpha} (\bar{\sigma}^\nu)_{\alpha\dot{\alpha}} = 2\eta^{\mu\nu}$. For everything to be consistent, the following relation must then hold

$$\bar{P}_{\alpha\dot{\alpha}} = (\bar{\sigma}^\mu)_{\alpha\dot{\alpha}} P_\mu \to \Lambda_\alpha{}^\beta \Lambda_{\dot{\alpha}}{}^{\dot{\beta}} (\bar{\sigma}^\mu)_{\beta\dot{\beta}} P_\mu = (\bar{\sigma}^\mu)_{\alpha\dot{\alpha}} (\Lambda^{-1})^T{}_\mu{}^\nu P_\nu , \tag{2.40}$$

$$\implies (\Lambda \bar{\sigma} \Lambda^\dagger)^\mu_{\alpha\dot{\alpha}} = (\bar{\sigma}(\Lambda^{-1})^T)^\mu_{\alpha\dot{\alpha}} . \tag{2.41}$$

This relation can be checked explicitly by using Eq. 2.28 and the Lorentz transformations obtained by exponentiating the generators in Eq. 2.22. It should be clear from the context that in the left-hand side of the above equation the Λ's refers to 2×2 matrices, whereas in the right-hand side it refers to the 4×4 version.

A further important insight concerns the relation between rank-two and rank-one spinors. Generally, they are independent, but what happens if the determinant of a rank-two spinor vanishes? In this case the rank is not two anymore, but one. Therefore, in this special case we must be able to write the 2×2 matrix representing the "rank-two" spinor with vanishing determinant in terms of the outer product of a right-handed and a left-handed spinor. We have already seen an example of this when looking at Weyl equation for massless fermions. The matrix in Eq. 2.31 represents the "rank-two" spinor $P^{\dot{\alpha}\alpha}$. Its determinant is the

---

[7] The convention for rank-two spinors is that they carry a bar if they are formed by contracting a four vector with a $\bar{\sigma}$, and vice versa. This is to keep track of contractions in index-free notation.

invariant mass $P^2 = 0$. By taking the outer product between the left-handed spinor in Eq. 2.36 and the right-handed spinor in Eq. 2.33 we indeed obtain the matrix in Eq. 2.31. This last relation, which in index notation reads

$$P^{\dot{\alpha}\alpha} = \bar{\lambda}^{\dot{\alpha}}\lambda^{\alpha} , \qquad (2.42)$$

allows us to decompose any null four-vector into two spinors. This is a crucial feature of the spinor helicity formalism. Lastly, note that the covariant normalisation $\lambda^\dagger \lambda = 2p^0$ is consistent with the trace of the rank two spinor.

Dirac Representation (1/2, 0) ⊕ (0, 1/2)

This representation is reducible into a left-handed and a right-handed one, whereas all previous representations are irreducible. However, it is still useful and widely used because Dirac mass terms mix left- and right-handed spinor components. The Dirac equation is

$$(\gamma^\mu P_\mu - m)\chi = \begin{pmatrix} -m & \bar{\sigma}^\mu P_\mu \\ \sigma^\mu P_\mu & -m \end{pmatrix} \begin{pmatrix} \chi_R \\ \chi_L \end{pmatrix} = 0 , \qquad (2.43)$$

where we chose to work in Weyl basis, meaning the γ-matrices are given by

$$\gamma^\mu = \begin{pmatrix} 0 & \bar{\sigma}^\mu \\ \sigma^\mu & 0 \end{pmatrix} \quad \text{and} \quad \gamma^5 = \begin{pmatrix} \mathbf{1} & 0 \\ 0 & -\mathbf{1} \end{pmatrix} . \qquad (2.44)$$

Clearly, in general these are two coupled equations for χ_R and χ_L, but in the massless limit they reduce to the Weyl equations (Eq. 2.30 and Eq. 2.35). Let us work with $m = 0$. We can easily write down the solutions for particle and anti-particle wavefunctions making use of our previous results. As by convention, we call the particle wavefunction u and the anti-particle wavefunction v. The left and right projection operators are as usual given by $P_{R,L} = (\mathbf{1} \pm \gamma^5)/2$. Let us start from the particle wavefunction, its positive helicity part and its negative helicity part. They are respectively:

$$u = \begin{pmatrix} \lambda_\alpha \\ \bar{\lambda}^{\dot{\alpha}} \end{pmatrix} , \quad u_+ = P_R u = \begin{pmatrix} \lambda_\alpha \\ 0 \end{pmatrix} , \quad \text{and} \quad u_- = P_L u = \begin{pmatrix} 0 \\ \bar{\lambda}^{\dot{\alpha}} \end{pmatrix} . \qquad (2.45)$$

The dual wavefunction and its projections are given by the Dirac adjoints

$$\bar{u} = u^\dagger \gamma^0, \quad \bar{u}_+ = (P_R u)^\dagger \gamma^0 = \bar{u} P_L = (0, \bar{\lambda}^{\dot{\alpha}}) , \qquad (2.46)$$

$$\text{and} \quad \bar{u}_- = (P_L u)^\dagger \gamma^0 = \bar{u} P_R = (\lambda_\alpha, 0) . \qquad (2.47)$$

To obtain the anti-particle wavefunction we could consider the negative energy solutions to

the Dirac equation and follow the "Feynman-Stuckelberg interpretation" to translate them to anti-particle wavefunctions. Alternatively, we can operate on the particle wavefunction with the charge conjugation operator $\hat{C} = i\gamma^2$

$$v = \hat{C}u^* = \begin{pmatrix} 0 & \epsilon_{\alpha\beta} \\ \epsilon^{\dot{\alpha}\dot{\beta}} & 0 \end{pmatrix} \begin{pmatrix} \bar{\lambda}_{\dot{\alpha}} \\ \lambda^{\alpha} \end{pmatrix} = \begin{pmatrix} \lambda_{\alpha} \\ \bar{\lambda}^{\dot{\alpha}} \end{pmatrix} = u \tag{2.48}$$

The helicity eigenstates are now given by

$$v_+ = \hat{C}u_+^* = \hat{C}P_R u^* = P_L\hat{C}u^* = P_L v = \begin{pmatrix} 0 \\ \bar{\lambda}^{\dot{\alpha}} \end{pmatrix} \quad \text{and} \quad v_- = P_R v = \begin{pmatrix} \lambda_{\alpha} \\ 0 \end{pmatrix} \tag{2.49}$$

where we have used the anti-commutation relation $\{\gamma^5, \gamma^\mu\} = 0$. Finally, the adjoint anti-particle wavefunction projections are

$$\bar{v}_+ = \bar{v}P_R = (\lambda_\alpha, 0) \quad \text{and} \quad \bar{v}_- = \bar{v}P_L = (0, \bar{\lambda}^{\dot{\alpha}}) \tag{2.50}$$

2.2.2 Representations of the Poincaré Group

For completeness, we will now mention the representations of the Poincaré group, although they are not crucial for the next topics we will cover.

In addition to boosts and rotations, the Poincaré group includes translations. Translations are generated by the momentum operator $P_\mu = i\partial_\mu$. It is convenient to combine the generators of boosts K_i and rotations J_i into a single tensor. This tensor is anti-symmetric and is known as the relativistic angular momentum tensor $M^{\alpha\beta}$. It is defined in its space-time components as $M^{0i} = -M^{i0} = K_i$, and in its space-space components as $M^{ij} = \epsilon_{ijk}J_k$. The Casimirs of the group, i.e. the operators that commute with both P^μ and $M^{\alpha\beta}$, are the square four-momentum $P_\mu P^\mu$, and the square Pauli-Lubanski four-vector $W_\mu W^\mu$. The latter is defined as

$$W_\mu = \frac{1}{2}\epsilon_{\mu\nu\rho\sigma}M^{\nu\rho}P^\sigma \ . \tag{2.51}$$

Thus, the representations of the Poincaré group are classified according to

$$P^2 = m^2 \quad \text{and} \quad W^2 = -m^2\,s(s+1)\ , \tag{2.52}$$

that is, according to mass and spin. The expression for W^2 given in Eq. 2.52 implies a zero value for massless particles, which is indeed the case for physical states, since $W^\mu \propto P^\mu$. Interestingly, however, there also exist solutions where this is not the case, but they correspond to unobserved degrees of freedom, such as tachyons.

2.2.3   Spinor Helicity Formalism

The spinor helicity formalism is, in essence, just a clever choice of variables for studying the scattering of massless particles[8]: amplitudes are expressed in terms of Weyl two-component spinors, instead of Dirac four-component spinors and four-vectors. This choice allows us to obtain very compact final expressions, and it is well suited to be used in conjunction with some powerful techniques for the computation of matrix elements (as will be discussed in Chapter 3). In this section, we will introduce the adopted conventions and notation, which will mostly reflect those in Refs. [75, 76], as well as review the main features of the spinor helicity formalism. Although the notation is fairly universal, its meaning is by no means unique, with several authors [77–79] using different conventions for index contraction, four-momentum signs (all-incoming vs. all-outgoing convention), notation associated with left-handed and right-handed spinors, and so forth.

The iconic building blocks of the spinor-helicity formalism are the angle and square bracket spinor products. They are defined in terms of the previously discussed right- and left-handed Weyl spinors as follows

$$\langle ij \rangle \equiv \lambda_i \lambda_j = (\lambda_i)^\alpha (\lambda_j)_\alpha \qquad \text{and} \qquad [ij] \equiv \bar{\lambda}_i \bar{\lambda}_j = (\bar{\lambda}_i)_{\dot\alpha} (\bar{\lambda}_j)^{\dot\alpha}. \qquad (2.53)$$

Both angle and square brackets are anti-symmetric

$$\langle ij \rangle = (\lambda_i)^\alpha (\lambda_j)_\alpha = \epsilon^{\alpha\beta} (\lambda_i)_\beta (\lambda_j)_\alpha = -\epsilon^{\beta\alpha} (\lambda_j)_\alpha (\lambda_i)_\beta = -(\lambda_j)^\beta (\lambda_i)_\beta = -\langle ji \rangle \,, \quad (2.54)$$

and similarly $[ij]$. In the case of real momenta, they are related by complex conjugation

$$\langle ij \rangle = \pm [ji]^* \quad \text{if } \text{sign}(P_i^{(0)}) = \pm \text{sign}(P_j^{(0)}). \qquad (2.55)$$

This is most easily understood in terms of the Mandelstam s_{ij} and the relation

$$s_{ij} = \langle ij \rangle [ji] = p_i^{(0)} p_j^{(0)} - \vec{p}_i \cdot \vec{p}_j \,. \qquad (2.56)$$

Clearly, if the two energies have the same sign, then s_{ij} is positive and we need the plus sign from Eq. 2.55; conversely if the energies have opposite sign. The formula of Eq. 2.56 can be understood starting from the relations between four-vectors and spinors

$$
\begin{aligned}
\langle ij \rangle [ji] &= & (\lambda_i)^\alpha (\lambda_j)_\alpha (\bar{\lambda}_j)_{\dot\alpha} (\bar{\lambda}_i)^{\dot\alpha} &= & (P_i)^{\dot\alpha\alpha} (\bar{P}_j)_{\alpha\dot\alpha} &= \\
&= & (P_i)_\mu (P_j)_\nu (\sigma^\mu)^{\dot\alpha\alpha} (\bar{\sigma}^\nu)_{\alpha\dot\alpha} &= & (P_i)_\mu (P_j)_\nu \, 2\eta^{\mu\nu} &= & 2 P_i \cdot P_j \,.
\end{aligned}
\qquad (2.57)
$$

---

[8]Massive particles can also be easily accommodated to some extent with certain tricks, see Chapter 8.

So far we have seen that both spinors and four-momenta can we easily expressed in terms of spinor helicity variables. To compute an amplitude in, say, massless QCD, using the Feynman rules from Appendix A, we would need one final ingredient: the positive and negative helicity polarisation tensors for massless vector bosons. These can be easily expressed in terms of spinors as follows[9]

$$(\epsilon_i^+)^{\dot\alpha\alpha} = \sqrt{2}\,\frac{|i]\langle q|}{\langle qi\rangle}\,, \qquad (\epsilon_i^-)^{\dot\alpha\alpha} = \sqrt{2}\,\frac{|q]\langle i|}{[iq]}\,. \tag{2.58}$$

As sanity checks, we see that they are manifestly transverse to the momenta $\epsilon_i^\pm \cdot P_i = 0$, and they are related by parity. Furthermore, both $\epsilon^\pm$ are transverse to q, an arbitrary reference momentum. Independence of an expression from the reference momenta is the spinor helicity equivalent of gauge invariance.

Lastly, let us mention two sets of identities satisfied by the spinor products. In the all outgoing convention, momentum conservation for an n-point massless phase space reads

$$\sum_{i=1}^{n}\langle j|i\rangle[i|k] = 0\,, \quad \forall j,k \in \{1,\ldots,n\}\,. \tag{2.59}$$

The second set of identities, called Schouten identities, follows from the simple observation that spinors are two component objects, hence any one of them can be written as a linear combination of other two

$$|k\rangle = \frac{\langle j|k\rangle}{\langle j|i\rangle}|i\rangle + \frac{\langle i|k\rangle}{\langle i|j\rangle}|j\rangle \tag{2.60}$$

These relations are non-linear, hence part of the difficulties in handling big expressions.

Spinor Contractions & Lorentz Invariants

When solving linear systems, it is often convenient to work with a basis of linearly independent variables. Hence, for instance, the use of twistors or minimal basis sets of Mandelstam invariants to reconstruct analytical expressions for amplitudes [15–31]. In Chapter 6, we will use a similar sets of variables, although in our case they will be products of angle and square spinor brackets, to solve linear systems for the numerators of amplitude coefficients. However, the linear redundancies of the spinor helicity variables provide a powerful tool which better describes the nuances of complex phase space, while keeping expressions compact. As we will argue in Chapter 5, singular limits[10] in complex phase space can be exploited to obtain insights in the structure of scattering amplitudes. Because

---

[9]Hence the name spinor helicity. These are already for outgoing particles, no complex conj. required.

[10]A singular phase space limit is a limit where a single invariant becomes arbitrarily small, and hence an amplitude diverges, if that invariant appears as a pole, see Eq. 5.8.

of this, we will generally try to express amplitudes in terms of sets of variables which are not necessarily linearly independent, but for which unique singular phase space configurations can be constructed. Such invariants will include, but not be limited to

$$\langle ij \rangle \equiv (\lambda_i)^\alpha (\lambda_j)_\alpha \ , \qquad [ij] \equiv (\bar\lambda_i)_{\dot\alpha} (\bar\lambda_j)^{\dot\alpha} \tag{2.61}$$

$$s_{ijk} \equiv (P_i + P_j + P_k)^2 \ , \tag{2.62}$$

$$\langle i|(j+k)|l] \equiv (\lambda_i)^\alpha (\bar P_j + \bar P_k)_{\alpha\dot\alpha} \bar\lambda_l^{\dot\alpha} \ , \tag{2.63}$$

$$\langle i|(j+k)|(l+m)|n\rangle \equiv (\lambda_i)^\alpha (\bar P_j + \bar P_k)_{\alpha\dot\alpha} (P_l + P_m)^{\dot\alpha\alpha} (\lambda_n)_\alpha \ , \tag{2.64}$$

$$tr_5(ijkl) \equiv tr(\gamma^5 P_i P_j P_k P_l) = [i\,|\,j\,|\,k\,|\,l\,|\,i\rangle - \langle i\,|\,j\,|\,k\,|\,l\,|\,i] \ . \tag{2.65}$$

All Outgoing Convention

All amplitudes we consider will be expressed in the all-outgoing labelling convention. Phase space configurations where some particles are incoming are easily translated to the all-outgoing convention by flipping signs of the incoming four-momenta.

Feynman rules and diagrams are converted to the all-outgoing convention in three steps:

1. incoming momenta have to be relabelled to be outgoing by introducing a minus sign;

2. incoming particle wavefunctions u are replaced by outgoing anti-particle wavefunctions v, and similarly incoming anti-particles $\bar v$ become outgoing particles $\bar u$;

3. finally, since spins are unchanged but momentum is inverted, we need to flip the helicity labelling as well. In the case of vector bosons, this means swapping the polarisation vectors $\epsilon^+ \leftrightarrow \epsilon^-$.

An example is given in the following diagram.
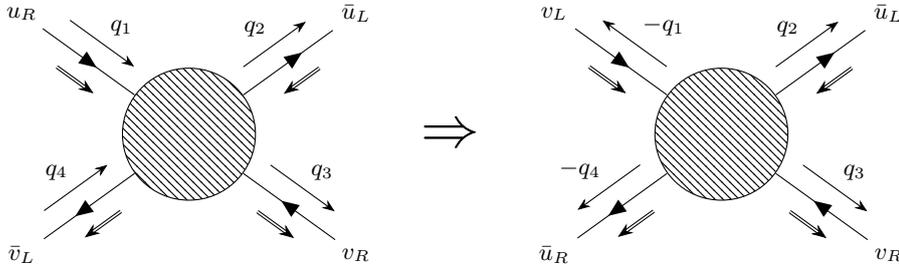
Negative helicity spin-1/2 (anti-) particles $(\bar u_-, v_-)$ are associate with a right handed spinor λ_α, and, vice versa, all positive helicity spin-1/2 (anti-) particles $(\bar u_+, v_+)$ are associated with a left-handed spinor $\bar\lambda_{\dot\alpha}$. Analogously, negative helicity massless vector bosons are associated with a factor of $\lambda_\alpha/\bar\lambda_{\dot\alpha}$, and positive helicity ones with $\bar\lambda_{\dot\alpha}/\lambda_\alpha$.

Special Kinematics

Out of all the possible n particle phase spaces, those for the two lowest values of n, that is $n = 3$ and $n = 4$, have some striking peculiarities which will become relevant in Chapter 3 and in Chapter 4, and are therefore interesting to discuss here.

Starting with the massless three-particle phase space, let us consider momentum conservation

$$P_1 + P_2 + P_3 = 0 \implies 2P_1 \cdot P_2 = (P_1 + P_2)^2 = (-P_3)^2 = 0 \,. \tag{2.66}$$

Rewriting this using the spinor helicity notation, we have that

$$\langle 12 \rangle [21] = 0 \,. \tag{2.67}$$

For this to hold, we have to choose either $\langle 12 \rangle = 0$ or $[12] = 0$. Without loss of generality, let us consider the case $\langle 12 \rangle \neq 0$ and $[12] = 0$. The other case will be related by parity, i.e. a swap of the right and left Lorentz representations (angle and square brackets)[11]. Consider now a slightly modified version of the above equation

$$\langle 12 \rangle [23] = \langle 1 | P_2 | 3] = \langle 1 | - P_1 - P_3 | 3] = 0 \,, \tag{2.68}$$

where the last equality follows from the anti-symmetry of the spinor products (or from Eq. 2.30). It follows that $[23] = 0$. Similarly, one can also show that $[13] = 0$.

Thus, either all square brackets or all angle brackets must vanish. This is only possible with complex kinematics. The last remaining case, that is the one where both all angle brackets and all square brackets vanish, corresponds to real momenta. Physically, this is equivalent to saying that it is kinematically impossible for a massless particle to decay into a pair of massless particles, unless they are all collinear.

Let us now consider the four-particle phase space. It is less constrained than the three-particle one, but it still has significant degeneracies among its invariants in specific regions. Starting again from momentum conservation, we have

$$P_1 + P_2 + P_3 + P_4 = 0 \,, \tag{2.69}$$

$$\implies 2P_1 \cdot P_2 = (P_1 + P_2)^2 = (-P_3 - P_4)^2 = 2P_3 \cdot P_4 \,. \tag{2.70}$$

---

[11]To clarify, calling this parity is a slight abuse of notation. We use the term parity interchangeably with the concept of swapping right and left Lorentz representations. Technically speaking, in our convention, this is equivalent to the improper Lorentz transformation $\text{diag}(1, 1, -1, 1)$, which is actually related to spatial inversion, i.e. $\text{diag}(1, -1, -1, -1)$, by a rotation by π around the y-axis.

In spinor-helicity notation, this implies

$$\langle 12\rangle [21] = \langle 34\rangle [43]\,. \tag{2.71}$$

To see the degeneracy of this phase space, we have to consider a singular limit, say

$$\langle 12\rangle \to \epsilon \ll 1\,, \quad [12] \sim \mathcal{O}(1)\,. \tag{2.72}$$

We can consider two cases $\langle 34\rangle \sim \epsilon$ and $[34] \sim \mathcal{O}(1)$, or vice versa. Let us consider the former case first. Following a similar argument as for the three-particle phase space, we pick a momentum contraction such as

$$0 = \langle 1| - P_1 - P_3 |3] = \langle 1| P_2 + P_4 |3] = \langle 12\rangle [23] + \langle 14\rangle [43]\,, \tag{2.73}$$

which implies $\langle 14\rangle \sim \epsilon$. This also assumes that no invariant is large, i.e. $\mathcal{O}(\epsilon^{-1})$. Proceeding further by considering other momentum contractions it can be shown that actually all angle brackets are $\mathcal{O}(\epsilon)$ in this case.

The latter case, with $\langle 34\rangle \sim \mathcal{O}(1)$ and $[34] \sim \epsilon$, is less degenerate, since it allows for all remaining invariants to be of order one. This is actually closer to the case of real momenta, where a collinear limit would imply

$$s = s_{12} = s_{34} \sim \epsilon\,, \tag{2.74}$$

and, in general,

$$t = s_{14} = s_{23} \sim u = s_{13} = s_{24} \sim \mathcal{O}(1)\,. \tag{2.75}$$

Physically, this is can also be seen from the equivalence of the MHV and $\overline{\text{MHV}}$ sectors. For example, in the case of four gluons we have

$$A_{4g}^{++--} = \frac{-i\langle 34\rangle^3}{\langle 12\rangle\langle 23\rangle\langle 41\rangle} = \frac{-i[12]^3}{[23][34][41]}\,. \tag{2.76}$$

These degeneracies make it harder to extract information from the singular limits, since the behaviour in the limit cannot be ascribed to a specific invariant, but these are such low multiplicity phase spaces that it is not truly an issue.

On-Shell Methods

The past twenty to thirty years have seen tremendous progress in the calculation of scattering amplitudes, especially at the one-loop order, so much so that we speak of a NLO revolution. This was achieved through what are known as generalised unitarity techniques for one-loop amplitudes [33–35, 41, 80–90], which have more recently started to see applications at the multi-loop level as well [16–19, 21–29]. A method to compute tree amplitudes which follows a similar philosophy (on-mass-shell and gauge-invariant building blocks) is the BCFW recursion [91, 92]. These methods rely on the existence of certain factorisation channels, probably best understood graphically in terms of Feynman diagrams, but in practice they can be formulated completely independently of the Feynman rules.

In this chapter, we review how these on-shell techniques work. More specifically, in Section 3.1 we show how, from very generic considerations about mass dimension and little group scalings, three-point tree-level amplitudes can be obtained. Afterwards, in Section 3.2, we will build on these to obtain tree-level amplitudes of any multiplicity by using BCFW recursion. Finally, in Section 3.3, we review the concepts at the foundations of generalised unitarity techniques. We give a detailed derivation of box- and triangle-integral coefficients through quadruple and triple cuts, following Ref. [82]. We conclude with a brief discussion of double cuts for bubble-integral coefficients, and of methods for the extraction of the rational terms.

Mass Dimension

Let us start by performing some straightforward dimensional analysis on amplitudes and integral coefficients, since much can be gained from it. For convenience, we reproduce here Eq. 1.40 for the partonic cross-section in a $2 \to n - 2$ process

$$d\hat{\sigma}_n = \frac{1}{2\hat{s}} d\Pi_{n-2} (2\pi)^4 \delta^4\big(\Sigma_{i=1}^n p_i\big) |\mathcal{A}_n(p_i, \mu_F, \mu_R)|^2 , \tag{3.1}$$

where the Lorentz invariant phase space is defined as

$$d\Pi_{n-2} = \prod_{i=1}^{n-2} \frac{d^3 p}{(2\pi)^3} \frac{1}{2E} . \tag{3.2}$$

From this, the mass dimension of an n-point amplitude is easily obtained

$$\big[d\hat{\sigma}_n\big]^{-2} = -\big[\hat{s}\big]^2 + (n-2)\Big[\frac{d^3 p}{E}\Big]^2 + \big[\delta^4\big]^{-4} + 2\big[\mathcal{A}\big] \implies \big[\mathcal{A}\big] = 4 - n . \tag{3.3}$$

Similarly, from Eq. 2.17 we can obtain the mass dimensions of the one-loop master-integral coefficient. Let us denote the loop momentum by l and the denominators form the loop propagators by D_i, where it is understood that $D_i = D_i(l) = l_i(l)^2 - m_i^2$, with l_i the momentum flowing through the relevant propagator and m_i its mass. We have

$$\big[I_{\text{Box}}\big] = \int \frac{\big[d^4 l\big]^4}{\big[D_1 D_2 D_3 D_4\big]^8} = -4 \implies \big[\text{Box coeff.}\big] = 8 - n , \tag{3.4}$$

$$\big[I_{\text{Tri}}\big] = \int \frac{\big[d^4 l\big]^4}{\big[D_1 D_2 D_3\big]^6} = -2 \implies \big[\text{Triangle coeff.}\big] = 6 - n , \tag{3.5}$$

$$\big[I_{\text{Bub}}\big] = \int \frac{\big[d^4 l\big]^4}{\big[D_1 D_2\big]^4} = 0 \implies \big[\text{Bubble coeff.}\big] = 4 - n . \tag{3.6}$$

Alternatively, these can be obtained by considering the relevant tree-level diagrams given by generalised unitarity cuts (this will become clear in Section 3.3).

In the next section, we will combine this information with some considerations about helicity to uniquely fix the kinematic dependence of three-point amplitudes in QCD.

3.1 The Little Group & Three-point Amplitudes

The transformations belonging to the little group are those that act on the $(1/2, 0)$ and $(0, 1/2)$ Lorentz spinor representations, while leaving the $(1/2, 1/2)$ vector representation unchanged. The fundamental relation to be kept in mind is that of Eq. 2.42

$$P^{\dot{\alpha}\alpha} = \bar{\lambda}^{\dot{\alpha}} \lambda^{\alpha} . \tag{3.7}$$

Clearly, it is sufficient to multiply and divide by some quantity respectively the left-handed and the right-handed spinor representations to keep the four-momentum unchanged

$$
\begin{aligned}
\lambda_i^\alpha &\to t_i\, \lambda_i^\alpha\,, \\
\bar\lambda_i^{\dot\alpha} &\to \bar\lambda_i^{\dot\alpha}/t_i\,, \\
P_i^{\dot\alpha\alpha} &\to P_i^{\dot\alpha\alpha}\,,
\end{aligned}
\tag{3.8}
$$

where the label i refers to the particle number in the phase space. This clarifies that there is one such transformation for each particle and that all these transformations are independent of one another. For real momenta, the parameters t_i must be phases $e^{i\tau_i}$ in order to preserve the relation between the spinors

$$
\bar\lambda^{\dot\alpha} = (\lambda^\alpha)^\dagger \quad \Leftrightarrow \quad P^\mu \in \mathbb{R}\,.
\tag{3.9}
$$

Such restriction does not apply to complex momenta. Nevertheless, we will still refer to the behaviour of a quantity with respect to little group transformations as *phase weights* or, in some cases, *little group scalings*, even if the phase space is complex.

Little group scalings are intimately related to the helicities of the particles of the considered process. This is easily understood by considering the Feynman rules for external lines in their spinor helicity formulation, as discussed in the Section 2.2.3. In that context, we saw that spin-1/2 particles with negative (positive) helicities carry factors of λ_α ($\bar\lambda_{\dot\alpha}$), and spin-1 particles with negative (positive) helicity carry factors $\lambda_\alpha/\bar\lambda_{\dot\alpha}$ ($\bar\lambda_{\dot\alpha}/\lambda_\alpha$). In general, under a little group transformation the following holds true

$$
\mathcal{A}(\{h_i, \dots\}) \to t_i^{-2h_i}\mathcal{A}(\{h_i, \dots\})\,,
\tag{3.10}
$$

where by h_i we denote the helicity of the ith particle. The phase weights are then simply the vector $\{-2h_i\}$[1].

We are now ready to obtain three-point amplitudes. In Section 2.2.3 we saw that they can only be functions of either angle or square brackets

$$
A_3(1,2,3) \propto \langle 12\rangle^\alpha \langle 23\rangle^\beta \langle 31\rangle^\gamma \quad \text{or} \quad A_3(1,2,3) \propto [12]^\alpha[23]^\beta[31]^\gamma\,,
\tag{3.11}
$$

and their phase weights are, respectively,

$$
\{\alpha+\gamma, \alpha+\beta, \beta+\gamma\} \quad \text{and} \quad \{-\alpha-\gamma, -\alpha-\beta, -\beta-\gamma\}\,.
\tag{3.12}
$$

Let us now consider two representative cases, $A_{3g}(1^+, 2^+, 3^+)$ and $A_{3g}(1^+, 2^+, 3^-)$. The rest of the all-gluon ones will follow from application of symmetries (permutation and parity); and the ones with a quark line can be obtained similarly to the ones we consider.

---

[1] Note that in this convention a positive helicity state has negative phase weight, and vice versa.

Example: $A_{3g}(1^+, 2^+, 3^+)$

The phase weights are $\{-2, -2, -2\}$. Thus, we have either

$$\begin{cases} -2 = \alpha + \gamma \\ -2 = \alpha + \beta \\ -2 = \beta + \gamma \end{cases} \implies \begin{cases} \alpha = -1 \\ \beta = -1 \\ \gamma = -1 \end{cases} \implies A_{3g}(1^+, 2^+, 3^+) \propto \frac{1}{\langle 12\rangle\langle 23\rangle\langle 31\rangle}, \qquad (3.13)$$

or

$$\begin{cases} -2 = -\alpha - \gamma \\ -2 = -\alpha - \beta \\ -2 = -\beta - \gamma \end{cases} \implies \begin{cases} \alpha = 1 \\ \beta = 1 \\ \gamma = 1 \end{cases} \implies A_{3g}(1^+, 2^+, 3^+) \propto [12][23][31]. \qquad (3.14)$$

Neither has the correct mass dimension (1), therefore this amplitude vanishes.

Example: $A_{3g}(1^+, 2^+, 3^-)$

The phase weights are $\{-2, -2, +2\}$. Thus, we have either

$$\begin{cases} -2 = \alpha + \gamma \\ -2 = \alpha + \beta \\ +2 = \beta + \gamma \end{cases} \implies \begin{cases} \alpha = -3 \\ \beta = 1 \\ \gamma = 1 \end{cases} \implies A_{3g}(1^+, 2^+, 3^+) \propto \langle 23\rangle\langle 31\rangle/\langle 12\rangle^3, \qquad (3.15)$$

or

$$\begin{cases} -2 = -\alpha - \gamma \\ -2 = -\alpha - \beta \\ +2 = -\beta - \gamma \end{cases} \implies \begin{cases} \alpha = 3 \\ \beta = -1 \\ \gamma = -1 \end{cases} \implies A_{3g}(1^+, 2^+, 3^+) \propto [12]^3/([23][31]). \qquad (3.16)$$

The first solution is not compatible with the mass dimension, but the latter is. This is indeed the result one would obtain by applying the Feynman rules, but we obtained it here in a much easier way. The only missing piece of information is the proportionality constant, which cannot be obtained this way, but is easy enough to reintroduce afterwards.

3.2   BCFW Recursion & Tree-Level Amplitudes

Recursion relations play a very important role in modern high energy physics. They provide a reliable and efficient method to compute tree-level amplitudes for virtually any multiplicity. There exist two types of recursion relations, off-mass-shell and on-mass-shell ones. An example of the former type of recursion is the Berends-Giele recursion [93],

which builds higher point amplitudes from lower point ones with an off-shell leg, effectively caching components of Feynman diagram computations. This type of recursions is very efficient when a full spin-averaged squared matrix element is required. An example of the latter type is the Britto–Cachazo–Feng–Witten (BCFW) recursion [91], which uses on-mass-shell, momentum conserving and gauge invariant building blocks. The trade-off is the necessity to introduce complex-valued four-momenta. On-shell recursions were first obtained from computations of components of one-loop amplitudes by unitarity techniques, for example by fusing box coefficients [94]. This type of recursion is best used when a specific helicity configuration is required, because it provides a targeted approach. Since our aim is not just to compute tree amplitudes for leading-order predictions, but rather to use them as ingredients for loop-level computations, where specific helicity states are required, here we focus on the BCFW recursion and review its proof based on Cauchy's residue theorem [92].

Let us consider an n-point colour-ordered amplitude $A(1^{\lambda_1}, 2^{\lambda_2}, \ldots, n^{\lambda_n})$. We want to modify two of the external legs, for simplicity say legs 1 and 2, such that they remain on-mass-shell, while, at the same time, sending an internal propagator on its mass-shell . For this purpose, we can introduce a complex number z and a four-momentum q such that

$$P_1 \quad \rightarrow \quad \hat{P}_1 = P_1 - zq \,, \tag{3.17}$$

$$P_2 \quad \rightarrow \quad \hat{P}_2 = P_2 + zq \,. \tag{3.18}$$

Maintaining the on-shellness requires

$$\hat{P}_1^2 = \left(P_1 + zq\right)^2 = P_1^2 - 2zP_1 \cdot q + q^2 = 0 \tag{3.19}$$

$$\hat{P}_2^2 = \left(P_2 - zq\right)^2 = P_2^2 + 2zP_2 \cdot q + q^2 = 0 \,, \tag{3.20}$$

which are satisfied by requiring

$$P_1 \cdot q = P_2 \cdot q = q^2 = 0 \,. \tag{3.21}$$

This can be easily achieved by choosing $q = |2\rangle[1|$ or $q = |1\rangle[2|$. Let us consider the former case, the shifted momenta become

$$\hat{P}_1 = |1]\big(\langle 1| - z\langle 2|\big) \quad \text{and} \quad \hat{P}_2 = \big(|2] + z|1]\big)\langle 2| \,. \tag{3.22}$$

In general, the amplitude will now be a function of the shift parameter z, and we are interested in obtaining it at the physical value $z = 0$. This is done by considering an

integral on a contour at infinity and applying Cauchy's residue theorem

$$0 = \oint \frac{dz}{2\pi i} \frac{\hat{A}(z)}{z} = \hat{A}(0) + \sum_i \frac{\text{Res}\big[\hat{A}(z)\big]_{z=z_i}}{z_i} \ , \tag{3.23}$$

$$\implies \hat{A}(0) = -\sum_i \frac{\text{Res}\big[\hat{A}(z)\big]_{z=z_i}}{z_i} \ . \tag{3.24}$$

In equation Eq. 3.23, we have assumed that the amplitude $\hat{A}(z)$ vanishes sufficiently fast at $z = \infty$ for the contour to evaluate to zero. If this is not the case, then Eq. 3.24 picks up an additional contribution.

The residues of $\hat{A}(z)$ originate from its simple poles, which can be located where a propagator goes on-shell. Assuming we are dealing with colour ordered amplitudes, such as in QCD, we can restrict momentum configurations to those with cyclically ordered external legs. For a propagator to depend on z we need the two shifted momenta to be on opposite sides of the propagator. Except for this restriction, all partitions of $\{1, \ldots, n\}$ into two sets are in principle allowed. To keep things general, let us have $\{2, \ldots, i\}$ on the right-hand side of the propagator and $\{i+1, \ldots, n, 1\}$ on the left hand side, as shown in the diagrammatic equation below. Let the propagator be $\hat{Q}_i^2$. Then, the locations of the poles z_i are obtained by putting the shifted propagator momentum $\hat{Q}_i$ on-shell

$$\hat{Q}_i = \hat{P}_1 + P_{i+1} + \cdots + P_n = \big(P_1 + P_{i+1} + \cdots + P_n\big) - zq = Q_i - zq \ , \tag{3.25}$$

$$0 \overset{!}{=} \hat{Q}_i^2 = Q_i^2 - 2z_i q \cdot Q_i \quad \Rightarrow \quad z_i = \frac{Q_i^2}{2q \cdot Q_i} \ , \ \hat{Q}_i^2 = -2q \cdot Q_i(z - z_i) \tag{3.26}$$

At the pole, i.e. when $z \to z_i$, the amplitude factorises into a sum of on-shell left and right lower-point sub-amplitudes, hence the recursion. The sum runs over the polarisations of the on-shell propagator and arises from the polarisation completeness relation. We have

$$\hat{A}(z)\big|_{z=z_i} = \sum_{\text{pol.}} \hat{A}_L(i+1, \ldots, n, \hat{1}, \hat{Q}_i) \frac{1}{\hat{Q}_i^2} \hat{A}_R(-\hat{Q}_i, \hat{2}, \ldots, i)\big|_{z=z_i} \ , \tag{3.27}$$

$$\hat{A}(0) = -\sum_i \frac{\text{Res}\big[\hat{A}(z)\big]_{z=z_i}}{z_i} = \sum_{i,\,\text{pol.}} \frac{1}{z_i} \hat{A}_L \frac{1}{2q \cdot Q_i} \hat{A}_R = \sum_{i,\,\text{pol.}} \hat{A}_L \frac{1}{Q_i^2} \hat{A}_R \ . \tag{3.28}$$

We can visualise Eq. 3.28 graphically as follows.

Amplitudes obtained via BCFW recursion are generally more compact and better represent their pole structure compared to those obtained via off-shell methods. However, they

contain spurious poles.

The proof presented here relies on the propagators to be quadratic. In theories with higher-derivative kinetic terms, the propagators may be quartic, which would make the poles of second order. It is then more complicated to extract the residues, and the factorisation is not as straightforward either. We'll discuss more about this in Chapter 9.

**Example: $A_{6g}(1^+, 2^-, 3^+, 4^-, 5^+, 6^-)$**

In the following, we give an example of BCFW recursion for one of the first NMHV amplitudes in QCD, $A_{6g}(1^+, 2^-, 3^+, 4^-, 5^+, 6^-)$. We make use of a $|2\rangle[1|$ shift, and, hence, of the hatted momenta of Eq. 3.22. There are three possible factorisation channels

$$1) \quad \{6^-, \hat{1}^+, Q_i^{\pm}\} \, \{-\hat{Q}_i^{\mp}, \hat{2}^-, 3^+, 4^-, 5^+\} \,, \tag{3.29}$$

$$2) \quad \{5^+, 6^-, \hat{1}^+, Q_i^{\pm}\} \, \{-\hat{Q}_i^{\mp}, \hat{2}^-, 3^+, 4^-\} \,, \tag{3.30}$$

$$3) \quad \{4^-, 5^+, 6^-, \hat{1}^+, Q_i^{\pm}\} \, \{-\hat{Q}_i^{\mp}, \hat{2}^-, 3^+\} \,. \tag{3.31}$$

Let us consider the first one. The corresponding diagram is
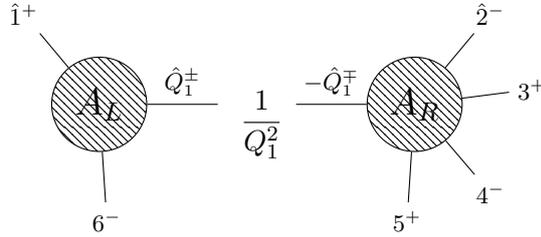
The un-shifted and shifted propagator are $Q_1 = -1 - 6$, $Q_1^2 = s_{16}$, $\hat{Q}_1 = -\hat{1} - 6$, hence

$$z_1 = Q_1^2 / 2q \cdot Q_1 = s_{16} / \langle 2|6|1] = \langle 16 \rangle [61] / \langle 26 \rangle [61] = \langle 16 \rangle / \langle 26 \rangle \,. \tag{3.32}$$

This implies that $\langle 6\hat{1} \rangle = \langle \hat{Q}_1 6 \rangle = \langle \hat{Q}_1 \hat{1} \rangle = 0$, and therefore that

$$A(\hat{1}, \hat{Q}_1^-, 6^-) = \frac{\langle \hat{Q}_1 6 \rangle^4}{\langle \hat{1}\hat{Q}_1 \rangle \langle \hat{Q}_1 6 \rangle \langle 6\hat{1} \rangle} = \frac{0^4}{0^3} = 0 \,, \tag{3.33}$$

where this is understood as being in the limit for $z \to z_1$. The other helicity choice is

$$A(\hat{1}, \hat{Q}^+, 6^-) \frac{1}{s_{16}} A(-\hat{Q}^-, \hat{2}^-, 3^+, 4^-, 5^+) = \tag{3.34}$$

$$= \frac{[\hat{1}\hat{Q}]^4}{[\hat{1}\hat{Q}][\hat{Q}6][6\hat{1}]} \frac{1}{s_{16}} \frac{[35]^4}{[-\hat{Q}\hat{2}][\hat{2}3][34][45][5-\hat{Q}]} = \tag{3.35}$$

$$= \frac{[\hat{1}\hat{Q}]^3}{[61]^2[\hat{Q}6]} \frac{\langle 26 \rangle [35]^4}{\langle 16 \rangle [34][45]\langle 6|1+2|3]} \frac{1}{[-\hat{Q}\hat{2}][5-\hat{Q}]} \times \frac{\langle \hat{Q}2 \rangle^3}{\langle \hat{Q}2 \rangle^3} \,. \tag{3.36}$$

Simplifying this expression[2], reintroducing factors of i and making use of two of the symmetries we obtain the full amplitude

$$
A_{6g}(1^+, 2^-, 3^+, 4^-, 5^+, 6^-) = \frac{-i \langle 26 \rangle^4 [35]^4}{\langle 12 \rangle \langle 16 \rangle [34][45] \langle 2|1+6|5] \langle 6|1+2|3] s_{345}} + \\
\left(123456 \to \overline{234561} \right) + \left(123456 \to 345612 \right) , \quad (3.37)
$$

where the two parenthesis indicate permutations, and the overline represents parity.

3.3   Generalised Unitarity & One-Loop Amplitudes

In a $i \to f$ process, the relation between the scattering matrix S, the forward scattering matrix T, defined as $S = \mathbb{1} + iT$, and the full amplitude $\mathcal{A}$ is given by

$$
\langle f|S-1|i \rangle = i \langle f|T|i \rangle = i(2\pi)^4 \delta^4(P_i - P_f) \mathcal{A}(i \to f) . \quad (3.38)
$$

Unitarity of the scattering matrix S is simply a statement of conservation of probability

$$
\sum_f \left| \langle f|S|i \rangle \right|^2 = \langle i|S^\dagger S|i \rangle = 1 \implies SS^\dagger = \mathbb{1} = S^\dagger S , \quad (3.39)
$$

that is, the probability for anything to happen is 1. This relation, in terms of the forward scattering matrix T, reads

$$
\mathbb{1} = S^\dagger S = (\mathbb{1} - iT^\dagger)(\mathbb{1} + iT^\dagger) = \mathbb{1} - iT^\dagger + iT + T^\dagger T , \quad (3.40)
$$

$$
\implies T^\dagger T = i(T^\dagger - T) = 2\text{Im}(T) \equiv \text{Disc}(T) . \quad (3.41)
$$

The "Disc" operation, defined as twice the imaginary part, refers to the discontinuity across a branch cut in the complex plane. As we will see shortly, propagators in scattering amplitudes are intimately related to this branch cut structure in the on-shell limit.

Going back to our pure gluon example and reintroducing the $0 \to n$ notation, we can expand T in the number of particles n and in powers of the strong coupling g_s

$$
T = T_4 + T_5 + \dots , \quad (3.42)
$$

$$
T_4 = g_s^2 T_4^{(0)} + g_s^4 T_4^{(1)} + g_s^6 T_4^{(2)} + \dots , \quad (3.43)
$$

$$
T_5 = g_s^3 T_5^{(0)} + g_s^5 T_5^{(1)} + g_s^5 T_5^{(2)} + \dots . \quad (3.44)
$$

---

[2]The following identities are being used $[\hat{2}3] = \langle 6|1+2|3]/\langle 62 \rangle, [5|-\hat{Q}|2 \rangle = [5|1+6|2 \rangle, [1|\hat{Q}|2 \rangle = [16]\langle 62 \rangle,$ $[6|\hat{Q}|2 \rangle = [61]\langle 12 \rangle$, and $[\hat{2}|-\hat{Q}|2 \rangle = s_{345}$.

By inserting these in Eq. 3.41 we obtain

$$\text{Disc}(T_4^{(0)}) = 0 , \tag{3.45}$$

$$\text{Disc}(T_4^{(1)}) = T_4^{(0)\dagger}T_4^{(0)} , \tag{3.46}$$

$$\text{Disc}(T_4^{(2)}) = T_4^{(1)\dagger}T_4^{(0)} + T_4^{(0)\dagger}T_4^{(1)} + T_5^{(0)\dagger}T_5^{(0)} , \tag{3.47}$$

and so forth. For example, we can picture Eq. 3.46 graphically as follows
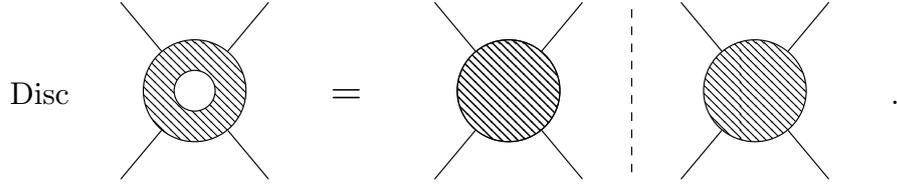
What we have discussed so far is unitarity, where two propagators are set to be on-mass-shell. In some cases, full amplitudes can be reconstructed by means of dispersion relations, but this is a highly non-trivial procedure. More information about the amplitude can be obtained by setting on-shell, or *cutting*, a different number of propagators. This is the fundamental idea behind generalised unitarity.

In the following, we will quantitatively define the procedure of cutting loop momenta, and, subsequently, we will apply generalised unitarity to extract one-loop integral coefficients.

3.3.1 Cut Rules

Let us consider a massless propagator in the "$i\epsilon$" prescription. It can be shown that its discontinuity is proportional to a δ-function [95]. Starting from the definition of discontinuity given in Eq. 3.41, we have

$$\text{Disc}\left(\frac{1}{P^2 + i\epsilon}\right) = 2\,\text{Im}\left(\frac{1}{P^2 + i\epsilon}\right) = 2\,\text{Im}\left(\frac{P^2 - i\epsilon}{P^4 + \epsilon^2}\right) = -\frac{2\epsilon}{P^4 + \epsilon^2} . \tag{3.48}$$

Taking first the on-shell limit $P^2 \to 0$, and then the zero contour deformation limit $\epsilon \to 0$, we see that it is indeed an infinitely peaked distribution at the origin

$$\frac{\epsilon}{P^4 + \epsilon^2} = \begin{cases} \frac{1}{\epsilon} \sim \infty & \text{if } P^2 = 0 , \\ \epsilon \sim 0 & \text{if } P^2 \neq 0 , \end{cases} \tag{3.49}$$

and the area is finite

$$\int \frac{\epsilon}{P^4 + \epsilon^2} dP^2 = \arctan\left(\frac{P^2}{\epsilon}\right) \sim \pi . \tag{3.50}$$

Therefore, we have that the *cut* procedure is defined by taking the discontinuity across a propagator branch cut, which is, up to factors of 2 and π, a δ-function enforcing the on-shell condition

$$\left(\frac{1}{P^2 + i\epsilon} \right) \rightarrow \text{Disc}\left(\frac{1}{P^2 + i\epsilon} \right) \sim \delta(P^2) \, . \tag{3.51}$$

If a particular diagram or expression does not contain the propagator being cut, then it does not have the correct branch cut and the discontinuity is zero.

Cutting the loop momenta can be regarded as a procedure to project a loop amplitude onto a known set of master integrals, and thus extract the coefficients of said integrals. As already anticipated in the context of colour-ordered amplitudes in the previous chapter, the scalar master integral decomposition at one loop reads

$$A_{n;1}^{1-loop} = \sum_i d_i I_{Box}^i + \sum_i c_i I_{Triangle}^i + \sum_i b_i I_{Bubble}^i + \sum_i a_i I_{Tadpoles}^i + R \, , \tag{3.52}$$

or graphically

This assumes the loop momentum is kept in $D = 4$, since the above equation is correct up to terms of $\mathcal{O}(D - 4)$. Throughout this thesis, we will not consider tadpoles, since they vanish in dim-reg if massless particles run through the loop (the integral becomes scale-less).

Depending on the number of cuts performed, a single integral coefficient or a combination of integral coefficients may be singled out. Quadruple cuts are *clean*, in the sense that they pick out only the relevant d_i coefficient. However, for instance, triple cuts pick out both a triangle coefficient c_i, as well as any box coefficient of an integral sharing the relevant propagators. Therefore, the strategy is to perform as many cuts as possible to extract the box coefficients. Afterwards, we may do one fewer cut, subtract the known box information, and obtain the triangle coefficients. Similarly, we may proceed to obtain bubbles and, if present, tadpole coefficients.

3.3.2   Maximal Cuts

In four dimensions the loop momentum has 4 components, therefore we can at most impose 4 on-shell conditions. This is called a maximal cut. On the cut, the left-hand side of

Eq. 3.52 factorises into the product of four on-shell tree amplitudes, as shown graphically here.
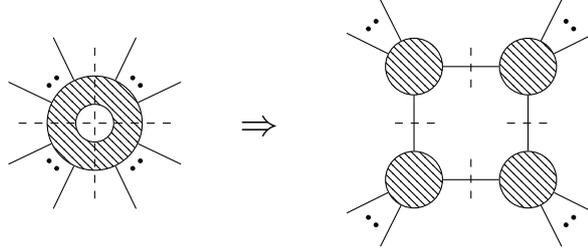
This is analogous to the factorisation in the context of BCFW recursion. On the right-hand side of Eq. 3.52 the quadruple cut picks out the relevant coefficient d_i. Note that, in principle, there is a Jacobian associated with the change of variable from the loop-integral measure $d\,l^4$ to the arguments of the four δ-functions, call them l_1^2, l_2^2, l_3^2, and l_4^2. However, the same Jacobian appears on both sides of the equal sign, and thus can be ignored.

Therefore, the box coefficient is given by

$$d_i = \frac{1}{2}\left(d_i^+ + d_i^-\right) , \quad \text{with} \quad d_i^\pm = A_1^{tree} A_2^{tree} A_3^{tree} A_4^{tree} \tag{3.53}$$

where, due to the quadratic nature of the on-shell cut conditions, we have to average over the two possible on-shell solutions for the cut-loop momenta. Finally, a summation over all possible intermediate physical states for the loop momentum is also implied. In the case of gluons, this is simply the helicity assignments for the cut-loop momenta.

Example: box coefficient

As an example, we are going to compute the box coefficient for $A_{6g}^{(1)}(1^+, 2^-, 3^+, 4^-, 5^+, 6^-)$ given by the diagram below. Note that different helicity assignments for the cut propagators are also possible, but for the purpose of this example we will consider only the one shown in the following diagram.
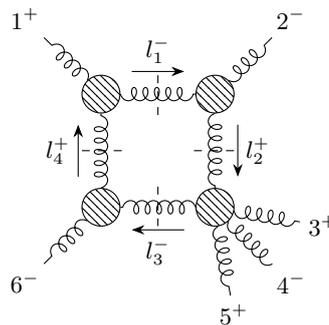
Algebraically, this corresponds to the following product of tree amplitudes[3]

$$A(-l_4^-, 1^+, l_1^-)\, A(-l_1^+, 2^-, l_2^+)\, A(-l_2^-, 3^+, 4^-, 5^+, l_3^-)\, A(-l_3^+, 6^-, l_4^+) = \tag{3.54}$$

$$\frac{i\,\langle l_1| - l_4\rangle^3}{\langle -l_4|1\rangle\langle 1|l_1\rangle} \times \frac{i\,[l_2| - l_1]^3}{[-l_1|2][2|l_2]} \times \frac{i\,[3|5]^4}{[-l_2|3][3|4][4|5][5|l_3][l_3| - l_2]} \times \frac{i\,[l_4| - l_3]^3}{[-l_3|6][6|l_4]}\,. \tag{3.55}$$

Because there are three massless corners, the loop momentum parametrisation is very straightforward. We will review the general mass case together with the triangle coefficients. The two possible on-shell solutions are $l_1 \propto |1\rangle[2|$ or $l_1 \propto |2\rangle[1|$. However, it is easy to see that the former choice leads to vanishing $A(-l_4^-, 1^+, l_1^-)$. Therefore, we only have to consider the latter parametrisation choice

$$l_1 = \xi|2\rangle[1| = \left(-\frac{\langle 16\rangle}{\langle 26\rangle}|2\rangle\right)[1|\,, \tag{3.56}$$

$$l_2 = l_1 - P_2 = |2\rangle\Big(\xi[1| - [2|\Big) = |2\rangle\left(-\frac{\langle 16\rangle}{\langle 26\rangle}[1| - [2|\right)\,, \tag{3.57}$$

$$l_4 = l_1 + P_1 = \Big(\xi|2\rangle + |1\rangle\Big)[1| = \left(-\frac{\langle 16\rangle}{\langle 26\rangle}|2\rangle + |1\rangle\right)[1|\,, \tag{3.58}$$

$$l_3 = l_1 + P_1 + P_6 = \Big(\xi|2\rangle + |1\rangle\Big)[1| + |6\rangle[6| = \left(-\frac{\langle 16\rangle}{\langle 26\rangle}|2\rangle + |1\rangle\right)\left([1| + \frac{\langle 26\rangle}{\langle 21\rangle}[6|\right).\tag{3.59}$$

In the above, the value of the proportionality constant ξ is fixed by requiring $l_3^2 = 0$, whereas the other three cut conditions are trivially satisfied. It is then straightforward to plug Eq.s 3.56 - 3.59 into the product of trees of Eq. 3.55. For example, up to numerical prefactors, some of the required manipulations are[4]

$$[5|l_3] \sim [5|\left(|1\rangle + \frac{\langle 26\rangle}{\langle 21\rangle}|6\rangle\right) = \frac{1}{\langle 21\rangle}\Big(\langle 21\rangle[51] + \langle 26\rangle[56]\Big) = \frac{\langle 2|1 + 6|5]}{\langle 12\rangle}\,, \tag{3.60}$$

$$[l_3| - l_2] \sim \left([1| + \frac{\langle 26\rangle}{\langle 21\rangle}[6|\right)\left(-\frac{\langle 16\rangle}{\langle 26\rangle}|1] - |2]\right) = [21] + \frac{\langle 16\rangle}{\langle 12\rangle}[61] + \frac{\langle 26\rangle}{\langle 12\rangle}[62] = \frac{s_{345}}{\langle 12\rangle}\,.$$

The final answer is given by

$$\frac{1/2\,i\,[12][16]\langle 26\rangle^4[35]^4}{[34][45]\langle 2|1 + 6|5]\langle 6|1 + 2|3]s_{345}}\,. \tag{3.61}$$

As expected, it is proportional to $s_{12}s_{16}$ times the part of the tree amplitude obtain by the BCFW shift of Eq. 3.29 (note that s_{12} and s_{16} can be thought of as the s and t channels of this diagram). The proportionality of box coefficients to tree amplitudes, or parts of

---

[3]Momenta and helicity signs are flipped in adjacent trees to respect the all-outgoing convention.

[4]Technically, the analytical continuation convention is $|-k\rangle = \pm i|k\rangle$ and $|-k] = \pm i|k]$, where the sign depends on the position of the branch cut for the complex square root, which is itself a matter of convention. We place the brunch cut in the negative real axis, which means $-\pi < \arg(z) \leq \pi$ for $z \in \mathbb{C}$. The sign is then negative if $\arg(k^{(0)} + k^{(3)}) > 0$, and vice versa.

them, is a general result, which, as mentioned, first lead to conjecturing on-shell recursions. However, further investigations on the topic are beyond the scope of the present analysis.

3.3.3   Triangle Coefficients

In this section, we are going to review the method of Ref. [82] for the extraction of triangle coefficients. Graphically, a triple cut acting on Eq. 3.52 will be as follows.
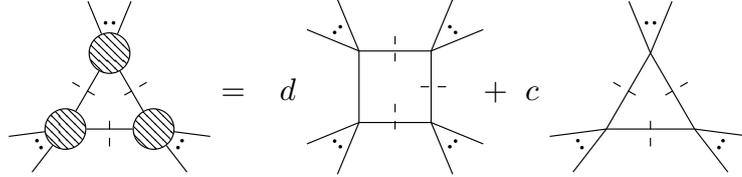
On the left-hand side, the one-loop amplitude factorises into a product of three tree amplitudes, integrated over one remaining degree of freedom, call it t. On the right-hand side, we pick out not only the relevant triangle coefficient, but also any box coefficient of scalar integrals sharing the three cut propagators. Mathematically, we may write the triple cut as

$$\int \mathrm{d}t\, J_t\, A_1 A_2 A_3 = \sum_i d_i \int \mathrm{d}t\, J_t\, \frac{1}{D_4^{(i)}} + c \int \mathrm{d}t\, J_t \ , \qquad (3.62)$$

where the integration over three δ-functions $\delta(l^2)\delta(l_1^2)\delta(l_2^3)$ has already been performed, and $J_t \propto 1/t$ is the Jacobian[5] arising from the change of variables $\mathrm{d}^4 l \to \mathrm{d}t\, \mathrm{d}l^2\, \mathrm{d}l_1^2\, \mathrm{d}l_2^3$.

Let us study the momentum parametrisation for a generic triple cut, where the external momenta have been clustered into three massive momenta K_1, K_2 and K_3, as described by the following diagram.
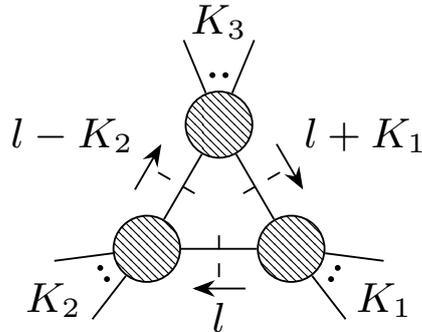
Since on the cut the loop momentum l is massless, we would like to express it in terms of

---

[5] A derivation of the Jacobian is given in Appendix B.

massless projections of K_1 and K_2, denoted by the flat symbol $\flat$, and defined as

$$\begin{cases} K_1^\mu = K_1^{\flat,\mu} + \alpha K_2^{\flat,\mu} \, , \\ K_2^\mu = K_2^{\flat,\mu} + \beta K_1^{\flat,\mu} \, . \end{cases} \tag{3.63}$$

To enforce $K_1^{\flat,2} = K_2^{\flat,2} = 0$, we can square the above relations and solve for α and β

$$K_1^2 = \alpha \, 2K_1^\flat \cdot K_2^\flat \, , \quad K_2^2 = \beta \, 2K_1^\flat \cdot K_2^\flat \, . \tag{3.64}$$

Let $\gamma = 2K_1^\flat \cdot K_2^\flat = \langle K_1^\flat | K_2^\flat | K_1^\flat] = \langle K_2^\flat | K_1^\flat | K_2^\flat]$ and $K_i^2 = S_i$, then we obtain the two coefficients $\alpha = S_1/\gamma$ and $\beta = S_2/\gamma$.

Inverting the relations of Eq. 3.63, we obtain

$$K_1^{\flat,\mu} = \frac{K_1^\mu - \frac{S_1}{\gamma} K_2^\mu}{1 - \frac{S_1 S_2}{\gamma^2}} \, , \quad \text{and} \quad K_2^{\flat,\mu} = \frac{K_2^\mu - \frac{S_2}{\gamma} K_1^\mu}{1 - \frac{S_1 S_2}{\gamma^2}} \, . \tag{3.65}$$

By squaring $K_1^{\flat,\mu}$, we can express γ as a function of the external momenta only

$$K_1^{\flat,2} = \left(\frac{1}{1 - \frac{S_1 S_2}{\gamma^2}} \right)^2 \left(K_1^\mu - \frac{S_1}{\gamma} K_2^\mu \right)^2 = 0 \, , \tag{3.66}$$

$$\implies K_1^2 + \frac{S_1^2}{\gamma^2} K_2^2 - \frac{S_1}{\gamma} 2K_1 \cdot K_2 = 0 \, . \tag{3.67}$$

Then, multiplying through by γ^2, we obtain the following quadratic

$$\Rightarrow \gamma^2 - 2K_1 \cdot K_2 \gamma + S_1 S_2 = 0 \, , \tag{3.68}$$

and, thus, two solutions for γ

$$\gamma_\pm = K_1 \cdot K_2 \pm \sqrt{\Delta} \, , \quad \Delta = (K_1 \cdot K_2)^2 - S_1 S_2 \, . \tag{3.69}$$

However, note that Eq. 3.67 for γ is not, strictly speaking, quadratic. Therefore, when either $S_1 = 0$ or $S_2 = 0$, the $\gamma = 0$ solution is not acceptable, and there is a single solution $\gamma = 2K_1 \cdot K_2$.

We can now express the loop momentum in terms of the flat momenta $K_1^\flat$ and $K_2^\flat$. The following is completely generic, since any massless momentum can be expressed as linear combination of spinors as follows

$$|l\rangle = a|K_1^\flat\rangle + b|K_2^\flat\rangle \, , \quad \text{and} \quad |l] = c|K_1^\flat] + d|K_2^\flat] \, . \tag{3.70}$$

The first cut condition l^2 is trivially satisfied for any value of the parameters a, b, c and d.

The other two cut conditions read

$$(l + K_1)^2 = l^2 + 2l \cdot K_1 + K_1^2 = 0 \tag{3.71}$$

$$\Rightarrow S_1 + \langle l|K_1|l] = 0 \tag{3.72}$$

$$\Rightarrow S_1 + acS_1 + bd\gamma = 0 \tag{3.73}$$

and

$$(l - K_2)^2 = l^2 - 2l \cdot K_1 + K_1^2 = 0 \tag{3.74}$$

$$\Rightarrow S_2 - \langle l|K_1|l] = 0 \tag{3.75}$$

$$\Rightarrow S_2 - ac\gamma - bdS_2 = 0 . \tag{3.76}$$

By solving the resulting system of equations

$$\begin{cases} S_1 + acS_1 + bd\gamma = 0 , \\ S_2 - ac\gamma - bdS_2 = 0 , \end{cases} \tag{3.77}$$

one obtains the following constraints for the products ac and bd

$$ac = \frac{S_2(\gamma + S_1)}{\gamma^2 - S_1 S_2} \equiv \alpha_{02} , \tag{3.78}$$

$$bd = -\frac{S_1(\gamma + S_2)}{\gamma^2 - S_1 S_2} \equiv \alpha_{01} . \tag{3.79}$$

The definitions for α_{01} and α_{02} are made in order to keep the notation as close as possible to the original of Ref. [82]. In addition to Eq. 3.78 and Eq. 3.79, there is the further freedom given by the little group. For instance, assuming $\alpha_{01} \neq 0$, we may pick $d = 1$, renamed $a = t$, and obtain

$$\begin{cases} |l\rangle = t|K_1^\flat\rangle + \alpha_{01}|K_2^\flat\rangle , \\ |l] = \frac{\alpha_{02}}{t}|K_1^\flat] + |K_2^\flat] . \end{cases} \tag{3.80}$$

However, if $\alpha_{01} = 0$, we also have to choose $b = 1$, $c = t$, and obtain

$$\begin{cases} |l\rangle = \frac{\alpha_{02}}{t}|K_1^\flat\rangle + |K_2^\flat\rangle , \\ |l] = t|K_1^\flat] + \alpha_{01}|K_2^\flat] . \end{cases} \tag{3.81}$$

The latter parametrisation is independent from the first one only if $\alpha_{01} = 0$ and/or $\alpha_{02} = 0$, otherwise the two are related by a little group transformation equal to α_{01} and a renaming of $t \to \frac{\alpha_{01}\alpha_{02}}{t}$. Therefore, summing up, there are always two distinct solutions for the loop momentum. If $S_1 \neq 0$ and $S_2 \neq 0$, then there are two choices for $\gamma_\pm$, but a single

momentum parametrisation for each of these choices. Conversely, if either $S_1 = 0$ or $S_2 = 0$ (or both), then there is a single γ but two momentum parametrisations.

The first choice of Eq. 3.80 is the one given in Ref. [82]. In four-vector notation it reads

$$l^\mu = \alpha_{01} K_1^{\flat,\mu} + \alpha_{02} K_2^{\flat,\mu} + \frac{t}{2}\langle K_1^\flat|\bar{\sigma}^\mu|K_2^\flat] + \frac{\alpha_{01}\alpha_{02}}{2t}\langle K_2^\flat|\bar{\sigma}^\mu|K_1^\flat] \tag{3.82}$$

$$\equiv a_0^\mu t + a_1^\mu \frac{1}{t} + a_2^\mu . \tag{3.83}$$

Let us now consider what happens in the case of a box integral. Graphically, by "zooming in" one of the vertices, we may resolve one more propagator, as shown below.
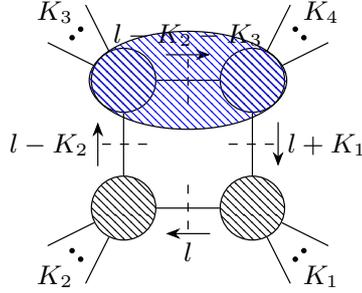
With a slight abuse of notation, we are now giving a new meaning to K_3, as seen by comparing the triangle and the box diagrams $K_3 \to K_3 + K_4$. The propagator that appears only in the box reads

$$D_4 = (l - K_2 - K_3)^2 = \overset{0}{\cancel{l^2}} + (K_2 + K_3)^2 - 2l \cdot (K_2 + K_3) . \tag{3.84}$$

By setting it to zero, we obtain the location of the poles in t-space corresponding to D_4 going on-shell[6]. We have

$$(t\langle K_1^\flat| + \alpha_{01}\langle K_2^\flat|)K_{23}(\frac{\alpha_{02}}{t}|K_1^\flat] + |K_2^\flat]) = K_{23}^2 , \tag{3.85}$$

$$\alpha_{02}\langle K_1^\flat|K_{23}|K_1^\flat] + t\langle K_1^\flat|K_{23}|K_2^\flat] + \frac{\alpha_{01}\alpha_{02}}{t}\langle K_2^\flat|K_{23}|K_1^\flat] + \alpha_{01}\langle K_2^\flat|K_{23}|K_2^\flat] = K_{23}^2 ,$$

$$t^2\langle K_1^\flat|K_{23}|K_2^\flat] + t\big(\alpha_{02}\langle K_1^\flat|K_{23}|K_1^\flat] + \alpha_{01}\langle K_2^\flat|K_{23}|K_2^\flat] - K_{23}^2\big) + \alpha_{01}\alpha_{02}\langle K_2^\flat|K_{23}|K_1^\flat] = 0 .$$

By solving the quadratic and doing a partial-fraction decomposition, we obtain an expression for the propagator

$$\frac{1}{D_4} = \frac{1}{(l - K_2 - K_3)^2} = \frac{t}{\langle K_1^\flat|K_{23}|K_2^\flat]\big(t_+ - t_-\big)}\left(\frac{1}{t - t_+} - \frac{1}{t - t_-}\right) , \tag{3.86}$$

where, again, we have assumed $S_1 \neq 0$ and $S_2 \neq 0$. If this is not the case, then Eq. 3.85 is

---

[6]This can also be used to compute box coefficients with arbitrary external legs.

not really quadratic, and there is a single pole

$$\frac{1}{D_4} = \frac{1}{(l - K_2 - K_3)^2} = \frac{1}{\langle K_1^\flat | K_{23} | K_2^\flat](t - t_0)} \ . \tag{3.87}$$

Crucially, the propagator of Eq. 3.86 vanishes at $t = 0$, whereas that of Eq. 3.87 does not. To understand why this is of any consequence, we need to look at the remaining piece of puzzle, namely the integral over t.

As explained in Ref. [82], and in references therein [96, 97], the integral in t behaves like a contour integral, with only simple pole contributing to the final result. It may be possible to understand this in terms of the 4d geometry of the change of variable, but it is easiest to consider the following Passarino-Veltman tensor reduction [73]

$$\int \mathrm{d}l \, \frac{l^{\mu_1} \dots l^{\mu_n}}{l^2 l_1^2 l_2^2} \sim f^{\mu_1 \dots \mu_2}(K_1, K_2, \eta) \int \mathrm{d}^4 l \, \frac{1}{l^2 l_1^2 l_2^2} \ , \tag{3.88}$$

where the tensor integral on the left-hand side has been expressed as a scalar integral times a function which depends on the only available tensor structures, namely the momenta K_1^μ and K_2^ν, and the metric tensor $\eta^{\mu\nu}$. Since this undetermined function $f^{\mu_1 \dots \mu_2}(K_1, K_2, \eta)$ vanishes when contracted with tensor structures like $|K_2^\flat]\langle K_1^\flat|$ or $|K_1^\flat]\langle K_2^\flat|$, we have

$$\int \mathrm{d}^4 l \, \frac{\langle K_1^\flat | l | K_2^\flat]^n}{l^2 l_1^2 l_2^2} = 0 \quad \Longrightarrow \quad \int \mathrm{d}t J_t \frac{1}{t^n} = 0 \quad \text{for} \quad n \geq 1 \ , \tag{3.89}$$

$$\int \mathrm{d}^4 l \, \frac{\langle K_2^\flat | l | K_1^\flat]^n}{l^2 l_1^2 l_2^2} = 0 \quad \Longrightarrow \quad \int \mathrm{d}t J_t t^n = 0 \quad \text{for} \quad n \geq 1 \ , \tag{3.90}$$

where it is important to recall that $J_t \propto 1/t$.

Finally, to sum up, let us consider again Eq. 3.62, and in particular the left-hand side integrand $A_1 A_2 A_3 / t$. The residues from poles away from zero correspond to box coefficients, whereas the residue at $t = 0$ corresponds to the genuine triangle coefficient, once the box contribution has been subtracted. This is necessary only if the box integral contributes as in Eq. 3.87, since propagators like that of Eq. 3.86 do not contribute at $t = 0$.

The lack of additional insights which we would obtain from a fully analytical computation do not warrant the increased complexity necessary to carry it out. Therefore, we do not present one in this context. However, we have implemented this generalised unitarity method in numerical Python code, and checked that the triangle coefficients reproduce those obtained by the BLACKHAT library [98] to a high precision.

3.3.4   Bubble Coefficients and Rational Parts

In order to perform a one-loop calculation from the ground up, we would need to obtain two more quantities: bubble coefficients and rational parts. An in-depth review of these would be fairly lengthy and is beyond the scope of the current work. In fact, for the analysis we are going to perform starting in Chapter 5, it is sufficient to consider already available numerical routines (e.g. BLACKHAT) as black boxes which provide a numerical value for a given quantity given a phase space point. For this same reason, the momentum parametrisation chosen for the cut loop momentum is not important, as long as the result is numerically stable and sufficiently precise. Furthermore, from the point of view of the analytical reconstruction, there is not fundamental difference between box, triangle and bubble coefficients and the rational part: they are all rational functions of kinematic invariants. The main difference will be which poles appear and with what degree, but since all poles are handled in a similar fashion no special treatment will be required for bubble coefficients and rational parts.

Let us briefly summarise possible computation methods. Bubble coefficients can be obtained in an analogous way to the triangle coefficients discussed in the previous section [82]. In this case, we would have only two on-shell conditions, resulting in one more residual degree of freedom from Eq. 3.70, call it y. Thus, the left over integration would be over both t and y, and we would need to identify contributions from both box and triangle integrals as poles in t and y, before being able to obtain the genuine bubble coefficients. Again, the momentum parametrisation is not unique, but it will always contain two residual degrees of freedom which need to be integrated over. As an alternative example, the parametrisation chosen in Ref. [90] results in a double integration over a complex variable z and it's c.c. $\bar{z}$.

The rational part is not cut constructible in four dimensions, meaning it cannot be obtained by generalised unitarity cuts in $d = 4$. Any spurious pole dependence can still be obtained in $d = 4$, by requiring it to match the un-cancelled spurious singularities from the cut constructible coefficients. However, this is not enough to fully constrain it. Several methods exist to obtain the rational part in its entirety [39, 86–88, 99]. These include performing the generalised unitarity cuts in higher number of dimensions, or - equivalently[7] - introducing a fictitious mass for the loop momenta. Other methods include Feynman-diagram and string-theory based methods [100–102].

---

[7]Any massless momentum in a higher number of dimensions would appear as a massive one in d = 4: $K^2 = K_{(4)}^2 - K_{(\epsilon)}^2 = 0 \Rightarrow K_{(4)}^2 = K_{(\epsilon)}^2 = m_{(\epsilon)}^2$.

The CHY Formalism

In this chapter we briefly review the theory underlining the Cachazo-He-Yuan (CHY) formalism [55–57]. In Appendix C we present an implementation in `Python` with floating point numbers to arbitrary precision. For a more thorough introduction to the subject, with explicit step-by-step derivations, please consider Ref. [103] and the references therein.

Let us consider the tree-level scattering of n massless particles in d dimensions. We denote with A the set $\{1, \ldots, n\}$, with k_a^μ ($a \in A$) the n momenta, and with z_a n special points of the Riemann sphere called punctures. The map from momentum space to the Riemann sphere, as defined in Ref. [55], is the given by

$$k_a^\mu = \frac{1}{2\pi i} \oint_{|z - z_a| = \epsilon} dz \frac{p^\mu(k, z)}{\prod_{b \in A}(z - z_b)} \, , \tag{4.1}$$

where $p^\mu(z)$ are d polynomials with coefficients depending on the momenta and the punctures. The contour is taken to encircle the punctures.

From Eq. 4.1 it can be shown, as a consistency condition, that the following equations have to be satisfied

$$f_a(z, k) \equiv \sum_{b \in A \setminus \{a\}} \frac{k_a \cdot k_b}{z_a - z_b} = 0, \qquad \forall a \in A \, . \tag{4.2}$$

These are the so-called *scattering equations*. As previously mentioned, the SE are invariant

under Möbius transformations $SL(2, \mathbb{C})$, that is under the following mapping

$$z \rightarrow \zeta = \frac{\alpha z + \beta}{\gamma z + \delta} \ . \tag{4.3}$$

Because Eq. 4.3 has effectively three free complex parameters, we can fix the position of three of the n punctures. A common choice in the literature, which we follow throughout this work, is given by

$$z_1 = \infty, \quad z_2 = 1, \quad z_n = 0 \ . \tag{4.4}$$

Scattering amplitudes for n massless particles A_n[1] are then obtained by integrating a CHY-integrand I_{CHY}[2] over the solutions of the SE. This can be achieved either with a normal integral over delta functions, or as a contour integral over the SE. As by prescription

$$A_n = i \int \frac{d^n z}{d^3 \omega} \ I_{CHY}(z; k; \epsilon) \prod_{a \in A}{}' \delta(f_a(z, k)) \tag{4.5}$$

$$= i \oint_O \frac{d^n z}{d^3 \omega} \ I_{CHY}(z; k; \epsilon) \prod_{a \in A}{}' \frac{1}{f_a(z, k)} \ , \tag{4.6}$$

where the Möbius measure $d\omega$ and the modified product symbol $\prod'$ are defined as

$$d^3 \omega = \frac{dz_r dz_s dz_t}{(z_r - z_s)(z_s - z_t)(z_t - z_s)} \ , \tag{4.7}$$

$$\prod_{a \in A}{}' = (z_i - z_j)(z_j - z_k)(z_k - z_i) \prod_{a \in A \backslash \{i, j, k\}} \ . \tag{4.8}$$

By substituting Eq. 4.7 and Eq. 4.8 back into Eq. 4.5 or Eq. 4.6 it can be shown that the amplitude A_n is invariant under Möbius transformations. Note that in principle the sets $\{i, j, k\}$ and $\{r, s, t\}$ are independent, but in practice they are often taken to be the same for convenience sake. Clearly the requirement of Möbius invariance also imposes a restriction on the valid CHY-integrands I_{CHY}, as we will see shortly.

We would like to use a purely algebraic approach, as it is more amenable to be implementation as computer code. To achieve this, we can recast Eq. 4.5 from an integral to a summation by changing variables from the punctures z_a to the scattering equations f_a. This introduces a Jacobian factor, i.e. the determinant of the Jacobian matrix defined as

$$\phi_{ab} = \frac{\partial f_a}{\partial z_b} = \begin{cases} \frac{2 k_a \cdot k_b}{(z_a - z_b)^2} & a \neq b \ , \\ -\sum\limits_{j \in A \backslash \{a\}} \frac{2 k_a \cdot k_j}{(z_a - z_j)^2} & a = b \ . \end{cases} \tag{4.9}$$

---

[1] Color ordering is assumed for gauge theories.

[2] More details on I_{CHY} are given in section 4.2. For now it suffices to say that in general it is a function of the punctures z, the momenta k and the polarisations ϵ.

Again, in the spirit of preserving Möbius invariance, since we have removed punctures i, j, and k from the above δ-function, we also have to remove the corresponding rows form the Jacobian. Similarly, we are not integrating over r, s and t, and therefore those columns have to be removed as well. The matrix of Eq. 4.9 with rows i, j, k and columns r, s, t removed is denoted by ϕ^{ijk}_{rst}. In the end, the relevant Jacobian for the change of variables, which is independent of the Möbius fixing choice, is given by[3]

$$J = \frac{(z_i - z_j)(z_j - z_k)(z_k - z_i)(z_r - z_s)(z_s - z_t)(z_t - z_r)}{\det(\phi^{ijk}_{rst})} \ . \tag{4.10}$$

If we impose the choice made in Eq. 4.4, we have

$$\{i, j, k\} = \{r, s, t\} = \{z_1, z_2, z_n\} = \{\infty, 1, 0\} \ . \tag{4.11}$$

We now write Eq. 4.5 for the scattering amplitudes as

$$A_n \ = \ z_1^4 \cdot i \sum_{j=1}^{(n-3)!} \frac{I_{CHY}(z^{(j)}(k); k; \epsilon)}{\det(\phi^{ijk}_{rst})(z^{(j)}(k); k)} \ , \tag{4.12}$$

where j labels the solution of the SE given by the set of punctures $z^{(j)}$, which are themselves function of the momenta k. Note that, because of Eq. 4.10 and our choice Eq. 4.11, the Jacobian J introduces the four powers of $z_1 = \infty$ in the numerator. Therefore, I_{CHY} must come with four powers of z_1 in the denominator for Eq. 4.12 to be sensible. This is a check of Mobius invariance.

4.1 Polynomial Form of the SE and their Solutions

We now turn to the problem of actually finding the solutions to the SE. It is easiest to consider the SE in the form found in Ref. [104], where the SE are reformulated as $n - 3$ polynomial equations. We can then follow Ref. [105, 106] in using an elimination theory algorithm to find the solutions.

The SE in polynomial form, which are equivalent to the original SE of Eq. 4.2, are given by

$$h_m = \sum_{S \subset A', |S|=m} k_{S_1}^2 z_S = 0 \,, \ \text{ with } 1 \leq m \leq n - 3 \,, \tag{4.13}$$

---

[3]We are also including in the Jacobian J the products of differences of punctures from Eq. 4.7 and Eq. 4.8.

where the sets A' and S_1 are defined as

$$A' = A \backslash \{1, n\}, \;\; S_1 = S \cup \{1\} \tag{4.14}$$

and where k_S and z_S are defined as

$$k_S = \sum_{b \in S} k_b \;\; \text{and} \;\; z_S = \prod_{b \in S} z_b \, . \tag{4.15}$$

In the above z_1 and z_n have already been set to ∞ and 0 respectively, but z_2 is still kept free.

This is a system of $n - 3$ polynomial equations ($h_{1 \leq m \leq n-3}$) in $n - 2$ variables ($z_{2 \leq i \leq n-1}$). As such, it can be solved by using an elimination theory algorithm. The idea underpinning elimination theory is to express the system of equations in matrix form and to introduce more variables and equations until the system is over-specified and yields a consistency condition in the form of $\det(M_n) = 0$. Here we are going to discuss directly the general n case. A more detailed discussion can be found in the original papers of Ref. [105, 106] or in Ref. [103].

In general, the aim is to obtain an equation of order $(n-3)!$ in the ratio z_{n-1}/z_{n-2}. The original set of 2^{n-4} monomials we wish to eliminate is given by

$$V^T = \{1, z_2\} \times \{1, z_3\} \times \, ... \, \times \{1, z_{n-3}\} \, . \tag{4.16}$$

We introduce an auxiliary set

$$W^T = \{1\} \times \{1, z_3\} \times \{1, z_4, z_4^2\} \times \, ... \, \times \{1, z_{n-3}, ..., z_{n-3}^{n-5}\} \, , \tag{4.17}$$

which contains $(n-4)!$ terms. The new set of monomials is then given by

$$V^T \to V^T \times W^T = \{1, z_2\} \times \{1, z_3, z_3^2\} \times \, ... \, \times \{1, z_{n-3}, ..., z_{n-3}^{n-4}\} \, , \tag{4.18}$$

which is of length $(n-3)!$. Similarly, the new $(n-3)!$ equations are given by

$$H^T \to H^T \times W^T \, , \tag{4.19}$$

where H^T denotes the vector of polynomial scattering equations $h_{1 \leq m \leq n-3}$. This procedure ensures that the number of monomials matches the number of equations, thus allowing to express the system in matrix form.

Then, by taking partial derivatives of the entries of the extended H of Eq. 4.19 w.r.t. those of the extended V of Eq. 4.18, we could construct the $(n-3)! \times (n-3)!$ matrix M_n whose

determinant is the required equation. However, this is not necessary in practice since the matrix M_n can be built recursively in a block-matrix format starting directly from the original set $h_{1 \le m \le n-3}$ and their derivatives w.r.t. $z_{2 \le i \le n-3}$. We denote the derivatives with superscripts $(M^z = \partial_z M)$ and we have

$$
M_i = \begin{pmatrix} M_{i-1} & M_{i-1}^{z_{i-3}} & 0 & \dots & 0 & 0 \\ 0 & M_{i-1} & M_{i-1}^{z_{i-3}} & \dots & 0 & 0 \\ \vdots & \vdots & \vdots & \ddots & \vdots & \vdots \\ 0 & 0 & 0 & \dots & M_{i-1} & M_{i-1}^{z_{i-3}} \end{pmatrix}, \quad M_4 = H, \quad H = \begin{pmatrix} h_1 \\ h_2 \\ \vdots \\ h_{n-3} \end{pmatrix},
$$
(4.20)

with M_i of dimensions $(i-4) \times (i-3)$ when written in terms of M_{i-1}. After the derivative is taken, z_{i-3} is set to zero. M_n is then a function of z_{n-1} and z_{n-2} only, the required equation of order $(n-3)!$ in z_{n-1}/z_{n-2} is simply $\det(M_n) = 0$, and its roots are the solutions we seek. Note that, as discussed in the introduction, it is feasible to perform this root-finding step analytically only for low phase space multiplicities.

Clearly we are not at the end of the calculation yet, because we want values or expressions for the punctures themselves not for ratios. This is achieved by reintroducing one variable at a time in M. More explicitly, we first check with Eq. 4.18 the position in the vector of the variable $\tilde{z}$ we want to reintroduce (say it is the jth entry), then we add $\tilde{z}$ times the jth column of M to its first column, and eventually remove the jth column and the last row. This leads to a matrix of size $(n-3)! - 1 \times (n-3)! - 1$ whose determinant will be a linear equation for $\tilde{z}$. There is one notable exception to this procedure, namely when $\tilde{z} = z_2$ we set $z_2 = 1$ and get a linear equation for z_{n-2} instead.

Finally, we are left with $(n-3)!$ sets of punctures $\{z_1 = \infty, z_2 = 1, z_3, \dots z_{n-1}, z_n = 0\}$ that solve the scattering equations.

4.2 CHY-Integrands

So far, we have treated the theory-independent part of Eq. 4.12. Now we consider the theory-dependent term I_{CHY}. It can be built in a modular way from various building blocks. Here we review the definition of some of those building blocks found in Ref. [107] and in Ref. [108] which we have implemented in the `Python` package presented in the appendix.

Starting from the building blocks that are matrices, we have the $2n \times 2n$ anti-symmetric matrix Ψ which is defined block-wise in terms of two $n \times n$ anti-symmetric matrices A and B and in terms of a third $n \times n$ matrix C. The definitions follow.

$$\Psi = \begin{pmatrix} A & -C^T \\ C & B \end{pmatrix} , \quad A_{ab} = \begin{cases} \frac{2k_a \cdot k_b}{(z_a - z_b)} & a \neq b , \\ 0 & a = b , \end{cases} \tag{4.21}$$

$$B_{ab} = \begin{cases} \frac{2\epsilon_a \cdot \epsilon_b}{(z_a - z_b)} & a \neq b , \\ 0 & a = b , \end{cases} \quad C_{ab} = \begin{cases} \frac{2\epsilon_a \cdot k_b}{(z_a - z_b)} & a \neq b , \\ -\sum\limits_{j \in A \setminus \{a\}} \frac{2\epsilon_a \cdot k_j}{(z_a - z_j)} & a = b . \end{cases} \tag{4.22}$$

Since these are matrices we have to define an operation which converts them to a rank-one object before we can use them to construct I_{CHY}. In the case of anti-symmetric matrices the determinant can be written as a square of a polynomial in the matrix entries. This polynomial is called the Pfaffian and it was shown to be the correct operation to perform. More specifically, since the matrix Ψ has two null vectors and its Pfaffian would be zero, it is necessary to define a reduced Pfaffian PF' as

$$\mathrm{PF}'(\Psi) = \frac{(-1)^{i+j}}{z_i - z_j} \mathrm{PF}(\Psi_{ij}^{ij}) , \tag{4.23}$$

where Ψ_{ij}^{ij} again denotes deletion of rows and columns i and j. The same reduction applies also to different arguments, such as the matrix A.

We also consider two scalar building blocks C_n and W_1. C_n is a cyclic Parke-Taylor-like factor simply defined as

$$C_n = \frac{1}{(z_1 - z_2) \dots (z_n - z_1)} , \tag{4.24}$$

and the W_1 function is defined as [4]

$$W_1 = \prod_{i \in A} \omega_i , \quad \text{with} \quad \omega_i = \sum_{j \in A \setminus \{i\}} \frac{\epsilon_i \cdot k_j (z_j - z_r)}{(z_r - z_i)(z_i - z_j)} , \quad r \neq i. \tag{4.25}$$

I_{CHY} is built from products of pairs of these building blocks. A more detailed analysis reveals that $\mathrm{PF}'(\Psi)$, C_n and W_1 come with a factor of z_1^{-2}, while $\mathrm{PF}'(A)$ comes with a factor of z_1^{-1}. This dictates which combinations are allowed by Möbius invariance (recall that overall we need four powers of z_1 to balance out those in Eq. 4.12).

Table 4.1 summarises the theories that can be built out of $\mathrm{PF}'(\Psi)$, C_n, $\mathrm{PF}'(A)^2$ and W_1: EG stands for Einstein Gravity, YM for Yang-Mills, BS for Biadjoint Scalar, BI for

---

[4] We use W_1 to denote the function $W_{1\dots1}$ from Ref. [108].

$\times$	PF$'(\Psi)$	C_n	PF$'(A)^2$	W_1
PF$'(\Psi)$	EG	YM	BI	CG
C_n	YM	BS	NLSM	(DF)^2
PF$'(A)^2$	BI	NLSM	Galileon	?
W_1	CG	(DF)^2	?	?

Table 4.1: Possible QFTs built out of PF$'(\Psi)$, C_n , PF$'(A)^2$ and W_1.
A product is implied between rows and columns, eg: $I_{CHY,\,EG} = \text{PF}'(\Psi) \times \text{PF}'(\Psi)$.

Born-Infeld, NLSM for Non Linear Sigma Model and CG for Conformal Gravity. The theories labelled with a question mark do not seem to have an agreed upon name, but they are discussed in the reference from which the W_1 function is taken.

This is by no means a complete recount of all possible integrands I_{CHY}, but it is sufficient to illustrate the framework. Also note that, as anticipated in the introduction, relations among theories through double copies are now manifest in the structure of the integrands.

For reference, we reproduce here the Lagrangians of pure Yang-Mills, Einstein gravity and bi-adjoint scalar

$$\mathcal{L}_{\text{Yang-Mills}} = -\frac{1}{4} F^{a,\mu\nu} F^a_{\mu\nu} \, , \tag{4.26}$$

$$\mathcal{L}_{\text{Einstein Gravity}} = R\sqrt{-g} \, , \tag{4.27}$$

$$\mathcal{L}_{\text{Bi-adjoint Scalar}} = 2\partial^\mu \Phi^{aa'} \partial_\mu \Phi^{aa'} + \frac{1}{3} f^{abc} \tilde{f}^{a'b'c'} \Phi^{aa'} \Phi^{bb'} \Phi^{cc'} \, . \tag{4.28}$$

The field strength tensor $F^a_{\mu\nu}$ was defined in Eq. 1.19, R is the Ricci scalar, $g = \det(g_{\mu\nu})$, where $g_{\mu\nu}$ is the perturbed metric tensor $g_{\mu\nu} = \eta_{\mu\nu} + h_{\mu\nu}$, and Φ is a scalar field carrying two indices of the adjoint representation of $SU(N_c)$, hence the name.

We don't reproduce the remaining Lagrangians since they would require several additional definitions which are not fundamental for the discussion in Chapter 9, but they can be easily found in the references.

Finally, remember that the CHY-integrands are not unique. For instance, a different integrand for conformal gravity is given in Ref. [109].

Pole Structure

In this chapter, we study how to access the pole structure of integral coefficients directly from numerical evaluations. This is of interest because the pole structure provides a powerful window into their full analytical form, thus considerably restricting the amount of information needed for their reconstruction by means of an ansatz, which is the topic of Chapter 6. Overall, the aim of these two chapters is to lay out a procedure to reconstruct rational Lorentz-invariant functions from numerical evaluations only.

In order to access the pole structure, we need to be able to manipulate the Lorentz invariant phase space, which we will consider as formed by n massless particles. In particular, we want to be able to generate specific sets of momenta with which to probe the expressions. We will first consider the case of singular limits, that is regions of phase space where a single Lorentz invariant becomes arbitrarily small, and see what information we can obtain from them. Since this is often insufficient, we will then study the generation of doubly singular limits, that is regions of phase space where pairs of invariants vanish.

Let us start from the construction of random phase space points which satisfy both momentum conservation and on-shell relations. Assuming we work in the all outgoing convention with massless particles only, these constraints read

$$\sum_{k=1}^{n} P_k = 0 \quad \text{and} \quad P_k^2 = 0 \quad \forall \quad k \in \{1, \ldots, n\}. \tag{5.1}$$

A possible way to proceed is the following: 1) generate random numbers, either real or complex, for all spatial components of the four-momenta; 2) compute the energy component of the four-momenta using the on-shell relation; 3) recoil two of the n particle four-momenta by solving the momentum conservation equations. The reason why two four-momenta need to be recoiled, and not just one, is that a four-momentum has three degrees of freedom (the fourth component being fixed by the on-shell relation), whereas there are four (scalar) momentum conservation equations. Alternatives include the randomisation of spinor components, or the use of momentum twistors.

The last step of restoring momentum conservation can be performed in different ways. We will now see two procedures, one for real and one for complex momenta.

Real Momenta

Although this first procedure works for both real and complex momenta, in practice it should only be used to generate real phase space points. Start by picking the two momenta P_i and P_j, which will be recoiled in order to satisfy momentum conservation, and group the rest of the momenta in a massive momentum K. We have

$$0 = \sum_k P_k = P_i + P_j + \sum_{k \neq i,j} P_k = P_i + P_j + K \,. \tag{5.2}$$

Given P_i, P_j is uniquely determined. Thus, we can manipulate the above to eliminate P_j, and obtain an equation for P_i only

$$P_j = -P_i - K \quad \Longrightarrow \quad 0 = P_j^2 = P_i^{2\,0} + K^{2\,m_K^2} + 2P_i \cdot K \,. \tag{5.3}$$

Clearly, there is no unique solution for the components of P_i. In fact, two four-momenta have six degrees of freedom but momentum conservation imposes only four constraints. Therefore, we can choose the only non-zero component of the 3 momentum of P_i to be $w \in \{x, y, z\}$, which leads to

$$P_i^{(0)} = P_i^{(w)} = \frac{-m_K^2}{2(K^{(0)} - K^{(w)})} \,. \tag{5.4}$$

This procedure does not introduce any imaginary component to a real phase space point, but it does modify both the left- and the right-handed spinors of both recoiled four-momenta. While the former property is useful to generate physical phase space points, the latter is more restrictive than necessary for complex kinematics.

Complex Momenta

This second procedure always results in a complex phase space point, but has the advantage of acting only on either the left- or the right-handed spinor components. Let us reconsider the momentum conservation equation, this time written in spinor notation

$$0 = \sum_k |k]\langle k| = |i]\langle i| + |j]\langle j| + \sum_{k \neq i,j} |k]\langle k| = |i]\langle i| + |j]\langle j| + K \,. \tag{5.5}$$

Contracting Eq. 5.5 from the left with $[i|$ and $[j|$, we obtain a solution which only modifies the angle brackets

$$[ji]\langle i| + [j|K = 0 \quad \Rightarrow \quad \langle i| = \frac{[j|K}{[ij]} \,, \quad \langle j| = -\frac{[i|K}{[ij]} \,. \tag{5.6}$$

Alternatively, the parity conjugate of Eq. 5.6 only modifies the square brackets

$$|i]\langle ij\rangle + K|j\rangle = 0 \quad \Rightarrow \quad |i] = -\frac{K|j\rangle}{\langle ij\rangle} \,, \quad |j] = \frac{K|j\rangle}{\langle ij\rangle} \,. \tag{5.7}$$

The freedom of deciding whether to modify the angle or the square brackets will turn out to be extremely useful to easily generate phase space configurations with multiple constraints.

5.1 Least Common Denominator from Singular Limits

In this section, we will see how the least common denominator of kinematic expressions can be obtained by probing them in singular limits.

5.1.1 Singular Limits

Let us start by considering how to generate phase space points in singular limits, defined as regions of phase space where a single Lorentz invariant vanishes. For real kinematics, this definition reduces to the concept of collinear limit, where two momenta become aligned and the particles potentially unresolved. For complex kinematics, we lose both geometric and physical interpretations, but gain much freedom for the construction of distinct phase space points.

As anticipated in Section 2.2.3, we are going to consider a set of invariants $\{r_i\}$ each of which can be made arbitrarily small while keeping the others of $\mathcal{O}(1)$, but which are not necessarily linearly independent. Mathematically, we define a singular limit, and the allowed invariants in $\{r_i\}$, by

$$r_i \to \epsilon \ll 1 \,, \quad \text{with} \quad r_{j \neq i} = \mathcal{O}(1) \,. \tag{5.8}$$

For instance, this implies that $\langle 12 \rangle \in \{r_i\}$ and $[12] \in \{r_i\}$, but $s_{12} \notin \{r_i\}$. However, note that, for multiplicities greater than 5, $s_{123} \in \{r_i\}$, since complex kinematics circumvents the triangle inequality which, for real kinematics, requires $s_{123} \sim \epsilon \Rightarrow s_{12} \sim s_{13} \sim s_{23} \sim \epsilon$.

The invariants that need to be included in the set $\{r_i\}$ depend on the amplitude under consideration. For instance, the poles appearing in colour-ordered amplitudes are restricted compared to those of, say, gravity amplitudes. Ultimately, the bottle neck is not in the generation of the phase space point, but in the evaluation of an amplitude at said point.

As a more concrete example, for the study of the one-loop six-gluon amplitudes, we considered the following set of invariants

$$
\begin{aligned}
\{r_i\} \;=\; & \{\langle 12 \rangle, \; \ldots, \; \langle 56 \rangle, \; [12], \; \ldots, \; [56], \\
& \langle 1|2+3|1], \; \ldots, \langle 6|4+5|6], \; \langle 1|3+4|2], \; \ldots \langle 6|2+4|3], \\
& \langle 1|2+3|2+6|1 \rangle, \; \ldots, \; [6|1+5|4+5|6], \\
& s_{123}, \; \ldots, \; s_{345}, \; \Delta_{135}, \; \Delta_{624}, \; \ldots \} \,,
\end{aligned}
\tag{5.9}
$$

where all $\langle ij \rangle$ and $[ij]$ invariants are considered, but, for instance, contractions of the type $\langle i|j+k|l]$ are restricted to those containing adjacent particles. The Gram determinant Δ is defined in Section 3.3.3, its subscripts denote the first particles in each momentum grouping, and the rest of the invariants are defined in Eq.s 2.62 to 2.65. In total $\{r_i\}$ contains more than 200 spinor contractions.

We are now going to consider how the relevant limits are generated. In general, we will need to solve a system of equations for the selected invariant equal to a small value, and four-momentum conservation.

Angle and Square Brackets

In the case of angle and square brackets, i.e. of invariants of the form $\langle ij \rangle$ or $[ij]$, we simply need to solve

$$
\langle ij \rangle = (\lambda^{(i)})^\alpha (\lambda^{(j)})_\alpha = \epsilon
\tag{5.10}
$$

for any of the components of either spinor, say

$$
(\lambda^{(i)})^1 = \frac{\epsilon - (\lambda^{(i)})^2 (\lambda^{(j)})_2}{(\lambda^{(j)})_1} \;.
\tag{5.11}
$$

Afterwards, we can use either Eq. 5.6 or Eq. 5.7 to restore momentum conservation, making sure the recoiled momenta are neither i or j, which we have just fine tuned. Note that this procedure can be used to set $\langle ij \rangle$ to any value, not just $\epsilon \ll 1$.

Multi-Particle Invariant

The case of invariants of the form

$$\langle i| \underbrace{(j + \cdots + k)| \ldots |(l + \cdots + m)}_{\text{odd}} |n] , \quad \text{or} \quad \langle i| \underbrace{(j + \cdots + k)| \ldots |(l + \cdots + m)}_{\text{even}} |n\rangle ,$$

$$\text{or} \quad [i| \underbrace{(j + \cdots + k)| \ldots |(l + \cdots + m)}_{\text{even}} |n] \tag{5.12}$$

is slightly more involved, but not significantly so. Let us consider two possible cases.

1) The easiest case is when either the first momentum (i) or the last one (n) do not appear slashed in the central block. In this case, we can just compute the rest of the contraction to obtain

$$\langle i|K\rangle , \quad \text{with, say,} \quad |K\rangle = \underbrace{(j + \cdots + k)| \ldots |(l + \cdots + m)}_{\text{odd}} |n] \tag{5.13}$$

and then set $\langle i|K\rangle$ using Eq. 5.11, and restore momentum conservation making sure not to recoil any momentum which appears in the contraction.

2) Another case is when both the first momentum (i) and the last one (n) appear more than once in the spinor contraction. An example could be $\langle 1|2 + 3|2 + 6|1\rangle$. A possible solution in this case is

$$\langle 1|2 + 3|2 + 6|1\rangle = \langle 1|3\rangle[3|2 + 6|1\rangle + \langle 1|2|2 + 6|1\rangle = \epsilon , \tag{5.14}$$

$$\implies \langle 1|3\rangle = \frac{\epsilon - \langle 1|2|2 + 6|1\rangle}{[3|2 + 6|1\rangle} \tag{5.15}$$

which, again, can be solved using Eq. 5.11 for the spinor $|3\rangle$.

This is not an exhaustive list, but it covers the vast majority of cases, especially since we can use momentum conservation on the sum of slashed momenta to obtain equivalent expressions for the same invariant.

Three-Particle Mandelstam Invariants

Given the above discussion, the case of three particle Mandelstam invariants, s_{ijk}, is simple

$$s_{ijk} = \langle i|j + k|i] + \langle j|k|j] = \epsilon , \tag{5.16}$$

$$\implies \langle i|j + k|i] = \epsilon - \langle j|k|j] , \tag{5.17}$$

which can be solved using Eq. 5.13.

Gram Determinant

A more involved singular limit is that for the Gram determinant Δ. Following the definition of Eq. 3.69, we want to solve

$$\Delta_{ijk} = (K_i \cdot K_j)^2 - K_i^2 K_j^2 = \epsilon \quad \text{and} \quad \sum_{i=0}^{n} P_i = 0 \,, \tag{5.18}$$

where P_i are the external momenta, $K_i = P_i + \cdots + P_{j-1}$, with the set $\{i, \ldots, j-1\}$ taken to be cyclic for colour order amplitudes, and similarly $K_j = P_j + \cdots + P_{k-1}$. Since Δ_{ijk} can be formulated independently of any momentum in the set $\{k, \ldots, i-1\}$, once the first equation is satisfied, momentum conservation can be easily restored by recoiling two of these momenta.

Let us write $K_i = P_0 + \tilde{P}$, where P_0 is any single momentum from the set $\{i, \ldots, j-1\}$, and $\tilde{P}$ sums the remaining momenta of the set. We are going to solve Eq. 5.18 for P_0, or, more precisely, for one of the components of either its left or right spinor. Expanding Eq. 5.18, we have

$$\left[(P_0 + \tilde{P}) \cdot K_j\right]^2 - (P_0 + \tilde{P})^2 K_j^2 = \epsilon \tag{5.19}$$

$$\Rightarrow \quad (P_0 \cdot K_j)^2 + 2\left[(P_0 \cdot K_j)(\tilde{P} \cdot K_j) - (P_0 \cdot \tilde{P})K_j^2\right] + (\tilde{P} \cdot K_j)^2 - \tilde{P}^2 K_j^2 - \epsilon = 0 \tag{5.20}$$

$$\Rightarrow \quad \frac{1}{4}\langle 0|K_j|0]^2 + \left[\langle 0|K_j|0](\tilde{P} \cdot K_j) - \langle 0|\tilde{P}|0]K_j^2\right] + (\tilde{P} \cdot K_j)^2 - \tilde{P}^2 K_j^2 - \epsilon = 0 \,. \tag{5.21}$$

Let us call

$$K_j|0] = \begin{pmatrix} \alpha \\ \beta \end{pmatrix} \,, \quad \tilde{P}|0] = \begin{pmatrix} \gamma \\ \delta \end{pmatrix} \,, \quad \langle 0| = \begin{pmatrix} a, b \end{pmatrix} \,. \tag{5.22}$$

Then, substituting Eq. 5.22 into Eq. 5.21 and grouping for a we obtain

$$a^2 \left(\frac{\alpha^2}{4}\right) + a \left[\frac{1}{2}\alpha b\beta + \alpha(\tilde{P} \cdot K_j) - \gamma K_j^2\right] +$$

$$+ \left[\frac{1}{4}b^2\beta^2 + b\beta(\tilde{P} \cdot K_j) - b\delta K_j^2 + (\tilde{P} \cdot K_j)^2 - \tilde{P}^2 K_j^2 - \epsilon\right] = 0 \,, \tag{5.23}$$

which is simply a quadratic equation. Of course, one can also solve for b, or, by taking the parity conjugate, for one of the components of the left spinor $|0]$.

The freedom of being able to solve the same equations for different variables will become very useful when considering the case of doubly singular limits, discussed in the Section 5.2. In that context, the increased number of constraints will require additional attention to how to separate the system of equations so that they can still be solved sequentially instead of simultaneously.
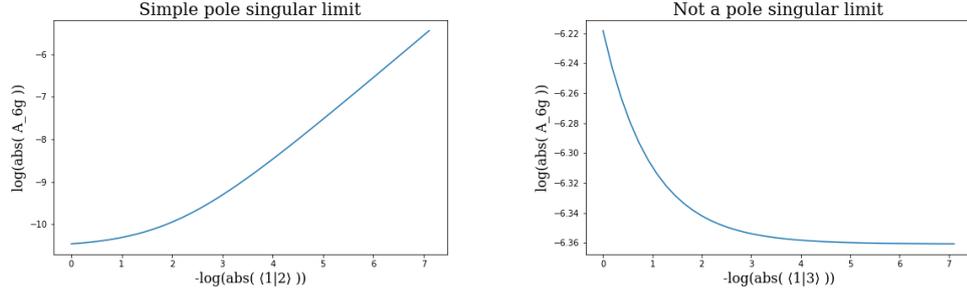
Figure 5.1: on the left, $A_{6g,+-+-+-}^{(0)}$ as it approaches a simple pole ($\langle 12 \rangle \to \epsilon$); on the right, the same tree amplitude at a regular point ($\langle 13 \rangle \to \epsilon$).

5.1.2 Least Common Denominator

Now that we understand how to generate singular phase space points, we can go back to consider scattering amplitudes. In general, a rational expression $\mathcal{E}$ can be expressed over a single denominator

$$\mathcal{E} = \frac{\mathcal{N}}{\mathcal{D}_{\mathcal{LCD}}}, \tag{5.24}$$

where $\mathcal{D}_{\mathcal{LCD}} = \prod r_i^{n_i}$ denotes the least common denominator, and r_i the real poles of $\mathcal{E}$. $\mathcal{D}_{\mathcal{LCD}}$ is unique and can be obtained directly from numerical evaluations, given a sufficiently complete set $\{r_i\}$ of possible denominator factors, by numerically probing $\mathcal{E}$ in limits where one of these factors vanishes. In a singular limit, a rational expression $\mathcal{E}$ will behave as[1]

$$\log(\mathcal{E}) \sim n_i \log(\epsilon) + \text{const}, \tag{5.25}$$

which means that the powers n_i are simply given by the slope of $\mathcal{E}$ in a log-log plot. Figure. 5.1 shows the scaling of the tree amplitude $A_{6g,+-+-+-}^{(0)}$ given in Eq. 3.37 in two limits, one of which corresponds to a pole.

Clearly, the same procedure also exposes overall factors in the numerator ($n_i > 0$). In this case, $\mathcal{E}$ vanishes when the limit is taken rather than exhibiting the diverging behaviour of denominator factors. To test for overall factors we can use a broader set of structures r_i that are not necessarily possible poles but satisfy the uniqueness of the limit in Eq. 5.8, in order to reliably ascribe the vanishing of the expression to a single overall factor.

In the simplest cases, the procedure described in this section yields the full expression $\mathcal{E}$ up to a numerical pre-factor, which can be obtained by performing a simple division. For example, this happens with all box coefficients in the six-gluon amplitudes (recall the expression in Eq. 3.61).

---

[1] This will hold also in the presence of radicals, but may be spoiled by transcendental functions.

5.2   Partial Fractions from Doubly Singular Limits

The information which can be extracted from the study of singular limits is important but quite limited, and in most cases not sufficient to make the reconstruction technique of the next chapter feasible. In fact, if the numerator $\mathcal{N}$ is not just an overall factor, but a sum of Lorentz invariants, then it cannot be identified by means of singular limits and it needs to be parametrised by an ansatz. If we refer back to Table 1.7, we see that the growth of the linear system is quite steep, and generally the mass dimension of $\mathcal{N}$ is not small.

5.2.1   Doubly Singular Limits

In order to learn more about the rational function $\mathcal{E}$, we will study its behaviour in doubly singular limits. In analogy with the singular limits described in Eq. 5.8, we define doubly singular limits as

$$r_i \to \epsilon \ll 1, \quad r_j \to \epsilon \ll 1. \tag{5.26}$$

In this case, it is not possible to guarantee that $r_{k \neq i,j} = \mathcal{O}(1)$. For example, if we have

$$\langle 1|2 \rangle \to \epsilon \quad \text{and} \quad \langle 2|3 \rangle \to \epsilon \tag{5.27}$$

we must also have

$$\langle 1|3 \rangle \sim \epsilon, \; s_{123} \sim \epsilon, \; ... \tag{5.28}$$

We call the double limit Eq. 5.26 *clean* if no factor $r_{k \neq i,j}$ other than r_i and r_j vanishes in this limit.

The singular limit of Eq. 5.26 is symmetric: r_i and r_j are both set to the same small ϵ. However, in some cases it is useful to study asymmetric limits as well: $r_i \to \epsilon_i$, $r_j \to \epsilon_j$, $\epsilon_i \neq \epsilon_j$. This is especially important to lift degeneracies that arise with higher order poles.

Since we are now interested in combinations of invariants (r_i, r_j), even with a relatively small initial set $\{r\}$, the number of possible cases is vastly bigger than that of the single limits considered in the previous section. For instance, at six-point, with about 200 invariants in the set $\{r\}$, we can take approximately $20,000$ combinations. We have implemented code that attempts to covers about $16,000$ cases. The remaining combinations are generally not required. In fact, thankfully, it is sufficient to consider small subsets of these combinations.

We are now going to review how to obtain doubly singular limits of complex phase space in a couple of scenarios.

⟨•|•⟩ and ⟨•|•⟩

The aim is to obtain a phase space point such that

$$\langle i|j\rangle \to \epsilon_1 , \quad \langle k|l\rangle \to \epsilon_2 , \quad \text{and} \quad \sum_{m=1}^{n} P_m = 0 . \tag{5.29}$$

In order to impose the first two conditions, we can use Eq. 5.11 twice, making sure that the spinor we modify does not appear in both contractions. To restore momentum conservation, ideally we would like to recoil two momenta not in the set $\{i, j, k, l\}$. If this is possible (e.g. for multiplicities ≥ 6), then we may use any one of Eq. 5.4, Eq. 5.6 or Eq. 5.7. However, if, say, $n = 5$ and i, j, k, l are all distinct, then there are no two momenta which do not appear in the contraction. In this case, we must use Eq. 5.7 to restore momentum conservation, since it acts on the square brackets only.

The cases involving an angle and a square bracket, or two square brackets follow by analogy.

⟨•|•⟩ and ⟨•| . . . |•]

We want a phase space point such that $\langle i|j\rangle$ is set to ϵ_1, together with any one of the invariants from Eq. 5.12 set to ϵ_2, and momentum conservation satisfied. The general strategy is to first set $\langle i|j\rangle \to \epsilon_1$ by modifying either spinor, then set the second invariant to ϵ_2 by modifying a spinor which does not appear in $\langle i|j\rangle$, and finally restore momentum conservation either via Eq. 5.6 or via Eq. 5.7. Clearly the first two steps are always possible, but the last one requires either two angle brackets or two square brackets in order not to appear in either Lorentz invariant. By using momentum conservation to obtain alternative expressions for the second invariant, this can be achieved in the vast majority of cases. A combination where this is not possible is, for instance, $\langle 1|3\rangle \to \epsilon_1$ and $[1|2+6|2+4|3] \to \epsilon_2$. This happens in roughly 1% of the cases we considered at six-point.

Additional Remarks

This same strategy can be applied to a number of cases, such as $(\langle i|j\rangle, s_{klm})$, $(\langle i|j\rangle, \Delta_{klm})$, most pairs of the form $(\langle a|b+c|d], \langle e|f+g|h])$, and so on. In some rare cases, it is necessary to properly solve the system of two equations for two variables simultaneously. For instance, this is the case for $\langle a|b+c|a]$, $\langle b|a+c|b]$, which is physically relevant for the rational part of one-loop six-gluon amplitudes, where these types of poles appear simultaneously.

Finally, note that, since the number of variables at our disposal is larger than the number of

equations, there may be multiple distinct solutions to the system. As an explicit example, let us consider the case $\langle a|b\rangle \sim \epsilon \ll 1$ and $s_{abc} \sim \epsilon \ll 1$. In order to set $\langle a|b\rangle = \epsilon$ we take

$$\langle a| = \lambda\langle b| + \frac{\epsilon}{\langle \eta|b\rangle}\langle \eta| \tag{5.30}$$

for some $\lambda \sim \mathcal{O}(1)$ and arbitrary spinor $\langle \eta|$. Plugging this into s_{abc} we obtain

$$s_{abc} = s_{ab} + s_{bc} + s_{ac} = \epsilon[b|a] + \langle c|a + b|c] \tag{5.31}$$

$$= \epsilon[b|a] + (\lambda\langle c|b\rangle[a|c] + \epsilon\langle c|\eta\rangle[a|c] + \langle c|b\rangle[b|c]) \tag{5.32}$$

$$= \epsilon([b|a] + \langle c|\eta\rangle[a|c]) + \langle c|b\rangle(\lambda[a|c] + [b|c]) . \tag{5.33}$$

Therefore, for s_{abc} to be also small, we need either $\langle c|b\rangle \sim \epsilon$ or $(\lambda[a|c] + [b|c]) \sim \epsilon$. The former case results in many more invariants being small compared to the latter. For example, for $a = 1$, $b = 2$ and $c = 3$, choosing $\langle c|b\rangle \sim \epsilon$ makes the following $\mathcal{O}(\epsilon)$

$$\langle 1|3\rangle,\ \langle 1|2\rangle,\ \langle 2|3\rangle,\ \langle 2|1+3|5],\ \langle 1|2+3|5],\ \langle 1|2+3|6],\ \langle 2|1+3|4],\ \langle 3|1+2|6],\ \langle 2|1+3|6],$$

$$\langle 2|1+3|2],\ \langle 3|1+2|5],\ \langle 1|2+3|4],\ \langle 3|1+2|3],\ \langle 1|2+3|1],\ \langle 3|1+2|4],\ s_{123}, \tag{5.34}$$

but choosing $\lambda[a|c] + [b|c] \sim \epsilon$ results in only the following invariants being small

$$\langle 1|2\rangle,\ \langle 5|1+2|3],\ \langle 6|1+2|3],\ \langle 4|1+2|3],\ \langle 3|1+2|3],\ s_{123}. \tag{5.35}$$

We would say that the latter case has lower degeneracy, or that it is *cleaner*, than the former one. In general, it is always best to choose the cleaner limit, since it makes ascribing the behaviour of the amplitude in a limit to a particular set of invariants easier. Quantitatively, we can define the degeneracy as the number of invariants in the set $\{r\}$ which are $\mathcal{O}(\epsilon)$.

5.2.2   Partial Fraction Decomposition

Similarly to the singular limits of Eq. 5.8, in doubly singular limits a rational expression $\mathcal{E}$ will behave as $\mathcal{E} \sim \epsilon^{-n_{ij}}$. However, now n_{ij} cannot be ascribed to a specific invariant, and instead is the combined scaling resulting from two or more invariants becoming small. This exponent can again be obtained by computing the slope in a log-log plot, as in Eq. 5.25.

By considering these exponents n_{ij}, we quickly realise that it is more natural[2] to think about $\mathcal{E}$ not as a single fraction, but as a sum of rational terms

$$\mathcal{E} = \sum_i \frac{\mathcal{N}_i}{\mathcal{R}_i \mathcal{S}_i}. \tag{5.36}$$

---

[2]Meaning that the singularity structure is better represented.

In the above, $\mathcal{R}_i$ are products of subsets of the factors in $\mathcal{D}_{\mathcal{LCD}}$, and $\mathcal{S}_i$ contain denominator factors that are not in the LCD, i.e. they cancel in the sum. The latter are known as spurious poles and arise naturally when using partial fractions to separate individual factors in the LCD. $\mathcal{N}_i$ are some numerator structures typically simpler than $\mathcal{N}$. Since the decomposition of Eq. 5.36 is not unique, it can be used to optimise the compactness of the expression representation or its stability in specific regions of phase space.

As anticipated, it is not necessary to consider all possible pairs of Lorentz invariants. The two most interesting sets of doubly singular limits are: a) for (r_i, r_j) both real poles; and b) for r_i a real pole, and $r_j \notin \mathcal{D}_{\mathcal{LCD}}$. Let us start with the former case, and for the sake of simplicity, let us consider an expression $\mathcal{E}$ which only involves simple poles, such as tree amplitudes. The reasoning for expressions involving higher order poles is similar. There are three distinct cases:

1. the limit Eq. 5.26 is clean and $n_{ij} = 1$: this implies that we can find a representation for $\mathcal{E}$ where r_i and r_j never appear in the same denominator. They can be split up without the need of a spurious pole;

2. the limit Eq. 5.26 is clean and $n_{ij} = 2$: this implies that r_i and r_j must appear at least once in the same denominator in the sum of Eq. 5.36, and our set $\{r\}$ does not contain a spurious pole able to separate them;

3. the limit Eq. 5.26 is not clean, i.e. there exist vanishing factors $r_k \sim \epsilon$ in the double limit:

   - if $n_{ij} = 1$ we cannot numerically distinguish the following situations:

   $$\mathcal{E} \sim \frac{r_k}{r_i r_j}, \quad \mathcal{E} \sim \frac{1}{r_i}, \quad \mathcal{E} \sim \frac{1}{r_j}; \tag{5.37}$$

   The implication is that in this case we cannot conclude from the doubly singular limit whether r_i and r_j have to be present at the same time in a denominator.

   - if $n_{ij} = 2$ we cannot numerically distinguish the following situations:

   $$\mathcal{E} \sim \frac{1}{r_i r_j}, \quad \mathcal{E} \sim \frac{1}{r_i r_k}, \quad \mathcal{E} \sim \frac{1}{r_j r_k}; \tag{5.38}$$

   and linear combinations of these scenarios are also possible.

The consequence of not being able to discriminate between these scenarios is that multiple possible ansatze for the denominator structure are possible and, as mentioned before, there is often no obvious optimal solution.

Let us consider the latter expression when r_k does not appear in $\mathcal{D}_{\mathcal{LCD}}$. There might be several distinct r_k's and among those one may recognise some as possible spurious poles, which now have a clear physical interpretation in that they preserve the correct doubly singular behaviour of each term when we separate the r_i and r_j poles in separate denominators.

For instance, let us consider the structure of the pair of poles r_i, $r_j = \langle 12 \rangle$, $[34]$ when $n_{ij} = 2$. This is the case for A_{tree}^{+-+-+-} which we derived via BCFW recursion in Section 3.2. The expression we obtained, with the symmetries made explicit, reads

$$
\begin{aligned}
A_{tree}(1^+, 2^-, 3^+, 4^-, 5^+, 6^-) \;=\; & \frac{i[13]^4 \langle 46 \rangle^4}{[12][23] \langle 45 \rangle \langle 56 \rangle \langle 4|2+3|1] \langle 6|1+2|3] s_{123}} \\
& + \frac{i[15]^4 \langle 24 \rangle^4}{[16] \langle 23 \rangle \langle 34 \rangle [56] \langle 2|1+6|5] \langle 4|2+3|1] s_{234}} \\
& + \frac{-i \langle 26 \rangle^4 [35]^4}{\langle 12 \rangle \langle 16 \rangle [34][45] \langle 2|1+6|5] \langle 6|1+2|3] s_{345}}. \quad (5.39)
\end{aligned}
$$

In this case we see that $\langle 12 \rangle$, $[34]$ appear in the same denominator, which corresponds to the first case of Eq. 5.38. However, there also exists another well-known representation of the same tree amplitude corresponding to a different BCFW shift, which reads

$$
\begin{aligned}
A_{tree}(1^+, 2^-, 3^+, 4^-, 5^+, 6^-) \;=\; & \frac{i \langle 2|1+3|5]^4}{\langle 12 \rangle \langle 23 \rangle [45][56] \langle 1|2+3|4] \langle 3|1+2|6] s_{123}} \\
& + \frac{i \langle 6|2+4|3]^4}{\langle 16 \rangle [23][34] \langle 56 \rangle \langle 1|2+3|4] \langle 5|1+6|2] s_{234}} \\
& + \frac{-i \langle 4|3+5|1]^4}{[12][16] \langle 34 \rangle \langle 45 \rangle \langle 3|1+2|6] \langle 5|1+6|2] s_{345}}. \quad (5.40)
\end{aligned}
$$

In this case, $\langle 12 \rangle$ and $[34]$ appear in different denominators, thanks to the spurious pole $\langle 1|2+3|4]$, which clearly vanishes in the double limit. The partial fraction identity reads

$$
\frac{1}{\langle 12 \rangle [34]} = \frac{\langle 13 \rangle}{\langle 12 \rangle \langle 1|2+3|4]} + \frac{[24]}{[34] \langle 1|2+3|4]}. \quad (5.41)
$$

Similarly, we see that $\langle 3|1+2|6]$ separates $\langle 23 \rangle$ and $[16]$, and $\langle 5|1+6|2]$ separates $\langle 56 \rangle$ and $[12]$, and so on. A good choice of spurious pole to introduce can be identified from the list of vanishing r_k's by looking at intersections between different r_k sets: for instance, the sets from $(\langle 12 \rangle, [34])$ and $(\langle 16 \rangle, [45])$ share $\langle 1|2+3|4]$ only[3].

If we consider a slightly simpler example, namely the six-gluon split NMHV tree amplitude, which contains fewer poles, we can visualise the full set of relations between the poles by means of a diagram.

---

[3]It is clear that $\langle 1|2+3|4]$ vanishes also when $\langle 16 \rangle$ and $[45]$ vanish, because we can rewrite it as $-\langle 1|5+6|4]$ by using momentum conservation.
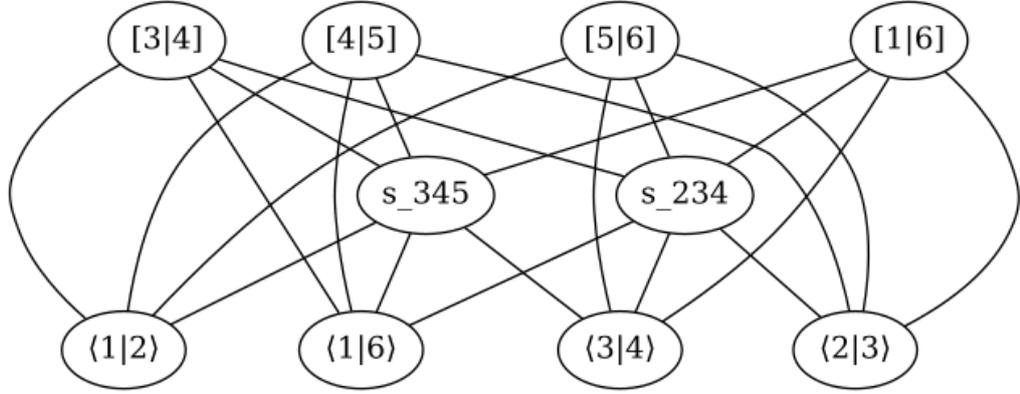
Figure 5.2: Shown are the real poles of A_{tree}^{+++---}. Two poles are connected by a line if $n_{ij} = 2$ in the relevant doubly singular limit. If $n_{ij} = 1$ they are not connected.

Figure 5.2 shows the real poles of A_{tree}^{+++---}, as obtained from singular limits, and their relations, as obtained from doubly singular limits. A line connecting two poles means that the doubly singular exponent n_{ij} is 2, otherwise it is 1. Note, however, that the diagram does not represent in any way whether a limit is clean or not. The full information obtained from doubly singular limits is displayed in Table 5.1. We will now analyse three different ways to write this amplitude, and highlight the differences.

The first and most compact way to split the poles is shown in Figure 5.3. The groupings attempt to keep invariant pairs with $n_{ij} = 2$ in the same denominator, but this is not always possible, meaning a spurious pole is necessary to perform the partial fraction decomposition. This figure corresponds to the following spinor expression

$$A_{tree}(1^+, 2^+, 3^+, 4^-, 5^-, 6^-) = \frac{i\langle 4|2+3|1]^3}{[16]\langle 23\rangle\langle 34\rangle[56]\langle 2|1+6|5]s_{234}} + \frac{-i\langle 6|1+2|3]^3}{\langle 12\rangle\langle 16\rangle[34][45]\langle 2|1+6|5]s_{345}}. \qquad (5.42)$$

To understand the origin of the spurious pole, let us denote the set of invariants $\{r_k\}$ that vanish together with r_i and r_j in their doubly singular limits as $\{r_i, r_j\}_\epsilon$. Then, we have a clear expression for the spurious pole $\langle 2|1+6|5]$ as the following intersection

$$\langle 2|1+6|5] = \{\langle 12\rangle, [56]\}_\epsilon \cap \{\langle 16\rangle, s_{234}\}_\epsilon \cap \{\langle 23\rangle, [45]\}_\epsilon \cap \{[34], s_{234}\}_\epsilon \ldots \qquad (5.43)$$

Note that some pairs of invariants appear in the same grouping, even if they are not connected by a line, i.e. even if $n_{ij} = 1$. For instance, this is the case for $\langle 12\rangle$ and $\langle 16\rangle$. We see that this is consistent because

$$\{\langle 12\rangle, \langle 16\rangle\}_\epsilon \supset \{\langle 12\rangle, \langle 16\rangle, \langle 2|1+6|5], s_{345}, \langle 6|1+2|3]\}, \qquad (5.44)$$

	$\langle 1\|2\rangle$	$\langle 1\|6\rangle$	$[1\|6]$	$\langle 2\|3\rangle$	$\langle 3\|4\rangle$	$[3\|4]$	$[4\|5]$	$[5\|6]$	s_{234}	s_{345}
$\langle 1\|2\rangle$		1; 30	1; 3	1; 31	1; 2	2; 12	2; 3	2; 10	1; 2	2; 10
$\langle 1\|6\rangle$	1; 30		1; 2	1; 2	1; 10	2; 4	2; 12	1; 3	2; 10	2; 10
$[1\|6]$	1; 3	1; 2		2; 12	2; 4	1; 10	1; 2	1; 30	2; 10	2; 10
$\langle 2\|3\rangle$	1; 31	1; 2	2; 12		1; 30	1; 3	2; 12	2; 3	2; 10	1; 2
$\langle 3\|4\rangle$	1; 2	1; 10	2; 4	1; 30		1; 2	1; 3	2; 12	2; 10	2; 10
$[3\|4]$	2; 12	2; 4	1; 10	1; 3	1; 2		1; 30	1; 2	2; 10	2; 10
$[4\|5]$	2; 3	2; 12	1; 2	2; 12	1; 3	1; 30		1; 31	1; 2	2; 10
$[5\|6]$	2; 10	1; 3	1; 30	2; 3	2; 12	1; 2	1; 31		2; 10	1; 2
s_{234}	1; 2	2; 10	2; 10	2; 10	2; 10	2; 10	1; 2	2; 10		1; 2
s_{345}	2; 10	2; 10	2; 10	1; 2	2; 10	2; 10	2; 10	1; 2	1; 2	

Table 5.1: Information obtained from doubly singular limits, displayed is the power of divergence n_{ij} (first number) and degeneracy of phase space (second number).

then $n_{ij} = 1$ follows by simple power counting. This degeneracy is in some cases problematic, since it is not easy to perform this reasoning *a priori*, that is, before the analytical expression is known. However, it can actually be useful to be able to guess numerator factors, and thus reduce the complexity of the anstaz for the numerator.

An alternative grouping is given in Figure 5.4. In this case we have three groups, corresponding to three terms in the expression for the amplitude, and we need a spurious pole to separate each pair of groups, for a total of three spurious poles. The spinor expression reads

$$
\begin{aligned}
A_{tree}(1^+, 2^+, 3^+, 4^-, 5^-, 6^-) \;=\; & \frac{i[23]^3\langle 56\rangle^3}{\langle 16\rangle[34]\langle 1|2+3|4]\langle 5|1+6|2]s_{234}} \\
& + \frac{-i[12]^3\langle 45\rangle^3}{[16]\langle 34\rangle\langle 3|1+2|6]\langle 5|1+6|2]s_{345}} \\
& + \frac{is_{123}^3}{\langle 12\rangle\langle 23\rangle[45][56]\langle 1|2+3|4]\langle 3|1+2|6]}, \quad (5.45)
\end{aligned}
$$

where again the same logic about set intersection and power counting apply. These two expressions for $A_{tree}(1^+, 2^+, 3^+, 4^-, 5^-, 6^-)$ that we just considered correspond to two BCFW shifts. They represent the structure of the poles as well as possible, but require the introduction of spurious singularities.

We can attempt to apply our reconstruction strategy to any denominator ansatz, even if
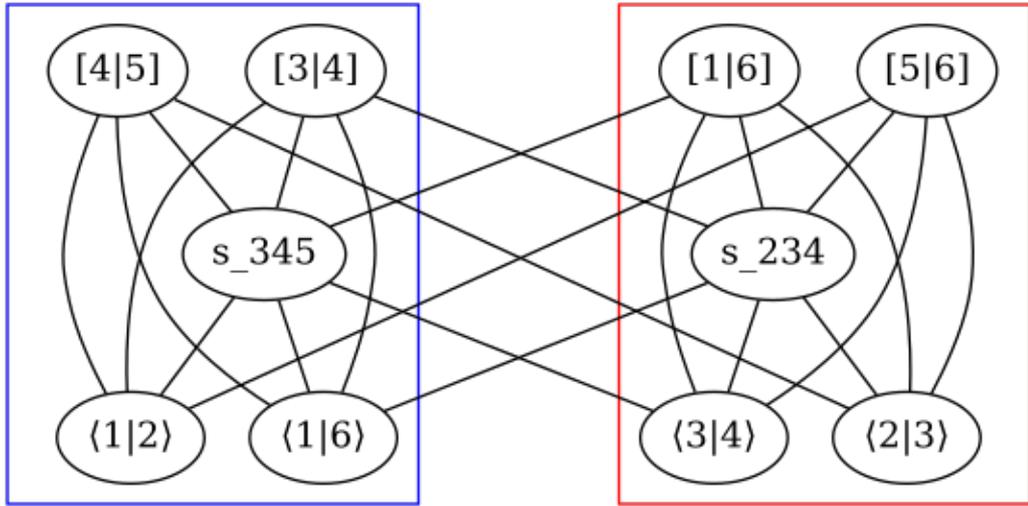
Figure 5.3: A first possible grouping of the real poles of A_{tree}^{+++---}. Different groups correspond to different denominators. A spurious pole is needed to split the two groups.
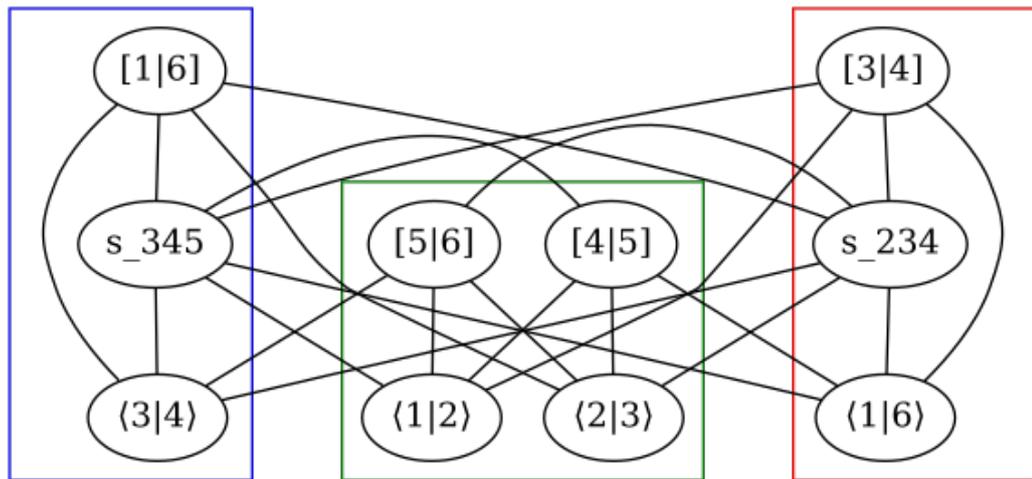

Figure 5.4: A second possible grouping of the real poles of A_{tree}^{+++---}. Different groups correspond to different denominators. Three spurious poles are needed to split the three groups.

it appears to violate the information from the doubly singular limits. For instance, if we place the three particle Mandelstam invariants in the same denominator, even if n_{ij} for s_{234} and s_{345} is 1, and the limit is clean, we can find the following expression

$$A_{tree}(1^+, 2^+, 3^+, 4^-, 5^-, 6^-) = \frac{i[12]\langle45\rangle\langle4|2+3|1]^2}{[16]\langle23\rangle\langle34\rangle[56]s_{234}s_{345}}$$
$$+ \frac{i[23]\langle56\rangle\langle6|1+2|3]^2}{\langle12\rangle\langle16\rangle[34][45]s_{234}s_{345}}$$
$$+ \frac{i\langle4|2+3|1]\langle6|1+2|3]s_{123}}{\langle12\rangle\langle23\rangle[45][56]s_{234}s_{345}}. \qquad (5.46)$$

This is similar, but not exactly identical, to the expression found in the '80s [75, 110].

From a practical point of view, for floating point evaluations, we see that these three expressions are numerically unstable in different regions of phase space. The two terms in the very first expression, in the limit $\langle2|1+6|5] \to \epsilon \ll 1$, behave like ϵ^{-1}, but their sum is $\mathcal{O}(1)$. This leads to a loss of significant digits. Similarly, the second expression is numerically unstable in the limits of $\langle1|2+3|4]$, $\langle3|1+2|6]$, $\langle5|1+6|2]$ being small. The third equation is instead unstable in the doubly singular limit $s_{234} \to \epsilon$ and $s_{345} \to \epsilon$, since each term is $\mathcal{O}(\epsilon^{-2})$ but the sum is $\mathcal{O}(\epsilon^{-1})$.

The other interesting set of doubly singular limits which we mentioned at the beginning is for r_i a real pole and $r_j \notin \mathcal{D}_{\mathcal{LCD}}$. Whenever in such a limit $\mathcal{E}$ diverges less drastically than n_i, that is $n_{ij} < n_i$ where n_i is the order of the single pole r_i, it means that in this doubly singular limit r_j may be a factor in the numerator of the term containing r_i in the denominator. As explained above, more or less information can be accessed this way depending on the degeneracy of the particular phase space point, i.e. how many $r_k \neq r_i, r_j$ vanish in this limit. This type of doubly singular limits turns out to be extremely useful to keep the complexity of the numerators manageable for complicated expressions, such as three mass triangles. In the case of A_{tree}^{+++---}, we see that the following doubly singular limits are regular ($\mathcal{E} \sim \mathcal{O}(1)$), even if they involve a simple pole

$$\{\langle12\rangle, \langle3|1+2|3]\}, \{\langle12\rangle, \langle4|1+2|3]\}, \ldots, \{s_{345}, \langle3|4+5|3]\}, \{s_{345}, \langle6|1+2|3]]\}. \quad (5.47)$$

Using these observations we can write an ansatz for the expression in the form of Eq. 5.36 where the denominators $\mathcal{D}_i = \mathcal{R}_i \mathcal{S}_i$ are free from combinations of factors that would lead to a worse scaling than observed in the doubly singular limits. Alternatively, we can attempt to express $\mathcal{E}$ as a sum of terms apparently violating the doubly singular scalings, but free from spurious poles.

All the examples we gave in this section are for colour-ordered tree amplitudes and simple poles. However, the same ideas are applicable to loop-integral coefficients and rational parts, as we will see in subsequent chapters. Similarly, colour-ordering introduces welcome simplifications in the structure of the poles, in the case of QCD by restricting them to cyclically-adjacent ones, but is not strictly speaking required. For instance, in Chapter 8 we apply this method to amplitudes involving a colour-singlet (the Higgs boson) and in Chapter 9 we study, among others, gravity amplitudes, which are clearly not colour-ordered and $(DF)^2$ amplitudes, which involve non-adjacent singularities despite being colour ordered.

In the next chapter we will discuss the parametrisation and reconstruction of the numerators, which we took as given in this chapter. If necessary, in that context it should be straightforward to obtain colour factors, which would appear as rational fractions in the numerators, and it may even be possible to reconstruct the dependence on the number of colours by repeating the evaluation over different values of N_c. However, this is a complication which is easily avoided by using the colour decomposition identities reviewed in Chapter 2.

Multivariate Coefficient Reconstruction

In the previous chapter, we considered how to extract information about the analytical structure of rational expressions from numerical evaluations in singular limits. In this chapter, we will first show how this fits in the overall reconstruction procedure, and then we will take a closer look at how to obtain the remaining numerator spinor structures.

The method is based on the iterative study of singular limits, and reconstruction of pole residues, until the full analytical expression is obtained. More specifically, the following steps have to be carried out

1. evaluate $\mathcal{E}$ in singular limits to obtain the list of all factors in the least common denominator, their exponents, as well as any common factor in the numerator;

2. consider $\mathcal{E}$ in doubly singular limits to expose the dependency structure of the poles;

3. select a pole from the LCD and identify the set of necessary other factors needed in the denominator to fit its residue;

4. fit the residue, subtract the term thus obtained from $\mathcal{E}$ and reiterate from step 1.

At every iteration, at least a pole is either removed or its power reduced. We repeat the process until the expression is fully reconstructed. This process is better represented diagrammatically in Figure 6.1.
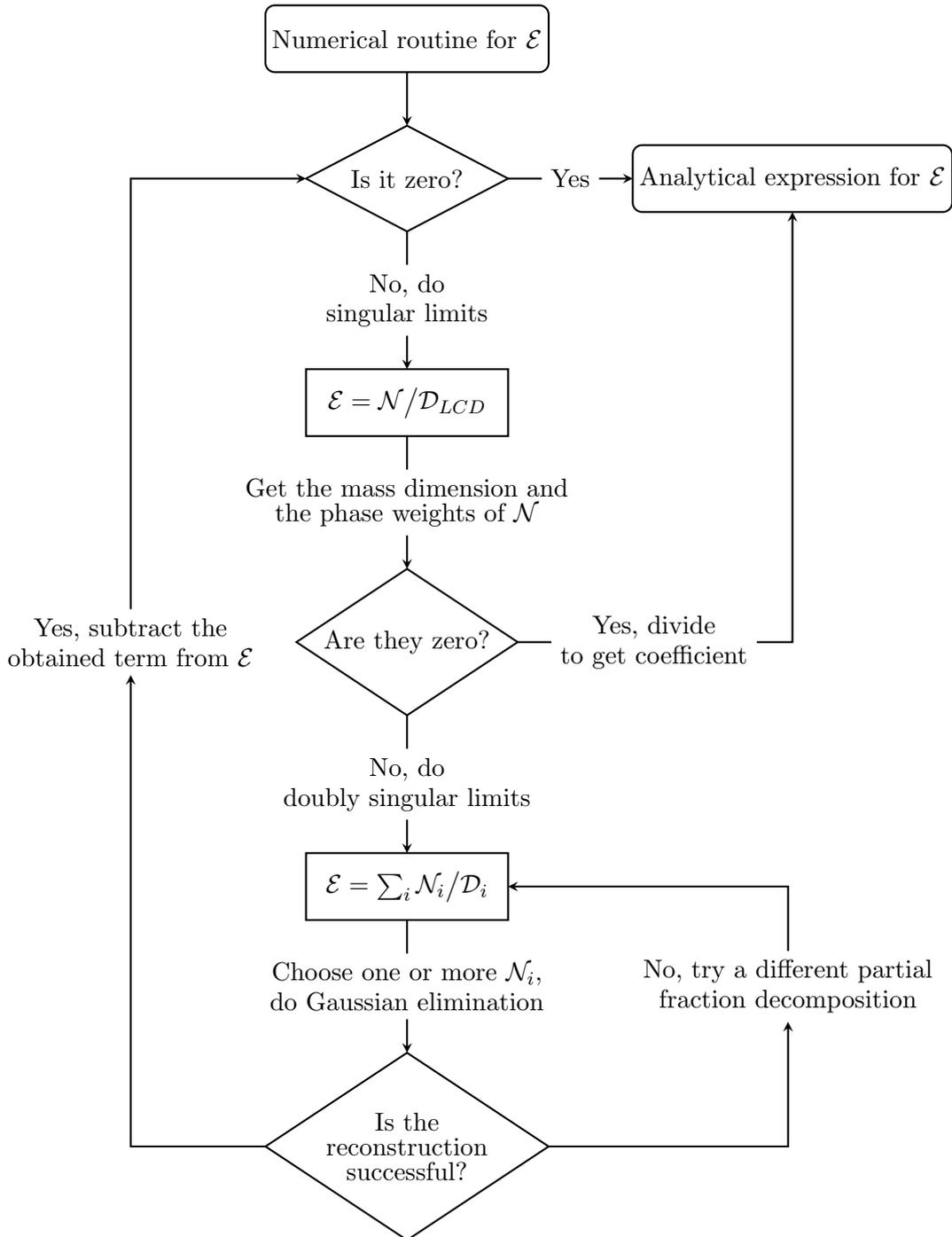
Figure 6.1: Decision tree for the analytical reconstruction strategy.

The diagram also shows that in some cases the residue reconstruction can fail. This is generally due to a bad choice for the partial fraction decomposition. As we already argued, the degeneracies in the doubly singular limits imply that multiple, equivalent expression may be possible. In some cases, decompositions that look consistent with the data from the doubly singular limits may not admit a correct numerator structure. This is generally fixed by simply trying a different denominator structure.

6.1 Numerator Ansatz and Reconstruction

In this section we discuss how to reconstruct a numerator whenever singular limits do not provide all of the required information. We start by building an ansatz out of products of spinor products $\langle i|j\rangle$ and $[i|j]$ and, if necessary, other linearly independent expressions, such as square roots of Gram determinants. However, the latter were not necessary for any of the quantities we considered so far, i.e. they are all manifestly rational expressions in spinor contractions. The coefficients of the terms in the ansatz are determined by solving a system of linear equations. The number of spinor products in each term of the ansatz can be determined by numerically inspecting the behaviour of the expression under uniform scaling of all momenta

$$p_i \to \lambda p_i \,, \qquad \langle i|j\rangle \to \lambda \langle i|j\rangle \,, \qquad [i|j] \to \lambda [i|j] \,, \qquad \forall \, i,j \in \{1,n\}. \qquad (6.1)$$

This is simply the mass dimension of the expression which needs to be determined. Alternatively, we may think of the mass dimension as the degree of the polynomial in the angle and square brackets, since they have mass dimension 1. We can further limit the size of the ansatz by looking at its phase weights. The phase weight with respect to momentum p_i is defined by the scaling of the expression under a little group transformation, i.e. a change in λ_i and $\tilde{\lambda}_i$ which leaves p_i unchanged

$$p_i \to p_i \,, \qquad |i\rangle \to t\,|i\rangle \,, \qquad [i| \to t^{-1}\,[i|. \qquad (6.2)$$

The phase weight for momentum i of the expression $\mathcal{E}$ is n if it scales as t^n. The mass dimension and phase-weights of the numerator ansatz combined with those of the denominator have to match the mass dimension and phase-weights of the expression $\mathcal{E}$. Both these concepts were already introduced in Chapter 3.

An ansatz built from all products of spinor products with the right mass dimension and phase weights is sufficient but not minimal, due to momentum conservation and Schouten identities. To ensure uniqueness of the numerator representation, we need to remove redundant elements from the ansatz by either using analytical rules or numerical Gaussian elimination. This operation only needs to be performed once per mass dimension and phase weights combination.

For our application we use a numerical Gaussian elimination implemented in the following way: for a candidate ansatz $\mathcal{A}$ with N elements $a_{j=1,\dots,N}$ we generate N distinct phase

space points P_i and build a $N \times N$ matrix M. The set of linear identities $\{v\}$ relating ansatz elements lives in the kernel of M, that is for each such identity v for which $\sum_j a_j v_j = 0$ we have

$$M_{ij} v_j = 0 \quad \text{with} \quad M_{ij} = a_j(P_i) \,. \tag{6.3}$$

Here we are not interested in the identities but merely wish to remove redundant ansatz elements that can be expressed in terms of other elements. Row-reducing M brings it in upper-triangular form and the existence of identities will manifest itself as the appearance of zeros in the diagonal of the transformed matrix. As the algorithm progresses, we remove each ansatz element that leads to a vanishing diagonal element in the transformed matrix and remove the corresponding column of M. At the end of the row-reduction procedure we are left with $N' \leq N$ elements in the ansatz. These N' elements are linearly independent.

Given a minimal ansatz, we can solve for the coefficients vector c of each term in the numerator by solving the equation

$$\sum_j \tilde{M}_{ij} \, c_j = \tilde{a}_j(P_i) \, c_j = \mathcal{E}(P_i) , \quad \Rightarrow \quad c_j = \sum_i \tilde{M}_{ji}^{-1} \mathcal{E}(P_i) \tag{6.4}$$

where $\tilde{M}$ is the matrix of the N' independent numerator ansatz elements $\tilde{a}$ that we constructed above through Gaussian elimination, divided by the corresponding denominator. $\mathcal{E}(P_i)$ is the vector of the expression $\mathcal{E}$ evaluated at the first N' phase space configurations. In all cases we considered the coefficients in c are expected to be rational numbers. The analytical, infinite precision values can be recovered from the numerical estimates obtained through the inversion in Eq. 6.4 with procedures such as that of continued fractions. One can easily check the validity of the expression obtained by testing a further distinct phase space point. Note also that the inverse $\tilde{M}^{-1}$ is not explicitly calculated: large matrix inverses constructed numerically are susceptible to instabilities. Instead, Eq. 6.4 is solved through the same row-reduction procedure used for Eq. 6.3.

Depending on the complexity of the expression to reconstruct, we can apply different strategies:

  a) full reconstruction,

  b) full reconstruction with separated denominators,

  c) iterated reconstruction by sequentially removing poles.

Furthermore, the reconstruction can be used to force an expression to be manifestly symmetric under one or more of its symmetries by symmetrising the ansatz.

mass dimension	2	4	6	8	10	12	14
independent terms	9	50	205	675	1886	4644	~12870

Table 6.1: Number of independent terms in an ansatz for six-point configurations with all zero phase weights as a function of the mass dimension.

6.1.1 Full Reconstruction

Strategy a) is the simplest and does not require doubly singular limits to be probed. Unfortunately, trying to solve for the numerator $\mathcal{N}$ of the least common denominator $\mathcal{D}_{\mathcal{LCD}}$ (see Eq. 5.24) is in general intractable. The mass dimension of $\mathcal{N}$ can easily exceed 12, with the worst of the six-point amplitudes coefficients being above 100. Table 6.1 shows the size of the minimal ansatz $\{\tilde{a}\}$ as a function of mass dimension at six-point for zero phase weights $\{0, 0, 0, 0, 0, 0\}$, extending on the information shown in Table 1.7.

For example, even the simple split-helicity tree amplitude A_{tree}^{+++---} that we considered in previous chapter in the single denominator form

$$A_{tree}(1^+, 2^+, 3^+, 4^-, 5^-, 6^-) = \frac{\mathcal{N}}{\langle 12\rangle\langle 16\rangle[16]\langle 23\rangle\langle 34\rangle[34][45][56]s_{234}s_{345}} \tag{6.5}$$

admits 1326 independent Lorentz invariant structures in $\mathcal{N}$ (mass dimension 10, phase weights $\{-1, 0, -1, 1, 0, 1\}$). This is clearly not optimal.

6.1.2 Full Reconstruction with Separated Denominator

For strategy b), we use the information from doubly singular limits to postulate possible partial fraction decompositions

$$\mathcal{E} = \sum_i \frac{\mathcal{N}_i}{\mathcal{D}_i}. \tag{6.6}$$

The denominators $\mathcal{D}_i$ are in general simpler than $\mathcal{D}_{LCD}$, and may or may not contain spurious poles. There are different ways of choosing the denominators $\mathcal{D}_i$ depending on the number of terms in the sum and which spurious poles are chosen.

We apply the technique described above to construct an ansatz for each numerator

$$\mathcal{N}_i = \sum_{j=1}^{N_i} c_{i,j} \, a_{i,j} \tag{6.7}$$

where N_i is the number of elements in the ansatz for the ith numerator $\mathcal{N}_i$. Generally the combined size of these ansatze is much less than that for the single numerator $\mathcal{N}$.

While each numerator ansatz is constructed with independent elements, the sum over the terms can still contain redundant terms. For example, if we have

$$\mathcal{E} = \frac{\mathcal{N}_A}{AB} + \frac{\mathcal{N}_B}{AC} \, , \tag{6.8}$$

a term proportional to BC in the numerator $\mathcal{N}_A$ can be moved to $\mathcal{N}_B$ and viceversa.

This redundancy can be removed with the same technique described above. In analogy to Eq. 6.3, we construct $N = \sum N_i$ distinct momentum configurations P_l and a matrix M:

$$M_{l,k} = A_k(P_l) \, , \qquad A_k(P_l) = \frac{a_{i,j}(P_l)}{\mathcal{D}_i(P_l)} \, , \qquad k = i + \sum_{\tilde{i} < i} N_{\tilde{i}} \tag{6.9}$$

where $a_{i,j}$ is the jth element of the ansatz of the ith numerator, and k enumerates through the elements of the combined ansatze of the terms in Eq. 6.6. Redundant elements are then removed with the row-reduction procedure. Once the ansatz is minimal, we can solve for the coefficients $c_{i,j}$ by inverting a numerical system of equation.

Going back to the A_{tree}^{+++---} example, we may write

$$
\begin{aligned}
A_{tree}(1^+,2^+,3^+,4^-,5^-,6^-) \;=\; & \frac{\mathcal{N}_1}{[16]\langle 23\rangle\langle 34\rangle[56]\langle 2|1+6|5]s_{234}} \\
& + \frac{\mathcal{N}_2}{\langle 12\rangle\langle 16\rangle[34][45]\langle 2|1+6|5]s_{345}}.
\end{aligned} \tag{6.10}
$$

In this case, the combined ansatz size for $\mathcal{N}_1$ and $\mathcal{N}_2$ is 20, a clear improvement from the 1326 of the single denominator form. Solving the system for $\mathcal{N}_1$ and $\mathcal{N}_2$ yields Eq. 5.42.

Even by separating the LCD into smaller denominators, the resulting system can get too large to be solved in a reasonable time. In the following sections we discuss two methods to resolve this issue through the use of singular limits and symmetries.

6.1.3   Iterated Reconstruction by Sequentially Removing Poles

For expressions for which strategies a) and b) are intractable, we use the full method outlined in the beginning of this chapter. The aim is to isolate the contribution of the highest order of a specific pole r in the expression $\mathcal{E}$. To achieve this, we identify the term i_r in Eq. 5.36 with the highest power k of the pole r, that is, we think of $\mathcal{E}$ in the form:

$$\mathcal{E} = \frac{\mathcal{N}_{i_r}}{r^k \bar{\mathcal{D}}_{i_r}} + \sum_{i \neq i_r} \frac{\mathcal{N}_i}{r^{k_i} \bar{\mathcal{D}}_i} \, , \tag{6.11}$$

where the powers of r in the denominators in the sum are lower than in the first term, i.e. $k_i < k$, and $\bar{\mathcal{D}}$ are the denominators with any power of the pole r factored out, i.e. $\mathcal{D}_i = r^{k_i} \bar{\mathcal{D}}_i$.

We can fit the numerator $\mathcal{N}_{i_r}$ in isolation if we generate the phase space points for the Gaussian elimination in the specific singular limit $r \to \epsilon$, thus making the i_r term dominant. Subtracting the term reconstructed in this limit from $\mathcal{E}$ results in an expression where the order of the pole r is decreased by one. Repeating the same operation for the new maximum power of r or for other factors reduces the mass dimension of the numerators until the remaining expression can be fitted without any particular limits.

In the example of A_{tree}^{+++---}, this method allows to obtain $\mathcal{N}_1$ in isolation from $\mathcal{N}_2$, by taking, for instance, $s_{234} \to \epsilon$. In this simple case, the ansatz size is only halved, but in cases where the partial fraction decomposition involves many terms, the improvement is much greater.

It is also possible to use doubly singular limits, especially with non-equal small parameters $\epsilon_1 \neq \epsilon_2$, to numerically isolate specific terms in the ansatz. This turns out especially useful when a simple singular limit does not isolate a single term, but still picks up a combination of terms. However, due to the degeneracies arising when multiple invariants are set small, it can be tricky to reliably identify the terms which become dominant.

There is a large amount of freedom in choosing the order in which to remove the poles, which can lead to very different forms of the reconstructed analytical expression. This freedom can be exploited for different goals. On the one hand, we can iterate through different choices to select the most compact version, in order to obtain the quickest evaluation. On the other hand, we can produce expressions that are numerically stable in specific limits by either removing the poles corresponding to the selected singular behaviour first or by avoiding the introduction of certain spurious singularities. In doing so we can produce a family of expressions, each tailored to maximise execution speed or numerical stability in specific phase-space regions.

The main bottleneck for this procedure, possibly together with the numerical computation of the rational function $\mathcal{E}$, is the row reduction of the matrix in Eq. 6.4. If the matrix is excessively large, extra floating-point precision is required, forcing the row reduction to happen on a central processing unit (CPU). However, given a reasonably efficient partial fraction decomposition (Eq. 6.11), it is sufficient to perform the Gaussian elimination with double precision[1]. In this case it can be performed significantly faster on a graphical processing unit (GPU). In Appendix E we discuss an implementation of the row reduction algorithm on NVIDIA GPUs with the CUDA parallel computing platform.

---

[1]In practice, only numerator ansatze exceeding a couple thousand entries require additional precision.

6.1.4 Reconstruction in the Presence of Symmetries

Symmetries of the coefficients also help in the analytical reconstruction. Different coefficients can be related by symmetry operations or a single coefficient may be invariant under them. In the former case, the symmetries reduce the number of coefficients we have to consider: it is sufficient to consider independent topologies. In the latter case, the number of pole residues that have to be fitted is reduced: once a pole has been removed all other poles related to it by a symmetry can also be removed by a simple symmetrisation; alternatively, if a pole is itself invariant under a symmetry, it can be made manifestly so by symmetrising the ansatz.

Ideally, one would generate an ansatz already invariant under the given symmetry. However, the use of momentum conservation and Schouten identities to make the ansatz minimal makes it complicated to have an ansatz which is at the same time minimal and which respects the given symmetry. Nevertheless, we can restore invariance under the symmetry as follows. Let us consider again Eq. 6.4 and expand upon it. Given a (minimal) ansatz $\tilde{a}_j$, let us call $\tilde{b}_j$ its image under the given symmetry. Thus, we have

$$\tilde{a}_j(P_i)\, c_j + \text{symm.} = \tilde{a}_j(P_i)\, c_j + \tilde{b}_j(P_i)\, d_j = \mathcal{E}(P_i) \,. \tag{6.12}$$

Naively, this appears to be doubling the number of coefficients to reconstruct. However, note that we must have $c_j = d_j$ for the expression to actually be invariant under the symmetry. Thus, the size of the system is actually unchanged, since we can write it as

$$\tilde{M}_{ij} c_j = \big(\tilde{a}_j + \tilde{b}_j\big)(P_i)\, c_j = \mathcal{E}(P_i) \,. \tag{6.13}$$

In fact, note that the null space of $\tilde{a}_j(P_i)$ and that of $\big(\tilde{a}_j + \tilde{b}_j\big)(P_i)$ may be different, and we may have extra redundancies in the symmetrised system (making it actually smaller than the original one). This easily handled by the Gaussian elimination, as explained beforehand. The result is guaranteed to respect the symmetry, but it may not be in a particular compact form. We can attempt to further simplify it by considering the reconstructed expression as the new input for the reconstruction, and study its behaviour in singular limits. If common factors can be factored out in the numerator they will be detected by our procedure, as long as they appear in the list of Lorentz invariants which are used to probe the expression.

As an example, let us consider pure gluon amplitudes. Symmetries are permutations of the external indices; they can be either cyclic or anti-cyclic, due to colour ordering, with anti-cyclic permutation involving a an overall factor of $(-1)^n$ from parity, where n is the

multiplicity of the phase space. Symmetries may involve a flip of all helicities, which corresponds to swapping the left and right Lorentz spinor representations. The latter operation is equivalent to complex conjugation in the case of real momenta, and is related to parity, as we saw in Chapter 2.

Therefore, we express a symmetry as a permutation of $(123...n)$, with a bar over the permutation denoting an helicity flip, and possibly a minus sign denoting anti-symmetry. Blocks of spinor helicity expressions are alternated with blocks of symmetries, with the convention that each symmetry in a symmetry block is applied to all the lines in the spinor helicity block preceding it. We have already used this notation in Eq. 3.37. Going back to that tree-level example, in the form given in Eq. 5.40, it can be written as

$$
\begin{aligned}
A_{tree}(1^+, 2^-, 3^+, 4^-, 5^+, 6^-) \;\; = \;\; & \frac{1i\langle 2|1+3|5]^4}{\langle 12\rangle\langle 23\rangle[45][56]\langle 1|2+3|4]\langle 3|1+2|6]s_{123}} \\
& + (123456 \to \overline{234561}) \\
& + (123456 \to 345612).
\end{aligned}
\tag{6.14}
$$

Symmetry blocks in general do not contain the full set of symmetries of an expression. Spinor helicity blocks are sometimes symmetric under the missing symmetries, but oftentimes a symmetry is preserved only by the full expression. For instance, the above tree amplitude has 11 symmetries in total, of which only two are used. Among other others, we can find $123456 \to 321654$, which maps the first spinor helicity line to itself, but also $123456 \to 165432$ whose action in this case is equivalent to that of $123456 \to \overline{234561}$.

One-Loop Six-gluon Amplitudes

To illustrate our reconstruction method, we obtain analytical expressions for the scalar integral coefficients of the one-loop six-gluon amplitudes with a gluon in the loop. More specifically, we obtain a complete, minimal set of independent integral coefficients for the colour-ordered helicity amplitudes $A_{n;1}^{(1)}$ (see Eq. 2.16). These amplitudes can be decomposed in terms of master scalar integrals as follows

$$\mathcal{A}_{6g;1}^{(1-loop)} = \frac{\Gamma(1+\epsilon)\Gamma(1-\epsilon)^2}{(2\pi)^{2-\epsilon}\Gamma(1-2\epsilon)} \left(\sum_i d_i I_i^4 + \sum_j c_j I_k^3 + \sum_k b_k I_k^2 + R \right), \qquad (7.1)$$

where, I_i^4, I_j^3 and I_k^2 are the scalar box, triangle, and bubble integrals respectively. The coefficients d_i, c_j, b_k and R are the rational functions of spinor products for which we applied our reconstruction method. The full list of coefficients, and their relations to the minimal set of independent ones, is given in Appendix F.

We emphasise that in extracting the analytical expressions for the coefficients we did not exploit any prior knowledge about the coefficients beyond the list of possible factors in the denominator. This list is a property of colour-ordered one-loop amplitudes with massless internal particles. Their powers and how they combine has been uncovered by the numerical exploration. More specifically, only knowledge about the general structure of these Lorentz invariants was used. We programmatically generate all strings of the form s_{ijk}, Δ_{ijk} (see Eq. 7.5), $\langle ij \rangle$, $[ij]$, $\langle i|j+k|l]$, and so forth, as shown in Eq. 5.9.

We used the BLACKHAT library [98] and its arbitrary precision implementation using the GNU Multi Precision library [111] to generate the numerical input for our method. These amplitudes were previously calculated numerically in Ref. [112] and combined to present the NLO four-jet cross section and distributions in Ref. [113] and Ref. [114].

In the accompanying files to Ref. [1] we provide expressions readable by the S@M [76] MATHEMATICA package as well as human readable formulae for a representative set of helicity configurations. All other configurations can be obtained through symmetries. We have validated all our analytical results by verifying their agreement with the output of BLACKHAT to 300 significant digits on several independent phase space points (i.e. phase space points that were not used in the determination of the coefficients of the ansatz).

In the MATHEMATICA files the results are presented with all symmetries unwrapped to make computations easier. However, to increase readability the symmetries are kept in the formulae in the human readable files, where blocks of spinor helicity expressions are alternated with blocks of symmetries. The convention is that each symmetry in a symmetry block is applied to all the lines in the spinor helicity block preceding it.

7.1   Execution Speed Comparison

For the reconstruction of the analytical expression for the integral coefficients we have treated each coefficient in isolation and did not use any knowledge about relationships between coefficients of related scalar integrals. This means that the resulting expressions could easily be re-written in a more compact way but we refrained from doing so as in the current form they are more illustrative of the type of output our method produces. This also provided us with additional validation methods for our results (for example, we checked that the sum of the bubble coefficients is proportional to the tree amplitude).

In order to assess the potential gain of using our analytical expression, we implemented the analytical expressions in BLACKHAT, which allows us to perform a comparison where the only difference is whether the numerical procedure or the analytical expressions are used. We observe significantly lower run times compared to the original numerical computation, with individual pieces receiving different speed-ups. The best speed improvement is by a factor of about 75 for the split NMHV configuration, while the worst is a factor of 2 for the alternating NMHV configuration. The remaining NMHV configuration is about 3 times faster. In the latter two cases, the analytical formulae for the cut part of the

amplitude led to slightly slower code. However, since the largest part of the calculation time in BLACKHAT is spent on the rational part, which is significantly faster analytically, we still measure an overall speed-up for the complete amplitude. On the entire cross section, the speed-up lies in between those of the various helicity configurations: it is a factor of about 4. Since the MHV and split NMHV configurations run much faster analytically than numerically, the bottlenecks for the entire cross section are the two harder NMHV configurations.

As pointed out earlier, the execution speed could be further improved if the expressions were simplified using some additional knowledge about the structure of the one-loop amplitude. Similarly, some post-processing of the reconstructed coefficients could be beneficial, but might misrepresent the method output. For instance, let us consider the following expression:

$$\mathcal{E} = \frac{\langle 1|2 + 3|5]\langle 3|1 + 2|5]^3}{\langle 13 \rangle^4} + O(\langle 13 \rangle^0). \tag{7.2}$$

Regardless of how complicated the $O(\langle 13 \rangle^0)$ part is, we can isolate the first term by considering phase space points in the $\langle 13 \rangle$ singular limit. However, since the expression above groups $\langle 13 \rangle$ sub-leading terms in $\langle 1|2 + 3|5]$ and $\langle 3|1 + 2|5]$, the reconstruction strategies presented in the previous section will yield a Laurent expansion in $\langle 13 \rangle$:

$$\begin{aligned}
\mathcal{E} = & -\frac{\langle 12 \rangle \langle 23 \rangle^3 [25]^4}{\langle 13 \rangle^4} - \frac{\langle 23 \rangle^2 [25]^3 (3\langle 12 \rangle [15] + \langle 23 \rangle [35])}{\langle 13 \rangle^3} + \\
& -\frac{[15]\langle 23 \rangle [25]^2 (3\langle 12 \rangle [15] + 3\langle 23 \rangle [35])}{\langle 13 \rangle^2} - \frac{[15]^2 [25]((\langle 12 \rangle [15] + 3\langle 23 \rangle [35])}{\langle 13 \rangle} + \\
& -[15]^3 [35] + O(\langle 13 \rangle^0)
\end{aligned} \tag{7.3}$$

The last spinor helicity term is actually itself $O(\langle 13 \rangle^0)$, and thus it would need to be obtained independently of the $\langle 13 \rangle$ singular limit, but we reproduce it here for completeness. Clearly Eq. 7.2 would evaluate much faster than Eq. 7.3.

Lastly, in some cases we stop splitting the pole structure into smaller denominators when the full reconstruction of the numerator becomes feasible. As future work, it might be interesting to try to further unravel the pole structure of such terms to potentially obtain more compact representations.
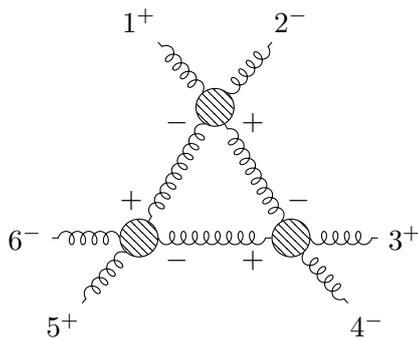
Figure 7.1: Three-mass triangle $c_{12\tilde{\times}34\tilde{\times}56\tilde{\times}}$ from Table F.9.

7.2   Rationality of the One-Loop Coefficients

Scalar loop-integral coefficients represent discontinuities across branch cuts in complex phase space and should be obtained following a *maximal* cut procedure: first all quadruple discontinuities are considered to obtain box-integral coefficients, subsequently all triple discontinuities give triangle-coefficients, and as so on. Therefore, the coefficients themselves must be free from branch cuts, or, in other words, they must be purely rational functions. Following a *reductio ad absurdum* argument, if, for instance, a triangle coefficient still contained a branch cut, then a quadruple-discontinuity should have been possible making the cut procedure not maximal. However, it is often the case that square roots appear in the loop-momentum parametrisation, e.g. in Eq. 3.69. In principle, it should always be possible to manipulate the final expression to remove such square roots, but in practice it is often not so straightforward to perform such simplifications.

It has already been shown in Ref. [81] that the coefficients of three-mass triangles in $\mathcal{N} = 1$ super Yang-Mills can be written in a manifestly rational form at six-point. We observe that this holds also without any super-symmetry, and for bubble coefficients, as well as the rational part. To achieve this, we use information on the singularity structure of these quantities, which explains why square roots of Gram determinants seem to appear and why the same behaviour can be reproduced by rational spinor structures.

For concreteness, let us consider one of the two three-mass triangles in the alternating NMHV helicity configuration shown in Figure 7.1. The real poles of this function, as obtained from the singular limits of Eq. 5.8, are:

$$\langle 12 \rangle, [12], \langle 34 \rangle, [34], \langle 56 \rangle, [56], \langle 1|3+4|2]^4, \langle 3|1+2|4]^4, \langle 5|1+2|6]^4, \Delta_{135}^3. \tag{7.4}$$

Following convention from the literature, in the above list Δ_{135} is the Gram determinant related to this diagram:

$$\Delta_{135} = (K_1 \cdot K_2)^2 - K_1^2 K_2^2, \tag{7.5}$$

where K_1 and K_2 are the sums of the momenta in any two corners of Figure 7.1.

Square roots seem to appear when we study doubly singular limits, for instance:

$$\langle 3|1+2|4] \to \epsilon, \ \Delta_{135} \to \epsilon, \quad \text{yields} \quad -\frac{\log(\mathcal{E})}{\log(\epsilon)} \to 3.5, \tag{7.6}$$

or:

$$\langle 12 \rangle \to \epsilon^3, \ \Delta_{135} \to \epsilon, \quad \text{yields} \quad -\frac{\log(\mathcal{E})}{\log(\epsilon)} \to 2.5, \tag{7.7}$$

and similarly for the other poles. Note how the asymmetric doubly singular limit in Eq. 7.7 was necessary to lift the $1/\langle 12 \rangle$ residue above the $1/\Delta_{135}^3$ one. Although this scaling can be explained by an irrational factor of $\sqrt{\Delta_{135}}$, there is a more appealing solution: in any limit exhibiting half integer scaling, Δ_{135} behaves like the square of some rational quantity, and it is sufficient to introduce this quantity in the numerator instead of $\sqrt{\Delta_{135}}$. Several such spinor structures are possible. Here we list a few with their relation to Δ_{135}:

$$(\Omega_{351})^2 \equiv (2s_{12}s_{56} - (s_{12} + s_{56} - s_{45})s_{123})^2 =$$
$$= 4s_{123}^2 \Delta_{135} - 4s_{12}s_{56}\langle 4|1+2|3]\langle 3|1+2|4] \tag{7.8}$$

$$(\Pi_{351})^2 \equiv (s_{123} - s_{124})^2 = 4\Delta_{135} - 4\langle 4|1+2|3]\langle 3|1+2|4] \tag{7.9}$$

$$(\langle 1|3+4|1] + \langle 2|3+4|2])^2 = 4\Delta_{135} + 4s_{12}s_{34} \tag{7.10}$$

$$-(s_{34} - s_{56})^2 = \Delta_{135} + \langle 12 \rangle ... \tag{7.11}$$

The first two quantities might be familiar from the numerators of the expressions obtained in Ref. [81]. The order of the subscripts in those quantities is important because there are 3 distinct ones, one for each corner of the triangle, whereas Δ_{135} is invariant under a permutation of its subscripts. As a concrete example, the $1/\Delta_{135}^3$ term is almost fully constrained by doubly singular limits and can be expressed as:

$$\frac{5/128i\langle 12\rangle[12]\langle 34\rangle[34]\langle 56\rangle[56]\langle 2|3+4|1]\langle 4|1+2|3]\langle 6|1+2|5]\Pi_{135}\Pi_{351}\Pi_{513}}{\langle 1|3+4|2]\langle 3|1+2|4]\langle 5|1+2|6]\Delta_{135}^3}. \tag{7.12}$$

The term of Eq. 7.12 is invariant under the following 5 symmetries:

$$345612, \ 561234, \ \overline{654321}, \ \overline{432165}, \ \overline{216543}. \tag{7.13}$$

The former two symmetries are pure permutations, whereas the latter three also involve a helicity flip. These are indeed the symmetries one expects from the three-mass triangle of Figure 7.1.

An issue with Eq. 7.12 is that it introduces spurious singularities in doubly singular regions where a pair of the three poles $\langle 1|3+4|2]$, $\langle 3|1+2|4]$ and $\langle 5|1+2|6]$ vanishes. This can be fixed by adding the following term:

$$\frac{5/32i\langle 12\rangle[12]\langle 34\rangle[34]\langle 56\rangle[56]\langle 2|3+4|1]\langle 4|1+2|3]\langle 6|1+2|5](\Pi_{135}+\Pi_{351}+\Pi_{513})}{\langle 1|3+4|2]\langle 3|1+2|4]\langle 5|1+2|6]\Delta_{135}^2}. \tag{7.14}$$

Finally, for comparison, the same triple pole in the bubbles reads:

$$\frac{5/256i\langle 12\rangle[12]\langle 2|3+4|1]\langle 4|1+2|3]\langle 6|1+2|5](s_{134}+s_{234})\Pi_{135}\Pi_{351}\Pi_{513}}{\langle 1|3+4|2]\langle 3|1+2|4]\langle 5|1+2|6]\Delta_{135}^3}, \tag{7.15}$$

whereas in the rational part it enters at order Δ_{135}^2 as:

$$\frac{5/96i\langle 2|3+4|1]\langle 4|1+2|3]\langle 6|1+2|5]\Pi_{135}\Pi_{351}\Pi_{513}}{\langle 1|3+4|2]\langle 3|1+2|4]\langle 5|1+2|6]\Delta_{135}^2}. \tag{7.16}$$

Expressions such as these in Eq. 7.12-7.16 exhibit a scaling consistent with square roots of Δ_{135} when considered in particular kinematic regions, but are fully rational. More generally, the use of the spinor structures in Eq. 7.8-7.11 allowed us to obtain rational analytical representations for all the pieces of the one-loop six-gluon amplitudes.

7.3   All Multiplicity One-Loop Integral Coefficients

The ultimate goal for a calculation at a given fixed order is to provide a numerical algorithm or an analytical expression valid for any multiplicity. At one-loop, the former has been achieved with numerical unitarity techniques, whereas the latter is only available for some specific cases, such as adjacent MHV amplitudes [115].

In this section, we show that fixed multiplicity results can in some cases lead to all-multiplicity expression for a class of coefficients, or, when this not possible due to new structures appearing at higher point, at least provide helpful insights. Having obtained all one-loop six-gluon integral coefficients, and, before that, all five-gluon ones, the parallel between the two becomes quite striking in some cases. For instance, consider the following two non-adjacent MHV bubble coefficient.

$$b_{5-1^+\times 2^+3^-4^+\times} = \qquad\qquad b_{6-1^+\times 2^+3^+4^-5^+\times} =$$

$$\frac{1/3i[12]^3\langle 15\rangle^2\langle 23\rangle^4}{\langle 12\rangle\langle 23\rangle\langle 24\rangle\langle 34\rangle\langle 2|1+5|2]^3}+ \qquad\qquad \frac{1/3i[12]^3\langle 16\rangle^2\langle 24\rangle^4}{\langle 12\rangle\langle 23\rangle\langle 25\rangle\langle 34\rangle\langle 45\rangle\langle 2|1+6|2]^3}+$$

$$\frac{1/2i[12]^2\langle 15\rangle\langle 23\rangle^4\langle 45\rangle}{\langle 12\rangle\langle 23\rangle\langle 24\rangle^2\langle 34\rangle\langle 2|1+5|2]^2}+ \qquad\qquad \frac{1/2i[12]^2\langle 16\rangle\langle 24\rangle^4\langle 56\rangle}{\langle 12\rangle\langle 23\rangle\langle 25\rangle^2\langle 34\rangle\langle 45\rangle\langle 2|1+6|2]^2}+$$

$$\frac{-2i[12]^2\langle 15\rangle\langle 23\rangle^3\langle 35\rangle}{\langle 12\rangle\langle 23\rangle\langle 24\rangle\langle 34\rangle\langle 2|1+5|2]^2}+ \qquad\qquad \frac{-2i[12]^2\langle 16\rangle\langle 24\rangle^3\langle 46\rangle}{\langle 12\rangle\langle 23\rangle\langle 25\rangle\langle 34\rangle\langle 45\rangle\langle 2|1+6|2]^2}+$$

$$\frac{1i[12]\langle 23\rangle^4\langle 45\rangle^2}{\langle 12\rangle\langle 23\rangle\langle 24\rangle^3\langle 34\rangle\langle 2|1+5|2]}+ \qquad\qquad \frac{1i[12]\langle 24\rangle^4\langle 56\rangle^2}{\langle 12\rangle\langle 23\rangle\langle 25\rangle^3\langle 34\rangle\langle 45\rangle\langle 2|1+6|2]}+$$

$$\frac{-4i[12]\langle 23\rangle^3\langle 35\rangle\langle 45\rangle}{\langle 12\rangle\langle 23\rangle\langle 24\rangle^2\langle 34\rangle\langle 2|1+5|2]}+$$

$$\frac{6i[12]\langle 23\rangle^2\langle 35\rangle^2}{\langle 12\rangle\langle 23\rangle\langle 24\rangle\langle 34\rangle\langle 2|1+5|2]}+$$

$$\frac{-1/3i[14]^3\langle 15\rangle^2\langle 34\rangle^3}{\langle 14\rangle\langle 23\rangle\langle 24\rangle\langle 4|1+5|4]^3}+$$

$$\frac{1/2i\langle 12\rangle[14]^2\langle 15\rangle\langle 34\rangle^3\langle 45\rangle}{\langle 14\rangle^2\langle 23\rangle\langle 24\rangle^2\langle 4|1+5|4]^2}+$$

$$\frac{1i[14]^2\langle 15\rangle^2\langle 34\rangle^3}{\langle 14\rangle^2\langle 23\rangle\langle 24\rangle\langle 4|1+5|4]^2}+$$

$$\frac{-1i\langle 12\rangle^2[14]\langle 34\rangle^3\langle 45\rangle^2}{\langle 14\rangle^3\langle 23\rangle\langle 24\rangle^3\langle 4|1+5|4]}+$$

$$\frac{-3i[14]\langle 15\rangle\langle 25\rangle\langle 34\rangle^3}{\langle 14\rangle^2\langle 23\rangle\langle 24\rangle^2\langle 4|1+5|4]}$$

$$\frac{-4i[12]\langle 24\rangle^3\langle 46\rangle\langle 56\rangle}{\langle 12\rangle\langle 23\rangle\langle 25\rangle^2\langle 34\rangle\langle 45\rangle\langle 2|1+6|2]}+$$

$$\frac{6i[12]\langle 24\rangle^2\langle 46\rangle^2}{\langle 12\rangle\langle 23\rangle\langle 25\rangle\langle 34\rangle\langle 45\rangle\langle 2|1+6|2]}+$$

$$\frac{-1/3i[15]^3\langle 16\rangle^2\langle 45\rangle^3}{\langle 15\rangle\langle 23\rangle\langle 25\rangle\langle 34\rangle\langle 5|1+6|5]^3}+$$

$$\frac{1/2i\langle 12\rangle[15]^2\langle 16\rangle\langle 45\rangle^3\langle 56\rangle}{\langle 15\rangle^2\langle 23\rangle\langle 25\rangle^2\langle 34\rangle\langle 5|1+6|5]^2}+$$

$$\frac{1i[15]^2\langle 16\rangle^2\langle 45\rangle^3}{\langle 15\rangle^2\langle 23\rangle\langle 25\rangle\langle 34\rangle\langle 5|1+6|5]^2}+$$

$$\frac{-1i\langle 12\rangle^2[15]\langle 45\rangle^3\langle 56\rangle^2}{\langle 15\rangle^3\langle 23\rangle\langle 25\rangle^3\langle 34\rangle\langle 5|1+6|5]}+$$

$$\frac{-3i[15]\langle 16\rangle\langle 26\rangle\langle 45\rangle^3}{\langle 15\rangle^2\langle 23\rangle\langle 25\rangle^2\langle 34\rangle\langle 5|1+6|5]}$$

It would not be unreasonable to conjecture that the all-multiplicity generalisation is as follows.

$$b_{n^-1+\times 2+\ldots(n-3)+(n-2)^-(n-1)^+\times} = \tag{7.17}$$

$$\frac{1/3i[12]^3\langle 1n\rangle^2\langle 2(n-2)\rangle^4}{\langle 12\rangle\ldots\langle (n-2)(n-1)\rangle\langle 2(n-1)\rangle\langle 2|1+n|2]^3}+$$

$$\frac{1/2i[12]^2\langle 1n\rangle\langle 2(n-2)\rangle^4\langle (n-1)n\rangle}{\langle 12\rangle\ldots\langle (n-2)(n-1)\rangle\langle 2(n-1)\rangle^2\langle 2|1+n|2]^2}+$$

$$\frac{-2i[12]^2\langle 1n\rangle\langle 2(n-2)\rangle^3\langle (n-2)n\rangle}{\langle 12\rangle\ldots\langle (n-2)(n-1)\rangle\langle 2(n-1)\rangle\langle 2|1+n|2]^2}+$$

$$\frac{1i[12]\langle 2(n-2)\rangle^4\langle (n-1)n\rangle^2}{\langle 12\rangle\ldots\langle (n-2)(n-1)\rangle\langle 2(n-1)\rangle^3\langle 2|1+n|2]}+$$

$$\frac{-4i[12]\langle 2(n-2)\rangle^3\langle (n-2)n\rangle\langle (n-1)n\rangle}{\langle 12\rangle\ldots\langle (n-2)(n-1)\rangle\langle 2(n-1)\rangle^2\langle 2|1+n|2]}+$$

$$\frac{6i[12]\langle 2(n-2)\rangle^2\langle (n-2)n\rangle^2}{\langle 12\rangle\ldots\langle (n-2)(n-1)\rangle\langle 2(n-1)\rangle\langle 2|1+n|2]}+$$

$$\frac{-1/3i[1(n-1)]^3\langle 1n\rangle^2\langle (n-2)(n-1)\rangle^3}{\langle 23\rangle\ldots\langle (n-3)(n-2)\rangle\langle 1(n-1)\rangle\langle 2(n-1)\rangle\langle (n-1)|1+n|(n-1)]^3}+$$

$$\frac{1/2i\langle 12\rangle[1(n-1)]^2\langle 1n\rangle\langle (n-2)(n-1)\rangle^3\langle (n-1)n\rangle}{\langle 23\rangle..\langle (n-3)(n-2)\rangle\langle 1(n-1)\rangle^2\langle 2(n-1)\rangle^2\langle (n-1)|1+n|(n-1)]^2}+$$

$$\frac{1i[1(n-1)]^2\langle 1n\rangle^2\langle (n-2)(n-1)\rangle^3}{\langle 23\rangle\ldots\langle (n-3)(n-2)\rangle\langle 1(n-1)\rangle^2\langle 2(n-1)\rangle\langle (n-1)|1+n|(n-1)]^2}+$$

$$\frac{-1i\langle 12\rangle^2[1(n-1)]\langle (n-2)(n-1)\rangle^3\langle (n-1)n\rangle^2}{\langle 23\rangle\ldots\langle (n-3)(n-2)\rangle\langle 1(n-1)\rangle^3\langle 2(n-1)\rangle^3\langle (n-1)|1+n|(n-1)]}+$$

$$\frac{-3i[1(n-1)]\langle 1n\rangle\langle 2n\rangle\langle (n-2)(n-1)\rangle^3}{\langle 23\rangle\ldots\langle (n-3)(n-2)\rangle\langle 1(n-1)\rangle^2\langle 2(n-1)\rangle^2\langle (n-1)|1+n|(n-1)]}$$

Indeed, this appears to be the case, having checked the latter expression for $n = 7$ and $n = 8$ against numerical evaluations from BLACKHAT.

We can even attempt to say something about NMHV amplitudes at all multiplicities, although we only have $n = 6$ to rely on in this case. For instance, the three-mass triangle

coefficient denoted by (see Appendix F for a definition of subscript notation)

$$c_{6-1+\tilde{\times}2+3-\tilde{\times}4+5-\tilde{\times}} \tag{7.18}$$

has a 4th order pole in the spinor variable $\langle 1|2 + 3|6]$, analogously to that of Figure 7.1. The expression we reconstructed for this pole reads

$$\frac{-1/2i\langle 13\rangle^3[46]^3 s_{123}^2(s_{456} - s_{451})}{\langle 12\rangle\langle 23\rangle[45][56]\langle 1|2 + 3|6]^4}. \tag{7.19}$$

It is then reasonable to guess that the corresponding pole in

$$c_{n-1+\tilde{\times}2+\ldots(n-4)+(n-3)-\tilde{\times}(n-2)+(n-1)-\tilde{\times}} \tag{7.20}$$

is given by

$$\frac{-1/2i\langle 1(n-3)\rangle^3[(n-2)n]^3 s_{(n-2)(n-1)n}^2(s_{(n-2)(n-1)n} - s_{(n-2)(n-1)1})}{\langle 12\rangle\ldots\langle (n-4)(n-3)\rangle[(n-2)(n-1)][(n-1)n]\langle 1|(n-2) + (n-1)|n]^4}. \tag{7.21}$$

Again, we checked numerically that this holds true for $n = 7$ and $n = 8$. However, things are not always so clear-cut. In some cases, the expressions we obtain for sub-leading poles are not yet compact enough to easily guess an all-n generalisation, and when new Lorentz structures appear things can be significantly more complicated. For example, the Δ_{624}^3 pole for the coefficient of Eq. 7.18, similarly to that of Eq. 7.12, reads

$$\frac{5/128i\langle 16\rangle[16]\langle 23\rangle[23]\langle 45\rangle[45]\langle 6|2 + 3|1]\langle 3|1 + 6|2]\langle 5|1 + 6|4]\Pi_{624}\Pi_{246}\Pi_{462}}{\langle 1|2 + 3|6]\langle 2|1 + 6|3]\langle 4|1 + 6|5]\Delta_{624}^3}. \tag{7.22}$$

If we try to guess the corresponding $\Delta_{n2(n-2)}^3$ pole for the all-multiplicity coefficient of Eq. 7.20 we realise that it is not entirely clear how some parts of the expression behave. More specifically, the pole $\langle 2|1 + 6|3]$ associated with the corner of the diagram where we want to insert additional positive helicity gluons becomes $\langle 2|1 + 7|3 + 4|2\rangle$ at seven-point, but the latter had to be obtained from singular limits again. In the following expression,

$$\frac{\langle 17\rangle[17]s_{234}\langle 56\rangle[56]\langle 7|5 + 6|1]\langle 6|1 + 7|5]\Pi_{725}}{\langle 1|5 + 6|7]\langle 5|1 + 7|6]\Delta_{725}^3}\frac{\mathcal{N}}{\langle 23\rangle\langle 34\rangle\langle 2|1 + 7|3 + 4|2\rangle} \tag{7.23}$$

the first fraction is a clear generalisation of Eq. 7.22, but the second one introduced new structures not clearly visible at six-point. The numerator $\mathcal{N}$ can be correctly reconstructed, but it has about ~ 270 non-zero entries. In analogy to Eq. 7.8-7.11, it will probably be necessary to insert new structures, such as

$$\left(\langle 2|1 + 7|5 + 6|3\rangle - \langle 2|5 + 6|1 + 7|3\rangle\right)/2 =$$
$$= \sqrt{\langle 23\rangle^2\Delta_{725} + \langle 2|1 + 7|3 + 4|2\rangle\langle 3|1 + 7|2 + 4|3\rangle} \tag{7.24}$$

in order to obtain a more compact expression, but we leave this type of study for future work.

One-Loop Higgs + Four-Parton Amplitudes

At the Large Hadron Collider the dominant mechanism for producing Higgs bosons is gluon fusion ($gg \to h$). As argued in Section 1.2.1 of the introduction, because of the relatively large strong coupling constant α_s, additional QCD radiation is often present, making the processes we consider here phenomenologically important. Gluon fusion is mediated, in the Standard Model, by a loop of massive coloured fermions. Since the Yukawa coupling (last line of Eq. 1.16) is proportional to the fermion mass, the main contribution comes from the top quark coupling to the Higgs boson. In the limit of large top mass, i.e. when the particle in the loop is unresolved, the top degree of freedom can be integrated out, giving rise to an effective field theory (EFT) in which the gluons couple directly to the Higgs boson. The effective Lagrangian reads

$$\mathcal{L}_{\text{eff}} = \frac{g_s^2}{48\pi^2 v} \, h \, G_{\mu\nu}^a G^{a,\mu\nu} \, , \tag{8.1}$$

where g_s is the strong coupling constant, v is the vacuum expectation value of the Higgs field, $G_{\mu\nu}$ is gluon field strength, and h is the Higgs boson field. This is analogous to the Fermi theory for weak interactions, which is understood as an effective theory in the limit of unresolved W bosons. The EFT in Eq. 8.1 has been used to compute higher-order corrections to the inclusive cross-section – most recently up to next-to-next-to-next-to-leading order [116, 117] – as well as rates for the production of Higgs bosons in association with up to three additional jets up to next-to-leading order [118, 119]. The effective field theory

description is expected to break down when, for example, the transverse momentum of produced gluons is of order of the top quark mass. This breakdown has most recently been investigated at NLO in ref. [120]. This kinematic regime is beginning to be explored at the LHC [121] and can give important information about the mediators in the loop that couple to the Higgs. For such configurations it is therefore important to make use of a calculation in which the full dependence on the top quark mass is retained. Such a calculation also allows a direct quantification of the breakdown of the EFT approach.

The increase in algebraic complexity between a Higgs + three-parton and a Higgs + four-parton amplitude is analogous to that between a five-gluon and a six-gluon amplitude. In fact, analytic results for the Higgs + three-parton amplitudes in the full theory have been known for a long time [122, 123], whereas the corresponding results for Higgs + four-parton amplitudes have been obtained more recently in Refs. [47, 49], and in both cases expressions for at least some of the amplitudes were too long to report. In addition, there are several automatic procedures that can provide numerical results for one-loop amplitudes [48, 124–126]. In Ref. [3] we present compact amplitudes for all contributing processes,

$$0 \to ggggh \,, \tag{8.2}$$

$$0 \to \bar{q}qggh \,, \tag{8.3}$$

$$0 \to \bar{q}q\bar{q}'q'h \,, \tag{8.4}$$

retaining all mass effects. Although our result is not new *per se*, it is the first time that a compact publishable analytic result has been obtained for all gluon helicities.

We checked our results for the amplitudes using an in-house implementation of the D-dimensional unitarity method [127], and also against a previous unitarity-based calculation [47]. Complete agreement was found at the amplitude level. Our results for the squared matrix elements are also in full agreement with those obtained using the code OpenLoops 2 [126]. A comparison of the evaluation time of squared matrix elements against both the previous code implemented in MCFM [128–130] and OpenLoops 2 indicates a speed-up by at least an order of magnitude over previously-available results. This will be beneficial for calculations requiring this amplitude in all regions of phase space, such as recent NLO predictions for Higgs boson plus 1-jet production in the full theory [120] and at large transverse momentum [131, 132].

8.1 Structure of the Calculation

We consider colour ordered amplitudes, as explained in Section 2.1.2. In addition to the colour decomposition for $0 \to gggg h$ presented in Eq. 2.18, those for $0 \to \bar{q}qggh$ and $0 \to \bar{q}q\bar{q}'q'h$ are given by

$$
\mathcal{H}_4^{\bar{q}qgg}(\{p_i, h_i, c_i, j_i\}) = i\,\frac{g_s^4}{16\pi^2}\Big(\frac{m^2}{v}\Big)\Big[(t^{c_3}\,t^{c_4})_{j_2\,j_1} H_4^{34}(1^{h_1}, 2^{-h_1}, 3^{h_3}, 4^{h_4}; h)
$$
$$
+ (t^{c_4}\,t^{c_3})_{j_2\,j_1} H_4^{43}(1^{h_1}, 2^{-h_1}, 3^{h_3}, 4^{h_4}; h)\Big], \quad (8.5)
$$
$$
\mathcal{H}_4^{4q}(\{p_i, h_i, j_i\}) = i\,\frac{g_s^4}{16\pi^2}\Big(\frac{m^2}{v}\Big)\,(t^{c_1})_{j_2\,j_1}\,(t^{c_1})_{j_4\,j_3} H_4^{4q}(1_{\bar{q}}^{h_1}, 2_q^{-h_1}, 3_{\bar{q}'}^{h_3}, 4_{q'}^{-h_3}) . \quad (8.6)
$$

Note that in principle Eq. 8.5 should also contain a term of the form $\mathrm{tr}(t^{c_3}\,t^{c_4})\delta_{j_2\,j_1}$. However, these contributions cancel at the diagram level and give no net contribution[1].

The colour-ordered amplitudes are themselves decomposed in terms of master integrals, as shown in Eq. 2.17. A set of generalised unitarity techniques are used to determined the scalar integral coefficients for boxes [80], triangles [82] and bubbles [84, 90, 133], whereas the rational part can be obtained from the mass-dependent part of triangle integral coefficients [88].

Furthermore, it is possible to manipulate the numerator tensor structures to decompose the massive fermion loop amplitude into one with a scalar in the loop plus a correction ΔF. The scalar theory has two advantages: it can be determined in the massless limits and avoids all tensor algebra. The correction term ΔF is cut constructible, lower rank than the full fermionic theory, and contributes only to certain parts of box and triangle coefficients.

Pentagon diagrams also warrant special attention, because they give raise to the only singularity which involves a mass. If we were to work with a D-dimensional loop momentum, then the master integral decomposition would explicitly contain pentagon integrals[2]

$$
A^{(1)} = \sum_i e_i I_{Pent.}^i + \sum_i d_i I_{Box}^i + \sum_i c_i I_{Tri.}^i + \sum_i b_i I_{Bub.}^i + \sum_i a_i I_{Tad.}^i + R . \quad (8.7)
$$

However, this pentagon part is not present in four dimensions because with four degrees of freedom in the loop momentum we can perform at most four unitarity cuts. In other

---

[1] We expect this cancellation to be due to some form of Furry's theorem, since this contribution arises from the $1/N_c$ photon-like term of Eq. 2.10, but we have not investigated it further.

[2] Note that if the loop momentum is made D dimensional, but the external momenta are kept in $D = 4$, then it is sufficient to add the pentagon integrals only, since any extra-dimensional component of the loop momentum can be rotated to point in a single extra dimension. No hexagons are required.

words, in $D = 4$ each pentagon integral can be written as a sum over five box integrals, each with one fewer propagator. We can write this identity as

$$
\begin{aligned}
E_0(p_1, p_2, p_3, p_4; m) &= \mathcal{C}^{(1)}_{1\times2\times3\times4} D_0(p_2, p_3, p_4; m) + \mathcal{C}^{(2)}_{1\times2\times3\times4} D_0(p_{12}, p_3, p_4; m) \\
&+ \mathcal{C}^{(3)}_{1\times2\times3\times4} D_0(p_1, p_{23}, p_4; m) + \mathcal{C}^{(4)}_{1\times2\times3\times4} D_0(p_1, p_2, p_{34}; m) \\
&+ \mathcal{C}^{(5)}_{1\times2\times3\times4} D_0(p_1, p_2, p_3; m) ,
\end{aligned}
\tag{8.8}
$$

where E_0 and D_0 are scalar pentagon and box integrals respectively, their arguments label the momenta in the corners of the diagram (with the last one left implicit), and m denotes the mass of the loop propagator. The reduction coefficients $\mathcal{C}^{(i)}$ are given by

$$
\mathcal{C}^{(i)} = -\frac{1}{2} \frac{\mathcal{N}^{(i)}(s_{12},\, s_{23},\, s_{34},\, s_{45},\, s_{51})}{16\,|S_{1\times2\times3\times4}|} ,
\tag{8.9}
$$

where the explicit numerator structures can be found in Ref. [3]. $|S_{1\times2\times3\times4}|$ is the determinant of the 5×5 matrix $[S_{1\times2\times3\times4}]_{ij} = [m^2 - \frac{1}{2}(q_{i-1} - q_{j-1})^2]$, where $q_i = \sum_{j\leq i} p_j$, with p_j the external momenta. Explicitly, the determinant is given by

$$
16\,|S_{1\times2\times3\times4}| = -s_{12}s_{23}s_{34}\langle 1|2+3|4]\langle 4|2+3|1] + m^2\,tr_5(1234)^2 .
\tag{8.10}
$$

We can understand Eq. 8.8 by considering a quadruple cut. The reduction coefficients are nothing more than the extra propagator in the pentagon evaluated on the cut which puts the other four propagators on-shell.

Although the decomposition that we use does not explicitly contain pentagon diagrams, the box coefficients we obtain contain the reduction coefficients of Eq. 8.9, multiplied by effective pentagon coefficients. Schematically, we have

$$
\text{box coef.} = \sum \text{redu. coef.} \times \text{pent. coef.} + \text{genuine box} ,
\tag{8.11}
$$

where the latter part is regular in $|S_{1\times2\times3\times4}|$, i.e. it has no contribution from the 5th propagator. The reason why we talk about *effective* pentagon coefficients, is that the decomposition of Eq. 8.11 is not unique: parts of the pentagon contribution can be reabsorbed into the genuine box part. We can exploit this freedom to explicitly eliminate the tr_5 spurious pole contributions between the pentagon and the genuine box part. This significantly improves the numerical stability of the expressions.

Similarly to the six-gluon case, we provide the full list of integral coefficients in Appendix G, whereas the full set of independent spinor-helicity expressions is too lengthy to reproduce here and can be found in Ref. [3].

8.2 High-Precision Floating-Point Reconstruction

The reconstruction strategy discussed in Chapters 5 and 6 proved useful to study these Higgs + 4-parton amplitudes as well, despite already having some form of analytical expressions. Reconstruction from numerical evaluations is particularly effective when unitarity techniques result in lengthy expressions that are hard to treat analytically using other simplification techniques, such as twistor variables. This is especially true in the case of some triangle and bubble coefficients. It is also convenient to bypass the algebra involved in removing artefacts of loop-momentum parametrisations, such as square roots and massless projections of non-lightlike external momenta [82, 96].

Apart from the $1/|S_{1\times2\times3\times4}|$ contribution from the reduction coefficients $\mathcal{C}^{(i)}$, all integral coefficients can be expressed as a sum of two terms, one which is independent of the mass, plus a term with m^2 dependence. From an analytical reconstruction point of view, factors of $1/|S_{1\times2\times3\times4}|$ can be isolated by choosing

$$m^2 = \frac{\epsilon + s_{12}s_{23}s_{34}\langle 1|2+3|4]\langle 4|2+3|1]}{tr_5(1234)^2}, \quad \text{with} \quad \epsilon \ll 1. \tag{8.12}$$

This is similar to a singular limit, but instead of manipulating momenta we manipulate the mass of the particle in the loop. By analysing the behaviour of box coefficients in this limit, a relation between the number of powers of m in the effective pentagon coefficient and the degree of the tr_5 spurious pole becomes apparent. This led us to the form of $|S_{1\times2\times3\times4}|$ given in Eq. 8.10.

The rest of the coefficients can be first reconstructed at $m = 0$, to obtain the part independent from the mass. This can then be subtracted from the numerical evaluation and the mass set to 1 to obtain the m^2 part of the coefficients. This easily accommodates a massive loop momentum in a framework built on massless kinematics.

The other slight complication arises from the Higgs momentum, which is the only external non-massless one. The easiest solution is to treat the Higgs as a pair of massless particles, which can be thought of as its decay products. For this reason, the kinematics of these Higgs + 4-parton amplitudes closely resembles that of six-gluon amplitudes. Using massless six-point kinematics to describe these processes results in a slight over-parametrisation, since, for instance, all coefficients must be symmetric under exchange of the momenta of the two massless decay products of the Higgs. In the end, we always remove any explicit dependence on the Higgs momentum using momentum conservation.

Finally, all the expressions we obtain are manifestly rational. In fact, the analysis of Section 7.2 is perfectly applicable in this context as well. For example, let us consider the following bubble coefficient in $0 \to g^+ g^- g^+ g^- h$ [3]

$$
\begin{aligned}
b_{34}(1^+, 2^-, 3^+, 4^-) \ = \ & \frac{3}{8} \frac{\langle 2|3+4|1] \langle 4|1+2|3] (s_{123} - s_{124})(s_{234} - s_{134})(s_{134} + s_{234})}{\langle 1|3+4|2] \langle 3|1+2|4] \Delta_{135}^2} \\
& + \mathcal{O}(\Delta_{135}^{-1}) \,.
\end{aligned}
\tag{8.13}
$$

First of all, note that it is manifestly symmetric under $(1234 \to \overline{2143})$, as expected. Secondly, note that the exact same structures as in Eq. 7.8-7.11 appear in the numerator to explain half-integer behaviour in doubly singular limits involving the Gram determinant. The similarity to Eq. 7.15 is striking, with the main difference being the absence of the $\langle 5|1+2|6]$ pole.

---

[3] There is a factor of 4 difference between the definition of Δ in Eq. 3.69 and that used in Ref. [3].

DF2 and Gravity Tree Amplitudes

In this chapter we consider how to recover analytical expressions for the tree-level scattering amplitudes discussed in Chapter 4. There are several reasons why analytical expressions are preferable to numerical ones, such as execution speed, numerical stability and general understanding of their analytical structure. The same reconstruction technique can be applied to all the theories from Table 4.1. In the accompanying files to Ref. [2] we provide sample analytical amplitudes for all these theories up to six-point. The results are given both in human readable format and as expressions readable by the `S@M Mathematica` package [76].

Here, we are going to explicitly discuss only the reconstruction of $(\mathrm{DF})^2$ and conformal gravity amplitudes, since they are the ones with a less well known analytical structure and therefore the most interesting to analyse. These theories are related by a double copy relation, similar to that between Yang-Mills and Einstein gravity, namely: $(\mathrm{DF})^2 \times \mathrm{YM} \sim CG$. $(\mathrm{DF})^2$ and conformal gravity present issues with renormalisability and unitarity, since for instance $(\mathrm{DF})^2$ is built out of dimension-six operators, as implied by the name. Despite this, they are of interest for a few reasons. Namely, one type of conformal gravity arises in Berkovits-Witten twistor string [134], it is the zero-mass limit of a mass-deformed theory that reproduces Einstein gravity in the infinite-mass limit [135], and it may be useful for computing Einstein gravity amplitude in curved backgrounds for cosmological applications [136, 137].

More specifically, in the following paragraphs we are going to provide: a) the first complete set of five-point $(\mathrm{DF})^2$ amplitudes (one of which we could confirm numerically with that found in Ref. [138]); b) an alternative expression to that of Ref. [134] for the five-point MHV conformal gravity amplitude; c) results for the leading three-particle sigularities of the six-point amplitudes in the MHV and NMHV helicity sectors. All the amplitudes we present are written in the spinor helicity language and are free from spurious singularities, unless explicitly stated. We think that, in order to obtain similar complete results at six-point, it could be necessary to use spurious sigularities (potentially of order higher than 1) which would introduce a further complication in the analysis.

We make use of the high floating-point precision provided by seampy and follow the reconstruction strategy discussed so far. Briefly summarised, we study the behaviour of amplitudes in singular limits of complex phase space to obtain the poles and their degrees. We then study the amplitudes in doubly singular regions to obtain information about the structure of the denominators of the amplitude. Using this information, we generate ansätze for the residues of different poles and solve linear systems for the coefficients of bases of spinor expressions in the numerators. If a reconstructed ansatz is correct, once subtracted from the numerical amplitude, it removes a singularity. We repeat the procedure until the amplitude is fully reconstructed.

Explicit examples are discussed in the following subsections.

9.1 Five-Point Amplitudes

$(\mathbf{DF})^2$: Five-Point All-Plus (explained example)

In contrast to QCD amplitudes, five-point $(\mathrm{DF})^2$ amplitudes are non-zero for all helicity configurations even at tree level. They are color ordered, like QCD, because their CHY-integrand contains the Parke-Taylor-like cyclic factor C_n of Eq. 4.24. Therefore, the symmetry group is restricted to cyclic and anti-cyclic permutations. It can be generated from two operations, which can be thought of as the rotations and reflections of a pentagon (i.e. the dihedral group D_5):

$$(12345 \to 23451) \quad \text{and} \quad (12345 \to -15432) \,. \tag{9.1}$$

The minus sign in the reflection comes from the partity operation applied to vector particles ($J^P = 1^-$). In total the group contains 10 elements (including the identity).

The poles and their order, as well as any common factor in the numerator, can be obtained by studying the behaviour of the amplitude in singular limits, as discussed in Section 5.1. We can see how this procedure works in practice in the case of angle and square spinor brackets with the following code snippet, which can be run with the packages discussed in the Appendices C and D:

```
>>> from __future__ import unicode_literals
>>> from lips import Particles
>>> from seampy import NumericalAmplitude
>>> import mpmath


>>> oDF2Amp = NumericalAmplitude("DF2", helconf="++++")
>>> oParticles = Particles(oDF2Amp.multiplicity)
>>> oParticles.set("⟨1|2⟩", 10 ** -30)
>>> a = oDF2Amp(oParticles)
>>> oParticles.set("⟨1|2⟩", 10 ** -31)
>>> b = oDF2Amp(oParticles)
>>> round(mpmath.log(abs(b)/abs(a))/mpmath.log(10))
2.0  # this is the order of the pole ⟨1|2⟩
```

What the above code does is to compute the amplitude at two phase space points and to calculate the slope of the line going through the two points in a log-log plot (Amplitude vs. spinor invariant), just like we showed in Figure 5.1.

Following this same procedure with the rest of the spinor invariants we obtain a first look at the analytical structure of the all plus amplitude:

$$A_{(\text{DF})^2}(1^+,\, 2^+,\, 3^+,\, 4^+,\, 5^+) = \frac{\mathcal{N}}{\langle 12 \rangle^2 \langle 13 \rangle \langle 14 \rangle \langle 15 \rangle^2 \langle 23 \rangle^2 \langle 24 \rangle \langle 25 \rangle \langle 34 \rangle^2 \langle 35 \rangle \langle 45 \rangle^2}\,, \tag{9.2}$$

where $\mathcal{N}$ is some numerator structure.

Two comments are now in order. Firstly, note that the adjacent particle singularities are of second order. This reflects the fact that this theory has a quartic propagator instead of the usual quadratic one. Secondly, although in this case it is possible to obtain an expression for the numerator $\mathcal{N}$, it is often not feasible to do so in this single fraction representation, especially with higher point amplitudes; and even when it is possible, the result is complicated and obscures the structure of the amplitude.

	$\langle 13 \rangle$	$\langle 14 \rangle$	$\langle 15 \rangle$	$\langle 23 \rangle$	$\langle 24 \rangle$	$\langle 25 \rangle$	$\langle 34 \rangle$	$\langle 35 \rangle$	$\langle 45 \rangle$
$\langle 12 \rangle$	2	2	2	2	2	2	3	2	3

Table 9.1: Doubly singular limits for $\langle 12 \rangle$ in $A_{(\mathrm{DF})^2}(1^+, 2^+, 3^+, 4^+, 5^+)$

In order to obtain a compact representation, we want to write the amplitude as a sum of fractions, each of which should have a simpler denominator structure than the expression above. It is generally convenient to start by considering the double poles, since they make it difficult to numerically access the corresponding simple poles. To study the doubly singular limits, we can use the same code snippet as above, by replacing the `oParticles.set` function with the `oParticles.set_pair` one. For example, for the pair $\langle 12 \rangle$, $\langle 23 \rangle$ we have:

```
>>> oParticles.set_pair("⟨1|2⟩", 10 ** -30, "⟨2|3⟩", 10 ** -30)
```

By repeating the same procedure with all pairs involving $\langle 12 \rangle$ and recording the behaviour of the amplitude in the corresponding doubly singular limit we can generate Table 9.1. Since $\langle 12 \rangle$ is already a double pole, it is not likely for any other invariant appearing with a 2 in the table to be in the same denominator as $\langle 12 \rangle^2$. Therefore, we make an ansatz where only $\langle 34 \rangle$ and $\langle 45 \rangle$ (as simple poles) appear together with $\langle 12 \rangle^2$. More rigorously, we conjecture that:

$$\lim_{\langle 12 \rangle \to 0} A_{(\mathrm{DF})^2}(1^+, 2^+, 3^+, 4^+, 5^+) = \frac{\mathcal{N}_{12}}{\langle 12 \rangle^2 \langle 34 \rangle \langle 45 \rangle} + O(\langle 12 \rangle^{-1}). \tag{9.3}$$

To check whether the above is true or not, we start by noting that the amplitude has mass dimension of 1 and little group weights of $[-2, -2, -2, -2, -2]$. Therefore, the numerator in the RHS must have mass dimension 5 and little group weights $[0, 0, -1, 0, -1]$ in order to match the LHS. We then generate a complete set of linearly independent products of spinor invariants consistent with these constraints. In this specific case, the basis contains 20 independent entries:

$\langle 12 \rangle \langle 13 \rangle [13][13][25]$, $\langle 12 \rangle \langle 15 \rangle [13][15][25]$, $\langle 12 \rangle \langle 23 \rangle [13][23][25]$, $\langle 12 \rangle \langle 25 \rangle [13][25][25]$,

$\langle 12 \rangle \langle 35 \rangle [13][25][35]$, $\langle 13 \rangle \langle 13 \rangle [13][13][35]$, $\langle 13 \rangle \langle 15 \rangle [13][15][35]$, $\langle 13 \rangle \langle 23 \rangle [13][23][35]$,

$\langle 13 \rangle \langle 25 \rangle [12][35][35]$, $\langle 13 \rangle \langle 25 \rangle [13][25][35]$, $\langle 13 \rangle \langle 35 \rangle [13][35][35]$, $\langle 15 \rangle \langle 15 \rangle [15][15][35]$,

$\langle 15 \rangle \langle 25 \rangle [15][25][35]$, $\langle 15 \rangle \langle 35 \rangle [15][35][35]$, $\langle 23 \rangle \langle 23 \rangle [23][23][35]$, $\langle 23 \rangle \langle 25 \rangle [23][25][35]$,

$\langle 23 \rangle \langle 35 \rangle [23][35][35]$, $\langle 25 \rangle \langle 25 \rangle [25][25][35]$, $\langle 25 \rangle \langle 35 \rangle [25][35][35]$, $\langle 35 \rangle \langle 35 \rangle [35][35][35]$.

Note that, the basis would have 290 entries if we were to generate it for the numerator of Eq. 9.2. Moreover, since we are not working in a generic phase space region but in the limit of small $\langle 12 \rangle$, it turns out that 10 of the 20 basis elements only contribute to the $O(\langle 12 \rangle^{-1})$ part of Eq. 9.3, and thus can be ignored. We can now generate 10 random phase space points in the $\langle 12 \rangle \to \epsilon \ll 1$ region and solve for the coefficients of the 10 elements. The solution has only one non zero coefficient:

$$\mathcal{N}_{12} = i[12]\langle 13 \rangle \langle 25 \rangle [35]^2. \tag{9.4}$$

To obtain the remaining four double poles, we can simply symmetrise the expression for the $\langle 12 \rangle$ double pole by applying the following cyclic permutations:

$$(12345 \to 23451), \quad (12345 \to 34512), \quad (12345 \to 45123), \quad (12345 \to 51234). \tag{9.5}$$

Once an expression for a particular pole has been reconstructed, it can be numerically subtracted from the amplitude and the left over quantity will not contain that particular singularity anymore. Its singular limits can then be studied, ansätze made and reconstructions performed until all the poles have been successfully obtained and the amplitude fully reconstructed.

The final result for the all plus $(\text{DF})^2$ amplitude follows. On the left hand side, we give the amplitude written using the symmetries discussed above. This is the notation discussed in Section 6.1.4. For the sake of clarity, below we reproduce on the right hand side the same expression with the meaning of the symmetries made explicit.

$$A_{(\text{DF})^2}(1^+, 2^+, 3^+, 4^+, 5^+) =$$

$$\frac{i[12]\langle 13 \rangle \langle 25 \rangle [35]^2}{\langle 12 \rangle^2 \langle 34 \rangle \langle 45 \rangle} + \frac{i[14][24][35]}{\langle 12 \rangle \langle 35 \rangle} +$$

$$(12345 \to 23451) +$$

$$(12345 \to 34512) +$$

$$(12345 \to 45123) +$$

$$(12345 \to 51234) +$$

$$\frac{2i[15][23]\langle 4|1+2|4]}{\langle 12 \rangle \langle 34 \rangle \langle 45 \rangle} +$$

$$\frac{2i[12][45]\langle 3|1+5|3]}{\langle 15 \rangle \langle 23 \rangle \langle 34 \rangle} +$$

$$\frac{2i[12][15][34]}{\langle 23 \rangle \langle 45 \rangle}$$

$$A_{(\text{DF})^2}(1^+, 2^+, 3^+, 4^+, 5^+) =$$

$$\frac{i[12]\langle 13 \rangle \langle 25 \rangle [35]^2}{\langle 12 \rangle^2 \langle 34 \rangle \langle 45 \rangle} + \frac{i[14][24][35]}{\langle 12 \rangle \langle 35 \rangle} +$$

$$\frac{i\langle 13 \rangle [14]^2[23]\langle 24 \rangle}{\langle 15 \rangle \langle 23 \rangle^2 \langle 45 \rangle} + \frac{i[14][25][35]}{\langle 14 \rangle \langle 23 \rangle} +$$

$$\frac{i\langle 24 \rangle [25]^2[34]\langle 35 \rangle}{\langle 12 \rangle \langle 15 \rangle \langle 34 \rangle^2} + \frac{i[13][14][25]}{\langle 25 \rangle \langle 34 \rangle} +$$

$$\frac{i[13]^2\langle 14 \rangle \langle 35 \rangle [45]}{\langle 12 \rangle \langle 23 \rangle \langle 45 \rangle^2} + \frac{i[13][24][25]}{\langle 13 \rangle \langle 45 \rangle} +$$

$$\frac{i\langle 14 \rangle [15][24]^2\langle 25 \rangle}{\langle 15 \rangle^2 \langle 23 \rangle \langle 34 \rangle} + \frac{i[13][24][35]}{\langle 15 \rangle \langle 24 \rangle} +$$

$$\frac{2i[15][23]\langle 4|1+2|4]}{\langle 12 \rangle \langle 34 \rangle \langle 45 \rangle} +$$

$$\frac{2i[12][45]\langle 3|1+5|3]}{\langle 15 \rangle \langle 23 \rangle \langle 34 \rangle} +$$

$$\frac{2i[12][15][34]}{\langle 23 \rangle \langle 45 \rangle}$$

$(\mathbf{DF})^2$: Five-Point Single-Minus

The single minus amplitude has a single element in its symmetry group besides the identity, namely $(12345 \to -43215)$, and is slightly more complicated than the all plus one.

$$A_{(\mathrm{DF})^2}(1^+, 2^+, 3^+, 4^+, 5^-) =$$

$$\frac{i/2[23]\langle 25\rangle^3\langle 34\rangle[45]}{\langle 12\rangle\langle 14\rangle\langle 23\rangle^2\langle 24\rangle} + \frac{[23]\langle 35\rangle(-i/2[12]\langle 13\rangle\langle 25\rangle + i/2\langle 15\rangle[15]\langle 35\rangle)}{\langle 13\rangle\langle 14\rangle\langle 23\rangle\langle 34\rangle} +$$

$$(12345 \to -43215) +$$

$$\frac{i[12]\langle 14\rangle\langle 15\rangle\langle 25\rangle\langle 35\rangle[45]}{\langle 12\rangle^2\langle 13\rangle\langle 34\rangle^2} + \frac{i\langle 35\rangle\mathcal{N}}{\langle 12\rangle\langle 15\rangle\langle 23\rangle\langle 34\rangle\langle 45\rangle} +$$

$$\frac{-i[12]\langle 14\rangle\langle 23\rangle[24]\langle 25\rangle\langle 45\rangle}{\langle 12\rangle\langle 13\rangle\langle 24\rangle\langle 34\rangle^2} + \frac{-i[14][24]\langle 25\rangle\langle 45\rangle}{\langle 13\rangle\langle 23\rangle\langle 24\rangle} + \frac{-i[13][14]^2[24]}{[15]\langle 23\rangle[45]} \quad,$$

In the above $\mathcal{N}$ is given by

$$\mathcal{N} = ([12][13]\langle 15\rangle^2\langle 25\rangle + [13]^2\langle 15\rangle^2\langle 35\rangle + [12]\langle 15\rangle[23]\langle 25\rangle^2$$

$$+ [13]\langle 15\rangle[23]\langle 25\rangle\langle 35\rangle + [23]^2\langle 25\rangle^2\langle 35\rangle) .$$

$(\mathbf{DF})^2$: Five-Point MHV (adjacent)

This MHV amplitude is the only one we could already find in the literature, specifically in Ref. [138], where it was written in terms of Mandelstam invariants. The expression we provide is more concise, makes its symmetry explicit and is free from spurious singularities. We have numerically checked that the two expressions agree. The one we found follows.

$$A_{(\mathrm{DF})^2}(1^+, 2^+, 3^+, 4^-, 5^-) =$$

$$\frac{i[12]\langle 14\rangle^2\langle 25\rangle^2\langle 45\rangle}{\langle 12\rangle^2\langle 15\rangle\langle 23\rangle\langle 34\rangle} + \frac{[13]\langle 45\rangle(i\langle 12\rangle[12] + i/2\langle 13\rangle[13] + i\langle 14\rangle[14])}{\langle 12\rangle\langle 23\rangle[45]} +$$

$$\frac{i[13]^2\langle 14\rangle\langle 35\rangle}{\langle 12\rangle\langle 23\rangle[45]} + \frac{-i[12]\langle 14\rangle\langle 25\rangle\langle 45\rangle^2}{\langle 12\rangle\langle 15\rangle\langle 23\rangle\langle 34\rangle} + \frac{i[12][13]\langle 15\rangle\langle 34\rangle}{\langle 13\rangle\langle 23\rangle[45]} +$$

$$(12345 \to -32154) +$$

$$\frac{i\langle 13\rangle[13][15][34]\langle 45\rangle}{\langle 12\rangle\langle 23\rangle[45]^2} + \frac{-i[12][13]^2[23]}{[15][34][45]} \quad.$$

$(\mathbf{DF})^2$: Five-Point MHV (non-adjacent)

The following is the last independent five-point amplitude. All others can be obtained by permutations and/or conjugation of the amplitudes presented here.

$$A_{(\mathrm{DF})^2}(1^+, 2^+, 3^-, 4^+, 5^-) =$$

$$\frac{i[12]\langle 15\rangle^2\langle 23\rangle\langle 35\rangle}{\langle 12\rangle^2\langle 14\rangle\langle 45\rangle} + \frac{i[34]\langle 35\rangle^3}{\langle 12\rangle\langle 15\rangle\langle 24\rangle} + \frac{i[12]\langle 23\rangle\langle 35\rangle^2}{\langle 12\rangle\langle 24\rangle\langle 34\rangle} +$$

$$(12345 \to -21543) +$$

$$\frac{i\langle 35\rangle\mathcal{N}}{\langle 12\rangle\langle 14\rangle\langle 24\rangle} +$$

$$\frac{i[14][24]\langle 35\rangle}{\langle 12\rangle[35]} + \frac{-i[12][14]^2[24]^2}{[15][23][34][45]}$$

In the above $\mathcal{N}$ is given by

$$\mathcal{N} = ([12]\langle 13\rangle\langle 25\rangle + \langle 13\rangle[13]\langle 35\rangle + \langle 15\rangle[15]\langle 35\rangle$$

$$+ \langle 23\rangle[23]\langle 35\rangle + \langle 25\rangle[25]\langle 35\rangle + 2\langle 35\rangle^2[35])$$

Conformal Gravity: Five-Point MHV

An all-multiplicities expression for MHV conformal gravity amplitudes exists thanks to work by Berkovits and Witten [134]. Here we present an expression specific to five point which makes manifest the absence of terms with pairs of double poles.

$$A_{CG}(1^{++}, 2^{++}, 3^{++}, 4^{--}, 5^{--}) =$$

$$\frac{-i[12]^2\langle 24\rangle[34]\langle 45\rangle^5}{\langle 12\rangle^2\langle 23\rangle\langle 34\rangle\langle 35\rangle} + \frac{i[12]^2[13]\langle 15\rangle\langle 45\rangle^4}{\langle 12\rangle\langle 13\rangle\langle 23\rangle\langle 35\rangle} +$$

$$(12345 \to 23145) + (12345 \to 31245) +$$

$$\frac{-2i[12][13][23]\langle 45\rangle^4}{\langle 12\rangle\langle 13\rangle\langle 23\rangle}$$

9.2 Six-Point Partial Results

$(\mathbf{DF})^2$: Six-Point MHV (adjacent) (partial)

In order to convey the increase in complexity that a six-point amplitude entails, here we present an expression for the three-particle double poles as well as for the simple poles of non-adjacent three-particle singularities in a six-point MHV $(\mathrm{DF})^2$ amplitude.

$$A_{(\mathrm{DF})^2}(1^+, 2^+, 3^+, 4^+, 5^-, 6^-) =$$

$$\frac{i[13][46]\langle 56\rangle \mathcal{N}_1}{\langle 12\rangle\langle 23\rangle\langle 45\rangle[56]^2 s_{123}^2} + \frac{i[12][34]\langle 26\rangle\langle 35\rangle \mathcal{N}_2}{\langle 12\rangle^2[16]\langle 34\rangle[45] s_{345}^2} +$$

$$\frac{-i[14][24][35][36]\langle 56\rangle}{\langle 12\rangle[56]^2 s_{124}} + \frac{-i[12]\langle 15\rangle\langle 25\rangle[34][45]\langle 46\rangle}{\langle 12\rangle^2\langle 34\rangle[56] s_{125}} +$$

$$\frac{i[14]^2[23]\langle 26\rangle\langle 36\rangle[46]}{\langle 23\rangle^2[45][56] s_{145}} + \frac{-i[14][23]\langle 26\rangle\langle 5|1+4|2]}{\langle 14\rangle\langle 23\rangle[56] s_{145}} +$$

$$(123456 \rightarrow 432165) +$$

$$\frac{-i[12][14]\langle 15\rangle[34]\langle 46\rangle}{\langle 12\rangle\langle 34\rangle[56] s_{125}} + \frac{-i[13]^2[24]^2\langle 25\rangle\langle 36\rangle}{\langle 13\rangle[16]\langle 24\rangle[45] s_{245}} +$$

$$\frac{\mathcal{N}}{\langle 12\rangle^2\langle 13\rangle\langle 14\rangle\langle 16\rangle[16]\langle 23\rangle^2\langle 24\rangle\langle 34\rangle^2\langle 45\rangle[45][56]^2 s_{123} s_{234} s_{345}}$$

Where $\mathcal{N}_1$ and $\mathcal{N}_2$ are given by:

$$\begin{aligned}
\mathcal{N}_1 = (& -2\langle 12\rangle^2[12]^2\langle 24\rangle[24] - 2\langle 12\rangle^2[12]^2\langle 25\rangle[25] - 2\langle 12\rangle^2[12][13][24]\langle 34\rangle \\
& -2\langle 12\rangle^2[12][13][25]\langle 35\rangle - \langle 12\rangle^2[12][14][25]\langle 45\rangle - 2\langle 12\rangle[12]^2\langle 13\rangle\langle 24\rangle[34] \\
& -2\langle 12\rangle[12]^2\langle 13\rangle\langle 25\rangle[35] - 2\langle 12\rangle[12]\langle 13\rangle[13]\langle 34\rangle[34] - 2\langle 12\rangle[12]\langle 13\rangle[13]\langle 35\rangle[35] \\
& -\langle 12\rangle[12]\langle 13\rangle[14][35]\langle 45\rangle - \langle 12\rangle[12]^2\langle 14\rangle\langle 25\rangle[45] - \langle 12\rangle[12][13]\langle 14\rangle\langle 35\rangle[45] \\
& +\langle 12\rangle[12]\langle 23\rangle[24][35]\langle 45\rangle + \langle 12\rangle[12][23]\langle 24\rangle\langle 35\rangle[45] + \langle 12\rangle[13][23]\langle 34\rangle\langle 35\rangle[45] \\
& + [12]\langle 13\rangle\langle 23\rangle[34][35]\langle 45\rangle)
\end{aligned}$$

$$\begin{aligned}
\mathcal{N}_2 = (& +3\langle 12\rangle[12]\langle 13\rangle[13][34] - 2\langle 12\rangle\langle 13\rangle[13]^2[24] - \langle 12\rangle[13]\langle 14\rangle[14][24] \\
& +\langle 12\rangle[12]\langle 15\rangle[15][34] - \langle 12\rangle[13][14]\langle 15\rangle[25] - \langle 12\rangle[13]\langle 23\rangle[23][24] \\
& -\langle 12\rangle[15][23][24]\langle 25\rangle + \langle 13\rangle^2[13]^2[34] - \langle 13\rangle[13]^2\langle 15\rangle[45] \\
& +\langle 13\rangle[13]\langle 15\rangle[15][34] + \langle 13\rangle[13]\langle 23\rangle[23][34] - \langle 13\rangle[13][23]\langle 25\rangle[45] \\
& +\langle 13\rangle[15][23]\langle 25\rangle[34] - \langle 14\rangle^2[14]^2[34] - [13]\langle 14\rangle[14]\langle 15\rangle[45] \\
& -\langle 14\rangle[14]\langle 15\rangle[15][34] - \langle 14\rangle[14]\langle 24\rangle[24][34] - [13]\langle 14\rangle[24]\langle 25\rangle[45] \\
& -\langle 14\rangle[15][24]\langle 25\rangle[34] - [13]\langle 15\rangle^2[15][45] - \langle 15\rangle[15][23]\langle 25\rangle[45])
\end{aligned}$$

In the above expression $\mathcal{N}$ would contain several thousand terms. It is therefore crucial to identify appropriate ways to perform a partial fraction decomposition, since smaller denominators would in turn imply smaller numerators and thus easier systems of linear equations to generate and solve. However, further studies will be necessary to check whether such a decomposition requires the introduction of spurious singularities, like for NMHV amplitudes in Yang-Mills, and if so what form these spurious poles would take.

Conformal Gravity: NMHV (partial)

To conclude, we present an expression for the three-particle double poles in the six-point NMHV conformal gravity amplitude. To the best of our knowledge this is the first analytical result, albeit a partial one, for NMHV conformal gravity amplitudes.

$$A_{CG}(1^{++}, 2^{++}, 3^{++}, 4^{--}, 5^{--}, 6^{--}) =$$

$$\frac{i[23]^4\langle 56\rangle^4 \mathcal{N}_1}{\langle 15\rangle\langle 16\rangle\langle 23\rangle^2[24][34][56]^2 s_{234}^2} +$$

$$(123456 \to 312645) + (123456 \to 231564) + (123456 \to 312564) +$$

$$(123456 \to 231645) + (123456 \to 312456) + (123456 \to 231456) +$$

$$(123456 \to 123645) + (123456 \to 123564) +$$

$$\frac{\mathcal{N}}{(\langle 12\rangle^2\langle 13\rangle^2\langle 14\rangle[14]\langle 15\rangle[15]\langle 16\rangle[16]\langle 23\rangle^2\langle 24\rangle[24]\langle 25\rangle[25]\langle 26\rangle[26]\langle 34\rangle[34]}$$

$$\times \langle 35\rangle[35]\langle 36\rangle[36][45]^2[46]^2[56]^2 s_{124}s_{125}s_{134}s_{135}s_{145}s_{234}s_{235}s_{245}s_{345})$$

In the above $\mathcal{N}_1$ is given by

$$
\begin{aligned}
\mathcal{N}_1 = \big(&- [12]^2\langle 13\rangle[15]\langle 23\rangle\langle 24\rangle^2[36] + [12]\langle 13\rangle[13][15]\langle 23\rangle\langle 24\rangle^2[26] - [12]\langle 13\rangle[13][15]\langle 23\rangle\langle 24\rangle\langle 34\rangle[36] \\
&+ \langle 13\rangle[13]^2[15]\langle 23\rangle\langle 24\rangle[26]\langle 34\rangle + [12]^2\langle 14\rangle[15]\langle 23\rangle^2\langle 24\rangle[36] - [12][13]\langle 14\rangle[15]\langle 23\rangle^2\langle 24\rangle[26] \\
&- [12]\langle 14\rangle[14][15]\langle 23\rangle\langle 24\rangle\langle 34\rangle[36] + [13]\langle 14\rangle[14][15]\langle 23\rangle\langle 24\rangle[26]\langle 34\rangle - [12][13]\langle 23\rangle^2\langle 24\rangle^2[25][26] \\
&- 2[12][13]\langle 23\rangle^2\langle 24\rangle[25]\langle 34\rangle[36] - [12][13]\langle 23\rangle^2\langle 34\rangle^2[35][36] - [12]\langle 14\rangle\langle 23\rangle\langle 24\rangle^3[25][26] \\
&- [12][13]\langle 23\rangle\langle 24\rangle^2[24]\langle 34\rangle[56] - 2[12]\langle 14\rangle\langle 23\rangle\langle 24\rangle^2[25]\langle 34\rangle[36] + [13]\langle 14\rangle\langle 23\rangle\langle 24\rangle^2[25][26]\langle 34\rangle \\
&- [12]\langle 14\rangle\langle 23\rangle\langle 24\rangle\langle 34\rangle^2[35][36] - [13]^2\langle 23\rangle\langle 24\rangle[24]\langle 34\rangle^2[56] + 2[13][14]\langle 23\rangle\langle 24\rangle[25]\langle 34\rangle^2[36] \\
&+ [13][14]\langle 23\rangle\langle 34\rangle^3[35][36] - [12][14]\langle 24\rangle^3[24]\langle 34\rangle[56] + [14]^2\langle 24\rangle^3[25][26]\langle 34\rangle \\
&- [13][14]\langle 24\rangle^2[24]\langle 34\rangle^2[56] + 2[14]^2\langle 24\rangle^2[25]\langle 34\rangle^2[36] + [14]^2\langle 24\rangle\langle 34\rangle^3[35][36] \big).
\end{aligned}
$$

Here $\mathcal{N}$ would contain even more terms then in the six-point $(\text{DF})^2$ example. Similar expressions where the symmetries of the poles are made manifest are also possible in Einstein gravity amplitudes; for example, the following represent the three-particle simple

poles in the six-point NMHV sector.

$$A_{EG}(1^{++}, 2^{++}, 3^{++}, 4^{--}, 5^{--}, 6^{--}) =$$

$$\frac{-i[12]^3\langle 56\rangle^3\langle 4|1+2|3]^4}{\langle 12\rangle\langle 14\rangle[14]\langle 24\rangle[24]\langle 35\rangle[35]\langle 36\rangle[36][56]s_{124}}+$$

$$(123456 \to 132456) + (123456 \to 123546) + (123456 \to 132546) +$$

$$(123456 \to 321456) + (123456 \to 123654) + (123456 \to 321654) +$$

$$(123456 \to 231546) + (123456 \to 132645)+$$

$$\frac{\mathcal{N}}{\langle 12\rangle\langle 13\rangle\langle 14\rangle[14]\langle 15\rangle[15]\langle 16\rangle[16]\langle 23\rangle\langle 24\rangle[24]\langle 25\rangle[25]\langle 26\rangle[26]\langle 34\rangle[34]\langle 35\rangle[35]\langle 36\rangle[36][45][46][56]}$$

However, this symmetric approach, which is also free from spurious singularities, makes it highly non trivial to obtain the rest of the amplitude (i.e. the numerator $\mathcal{N}$). Indeed, the compact expressions that we are aware of come from BCFW recursions and have a quite different structure:

$$A_{EG}(1^{++}, 2^{++}, 3^{++}, 4^{--}, 5^{--}, 6^{--}) =$$

$$\frac{-i[23]^7\langle 34\rangle\langle 56\rangle^7[56]}{\langle 15\rangle\langle 16\rangle[24][34]\langle 1|2+4|3]\langle 1|2+3|4]\langle 5|1+6|2]\langle 6|1+5|2]s_{234}}+$$

$$\frac{i[24]\langle 4|1+2|3]^7\left(\begin{array}{c}-\langle 12\rangle[12]\langle 13\rangle[35]\langle 45\rangle + \langle 12\rangle[13]\langle 14\rangle[25]\langle 35\rangle + \langle 12\rangle[23]\langle 24\rangle[25]\langle 35\rangle - \langle 12\rangle[24]\langle 34\rangle[35]\langle 45\rangle\\-\langle 13\rangle\langle 14\rangle[14][35]\langle 45\rangle + [13]\langle 14\rangle^2\langle 35\rangle[45] - \langle 14\rangle\langle 24\rangle[25][34]\langle 35\rangle + \langle 14\rangle[24]\langle 25\rangle\langle 34\rangle[35]\end{array}\right)}{\langle 12\rangle^2\langle 24\rangle[35][36][56]\langle 1|2+4|3]\langle 1|2+4|5]\langle 1|2+4|6]\langle 4|1+2|5]\langle 4|1+2|6]s_{124}}+$$

$$\frac{i[12]^6\langle 14\rangle\langle 56\rangle^7\left(\begin{array}{c}-\langle 12\rangle[12][23]\langle 35\rangle[45] - [12]\langle 13\rangle\langle 14\rangle\langle 15\rangle[35] + [12]\langle 14\rangle[34]\langle 35\rangle[45] + \langle 14\rangle[15][24][34]\langle 35\rangle\\-[12]\langle 15\rangle\langle 23\rangle[24][35] - [14]\langle 15\rangle[24]\langle 34\rangle[35] + \langle 23\rangle[24]^2[35]\langle 45\rangle - [23]\langle 24\rangle[24]\langle 35\rangle[45]\end{array}\right)}{[14]\langle 35\rangle\langle 36\rangle\langle 3|1+4|2]\langle 3|1+2|4]\langle 5|1+4|2]\langle 5|1+2|4]\langle 6|1+4|2]\langle 6|1+2|4]s_{124}}+$$

$$\frac{-i[34]\langle 56\rangle\langle 4|1+3|2]^7}{\langle 13\rangle\langle 14\rangle[25][26]\langle 34\rangle[56]\langle 1|2+6|5]\langle 1|2+5|6]\langle 3|1+4|2]s_{134}}+$$

$$(123456 \to 123546) + (123456 \to 123654) +$$

$$\frac{i[23]s_{123}^7\left(\begin{array}{c}\langle 12\rangle\langle 13\rangle[14][25]\langle 45\rangle - \langle 12\rangle[12]\langle 14\rangle\langle 35\rangle[45] + \langle 12\rangle\langle 23\rangle[24][25]\langle 45\rangle + \langle 12\rangle[23]\langle 34\rangle\langle 35\rangle[45]\\+\langle 13\rangle^2[14][35]\langle 45\rangle - \langle 13\rangle[13]\langle 14\rangle\langle 35\rangle[45] + \langle 13\rangle\langle 23\rangle[25][34]\langle 45\rangle - \langle 13\rangle[23]\langle 25\rangle\langle 34\rangle[45]\end{array}\right)}{\langle 12\rangle^2\langle 23\rangle[45][46][56]\langle 1|2+3|4]\langle 1|2+3|5]\langle 1|2+3|6]\langle 3|1+2|4]\langle 3|1+2|5]\langle 3|1+2|6]}$$

We have reproduced this result already known in the literature by applying our analytical reconstruction strategy to a single BCFW factorisation channel at a time, which is significantly simpler than the full amplitude[1]. Compared to the previous partial result, we note that this representation manifestly does not contain two-particle Mandelstam invariants, but introduces many spurious singularities and hides the symmetries which were manifest in the above partial result.

---

[1] In this case a $\langle 21]$ shift was used.

The strategy of studying a factorisation channel at a time could prove fruitful also in the case of conformal gravity and $(DF)^2$ amplitudes, but the quartic propagator introduces a significant complication in the BCFW recursion.

In fact, the usual $A_L A_R / p^2$ factorisation is broken by the presence of higher order poles in the Laurent expansion in the shift parameter. We attempted to achieve such a factorisation by means of a Taylor expansion of the numerator $A_L A_R$ around the pole. However, this involves taking a derivative with respect to the shift parameter which, in turns, requires the amplitudes to be well defined in the neighbourhood of the factorisation point. This seems to be equivalent to the factorisation formula (Eq. 2.18) given in Ref. [135], where the derivative is implicit in the fact that we have to take the zero mass limit of expressions like $(A_L(m^2) - A_L(0))/m^2$. This would also explain why our approach fails: the amplitudes we use are well defined only exactly at the factorisation point, where the legs are on-shell and massless.

However, we do have the six-point amplitude through the CHY formula and there is no need to generate it recursively from lower point amplitudes. At the same time, we expect single factorisation channels to have an easier analytical structure than the full amplitude. This suggests to still look at the amplitude via the residue theorem:

$$\frac{1}{2\pi i} \oint \frac{\hat{A}(z)}{z} dz = \hat{A}(0) + \sum_i \frac{\operatorname{Res}\hat{A}(z)|_{z=z_i}}{z_i}. \tag{9.6}$$

We can then study one term in the sum in the RHS at a time. Note that the simultaneous need to generate singular phase space limits and to numerically extract the residue from a Laurent expansion in some cases requires to increase the working numerical of precision.

As an example, let us consider the same $\langle 21]$ shift as before, and more specifically the $(2,3,4)_L$, $(1,5,6)_R$ channel, which for Einstein gravity yields the first term from the previous expression, i.e.:

$$\frac{\operatorname{Res}\hat{A}_{EG}^{NMHV}(z)}{z}\bigg|_{z=z_{(2,3,4)_L,(1,5,6)_R}} = \frac{i[23]^7\langle 34\rangle\langle 56\rangle^7[56]}{\langle 15\rangle\langle 16\rangle[24][34]\langle 1|2+4|3]\langle 1|2+3|4]\langle 5|1+6|2]\langle 6|1+5|2]s_{234}}.$$

The same shift in the same channel in the case of conformal gravity instead yields:

$$\frac{\operatorname{Res}\hat{A}_{CG}^{NMHV}(z)}{z}\bigg|_{z=z_{(2,3,4)_L,(1,5,6)_R}} = \frac{\mathcal{N}}{(\langle 12\rangle^2\langle 13\rangle^2\langle 15\rangle\langle 16\rangle[24]\langle 34\rangle^2[34][46]^2[56]^2\langle 1|3+4|2]^2\langle 1|2+4|3]}$$

$$\times \langle 1|2+3|4]^3\langle 5|1+6|2]\langle 6|1+5|2]s_{124}^2 s_{125}^2 s_{234}^2).$$

The numerator $\mathcal{N}$, having mass dimension of 46, is unfortunately still too complicated to be determined. We see that the conformal gravity residue has more poles and poles of

higher order compared to Einstein gravity one, as well as some spurious singularities of order higher than one. Furthermore, note that for this shift the contour integral vanishes for Einstein gravity but not for conformal gravity. Therefore, in the latter case we would have to include a boundary term coming from the residue at infinity. Some of the other possible shifts have the advantage of vanishing on the contour, but the structure of the residues remains similarly complicated. Further work will be required to see whether a reasonably compact analytical expression can be obtained for these residues.

Conclusions

In this thesis we have presented a new method to obtain compact analytical expressions for high-multiplicity scattering amplitudes from numerical evaluations only. We leveraged this method to obtain new analytical expressions for two phenomenologically relevant processes at one-loop, namely six-gluon and Higgs + 4-parton scattering, as well as for more theoretical amplitudes in higher derivative theories at tree-level.

The complexity of the calculations for scattering amplitudes, together with the quadratic increase in the number of scales needed to describe them, means that numerical programs have to be employed whenever analytical calculations become unfeasible. Yet most of the complexity is usually in the intermediate stages of the calculation, and expressions in their final form are often much more compact than in the intermediate stages needed to compute them. Therefore, reconstructing analytical expressions after the calculation has been performed numerically largely bypasses the complexity usually inherent to an analytical calculation, while retaining the benefits of analytical results.

From a phenomenological point of view, the benefits include faster and more stable evaluations for Monte Carlo integration, which save on computation time and reduce integration errors. From a more theoretical point of view, the benefits include a better understanding of the mathematical properties of the amplitudes, and, as shown previously, can even provide some information about all-multiplicity expressions.

The reconstruction method we developed is based on the analysis of high-precision floating-point evaluations of rational kinematic quantities, such as loop integral coefficients. First of all, the singularity structure of the expressions is probed numerically through evaluations in singular limits of complex phase space. This yields the poles of the expression, their degrees, as well as any common factor in the numerator. In some simple cases this is sufficient to reconstruct the analytical expression. However, more generally, it is necessary to further probe the quantity in doubly singular limits to obtain information about the relations among the poles and, thereafter, postulate possible partial fraction decompositions. Finally, individual terms in the partial fraction decomposition can be numerically isolated by choosing appropriate regions of phase space and reconstructed by solving linear systems of equations for the coefficients of generic ansatze.

The reconstruction strategies presented in Chapter 6 offer different trade-offs between scalability and uniqueness of the result. While in principle the first strategy presented should always work and yield a result with a predictable structure, in practice it scales badly with the complexity of the expression. On the contrary, the last two strategies involve some trial and error, since a given partial fraction decomposition is not guaranteed to be valid before we actually attempt to reconstruct the numerator, but they offer more options to control the structure of the outcome and scale much better with the complexity of the problem. An advantage of this flexibility is that it allows to tailor the form of the reconstructed analytical expression for different goals, such as evaluation speed or numerical stability. For the latter goal, we can generate equivalent representations of the same expression that are numerically stable in different singular limits.

Firstly, we applied this method time to obtain analytical expressions for the six-gluon one-loop helicity amplitudes with a gluon in the loop from numerical evaluations from BLACKHAT. Analytical expressions for these amplitudes were already available in the literature, but had never been presented all together in a single place with a single notation. Furthermore, the expressions we obtained are both manifestly rational in the spinor products and manifestly gauge invariant. Implementing these expressions analytically in BLACKHAT has resulted in a significant speed-up compared to the numerical procedure. These amplitudes will be useful to obtain predictions for 3-jet production at next-to-next-to-leading order.

Secondly, the method we developed proved to be very useful in simplifying one-loop Higgs + 4-parton amplitudes in the full theory. Although originally developed for entirely massless

processes, it proved easy to adapt to the presence of some masses. Also in this case the expressions we obtained are manifestly rational, and they resulted in a speed-up of at least an order of magnitude. These results will be important for improving calculations of the Higgs + jet production at next-to-leading order in the full theory.

Thirdly, we used this method to reconstruct analytical tree-level amplitudes from numerical evaluations up to six-point in the following theories: Yang-Mills, Einstein gravity, biadjoint scalar, Born-Infeld, non-linear sigma model, Galileon, conformal gravity and $(\mathrm{DF})^2$. In this case, we developed a `Python` package (seampy) to numerically solve the scattering equations and to compute tree amplitudes with the high floating-point precision need by our reconstruction technique. In particular, we obtained the first complete set of five-point $(\mathrm{DF})^2$ amplitudes, a new form for the five-point MHV conformal gravity amplitude and we presented a discussion with partial results for six-point amplitudes in both $(\mathrm{DF})^2$ and conformal gravity. Let us remark that despite the fact that not all the solutions to the scattering equations are rational (except at three- and four-point), and in some cases are not even expressible in terms of radicals (beyond six-point), the tree-level amplitudes built from them are purely rational functions. This is made clear by reconstructing explicit rational analytical expressions from numerical evaluations.

Let us now point out possible future directions of enquiry and potential limitations of the reconstruction method.

An compelling and within reach further application would be to reconstruct rational coefficients of logarithms instead of master integrals. This should simply amount to reconstructing combinations of the master-integral coefficients considered so far, but may elucidate spurious-pole cancellations among different components of the amplitude. In principle, it may even be possible to reconstruct the dependence on the logarithms from numerical computations of the entire loop-amplitude. For instance, if the only logarithm to reconstruct depended on the renormalisation scale μ_R, then this could be easily accommodated by first performing the reconstruction at $\mu_R = 1$, which would kill the logarithm, and then at $\mu_R = e$ to obtain the coefficient of the log. However, in practice, if the argument of the logarithms were arbitrary ratios of kinematic invariants, a naive approach where the logarithms are added to the linear systems for the numerators may easily result in too large systems to be solved efficiently.

This brings us to the main limitation of the method presented, that is the size of the linear systems to be solved for the reconstruction of the numerators. We observed that systems of

up to a few thousands linear equations can be very efficiently solved with double-precision pivoted Gaussian elimination on a GPU in a matter of seconds. The larger the linear system, the more complicated it is to maintain numerical errors under control and eventually it is necessary to resort to performing the Gaussian elimination with higher floating-point precision on CPUs, which is significantly slower. However, the method presented for fitting individual terms in partial fraction decompositions by exploiting the singular limits severely reduces the size of the systems that have to be considered. Furthermore, it is usually the case that the numerator structures are not completely arbitrary and can be constrained by the study of doubly singular limits, which allow to make educated guesses for common factors in the numerators and thus reduce the size of systems to solve.

Finally, the application of the reconstruction method presented in this thesis is not limited to coefficients of one-loop scalar integrals, one-loop rational remainders or tree-level amplitudes. In a future study we plan to use it to rewrite analytical two-loop integral coefficients expressed in terms of twistor or Mandelstam variables as functions of spinor products, where the pole structure and physical limits are easier to interpret.

Appendices

Feynman Rules in the Standard Model

In this section of the Appendix, we give explicit Feynman rules for QCD and discuss the remaining electroweak ones. The latter either have the same tensor structure as QCD, up to simplifications arising from substituting $SU(3)$ structure constants with $SU(2)$ ones and adding projection operators to enforce the chiral nature of the weak interaction, or have trivial Lorentz structure, in the case of those involving the Higgs boson. In the following, we ignore technicalities concerning gauge choice and ghosts, since they do not play a role when working with gauge-invariant on-shell quantities.

A massless vector boson propagator, associated to the gauge-kinetic part of the Lagrangian of Eq. 1.23, in the axial gauge reads

$$a, \mu \; \xrightarrow{\quad p \quad} \; b, \nu \quad = \quad \frac{-i}{p^2 + i\epsilon} \left(\eta^{\mu\nu} - \frac{p^\mu n^\nu + n^\mu p^\nu}{p \cdot n} \right) \delta^{ab} , \tag{A.1}$$

where the n is an arbitrary massless reference momentum. The Kronecker's delta δ^{ab} is the only QCD specific part, it simply enforces the outgoing gluon to be the same as the incoming one. The photon propagator will look much the same, whereas the $W^\pm$ and Z propagators will be slightly different due to their non-zero mass.

The double product between the derivative part of the field strength and its commutator

part, denoted as triple-gauge in Eq. 1.24, gives rise to the three-point interaction between gluons
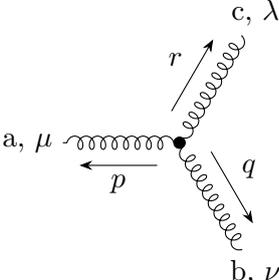
$$g_s f^{abc} \left[\eta^{\mu\nu}(p-q)^\lambda + \eta^{\nu\lambda}(q-r)^\mu + \eta^{\lambda\mu}(r-p)^\nu \right] . \quad \text{(A.2)}$$

Note that the sum over permutations arises from the 3! possible contractions with external fields from Wick's Theorem Eq. 1.14. This also takes care of the factor of $1/2$ from the Lagrangian. The momenta arise from the single derivative terms in the Lagrangian. The double product from the contraction of W field strength tensors from Eq. 1.20 leads to the exact same Lorentz structure, but now the structure constant f^{abc} becomes ϵ^{ijk}. This can be set to 1 as long as we remember that the three fields must be distinct, i.e. only W^+W^-Z and W^+W^-A vertices exist. The coupling g_s also has to be adjusted accordingly to $g_2 \cos\theta_W$ or e respectively.

The last part of the product of fields strength tensors is the square of the commutator part, which leads to four-point gauge interactions. The Feynman rule is
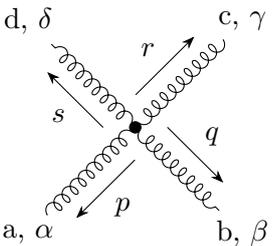
$$
\begin{aligned}
&-ig_s^2 f^{abe} f^{cde} \left(\eta^{\alpha\gamma}\eta^{\beta\delta} - \eta^{\alpha\delta}\eta^{\beta\gamma} \right) \\
&-ig_s^2 f^{ace} f^{bde} \left(\eta^{\alpha\beta}\eta^{\gamma\delta} - \eta^{\alpha\delta}\eta^{\beta\gamma} \right) \\
&-ig_s^2 f^{ade} f^{bce} \left(\eta^{\alpha\beta}\eta^{\gamma\delta} - \eta^{\alpha\gamma}\eta^{\beta\delta} \right) .
\end{aligned}
\quad \text{(A.3)}
$$

Again, the sum over permutations and the factor of $1/4$ are understood in terms of the 4! possible contractions with external fields. In the case of W field strengths, the $SU(2)$ indices can only take three values, therefore one of the three lines in the above Feynman rule has to vanish. Then, the remaining two lines can be combined, and the Levi-Civita tensors set to 1 as long as we remember the allowed combinations: $W^+W^-W^+W^-$, W^+W^-ZZ, W^+W^-AA, and W^+W^-AZ. The coupling constants also need to be adjusted accordingly.

Moving on to the matter part of the Standard Model, we have the fermion propagator

$$i \xrightarrow[\ m_f\ ]{\ \ p\ \ } j \quad = \quad \delta_{ij}\frac{i\slashed{p} + m_f}{p^2 - m_f^2 + i\epsilon} \; , \tag{A.4}$$

which is associated with the kinetic term of Eq. 1.26. The mass can be often neglected in the computation of high energy matrix elements. This is particularly useful since the mass term is the only one which mixes left and right handed chiralities.

The last Feynman diagram in QCD is the quark-gluon interaction

$$\quad = \quad -ig_s(T^a)_{ij}\gamma^\mu \; , \tag{A.5}$$

where T^a is the $SU(3)$ generator $T^a = \lambda^a/2$. This rule corresponds to Eq. 1.27 from the Lagrangian. Similar vertex factors exist for the electroweak part of the Lagrangian, but we are not going to list them all here. They are easily obtained by expanding out the $SU(2)$ doublet representations and adding left projection operators P_L. The only possible complication is the mixing of the B and W^3 currents into the photon and Z ones. On the one hand, the photon current yields the unification condition and the relation among charge, hypercharge and isospin, respectively

$$e = g_2 \sin\theta_W = g_1 \cos\theta_W \quad \text{and} \quad Q = I_3 + Y/2 \; . \tag{A.6}$$

On the other hand, the Z current gives the following left and right handed couplings

$$g_L = I_3 - Q\sin^2\theta_W \quad \text{and} \quad g_R = -Q\sin^2\theta_W \; . \tag{A.7}$$

Vertices involving the Higgs boson are obtained from three terms in the Lagrangian: the Yukawa term gives Higgs-fermion vertices, the covariant derivative acting on the Higgs field give Higgs-gauge vertices, just like Eq. 1.31 gave masses to some of the gauge bosons, and the Higgs potential gives Higgs self-interactions. All these vertices have trivial Lorentz structure (either the identity or the metric) and the coupling can be read off the Lagrangian.

Finally, external fermions and vectors require the introduction of the appropriate spinor (Dirac or Weyl) and polarisation tensor, respectively. These are given in Section 2.2.3.

Triple Cut Jacobian

In this section of the Appendix, we give an explicit derivation of the Jacobian J_t for the change of variable in the triple-cut momentum parametrisation of Section 3.3.3. This is still a review of Ref. [82]. The change of variables reads

$$\mathrm{d}^4 l \longrightarrow \mathrm{d}l^2 \mathrm{d}(l + K_1)^2 \mathrm{d}(l - K_2)^2 \mathrm{d}t \times |J_t| \,, \tag{B.1}$$

where $|J_t|$ is the determinant of the Jacobian, which is given by

$$\left(J_t^{-1}\right)_{\mu\nu\rho\sigma} = (\partial l^2 / \partial l^\mu)(\partial(l + K_1)^2 / \partial l^\nu)(\partial(l - K_2)^2 / \partial l^\rho)(\partial t / \partial l^\sigma) \tag{B.2}$$

$$= 8 l^\mu (l + K_1)^\nu (l - K_2)^\rho \partial t / \partial l^\sigma \,. \tag{B.3}$$

The first three partial derivatives are trivial, whereas the one involving the parameter t is slightly trickier. By contracting Eq. 3.82 with a_1 we obtain

$$a_1 \cdot l = a_1 \cdot a_0 t + a_1^2 \frac{1}{t} + a_1 \cdot a_2 \,, \tag{B.4}$$

$$a_{1,\mu} \mathrm{d}l^\mu = a_1 \cdot a_0 \mathrm{d}t = \frac{\alpha_{01} \alpha_{02}}{2} \langle K_2^\flat K_1^\flat \rangle [K_2^\flat K_1^\flat] \mathrm{d}t \,, \tag{B.5}$$

$$\implies \frac{\partial t}{\partial l^\mu} = -\frac{2 a_{1,\mu}}{\alpha_{01} \alpha_{02} \gamma} \,. \tag{B.6}$$

Note that the choice to contract l with a_1 is arbitrary, but convenient for analytical manipulations. We have checked numerically that the result is independent of the vector used in this contraction.

By repeatedly exploiting the anti-symmetry of Levi-Civita tensor, and using Eq. 3.82 and Eq. 3.63, we obtain

$$
\begin{aligned}
|J_t|^{-1} &= -8\epsilon^{\mu\nu\rho\sigma} l^\mu (K_1)^\nu (K_2)^\rho \partial t/\partial l^\sigma &\text{(B.7)}\\
&= -8\epsilon^{\mu\nu\rho\sigma}(a_{0,\mu} t + a_{1,\mu}\frac{1}{t})(K^\flat_{1,\nu} K^\flat_{2,\rho} + \frac{S_1 S_2}{\gamma^2} K^\flat_{2,\nu} K^\flat_{1,\rho})\partial t/\partial l^\sigma &\text{(B.8)}\\
&= 16t(1 - \frac{S_1 S_2}{\gamma^2})\epsilon^{\mu\nu\rho\sigma} a_{0,\mu} K^\flat_{1,\nu} K^\flat_{2,\rho}\frac{a_{1,\sigma}}{\alpha_{01}\alpha_{02}\gamma} &\text{(B.9)}\\
&= \frac{16t}{\gamma}(1 - \frac{S_1 S_2}{\gamma^2})\frac{1}{4i}\mathrm{tr}_5\big(|K^\flat_{1,\nu}\rangle[K^\flat_{2,\rho}|,\ |K^\flat_{1,\nu}\rangle[K^\flat_{1,\rho}|,\ |K^\flat_{2,\nu}\rangle[K^\flat_{2,\rho}|,\ |K^\flat_{2,\nu}\rangle[K^\flat_{1,\rho}|\big)\ .
\end{aligned}
$$

We can now use the following relation

$$
\mathrm{tr}_5(a, b, c, d) = [a|b|c|d|a\rangle - \langle a|b|c|d|a]\ , \tag{B.10}
$$

to evaluate the tr_5 part to $-\gamma^2$. Therefore, the determinant of the Jacobian is

$$
|J_t|^{-1} = 4it\gamma\big(1 - \frac{S_1 S_2}{\gamma^2}\big)\ . \tag{B.11}
$$

This is slightly different from the result quoted in [82] (there is an extra factor of $1 - \frac{S_1 S_2}{\gamma^2}$). However, since the difference is not in the t dependence, but in the kinematic part, which cancels between left- and right-hand sides of Eq. 3.62, no integral coefficient is affected by this discrepancy.

Scattering Equations and Amplitudes in Python

In this section of the Appendix, we show how to solve the scattering equations and compute scattering amplitudes using two new packages developed in `Phyton 2.7`:

- `seampy` (Scattering equations and amplitudes in `Python`),

- `lips` ($d = 4$ Lortenz invariant phase space).

The former provides high-precision floating-point solutions to the scattering equations in d dimensions and a variety of numerical scattering amplitudes built from their solutions. The latter is used to manipulate and pass a high-precision phase space point as input to the numerical amplitude.

Both packages are available on the Python Package Index. The source code is available on github and the documentation on the associated github pages seampy and lips. Their installation is straightforward thanks to pip:

```
pip install --upgrade seampy    # this installs lips as well
pip install --upgrade lips      # but it can be installed separately
```

The same commands can be used to update the libraries. The `--upgrade` option ensures that the latest version is always used. A review of the key features of these packages is now provided. Further examples are given in Chapter 9, and more details in the Appendix D.

C.1   Solving the Scattering Equations

In this section we show how to easily obtain solutions for the scattering equations. All the following examples have $n = 6$.

The SE in polynomial form as in Eq. 4.13 can be accessed as follows:

```
>>> hms(6)
```
$$\begin{bmatrix} s_{12} \cdot z_2 + s_{13} \cdot z_3 + s_{14} \cdot z_4 + s_{15} \cdot z_5 \\ s_{123} \cdot z_2 \cdot z_3 + s_{124} \cdot z_2 \cdot z_4 + s_{125} \cdot z_2 \cdot z_5 + s_{134} \cdot z_3 \cdot z_4 + s_{135} \cdot z_3 \cdot z_5 + s_{145} \cdot z_4 \cdot z_5 \\ s_{1234} \cdot z_2 \cdot z_3 \cdot z_4 + s_{1235} \cdot z_2 \cdot z_3 \cdot z_5 + s_{1245} \cdot z_2 \cdot z_4 \cdot z_5 + s_{1345} \cdot z_3 \cdot z_4 \cdot z_5 \end{bmatrix}$$

They are functions of the punctures and of Mandelstam invariants, which are given here as they appear in the SE:

```
>>> punctures(6)
```
$(z_1, \ z_2, \ z_3, \ z_4, \ z_5, \ z_6)$
```
>>> mandelstams(6)
```
$(s_{12}, \ s_{13}, \ s_{14}, \ s_{15}, \ s_{123}, \ s_{124}, \ s_{125}, \ s_{134}, \ s_{135}, \ s_{145}, \ s_{1234}, \ \ldots)$

The SE can be solved by calling the function `solve_scattering_equations`. It requires two inputs: the multiplicity of the phase space, `n`, and a `Python` dictionary with the numerical values for the Mandelstam invariants, `num_ss`. We therefore need a phase space point. This is easily done through the lips toolkit object `Particles` which generates a random phase space point:

```
>>> oPs = Particles(6)   # arg. is multiplicity of phase space
>>> num_ss = {str(s): oPs.compute(str(s)) for s in mandelstams(6)}
```

Alternatively, it is possible to set the momenta from a list by modifying the `four_mom` attribute of each `Particle` in the list subclass `Particles` or to provide an independently constructed set of Mandelstam invariants. More of this in appendix D.1.

We can then solve the scattering equations by calling:

```
>>> sols = solve_scattering_equations(6, num_ss)
```

the output, `sols`, is a list of length $(n-3)!$, in this case 6. Each solution in the list is a dictionary for the non-arbitrarily fixed punctures, in this case of the form:

```
>>> sols[0]
{'z3': mpc(real='#nbr', imag='#nbr'),
↪  'z4': mpc(real='#nbr', imag='#nbr'),
↪  'z5': mpc(real='#nbr', imag='#nbr')}
```

where each `'#nbr'` has by default 300 digits of precision.

C.2   Computing Scattering Amplitudes

First of all we can list the theories directly available for computation:

```
>>> theories
[YM, EG, BS, BI, NLSM, Galileon, CG, DF2]
```

To calculate an amplitude we need to generate a phase space point, as in the example for the solutions of the scattering equations:

```
>>> oParticles = Particles(6)  # arg. is multiplicity of phase space
```

We then need to declare what quantity we want to compute. This requires us to specify a theory and a multiplicity. For example, biadjoint scalar theory (BS) amplitudes or non-linear sigma model (NLSM) amplitudes can be accessed as follows:

```
>>> oBSAmp = NumericalAmplitude(theory='BS', multiplicity=6)
>>> oNLSMAmp = NumericalAmplitude(theory='NLSM', multiplicity=6)
```

Gauge and gravity theories also require a helicity configuration to be specified (the multiplicity is then deduced from it). Note that for gravity theories we are suppressing the repeated helicity sign since we do not have mixed cases such as dilatons. This means that in the following code snippet for conformal gravity (CG) `helconf=pmpmpm` stands for $1^{++}2^{--}3^{++}4^{--}5^{++}6^{--}$.

```
>>> oDFAmp = NumericalAmplitude(theory='DF2', helconf='pmpmpm')
>>> oCGAmp = NumericalAmplitude(theory='CG', helconf='pmpmpm')
```

It is then simply a matter of evaluating any amplitude at the phase space point:

```
>>> oBSAmp(oParticles)
mpc(real='#nbr', imag='#nbr')
```

Since most of these helicity amplitudes come with pre-factors of $\sqrt{2}$, we decided to normalise them in such a way that numerical coefficients in analytical expressions are rational fractions and often simply the imaginary unit. This also allows for easier comparison to other codes, which usually adopt such a normalisation. For instance, in the case of Yang-Mills amplitudes the right hand side of Eq. 4.12 is multiplied by $1/(\sqrt{2})^{n-2}$, so that the numerical coefficient in the Parke-Taylor expression for MHV amplitudes is i instead of $(\sqrt{2})^{n-2}i$, where n is the multiplicity of the process.

C.3   Validations

A first validation of the code is to check the solutions of the scattering questions. This is simply a matter of inserting each of the solutions back in the polynomial SE and check they vanish to working precision. This can easily be done in practice:

```
>>> sol = solve_scattering_equations(n, num_ss)[0]
>>> simplify(hms(n).subs(sol).subs(num_ss).subs({punctures(n)[1]: 1}))
[~10 ** -290, ~10 ** -290, ~10 ** -290]  # for n = 6 there are 3 SE
```

Additional checks not requiring independent implementations of amplitudes include checking the little group scalings, mass dimensions, pole structure (more of this in section **??**) or properties such as color ordering. For instance, as a sanity check, we can see that $(\text{DF})^2$ is color ordered whereas conformal gravity is not. This is shown in the following snippet (we are still using the `helconf=pmpmpm` amplitudes declared above):

```
>>> oNewParticles = oParticles.image("321456")  # swap momenta 1 & 3
```

```
>>> abs(oCGAmp(oParticles) - oCGAmp(oNewParticles)) < 10 ** -270
True
>>> abs(oDFAmp(oParticles) - oDFAmp(oNewParticles)) < 10 ** -270
False
```

However, picking the correct cyclic permutation of the external legs leaves the $(DF)^2$ amplitude unchanged as well.

Finally, the most stringent tests come from comparing to independent libraries. We have checked all pure gluon (Yang-Mills) tree amplitudes at 3, 4, 5, 6, and 7 point against BLACKHAT [139] and Yang-Mills, Einstein and conformal gravity against the code of Ref. [66]. They all match, that is their ratio differs at most by a normalisation factor fixed by convention.

Python Libraries (further details)

In this appendix we provide more details on the lips and seampy packages. Although not essential from a user point of view, it may be of interest to have more control over the phase space used or over the theories computed.

D.1 Lips (Lorentz Invariant Phase Space)

The lips `Python` package is an object-oriented high-precision floating-point phase space generator built on two layers. The lower one, called `Particle`, describes the kinematics of a single particle. Though setters and getters, it provides self-updating numerical tensors for the left and right spinors, four vectors and rank two spinors. This means that if, say, the value of the four-momentum is changed, then the values of the spinor attributes are immediately recalculated to reflect the change. We can see the naming conventions in the following code snippet:

```
>>> oParticle = Particle()
>>> oParticle.l_sp_u      # left spinor with index up ($\bar{\lambda}^{\dot{\alpha}}$)
>>> oParticle.r_sp_d      # right spinor with index down ($\lambda_\alpha$)
>>> oParticle.four_mom    # four-momentum with index up ($P^\mu$)
>>> oParticle.r2_sp       # rank two spinor ($P^{\dot{\alpha}\alpha}$)
```

By default, the `Particle` object is initialised with random complex momenta. However, this can be overruled by specifying the optional parameter `real_momentum=True`. A custom value for any of the above attributes can also be passed. For instance, we can set the momentum to be along the x axis:

```
>>> oParticle.four_mom = numpy.array([1, 1, 0, 0])
```

The second layer is a list subclass, called `Particles`. It is a base-one list of Particle objects with several methods associated to it. The reason why the list is rebased to start from 1 instead of 0 is simply to match the notation in the amplitudes community. As we have observed, it is initialised as follows:

```
>>> oParticles = Particles(6)  # argument is the multiplicity
```

It also accepts an optional parameter, now called `real_momenta`, which is by default set to `False`, and which gets automatically passed down to all the `Particle` objects in the `Particles` list, thus generating a complex or real phase space point.

Furthermore, as discussed in conjunction with the analytical reconstruction, the `Particles` phase space can be manipulated to generate specific configurations. For instance, we can generate phase space point with vanishing angle bracket $\langle 12 \rangle$ by calling:

```
>>> oParticles.set("⟨1|2⟩", 10 ** -30)
```

Doubly singular limits for pairs of invariants can be similarly generated. For instance, we can make both $\langle 12 \rangle$ and $\langle 23 \rangle$ small:

```
>>> oParticles.set_pair("⟨1|2⟩", 10 ** -30, "⟨2|3⟩", 10 ** -30)
```

At present these functions only work with complex momenta, because with complex momenta it is possible to construct phase space points where, say, $\langle 12 \rangle$ is small but $[12]$ is not, while with real momenta this is not possible ($[12] \sim \langle 12 \rangle^*$).

Other notable functions are:

```
>>> oParticles.randomise_all()  # randomises all momenta
>>> oParticles.angles_for_squares()  # swaps right/left spinors
>>> oParticles.image("234561")  # argument is a permutation of 123...n
```

For more details please consult the package documentation at the relevant github pages.

D.2   Seampy (Scattering Equations and Amplitudes in Python)

In Appendix C we have given a high-level overview on how to use seampy to solve the scattering equations and compute scattering amplitudes. Here, we provide a few further details which reflect the implementation of the CHY formalism discussed in Chapter 4.

Still using $n = 6$ for our examples, we can see two important elements of the elimination theory algorithm:

$\circ$ the vector of variables to be removed via elimination theory from Eq. 4.18:

```
>>> V(6)
```
$$[1, \ z_2, \ z_3, \ z_2 \cdot z_3, \ z_3^2, \ z_2 \cdot z_3^2]$$

$\circ$ the elimination theory matrix obtained with the recursion algorithm of Eq. 4.20:

```
>>> M(6)
```

$$\begin{bmatrix} S_{14} \cdot Z_4 + S_{15} \cdot Z_5 & S_{12} & S_{13} & 0 & 0 & 0 \\ S_{145} \cdot Z_4 \cdot Z_5 & S_{124} \cdot Z_4 + S_{125} \cdot Z_5 & S_{134} \cdot Z_4 + S_{135} \cdot Z_5 & S_{123} & 0 & 0 \\ 0 & S_{1245} \cdot Z_4 \cdot Z_5 & S_{1345} \cdot Z_4 \cdot Z_5 & S_{1234} \cdot Z_4 + S_{1235} \cdot Z_5 & 0 & 0 \\ 0 & 0 & S_{14} \cdot Z_4 + S_{15} \cdot Z_5 & S_{12} & S_{13} & 0 \\ 0 & 0 & S_{145} \cdot Z_4 \cdot Z_5 & S_{124} \cdot Z_4 + S_{125} \cdot Z_5 & S_{134} \cdot Z_4 + S_{135} \cdot Z_5 & S_{123} \\ 0 & 0 & 0 & S_{1245} \cdot Z_4 \cdot Z_5 & S_{1345} \cdot Z_4 \cdot Z_5 & S_{1234} \cdot Z_4 + S_{1235} \cdot Z_5 \end{bmatrix}$$

These are the basis for the `solve_scattering_equations` function, which involves taking the determinant of `M` and finding its roots.

We can also consider the CHY-integrands and the Jacobian for the change of variables. We denote with the term *reduced* the following sequence of operations: a) removing rows and

columns: two of them for arguments of Pfaffians and three of them for the Jacobian; b) imposing the Möbius fixing choice of Eq. 4.4; c) removing any factorised factor of $z_1 = \infty$. In the following code snippets we reproduce some examples:

∘ the reduced Jacobian Matrix ϕ of Eq. 4.9:

```
>>> Phi(6)
```

$$
\begin{bmatrix}
-\dfrac{2 \cdot k_2 \cdot k_3}{(z_3-1)^2} - \dfrac{2 \cdot k_3 \cdot k_4}{(z_3-z_4)^2} - \dfrac{2 \cdot k_3 \cdot k_5}{(z_3-z_5)^2} - \dfrac{2 \cdot k_3 \cdot k_6}{z_3^2} & \dfrac{2 \cdot k_3 \cdot k_4}{(z_3-z_4)^2} & \dfrac{2 \cdot k_3 \cdot k_5}{(z_3-z_5)^2} \\[2em]
\dfrac{2 \cdot k_3 \cdot k_4}{(z_3-z_4)^2} & -\dfrac{2 \cdot k_2 \cdot k_4}{(z_4-1)^2} - \dfrac{2 \cdot k_3 \cdot k_4}{(-z_3+z_4)^2} - \dfrac{2 \cdot k_4 \cdot k_5}{(z_4-z_5)^2} - \dfrac{2 \cdot k_4 \cdot k_6}{z_4^2} & \dfrac{2 \cdot k_4 \cdot k_5}{(z_4-z_5)^2} \\[2em]
\dfrac{2 \cdot k_3 \cdot k_5}{(z_3-z_5)^2} & \dfrac{2 \cdot k_4 \cdot k_5}{(z_4-z_5)^2} & -\dfrac{2 \cdot k_2 \cdot k_5}{(z_5-1)^2} - \dfrac{2 \cdot k_3 \cdot k_5}{(-z_3+z_5)^2} - \dfrac{2 \cdot k_4 \cdot k_5}{(-z_4+z_5)^2} - \dfrac{2 \cdot k_5 \cdot k_6}{z_5^2}
\end{bmatrix}
$$

∘ the reduced matrix A of Eq. 4.21:

```
>>> A(6)
```

$$
\begin{bmatrix}
0 & \dfrac{2 \cdot k_3 \cdot k_4}{z_3-z_4} & \dfrac{2 \cdot k_3 \cdot k_5}{z_3-z_5} & \dfrac{2 \cdot k_3 \cdot k_6}{z_3} \\[1.5em]
\dfrac{-2 \cdot k_3 \cdot k_4}{z_3-z_4} & 0 & \dfrac{2 \cdot k_4 \cdot k_5}{z_4-z_5} & \dfrac{2 \cdot k_4 \cdot k_6}{z_4} \\[1.5em]
\dfrac{-2 \cdot k_3 \cdot k_5}{z_3-z_5} & \dfrac{-2 \cdot k_4 \cdot k_5}{z_4-z_5} & 0 & \dfrac{2 \cdot k_5 \cdot k_6}{z_5} \\[1.5em]
\dfrac{-2 \cdot k_3 \cdot k_6}{z_3} & \dfrac{-2 \cdot k_4 \cdot k_6}{z_4} & \dfrac{-2 \cdot k_5 \cdot k_6}{z_5} & 0
\end{bmatrix}
$$

∘ the reduced cyclic Parke-Taylor-like factor C_n of Eq. 4.24:

```
>>> Cyc(6)
```

$$
\frac{-1}{z_5 \cdot (-z_3 + 1) \cdot (z_3 - z_4) \cdot (z_4 - z_5)}
$$

All these symbolic quantities are built with sympy. However, note that the symbolical substitution function from sympy is very slow, therefore we use regular expressions from the re library to perform substitutions in the conversion from symbolic to numeric.

For more details please consult the package documentation at the relevant github pages.

Gaussian Elimination on GPGPU

It is often the case that scientific computations require the execution of code that highly benefits from parallelisation. Normally this is done by distributing the instructions across different cores of the central processing unit (CPU). A high-end i7 Intel processor from 2018 has 8 virtual[1] cores. By contrast, a nVidia GTX 1050 general purpose graphical processor unit (GPGPU) from the same year has 640 `CUDA`[2] cores, distributed across 5 multi-processors. As a consequence, speed-up factors from one to two orders of magnitude are not uncommon when moving from CPU to GPGPU. However, not all code can be parallelised for efficient execution on GPGPUs because of some limitations. Firstly, while instructions running in different threads of a CPU are completely independent, those in simultaneously executed threads of a GPGPU multi-processor must be the exact same. Secondly, GPGPU performance on non-natively supported number types (e.g. double precision if it is natively single precision) is significantly lower. Lastly, the structure of code for execution on `CUDA` cores is substantially different from usual, requiring completely new implementations; whereas parallelisation in, say, `C++` can be as easy as adding `#pragma omp parallel for` before a for loop.

In our case, a good candidate for parallelisation on graphics cards is the Gaussian elimination procedure, which essentially involves repeatedly dividing matrix rows by their first non-zero

---

[1] The number of virtual cores is double the number of physical ones due to hyper-threading.

[2] Compute Unified Device Architecture.

entry and subtracting them from the rows beneath. More specifically, the code we implemented performs Gaussian elimination with scaled partial pivoting. Partial pivoting entails exchanging the order of the equations (i.e. rows) to maximise numerical stability, but not that of the variables (i.e. columns). The latter would be total pivoting. It is *scaled* partial pivoting because the row with the largest leading element in relation to the rest of entries in the row is chosen for the subtraction; note that this minimises round-off errors.

Our `CUDA` code is invoked from `Python` via the pyCUDA module, which acts as global synchronisation among all code running on the GPGPU. This is necessary because `CUDA` code is run asynchronously on a two dimensional grid of three dimensional blocks of threads and, whereas it is possible to synchronise threads within a block by calling the `__syncthreads();` instruction, there is no way to synchronise different blocks across the grid from within the device[3]. Figure E.1 shows the host side of the code, with every function beginning by `Cuda` being a custom written kernel invocation, acting on the grid of blocks of threads. The size of the blocks and grids are passed as keyword arguments, making sure not to exceed the device constraints, for instance `MAX_BLOCK_DIM_X` is 1024 on a GTX 1050. If a block x-dimension needs to be 1025 it is better to have two blocks, one of x-dimension 513 and one of x-dimension 512, rather than a block of x-dimension 1024 and one with a single thread, hence the `folded_number_of_columns` function for the block dimension and `number_of_foldings` function for the grid dimension. We are now going to analyse the code in more details.

- ○ `cuda.mem_alloc` stands for memory allocation; it simply reserves enough memory on the device to hold a matrix of given size with specific number type (128-bit complex floats in our case);

- ○ `cuda.memcpy_htod` stands for memory copy from host to device; this pushes the matrix from the RAM to the GPU memory, and is performed once at the beginning, since host-device communication is slow;

- ○ `CudaSetRowScales` finds the maximum entry, or *scale*, in every row; this is necessary for partially pivoting the row reduction;

- ○ `CudaThreadsReduceToMaxIndex` and, if necessary, `CudaBlocksReduceToMaxIndex`, find the index of the row with the largest leading element in relation to its row scale;

---

[3]*Device* refers to the GPU, *host* refers to the CPU.

- ○ `CudaSwitchRows` moves the row with index just found to the top of the sub-matrix being row reduced;

- ○ `CudaCompareScaledHeadToTollerance` checks whether the leading entry is compatible with 0 at the current working precision (we use $10^{-9} \sim 0$ with double precision), and saves the result of the comparison in a boolean on the device (it is expensive to return it to the host);

- ○ `CudaDoStuff` on the first invocation either calls a `__device__`[4] function called `RescaleRow`, which divides a row by the leading entry, or calls a different `__device__` function called `RowAndColumnSetToZero` which sets an entire row and column to zero (effectively throwing away a redundant variable and equation), depending on the result of the comparison at the above step;

- ○ `CudaIncrement_functionCounter` acts as synchronisation and increments a counter on the device;

- ○ `CudaDoStuff` on the second invocation calls `RowReduce`, which subtracts the rescaled row from the sub-matrix beneath, or does nothing, depending on the result of the previous comparison;

- ○ `CudaIncrement_i` increases the counter on the device which moves you down the diagonal by one row and one column, before restarting the loop;

- ○ `cuda.memcpy_dtoh` in the end copies the row-reduced matrix back to RAM.

Unfortunately, the need to avoid a `cuda.memcpy_dtoh` call at every iteration of the loop, leads to a quite awkward implementation of the if-statement for the comparison to the numerical zero threshold. Still, an empty `CUDA` kernel call is much cheaper than returning a value from the GPU memory to the RAM.

In the following code snippet of Figure E.2, as an example of `CUDA` code, we show the device function for the actual row subtraction. This code is run asynchronously on the grid of blocks of threads, both of which are taken to be one-dimensional. Threads across a block handle columns within a row, and each block within the grid handles a specific row. Each thread knows its position within the two dimensional grid-block array through the parameters `blockId.x` and `threadIdx.x`, as well as the overall block dimension via

---

[4]*Device* functions are accessible only from within the device, as opposed to *global* functions with can be invoked from the host.

```python
# Push Matrix To Device
Matrix_gpu = cuda.mem_alloc(Matrix.size * Matrix.dtype.itemsize)
cuda.memcpy_htod(Matrix_gpu, Matrix)
# Set The Row Scales Array On The Gpu
CudaSetRowScales(Matrix_gpu,
                block=(int(math.ceil(folded_number_of_columns(
                        NbrColumns, FoldingMaxLength=2048) / 2.0)), 1, 1),
                grid=(NbrRows, 1))


for i in xrange(NbrRows):  # Loop Over Rows
    # Scaled Partial Pivoting
    CudaThreadsReduceToMaxIndex(Matrix_gpu,
                                block=(int(math.ceil(folded_number_of_columns(
                                NbrColumns - i, FoldingMaxLength=2048) / 2.0)), 1, 1),
                                grid=(number_of_foldings(NbrColumns - i), 1))
    if number_of_foldings(NbrColumns - i) > 1:
        CudaBlocksReduceToMaxIndex(Matrix_gpu,
                                block=(number_of_foldings(NbrColumns - i), 1, 1),
                                grid=(1, 1))
    CudaSwitchRows(Matrix_gpu,
                block=(folded_number_of_columns(NbrColumns), 1, 1),
                grid=(number_of_foldings(NbrColumns) + 1, 1))
    # Cuda Row Reduction To Echelon Form
    CudaCompareScaledHeadToTollerance(Matrix_gpu,
                                block=(1, 1, 1),
                                grid=(1, 1))
    CudaDoStuff(Matrix_gpu,
                block=(folded_number_of_columns(NbrColumns), 1, 1),
                grid=(number_of_foldings(NbrColumns), 1))
    CudaIncrement_functionCounter(Matrix_gpu,
                                block=(2, 1, 1),
                                grid=(1, 1))
    CudaDoStuff(Matrix_gpu,
                block=(folded_number_of_columns(NbrColumns), 1, 1),
                grid=(NbrRows, 1))
    # Increment Mirrored Counter
    CudaIncrement_i(block=(1, 1, 1), grid=(1, 1))


# Pull Matrix From Device
cuda.memcpy_dtoh(Matrix, Matrix_gpu)
```

Figure E.1: Host code for partially pivoted row reduction on CUDA device.

```
__device__ void RowReduce(pycuda::complex<double> *Matrix) {
    int FoldingLength = blockDim.x;
    int NbrFoldings = ceil(NbrColumns / (1.0 * FoldingLength));
    int id_j_head = blockIdx.x * NbrColumns + i;
    int idMax = (blockIdx.x + 1) * NbrColumns;
    for (int s = 0; s < NbrFoldings; s++) {
        int id = blockIdx.x * NbrColumns + s * FoldingLength + threadIdx.x;
        int id_i = i * NbrColumns + s * FoldingLength + threadIdx.x;
        if (blockIdx.x > i && s * FoldingLength + threadIdx.x > i && id < MaxMatrixId &&
↪   id < idMax){
            Matrix[id] = Matrix[id] - Matrix[id_i] * Matrix[id_j_head];
        }
    }
    __syncthreads();
    if (blockIdx.x > i && threadIdx.x == 0 && id_j_head < MaxMatrixId) {
        Matrix[id_j_head] = 0;
    }
}
```

Figure E.2: Device code example for partially pivoted row reduction on CUDA device.

`blockDim.x`. The indexing to access the matrix elements is arguably quite convoluted, because the matrix is stored in the GPGPU memory as a one-dimensional array. Hence, each (x, y) coordinate has to be written as $x + NbrColumns * y$. Furthermore, as argued in precedence, if a row exceeds 1024 elements it is *folded* onto itself. Therefore, if, say, the row has 1025 elements, the first thread will run through the loop with counter `s` twice, the first time acting on element at position `0`, and the second time on the element at position `513`. The position of the element being modified is thus

$$id = \overbrace{blockIdx.x * NbrColumns}^{\text{row length}} + \underbrace{s * FoldingLength}_{\text{counter} \times \text{iteration length}} + threadIdx.x. \qquad (E.1)$$

Lastly, after the subtraction has finished for a given row, and all threads within the block have reached `__syncthreads()`, it is safe to set the row element in column i to zero.

Six Gluon Coefficient Tables

There are eight independent helicity configurations for six-gluon scattering:

1. $1^+2^+3^+4^+5^+6^+$,   3. $1^+2^+3^+4^+5^-6^-$,   5. $1^+2^+3^+4^-5^-6^-$,   7. $1^+2^+3^-4^+5^-6^-$,

2. $1^+2^+3^+4^+5^+6^-$,   4. $1^+2^+3^+4^-5^+6^-$,   6. $1^+2^+3^-4^+5^+6^-$,   8. $1^+2^-3^+4^-5^+6^-$.

The all-plus and single-minus configurations are purely rational at one loop, since they vanish at tree level. The remaining six have both rational and cut-constructible parts. The following tables show all integral coefficients in relation to a minimal set of independent ones. Box, triangle and bubble coefficients are denoted as d, c and b respectively. The subscripts refer to the external particles in the corners of the diagram. Each coefficient corresponds to a specific internal propagator helicity assignment on the cut, with $\times$ representing a $-+$ propagator, and $\tilde{\times}$ a $+-$ one. In the cases where multiple, distinct symmetries have to be used to obtain the related coefficients, we also provide a table of conversion rules. The cases where a single symmetry is sufficient follow.

Helicity Configuration	Conversion rule	Helicity Configuration	Conversion rule
$1^+2^+3^+4^+5^-6^-$	(432165)	$1^+2^+3^+4^-5^+6^-$	(321654)
$1^+2^+3^-4^+5^-6^-$	$(\overline{654321})$		

Table F.1: Conversion rules for $1^+2^+3^+4^+5^-6^-$, $1^+2^+3^+4^-5^+6^-$ and $1^+2^+3^-4^+5^-6^-$ integral coefficients.

Coefficient	Related coefficients	Coefficient	Related coefficients
$d_{1\tilde\times2\times3\times456\tilde\times}$	$d_{561\tilde\times2\tilde\times3\times4\times}$	$d_{1\tilde\times234\times5\tilde\times6\tilde\times}$	$d_{123\times4\times5\times6\tilde\times}$
$d_{1\times2\times345\times6\tilde\times}$	$d_{612\tilde\times3\tilde\times4\times5\tilde\times}$	$d_{61\tilde\times2\tilde\times34\times5\tilde\times}$	$d_{12\times3\times45\times6\tilde\times}$
$d_{1\tilde\times23\times4\times56\tilde\times}$			
$c_{1\tilde\times2\times3456\tilde\times}$	$c_{5612\tilde\times3\times4\times}$	$c_{61\tilde\times2\tilde\times345\tilde\times}$	$c_{612\times3\times45\times}$
$c_{1\times2\times3456\tilde\times}$	$c_{5612\tilde\times3\tilde\times4\times}$	$c_{12\times3\times456\tilde\times}$	$c_{561\tilde\times2\tilde\times34\times}$
$c_{1\tilde\times23\times456\tilde\times}$	$c_{561\tilde\times23\times4\times}$	$c_{61\times2\times345\times}$	$c_{612\tilde\times3\tilde\times45\tilde\times}$
$c_{1\tilde\times234\times56\tilde\times}$	$c_{123\times4\times56\tilde\times}$	$c_{61\tilde\times234\times5\tilde\times}$	$c_{123\times45\times6\tilde\times}$
$c_{1\tilde\times2345\tilde\times6\tilde\times}$	$c_{6123\times4\times5\times}$	$c_{12\times345\times6\tilde\times}$	$c_{612\tilde\times34\times5\tilde\times}$
$c_{1\times2345\times6\tilde\times}$	$c_{6123\tilde\times4\times5\tilde\times}$	$c_{1234\times5\tilde\times6\tilde\times}$	$c_{1234\times5\times6\tilde\times}$
$c_{1\times2345\times6\times}$	$c_{6123\tilde\times4\tilde\times5\tilde\times}$	$c_{4561\tilde\times2\tilde\times3\times}$	$c_{4561\tilde\times2\times3\times}$
$b_{61\tilde\times2345\tilde\times}$	$b_{6123\times45\times}$	$b_{123\times456\tilde\times}$	$b_{561\tilde\times234\times}$
$b_{12\times3456\tilde\times}$	$b_{5612\tilde\times34\times}$	$b_{1234\times56\tilde\times}$	
$b_{61\times2345\times}$	$b_{6123\tilde\times45\tilde\times}$	$b_{4561\tilde\times23\times}$	
$b_{612\tilde\times345\tilde\times}$	$b_{612\times345\times}$		

Table F.2: Minimal set of integral coefficients for $1^+2^+3^+4^+5^-6^-$.

Coefficient	Related coefficients	Coefficient	Related coefficients
$d_{1\tilde\times2\times3\times456\tilde\times}$		$d_{1\times234\times5\times6\times}$	$d_{612\tilde\times3\tilde\times4\tilde\times5\tilde\times}$
$d_{1\times2\times345\times6\tilde\times}$	$d_{561\tilde\times2\tilde\times3\times4\tilde\times}$	$d_{61\tilde\times2\tilde\times34\times5\tilde\times}$	$d_{61\times2\times34\times5\times}$
$d_{1\tilde\times23\times4\tilde\times56\tilde\times}$	$d_{12\times3\times45\times6\tilde\times}$	$d_{123\times4\tilde\times5\times6\tilde\times}$	
$d_{1\tilde\times234\tilde\times5\tilde\times6\tilde\times}$	$d_{612\times3\times4\times5\times}$		
$c_{1\tilde\times2\times3456\tilde\times}$	$c_{4561\tilde\times2\times3\times}$	$c_{61\times2\times345\times}$	$c_{561\tilde\times2\tilde\times34\times}$
$c_{1\times2\times3456\tilde\times}$	$c_{4561\tilde\times2\times3\times}$	$c_{61\tilde\times234\tilde\times5\tilde\times}$	$c_{612\times34\times5\times}$
$c_{1\tilde\times23\times456\tilde\times}$	$c_{12\times3\times456\tilde\times}$	$c_{12\times345\times6\tilde\times}$	$c_{561\tilde\times23\times4\tilde\times}$
$c_{1\tilde\times234\tilde\times56\tilde\times}$	$c_{612\times3\times45\times}$	$c_{61\times234\times5\times}$	$c_{612\tilde\times34\tilde\times5\tilde\times}$
$c_{1\times234\times56\times}$	$c_{612\tilde\times3\tilde\times45\tilde\times}$	$c_{123\times4\tilde\times56\times}$	$c_{123\times45\times6\tilde\times}$
$c_{1\tilde\times2345\tilde\times6\tilde\times}$	$c_{5612\times3\times4\times}$	$c_{1234\tilde\times5\tilde\times6\tilde\times}$	$c_{6123\times4\times5\times}$
$c_{1\times2345\times6\tilde\times}$	$c_{5612\tilde\times3\times4\tilde\times}$	$c_{6123\tilde\times4\tilde\times5\tilde\times}$	$c_{1234\times5\times6\times}$
$c_{1\times2345\times6\times}$	$c_{5612\tilde\times3\tilde\times4\tilde\times}$	$c_{1234\tilde\times5\times6\tilde\times}$	$c_{6123\times4\tilde\times5\times}$
$c_{61\tilde\times2\tilde\times345\tilde\times}$	$c_{561\times2\times34\times}$		

Coefficient	Related coefficients	Coefficient	Related coefficients
$b_{61\tilde{\times}2345\tilde{\times}}$	$b_{5612\times34\times}$	$b_{561\tilde{\times}234\tilde{\times}}$	$b_{612\times345\times}$
$b_{12\times3456\tilde{\times}}$	$b_{4561\tilde{\times}23\times}$	$b_{123\times456\tilde{\times}}$	
$b_{61\times2345\times}$	$b_{5612\tilde{\times}34\tilde{\times}}$	$b_{1234\tilde{\times}56\tilde{\times}}$	$b_{6123\times45\times}$
$b_{612\tilde{\times}345\tilde{\times}}$	$b_{561\times234\times}$	$b_{6123\tilde{\times}45\tilde{\times}}$	$b_{1234\times56\times}$

Table F.3: Minimal set of integral coefficients for $1^+2^+3^+4^-5^+6^-$.

Coefficient	Related coefficients	Coefficient	Related coefficients
$d_{1\tilde{\times}2\times3\times456\tilde{\times}}$	$d_{123\times4\times5\tilde{\times}6\tilde{\times}}$	$d_{1\tilde{\times}2\times345\tilde{\times}6\tilde{\times}}$	$d_{1\tilde{\times}234\times5\tilde{\times}6\tilde{\times}}$, $d_{612\times3\times4\times5\tilde{\times}}$, $d_{561\tilde{\times}2\times3\times4\times}$
$d_{1\tilde{\times}2\times34\times56\tilde{\times}}$	$d_{61\tilde{\times}2\times3\times45\tilde{\times}}$, $d_{61\tilde{\times}23\times4\times5\tilde{\times}}$, $d_{12\times34\times5\tilde{\times}6\tilde{\times}}$	$d_{1\times2\times345\times6\tilde{\times}}$	$d_{1\times234\times5\times6\tilde{\times}}$, $d_{561\tilde{\times}2\tilde{\times}3\times4\times}$, $d_{612\tilde{\times}3\times4\tilde{\times}5\tilde{\times}}$
$d_{1\times2\times34\times56\tilde{\times}}$	$d_{61\tilde{\times}2\tilde{\times}3\times45\tilde{\times}}$, $d_{61\tilde{\times}23\times4\tilde{\times}5\tilde{\times}}$, $d_{12\times34\times5\times6\tilde{\times}}$	$d_{1\tilde{\times}23\times45\tilde{\times}6\tilde{\times}}$	$d_{12\times3\times4\times56\tilde{\times}}$
$c_{1\tilde{\times}2\times3456\tilde{\times}}$	$c_{1234\times5\tilde{\times}6\tilde{\times}}$, $c_{6123\times4\times5\tilde{\times}}$, $c_{4561\tilde{\times}2\times3\times}$	$c_{1\times2345\times6\tilde{\times}}$	$c_{5612\tilde{\times}3\times4\tilde{\times}}$
$c_{1\times2\times3456\tilde{\times}}$	$c_{6123\times4\tilde{\times}5\tilde{\times}}$, $c_{1234\times5\times6\tilde{\times}}$, $c_{4561\tilde{\times}2\tilde{\times}3\times}$	$c_{1\times2345\times6\times}$	$c_{5612\tilde{\times}3\tilde{\times}4\tilde{\times}}$
$c_{1\tilde{\times}23\times456\tilde{\times}}$	$c_{12\times3\times456\tilde{\times}}$, $c_{123\times4\times56\tilde{\times}}$, $c_{123\times45\tilde{\times}6\tilde{\times}}$	$c_{61\tilde{\times}2\tilde{\times}345\tilde{\times}}$	$c_{61\tilde{\times}234\tilde{\times}5\tilde{\times}}$, $c_{561\times2\times34\times}$, $c_{612\times34\times5\times}$
$c_{1\tilde{\times}234\times56\tilde{\times}}$	$c_{12\times345\tilde{\times}6\tilde{\times}}$, $c_{612\times3\times45\tilde{\times}}$, $c_{561\tilde{\times}23\times4\times}$	$c_{61\tilde{\times}2\times345\tilde{\times}}$	$c_{61\tilde{\times}234\times5\tilde{\times}}$, $c_{561\tilde{\times}2\times34\times}$, $c_{612\times34\times5\tilde{\times}}$
$c_{1\times234\times56\tilde{\times}}$	$c_{12\times345\times6\tilde{\times}}$, $c_{612\tilde{\times}3\times45\tilde{\times}}$, $c_{561\tilde{\times}23\times4\tilde{\times}}$	$c_{61\times2\times345\times}$	$c_{61\times234\times5\times}$, $c_{561\tilde{\times}2\tilde{\times}34\times}$, $c_{612\times34\tilde{\times}5\tilde{\times}}$
$c_{1\tilde{\times}2345\tilde{\times}6\tilde{\times}}$	$c_{5612\times3\times4\times}$	$c_{61\tilde{\times}23\times45\tilde{\times}}$	$c_{12\times34\times56\tilde{\times}}$
$b_{61\tilde{\times}2345\tilde{\times}}$	$b_{5612\times34\times}$	$b_{612\tilde{\times}345\tilde{\times}}$	$b_{561\tilde{\times}234\tilde{\times}}$, $b_{612\times345\times}$, $b_{561\times234\times}$
$b_{12\times3456\tilde{\times}}$	$b_{1234\times56\tilde{\times}}$, $b_{6123\times45\tilde{\times}}$, $b_{4561\tilde{\times}23\times}$	$b_{123\times456\tilde{\times}}$	
$b_{61\times2345\times}$	$b_{5612\tilde{\times}34\tilde{\times}}$	$b_{612\times345\tilde{\times}}$	$b_{561\tilde{\times}234\times}$

Table F.4: Minimal set of integral coefficients for $1^+2^+3^+4^-5^-6^-$.

Coefficient	Conversion rule	Coefficient	Conversion rule
$d_{1\tilde{\times}2\times3\times456\tilde{\times}}$	$(\overline{456123})$	$d_{1\tilde{\times}2\times345\tilde{\times}6\tilde{\times}}$	$(\overline{654321})$, $(\overline{456123})$, (321654)
$d_{1\tilde{\times}2\times34\times56\tilde{\times}}$	(321654), $(\overline{456123})$, $(\overline{654321})$	$d_{1\times2\times345\times6\tilde{\times}}$	$(\overline{654321})$, (321654), $(\overline{456123})$
$d_{1\times2\times34\times56\tilde{\times}}$	(321654), $(\overline{456123})$, $(\overline{654321})$	$d_{1\tilde{\times}23\times45\tilde{\times}6\tilde{\times}}$	(321654)
$c_{1\tilde{\times}2\times3456\tilde{\times}}$	$(\overline{654321})$, $(\overline{456123})$, (321654)	$c_{1\times2345\times6\tilde{\times}}$	(321654)
$c_{1\times2\times3456\tilde{\times}}$	$(\overline{456123})$, $(\overline{654321})$, (321654)	$c_{1\times2345\times6\times}$	(321654)
$c_{1\tilde{\times}23\times456\tilde{\times}}$	(321654), $(\overline{456123})$, $(\overline{654321})$	$c_{61\tilde{\times}2\tilde{\times}345\tilde{\times}}$	$(\overline{654321})$, (321654), $(\overline{456123})$
$c_{1\tilde{\times}234\times56\tilde{\times}}$	$(\overline{654321})$, (321654), $(\overline{456123})$	$c_{61\tilde{\times}2\times345\tilde{\times}}$	$(\overline{654321})$, (321654), $(\overline{456123})$
$c_{1\times234\times56\tilde{\times}}$	$(\overline{654321})$, (321654), $(\overline{456123})$	$c_{61\times2\times345\times}$	$(\overline{654321})$, (321654), $(\overline{456123})$
$c_{1\tilde{\times}2345\tilde{\times}6\tilde{\times}}$	(321654)	$c_{61\tilde{\times}23\times45\tilde{\times}}$	$(\overline{456123})$
$b_{61\tilde{\times}2345\tilde{\times}}$	$(\overline{456123})$	$b_{612\tilde{\times}345\tilde{\times}}$	$(\overline{654321})$, $(\overline{456123})$, (321654)
$b_{12\times3456\tilde{\times}}$	$(\overline{654321})$, $(\overline{456123})$, (321654)	$b_{123\times456\tilde{\times}}$	
$b_{61\times2345\times}$	$(\overline{456123})$	$b_{612\times345\tilde{\times}}$	$(\overline{654321})$

Table F.5: Conversion rules for $1^+2^+3^+4^-5^-6^-$ integral coefficients.

Coefficient	Related coefficients	Coefficient	Related coefficients
$d_{1\tilde{\times}2\times3\tilde{\times}456\tilde{\times}}$	$d_{1\times2\times345\times6\tilde{\times}}$, $d_{123\tilde{\times}4\tilde{\times}5\times6\tilde{\times}}$, $d_{612\times3\tilde{\times}4\times5\times}$	$d_{1\tilde{\times}234\tilde{\times}5\tilde{\times}6\tilde{\times}}$	$d_{1\times234\times5\times6\times}$, $d_{561\tilde{\times}2\tilde{\times}3\tilde{\times}4\tilde{\times}}$, $d_{561\times2\times3\times4\times}$
$d_{1\tilde{\times}23\tilde{\times}4\tilde{\times}56\tilde{\times}}$	$d_{61\times2\times34\times5\times}$	$d_{12\times3\tilde{\times}45\times6\tilde{\times}}$	
$d_{1\times23\times4\times56\times}$	$d_{61\tilde{\times}2\tilde{\times}34\tilde{\times}5\tilde{\times}}$		
$c_{1\tilde{\times}2\times3456\tilde{\times}}$	$c_{1\times2\times3456\tilde{\times}}$, $c_{6123\tilde{\times}4\tilde{\times}5\times}$, $c_{6123\tilde{\times}4\times5\times}$	$c_{1\tilde{\times}2345\tilde{\times}6\tilde{\times}}$	$c_{5612\tilde{\times}3\tilde{\times}4\tilde{\times}}$, $c_{1234\times5\times6\times}$, $c_{4561\times2\times3\times}$

Coefficient	Related coefficients	Coefficient	Related coefficients
$c_{1\tilde\times23\tilde\times456\tilde\times}$	$c_{61\times2\times345\times}$, $c_{123\tilde\times4\tilde\times56\tilde\times}$, $c_{612\times34\times5\times}$	$c_{1\times2345\times6\tilde\times}$	$c_{1234\tilde\times5\times6\tilde\times}$, $c_{4561\tilde\times2\times3\tilde\times}$, $c_{5612\times3\tilde\times4\times}$
$c_{1\times23\times456\times}$	$c_{61\tilde\times2\tilde\times345\tilde\times}$, $c_{123\times4\times56\times}$, $c_{612\tilde\times34\tilde\times5\tilde\times}$	$c_{1\times2345\times6\times}$	$c_{1234\tilde\times5\tilde\times6\times}$, $c_{4561\tilde\times2\tilde\times3\tilde\times}$, $c_{5612\times3\times4\times}$
$c_{1\tilde\times234\tilde\times56\tilde\times}$	$c_{61\times234\times5\times}$, $c_{561\times2\times34\times}$, $c_{561\tilde\times23\tilde\times4\tilde\times}$	$c_{12\times3\tilde\times456\tilde\times}$	$c_{12\times345\times6\tilde\times}$, $c_{612\times3\tilde\times45\times}$, $c_{123\tilde\times45\times6\tilde\times}$
$c_{1\times234\times56\times}$	$c_{61\tilde\times234\tilde\times5\tilde\times}$, $c_{561\tilde\times2\tilde\times34\tilde\times}$, $c_{561\times23\times4\times}$		
$b_{61\tilde\times2345\tilde\times}$	$b_{5612\tilde\times34\tilde\times}$, $b_{1234\times56\times}$, $b_{4561\times23\times}$	$b_{123\tilde\times456\tilde\times}$	$b_{612\times345\times}$
$b_{12\times3456\tilde\times}$	$b_{6123\tilde\times45\times}$	$b_{612\tilde\times345\tilde\times}$	$b_{123\times456\times}$
$b_{61\times2345\times}$	$b_{1234\tilde\times56\tilde\times}$, $b_{4561\tilde\times23\tilde\times}$, $b_{5612\times34\times}$	$b_{561\tilde\times234\tilde\times}$	$b_{561\times234\times}$

Table F.6: Minimal set of integral coefficients for $1^+2^+3^-4^+5^+6^-$.

Coefficient	Conversion rule	Coefficient	Conversion rule
$d_{1\tilde\times2\times3\tilde\times456\tilde\times}$	(216543), (456123), (543216)	$d_{1\tilde\times234\tilde\times5\tilde\times6\tilde\times}$	(543216), (456123), (216543)
$d_{1\tilde\times23\tilde\times4\tilde\times56\tilde\times}$	(216543)	$d_{12\times3\tilde\times45\times6\tilde\times}$	
$d_{1\times23\times4\times56\times}$	(216543)		
$c_{1\tilde\times2\times3456\tilde\times}$	(216543), (456123), (543216)	$c_{1\tilde\times2345\tilde\times6\tilde\times}$	(456123), (543216), (216543)
$c_{1\tilde\times23\tilde\times456\tilde\times}$	(216543), (456123), (543216)	$c_{1\times2345\times6\tilde\times}$	(543216), (216543), (456123)
$c_{1\times23\times456\times}$	(216543), (456123), (543216)	$c_{1\times2345\times6\times}$	(543216), (216543), (456123)
$c_{1\tilde\times234\tilde\times56\tilde\times}$	(543216), (216543), (456123)	$c_{12\times3\tilde\times456\tilde\times}$	(216543), (543216), (456123)
$c_{1\times234\times56\times}$	(543216), (216543), (456123)		

Coefficient	Conversion rule	Coefficient	Conversion rule
$b_{61\tilde{\times}2345\tilde{\times}}$	(456123), (543216), (216543)	$b_{123\tilde{\times}456\tilde{\times}}$	(216543)
$b_{12\times3456\tilde{\times}}$	(456123)	$b_{612\tilde{\times}345\tilde{\times}}$	(216543)
$b_{61\times2345\times}$	(543216), (216543), (456123)	$b_{561\tilde{\times}234\tilde{\times}}$	(543216)

Table F.7: Conversion rules for $1^{+}2^{+}3^{-}4^{+}5^{+}6^{-}$ integral coefficients.

Coefficient	Related coefficients	Coefficient	Related coefficients
$d_{1\tilde{\times}2\times3\tilde{\times}456\tilde{\times}}$	$d_{123\tilde{\times}4\times5\tilde{\times}6\tilde{\times}}$	$d_{61\tilde{\times}2\tilde{\times}3\tilde{\times}45\tilde{\times}}$	$d_{61\tilde{\times}23\tilde{\times}4\tilde{\times}5\tilde{\times}}$
$d_{1\times2\times3\tilde{\times}456\tilde{\times}}$	$d_{123\times4\times5\times6\tilde{\times}}$	$d_{61\tilde{\times}2\times3\tilde{\times}45\tilde{\times}}$	$d_{61\tilde{\times}23\tilde{\times}4\times5\tilde{\times}}$
$d_{1\tilde{\times}2\times34\times56\tilde{\times}}$	$d_{12\times34\times5\tilde{\times}6\tilde{\times}}$	$d_{12\times3\tilde{\times}4\times56\tilde{\times}}$	
$d_{1\times2\times34\times56\tilde{\times}}$	$d_{12\times34\times5\times6\tilde{\times}}$	$d_{12\times3\times4\times56\tilde{\times}}$	
$d_{1\tilde{\times}2\times345\tilde{\times}6\tilde{\times}}$	$d_{1\tilde{\times}234\times5\tilde{\times}6\tilde{\times}}$	$d_{61\times2\times3\times45\times}$	$d_{61\times23\times4\times5\times}$
$d_{1\times2\times345\times6\tilde{\times}}$	$d_{1\times234\times5\times6\tilde{\times}}$	$d_{612\tilde{\times}3\tilde{\times}4\tilde{\times}5\tilde{\times}}$	$d_{561\tilde{\times}2\tilde{\times}3\tilde{\times}4\tilde{\times}}$
$d_{1\tilde{\times}23\tilde{\times}45\times6\tilde{\times}}$		$d_{612\tilde{\times}3\tilde{\times}4\times5\tilde{\times}}$	$d_{561\tilde{\times}2\tilde{\times}3\tilde{\times}4\times}$
$d_{1\times23\times45\times6\tilde{\times}}$		$d_{612\times3\times4\times5\times}$	$d_{561\times2\times3\times4\times}$
$d_{1\times23\times45\times6\times}$			
$c_{1\tilde{\times}2\times3456\tilde{\times}}$	$c_{1234\times5\tilde{\times}6\tilde{\times}}$	$c_{61\tilde{\times}23\tilde{\times}45\tilde{\times}}$	
$c_{1\times2\times3456\tilde{\times}}$	$c_{1234\times5\times6\tilde{\times}}$	$c_{12\times34\times56\tilde{\times}}$	
$c_{1\tilde{\times}23\tilde{\times}456\tilde{\times}}$	$c_{123\tilde{\times}45\tilde{\times}6\tilde{\times}}$	$c_{61\times23\times45\times}$	
$c_{1\times23\times456\tilde{\times}}$	$c_{123\times45\times6\tilde{\times}}$	$c_{612\tilde{\times}3\tilde{\times}45\tilde{\times}}$	$c_{561\tilde{\times}23\tilde{\times}4\tilde{\times}}$
$c_{1\times23\times456\times}$	$c_{123\times45\times6\times}$	$c_{561\tilde{\times}2\tilde{\times}34\tilde{\times}}$	$c_{612\tilde{\times}34\tilde{\times}5\tilde{\times}}$
$c_{1\tilde{\times}234\times56\tilde{\times}}$	$c_{12\times345\tilde{\times}6\tilde{\times}}$	$c_{612\tilde{\times}3\tilde{\times}45\tilde{\times}}$	$c_{561\tilde{\times}23\tilde{\times}4\times}$
$c_{1\times234\times56\tilde{\times}}$	$c_{12\times345\times6\tilde{\times}}$	$c_{561\tilde{\times}2\times34\times}$	$c_{612\tilde{\times}34\times5\tilde{\times}}$
$c_{1\tilde{\times}2345\tilde{\times}6\tilde{\times}}$		$c_{612\times3\times45\times}$	$c_{561\times23\times4\times}$
$c_{1\times2345\times6\tilde{\times}}$		$c_{561\times2\times34\times}$	$c_{612\times34\times5\times}$
$c_{1\times2345\times6\times}$		$c_{6123\tilde{\times}4\tilde{\times}5\tilde{\times}}$	$c_{4561\tilde{\times}2\tilde{\times}3\tilde{\times}}$
$c_{61\tilde{\times}2\tilde{\times}345\tilde{\times}}$	$c_{61\tilde{\times}234\tilde{\times}5\tilde{\times}}$	$c_{5612\tilde{\times}3\tilde{\times}4\tilde{\times}}$	
$c_{61\tilde{\times}2\times345\tilde{\times}}$	$c_{61\tilde{\times}234\times5\tilde{\times}}$	$c_{6123\tilde{\times}4\times5\tilde{\times}}$	$c_{4561\tilde{\times}2\times3\tilde{\times}}$
$c_{12\times3\tilde{\times}456\tilde{\times}}$	$c_{123\tilde{\times}4\times56\tilde{\times}}$	$c_{5612\times3\tilde{\times}4\times}$	
$c_{12\times3\tilde{\times}456\tilde{\times}}$	$c_{123\tilde{\times}4\times56\tilde{\times}}$	$c_{6123\times4\times5\times}$	$c_{4561\times2\times3\times}$

Coefficient	Related coefficients	Coefficient	Related coefficients
$c_{61×2×345×}$	$c_{61×234×5×}$	$c_{5612×3×4×}$	
$b_{61\tilde{×}2345\tilde{×}}$		$b_{123×456×}$	
$b_{12×3456\tilde{×}}$	$b_{1234×56\tilde{×}}$	$b_{612×345×}$	$b_{561×234×}$
$b_{61×2345×}$		$b_{6123\tilde{×}45\tilde{×}}$	$b_{4561\tilde{×}23\tilde{×}}$
$b_{123\tilde{×}456\tilde{×}}$		$b_{5612\tilde{×}34\tilde{×}}$	
$b_{612\tilde{×}345\tilde{×}}$	$b_{561\tilde{×}234\tilde{×}}$	$b_{6123×45×}$	$b_{4561×23×}$
$b_{123×456\tilde{×}}$		$b_{5612×34×}$	
$b_{612×345\tilde{×}}$	$b_{561\tilde{×}234×}$		

Table F.8: Minimal set of integral coefficients for $1^+2^+3^-4^+5^-6^-$.

Coefficient	Related coefficients	Coefficient	Related coefficients
$d_{1\tilde{×}2\tilde{×}3\tilde{×}456\tilde{×}}$	$d_{1×2×3×456×}$, $d_{1\tilde{×}2\tilde{×}345\tilde{×}6\tilde{×}}$, $d_{1×2×345×6×}$, $d_{1\tilde{×}234\tilde{×}5\tilde{×}6\tilde{×}}$, $d_{1×234×5×6×}$, $d_{123\tilde{×}4\tilde{×}5\tilde{×}6\tilde{×}}$, $d_{612\tilde{×}3\tilde{×}4\tilde{×}5\tilde{×}}$, $d_{561\tilde{×}2\tilde{×}3\tilde{×}4\tilde{×}}$, $d_{123×4×5×6×}$, $d_{612×3×4×5×}$, $d_{561×2×3×4×}$	$d_{1×2\tilde{×}34\tilde{×}56\tilde{×}}$	$d_{1×23×45×6\tilde{×}}$, $d_{12\tilde{×}3×4\tilde{×}56\tilde{×}}$, $d_{61×2\tilde{×}3×45×}$, $d_{12\tilde{×}34\tilde{×}5×6\tilde{×}}$, $d_{61×23×4\tilde{×}5×}$
$d_{1×2\tilde{×}3×456\tilde{×}}$	$d_{1×2\tilde{×}345×6\tilde{×}}$, $d_{1×234\tilde{×}5×6\tilde{×}}$, $d_{123×4\tilde{×}5×6\tilde{×}}$, $d_{561×2\tilde{×}3×4\tilde{×}}$, $d_{612\tilde{×}3×4\tilde{×}5×}$	$d_{1×2×34×56×}$	$d_{1\tilde{×}23\tilde{×}45\tilde{×}6\tilde{×}}$, $d_{61\tilde{×}2\tilde{×}3\tilde{×}45\tilde{×}}$, $d_{12×3×4×56×}$, $d_{61\tilde{×}23\tilde{×}4\tilde{×}5\tilde{×}}$, $d_{12×34×5×6×}$
$d_{1\tilde{×}2\tilde{×}34\tilde{×}56\tilde{×}}$	$d_{1×23×45×6×}$, $d_{12\tilde{×}3\tilde{×}4\tilde{×}56\tilde{×}}$, $d_{61×2×3×45×}$, $d_{12\tilde{×}34\tilde{×}5\tilde{×}6\tilde{×}}$, $d_{61×23×4×5×}$		
$c_{1\tilde{×}2\tilde{×}3456\tilde{×}}$	$c_{1×2345×6×}$, $c_{1234\tilde{×}5\tilde{×}6\tilde{×}}$, $c_{5612\tilde{×}3\tilde{×}4\tilde{×}}$, $c_{6123×4×5×}$, $c_{4561×2×3×}$	$c_{1×23×456\tilde{×}}$	$c_{1×234\tilde{×}56\tilde{×}}$, $c_{12\tilde{×}3×456\tilde{×}}$, $c_{61×2\tilde{×}345×}$, $c_{12\tilde{×}345×6\tilde{×}}$, $c_{61×234\tilde{×}5×}$, $c_{123×4\tilde{×}56\tilde{×}}$, $c_{561×2\tilde{×}34\tilde{×}}$, $c_{612\tilde{×}3×45×}$, $c_{123×45×6\tilde{×}}$, $c_{561×23×4\tilde{×}}$, $c_{612\tilde{×}34\tilde{×}5×}$

Coefficient	Related coefficients	Coefficient	Related coefficients
$c_{1\times2\tilde{\times}3456\tilde{\times}}$	$c_{1\times2345\times6\tilde{\times}}$, $c_{1234\tilde{\times}5\times6\tilde{\times}}$, $c_{5612\tilde{\times}3\times4\tilde{\times}}$, $c_{6123\times4\tilde{\times}5\times}$, $c_{4561\times2\tilde{\times}3\times}$	$c_{1\times23\times456\times}$	$c_{1\tilde{\times}234\tilde{\times}56\tilde{\times}}$, $c_{12\tilde{\times}3\tilde{\times}456\tilde{\times}}$, $c_{61\times2\times345\times}$, $c_{12\tilde{\times}345\tilde{\times}6\tilde{\times}}$, $c_{61\times234\times5\times}$, $c_{123\tilde{\times}4\tilde{\times}56\tilde{\times}}$, $c_{561\tilde{\times}2\tilde{\times}34\tilde{\times}}$, $c_{612\times3\times45\times}$, $c_{612\tilde{\times}34\tilde{\times}5\tilde{\times}}$, $c_{123\times45\times6\times}$, $c_{561\times23\times4\times}$
$c_{1\times2\times3456\times}$	$c_{1\tilde{\times}2345\tilde{\times}6\tilde{\times}}$, $c_{6123\tilde{\times}4\tilde{\times}5\tilde{\times}}$, $c_{4561\tilde{\times}2\tilde{\times}3\tilde{\times}}$, $c_{1234\times5\times6\times}$, $c_{5612\times3\times4\times}$	$c_{12\tilde{\times}34\tilde{\times}56\tilde{\times}}$	$c_{61\times23\times45\times}$
$c_{1\tilde{\times}23\tilde{\times}456\tilde{\times}}$	$c_{1\times234\times56\times}$, $c_{61\tilde{\times}2\tilde{\times}345\tilde{\times}}$, $c_{12\times3\times456\times}$, $c_{61\tilde{\times}234\tilde{\times}5\tilde{\times}}$, $c_{12\times345\times6\times}$, $c_{612\tilde{\times}3\tilde{\times}45\tilde{\times}}$, $c_{123\times4\times56\times}$, $c_{561\times2\times34\times}$, $c_{123\tilde{\times}45\tilde{\times}6\tilde{\times}}$, $c_{561\tilde{\times}23\tilde{\times}4\tilde{\times}}$, $c_{612\times34\times5\times}$	$c_{61\tilde{\times}23\tilde{\times}45\tilde{\times}}$	$c_{12\times34\times56\times}$
$b_{12\tilde{\times}3456\tilde{\times}}$	$b_{61\times2345\times}$, $b_{1234\tilde{\times}56\tilde{\times}}$, $b_{5612\tilde{\times}34\tilde{\times}}$, $b_{6123\times45\times}$, $b_{4561\times23\times}$	$b_{123\tilde{\times}456\tilde{\times}}$	$b_{612\tilde{\times}345\tilde{\times}}$, $b_{561\tilde{\times}234\tilde{\times}}$, $b_{123\times456\times}$, $b_{612\times345\times}$, $b_{561\times234\times}$
$b_{61\tilde{\times}2345\tilde{\times}}$	$b_{12\times3456\times}$, $b_{6123\tilde{\times}45\tilde{\times}}$, $b_{4561\tilde{\times}23\tilde{\times}}$, $b_{1234\times56\times}$, $b_{5612\times34\times}$	$b_{123\times456\tilde{\times}}$	$b_{561\times234\tilde{\times}}$, $b_{612\tilde{\times}345\times}$

Table F.9: Minimal set of integral coefficients for $1^+2^-3^+4^-5^+6^-$.

Coefficient	Conversion rule	Coefficient	Conversion rule
$d_{1\tilde{\times}2\tilde{\times}3\tilde{\times}456\tilde{\times}}$	(321654), $(\overline{216543})$, $(\overline{612345})$, (561234), (165432), $(\overline{654321})$, (345612), $(\overline{432165})$, $(\overline{456123})$, (543216), $(\overline{234561})$	$d_{1\times2\tilde{\times}34\tilde{\times}56\tilde{\times}}$	(165432), (345612), $(\overline{234561})$, (561234), $(\overline{456123})$

Coefficient	Conversion rule	Coefficient	Conversion rule
$d_{1\times2\tilde\times3\times456\tilde\times}$	$(\overline{216543})$, (165432), $(\overline{456123})$, $(\overline{234561})$, (345612)	$d_{1\times2\times34\times56\times}$	(165432), $(\overline{234561})$, (345612), $(\overline{456123})$, (561234)
$d_{1\tilde\times2\tilde\times34\tilde\times56\tilde\times}$	(165432), (345612), $(\overline{234561})$, (561234), $(\overline{456123})$		
$c_{1\tilde\times2\tilde\times3456\tilde\times}$	(165432), (561234), (345612), $(\overline{456123})$, $(\overline{234561})$	$c_{1\times23\times456\tilde\times}$	(165432), (321654), $(\overline{216543})$, $(\overline{612345})$, (561234), $(\overline{456123})$, $(\overline{234561})$, (345612), $(\overline{654321})$, $(\overline{432165})$, (543216)
$c_{1\times2\tilde\times3456\tilde\times}$	(165432), (561234), (345612), $(\overline{456123})$, $(\overline{234561})$	$c_{1\times23\times456\times}$	(165432), (321654), $(\overline{216543})$, $(\overline{612345})$, (561234), $(\overline{456123})$, $(\overline{234561})$, (345612), (543216), $(\overline{654321})$, $(\overline{432165})$
$c_{1\times2\times3456\times}$	(165432), $(\overline{456123})$, $(\overline{234561})$, (561234), (345612)	$c_{12\tilde\times34\tilde\times56\tilde\times}$	(165432)
$c_{1\tilde\times23\tilde\times456\tilde\times}$	(165432), $(\overline{216543})$, (321654), (561234), $(\overline{612345})$, (345612), $(\overline{456123})$, $(\overline{234561})$, $(\overline{654321})$, $(\overline{432165})$, (543216)	$c_{61\tilde\times23\tilde\times45\tilde\times}$	$(\overline{234561})$
$b_{12\tilde\times3456\tilde\times}$	(165432), (561234), (345612), $(\overline{456123})$, $(\overline{234561})$	$b_{123\tilde\times456\tilde\times}$	$(\overline{216543})$, $(\overline{432165})$, (321654), (543216), (165432)

Coefficient	Conversion rule	Coefficient	Conversion rule
$b_{61\tilde{\times}2345\tilde{\times}}$	$(\overline{234561})$, (561234), (345612), $(\overline{612345})$, $(\overline{456123})$	$b_{123\times456\tilde{\times}}$	(165432), $(\overline{216543})$

Table F.10: Conversion rules for $1^+2^-3^+4^-5^+6^-$ integral coefficients.

Higgs + 4 Partons Coefficient Tables

In the four-gluon case $(0 \to ggggh)$, there are four independent helicity assignments

1. $1_g^+ 2_g^+ 3_g^+ 4_g^+$, 2. $1_g^+ 2_g^+ 3_g^+ 4_g^-$, 3. $1_g^+ 2_g^+ 3_g^- 4_g^-$, 4. $1_g^+ 2_g^- 3_g^+ 4_g^-$.

For the two-quark two-gluon case $(0 \to qqggh)$, there are three independent helicity assignments, because of helicity conservation along the external quark line

1. $1_{\bar{q}}^+ 2_q^+ 3_g^+ 4_g^+$, 2. $1_{\bar{q}}^+ 2_q^+ 3_g^+ 4_g^-$, 3. $1_{\bar{q}}^+ 2_q^+ 3_g^- 4_g^-$.

The four-quark amplitude $(0 \to qqggh)$ can be expressed in a single compact formula via two form factors [49]. Thus, it does not need to be included in the following master-integral decomposition tables.

The convention used in the following tables is slightly different from the one used in the previous section of the Appendix. The sum over the degrees of freedom (left/right chiral) of the massive top-quark propagating in the loop has already been performed, hence $\times$ is a generic delimiter for the corners of the diagram and does not carry any helicity meaning[1]. Furthermore, box, triangle and bubble integrals carry three, two and one subscript indices respectively, i.e. one index less than in the previous section. The convention is that the omitted one contains all particles not appearing the ones given explicitly.

---

[1] Helicity would not even be a good quantum number, since the loop propagator is massive.

For instance, the coefficient in $1_g^+\, 2_g^+\, 3_g^+\, 4_g^+$ labeled as $d_{1\times2\times34}$ corresponds to the following cut diagram
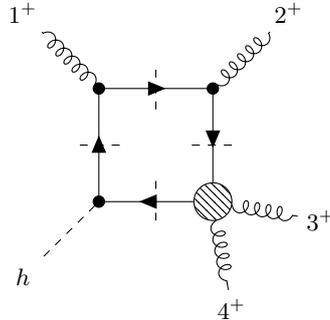
where in the loop we have a massive top quark. Note that three of the four corners correspond to individual vertices in standard Feynman diagrams, but the one in the bottom right corner represents any possible tree topology. In this case there are two possibilities: a gluon "s" channel or a fermion "t" channel exchange. The latter is what, in four dimensions, gives raise to the reduction × pentagon coefficient contribution to this box coefficient.

The tables of coefficients follow.

Coefficient	Related coefficients		Coefficient	Related coefficients
$d_{1\times2\times34}$	$d_{2\times3\times41}, d_{3\times4\times12}, d_{4\times1\times23},$		$c_{1\times234}$	$c_{2\times341}, c_{3\times412}, c_{4\times123}$
	$d_{1\times4\times32}, d_{2\times1\times43}, d_{3\times2\times14}, d_{4\times3\times21}$			
$d_{1\times23\times4}$	$d_{2\times34\times1}, d_{3\times41\times2}, d_{4\times12\times3}$			
$d_{1\times2\times3}$	$d_{2\times3\times4}, d_{3\times4\times1}, d_{4\times1\times2}$			

Table G.1: Minimal set of integral coefficients for $1_g^+\, 2_g^+\, 3_g^+\, 4_g^+$.

Coefficient	Related coefficients	Coefficient	Related coefficients
$d_{1\times2\times34}$	$d_{3\times2\times14}$	$c_{3\times4}$	$c_{4\times1}$
$d_{1\times4\times32}$	$d_{3\times4\times12}$	$c_{2\times34}$	$c_{2\times14}$
$d_{2\times1\times43}$	$d_{2\times3\times41}$	$c_{1\times43}$	$c_{3\times41}$
$d_{2\times34\times1}$	$d_{3\times41\times2}$	$c_{4\times123}$	
$d_{4\times3\times21}$	$d_{4\times1\times23}$	$c_{1\times234}$	$c_{3\times412}$
$d_{1\times23\times4}$	$d_{4\times12\times3}$	$c_{2\times341}$	
$d_{2\times3\times4}$	$d_{4\times1\times2}$	$c_{12\times34}$	$c_{23\times41}$
$d_{1\times2\times3}$		b_{34}	b_{14}

Coefficient	Related coefficients	Coefficient	Related coefficients
$d_{3\times4\times1}$		b_{234}	b_{412}, b_{341}
		b_{1234}	

Table G.2: Minimal set of integral coefficients for $1_g^+ 2_g^+ 3_g^+ 4_g^-$.

Coefficient	Related coefficients	Coefficient	Related coefficients
$d_{1\times2\times34}$	$d_{2\times1\times43}, d_{3\times4\times12}, d_{4\times3\times21}$	$c_{2\times3}$	$c_{4\times1}$
$d_{1\times4\times32}$	$d_{3\times2\times14}, d_{4\times1\times23}, d_{2\times3\times41}$	$c_{1\times23}$	$c_{2\times14}, c_{3\times41}, c_{4\times32}$
$d_{2\times34\times1}$	$d_{4\times12\times3}$	$c_{23\times41}$	
$d_{1\times23\times4}$	$d_{3\times41\times2}$	$c_{1\times234}$	$c_{2\times341}, c_{3\times412}, c_{4\times123}$
$d_{1\times2\times3}$	$d_{3\times4\times1}, d_{4\times1\times2}, d_{2\times3\times4}$	b_{23}	b_{41}
		b_{234}	$b_{341}, b_{412}, b_{123}$
		b_{1234}	

Table G.3: Minimal set of integral coefficients for $1_g^+ 2_g^+ 3_g^- 4_g^-$.

Coefficient	Related coefficients	Coefficient	Related coefficients
$d_{4\times3\times21}$	$d_{2\times1\times43}, d_{3\times2\times14}, d_{1\times4\times32},$	$c_{3\times4}$	$c_{4\times1}, c_{2\times3}, c_{1\times2}$
	$d_{1\times2\times34}, d_{2\times3\times41},$	$c_{2\times34}$	$c_{3\times41}, c_{4\times12}, c_{1\times23}$
	$d_{3\times4\times12}, d_{4\times1\times23}$		$c_{1\times43}, c_{2\times14}, c_{3\times21}, c_{4\times32}$
$d_{1\times23\times4}$	$d_{2\times34\times1}, d_{3\times41\times2}, d_{4\times12\times3}$	$c_{12\times34}$	$c_{23\times41}$
$d_{1\times2\times3}$	$d_{2\times3\times4}, d_{3\times4\times1}, d_{4\times1\times2}$	$c_{1\times234}$	$c_{2\times341}, c_{3\times412}, c_{4\times123}$
		b_{34}	b_{12}, b_{23}, b_{41}
		b_{234}	$b_{341}, b_{412}, b_{123}$
		b_{1234}	

Table G.4: Minimal set of integral coefficients for $1_g^+ 2_g^- 3_g^+ 4_g^-$.

$1_{\bar{q}}^+, 2_q^-, 3_g^+, 4_g^+$		$1_{\bar{q}}^+, 2_q^-, 3_g^-, 4_g^+$		$1_{\bar{q}}^+, 2_q^-, 3_g^+, 4_g^-$	
Coefficient	Related coefficients	Coefficient	Related coefficients	Coefficient	Related coefficients
$d_{3\times21\times4}$		$d_{3\times21\times4}$		$c_{4\times123}$	$c_{3\times412}$

$1^+_{\bar{q}}, 2^-_q, 3^+_g, 4^+_g$		$1^+_{\bar{q}}, 2^-_q, 3^-_g, 4^+_g$		$1^+_{\bar{q}}, 2^-_q, 3^+_g, 4^-_g$	
Coefficient	Related coefficients	Coefficient	Related coefficients	Coefficient	Related coefficients
$d_{4 \times 3 \times 21}$	$d_{3 \times 4 \times 12}$	$d_{4 \times 3 \times 21}$	$d_{3 \times 4 \times 12}$	b_{123}	b_{412}
$c_{3 \times 21}$	$c_{4 \times 12}$	$c_{3 \times 21}$	$c_{4 \times 12}$		
$c_{12 \times 34}$		$c_{3 \times 4}$			
$c_{4 \times 123}$		$c_{12 \times 34}$			
$c_{3 \times 412}$		$c_{4 \times 123}$	$c_{3 \times 412}$		
b_{12}		b_{34}			
b_{123}		b_{12}			
b_{412}		b_{123}	b_{412}		
b_{1234}		b_{1234}			

Table G.5: Minimal set of integral coefficients for $H^{34}_4(1^+_{\bar{q}}, 2^-_q, 3^+_g, 4^+_g)$, $H^{34}_4(1^+_{\bar{q}}, 2^-_q, 3^-_g, 4^+_g)$ and $H^{34}_4(1^+_{\bar{q}}, 2^-_q, 3^+_g, 4^-_g)$ together with the related coefficients that can be obtained from the base set.

Bibliography

[1] G. De Laurentis and D. Maître, *Extracting analytical one-loop amplitudes from numerical evaluations*, *JHEP* **07** (2019) 123 [1904.04067].

[2] G. De Laurentis, *Analytical amplitudes from numerical solutions of the scattering equations*, *JHEP* **02** (2020) 194 [1910.11355].

[3] L. Budge, J. M. Campbell, G. De Laurentis, R. Keith Ellis and S. Seth, *The one-loop amplitudes for Higgs + 4 partons with full mass effects*, 2002.04018.

[4] M. D'Onofrio and K. Rummukainen, *Standard model cross-over on the lattice*, *Phys. Rev.* **D93** (2016) 025003 [1508.07161].

[5] M. Johnson and D. Maître, *Strong coupling constant extraction from high-multiplicity Z+jets observables*, *Phys. Rev.* **D97** (2018) 054013 [1711.01408].

[6] L. Smaldone, *Dynamical Generation of Fermion Mixing*, Ph.D. thesis, 09, 2015. 10.13140/RG.2.1.2118.8728.

[7] R. K. Ellis and G. Zanderighi, *Scalar one-loop integrals for QCD*, *JHEP* **02** (2008) 002 [0712.1851].

[8] T. D. Lee and M. Nauenberg, *Degenerate systems and mass singularities*, *Phys. Rev.* **133** (1964) B1549.

[9] J. D. Bjorken, *Asymptotic sum rules at infinite momentum*, *Phys. Rev.* **179** (1969) 1547.

[10] S. J. Parke and T. R. Taylor, *Amplitude for n-gluon scattering*, *Phys. Rev. Lett.* **56** (1986) 2459.

[11] A. von Manteuffel and R. M. Schabinger, *A novel approach to integration by parts reduction*, *Phys. Lett.* **B744** (2015) 101 [1406.4513].

[12] P. Maierhöfer, J. Usovitsch and P. Uwer, *Kira—A Feynman integral reduction program*, *Comput. Phys. Commun.* **230** (2018) 99 [1705.05610].

[13] A. V. Smirnov and F. S. Chukharev, *FIRE6: Feynman Integral REduction with Modular Arithmetic*, 1901.07808.

[14] J. Klappert and F. Lange, *Reconstructing Rational Functions with* `FireFly`, 1904.00009.

[15] T. Peraro, *Scattering amplitudes over finite fields and multivariate functional reconstruction*, *JHEP* **12** (2016) 030 [1608.01902].

[16] M. Zeng, *Differential equations on unitarity cut surfaces*, *JHEP* **06** (2017) 121 [1702.02355].

[17] S. Abreu, F. Febres Cordero, H. Ita, M. Jaquier, B. Page and M. Zeng, *Two-Loop Four-Gluon Amplitudes from Numerical Unitarity*, *Phys. Rev. Lett.* **119** (2017) 142001 [1703.05273].

[18] S. Badger, C. Brønnum-Hansen, H. B. Hartanto and T. Peraro, *First look at two-loop five-gluon scattering in QCD*, *Phys. Rev. Lett.* **120** (2018) 092001 [1712.02229].

[19] S. Abreu, F. Febres Cordero, H. Ita, B. Page and M. Zeng, *Planar Two-Loop Five-Gluon Amplitudes from Numerical Unitarity*, *Phys. Rev.* **D97** (2018) 116014 [1712.03946].

[20] X. Liu and Y.-Q. Ma, *Determine Arbitrary Feynman Integrals by Vacuum Integrals*, 1801.10523.

[21] S. Abreu, F. Febres Cordero, H. Ita, B. Page and M. Zeng, *Five-Point Two-Loop Amplitudes from Numerical Unitarity*, *PoS* **LL2018** (2018) 016 [1807.09447].

[22] S. Abreu, F. Febres Cordero, H. Ita, B. Page and V. Sotnikov, *Planar Two-Loop Five-Parton Amplitudes from Numerical Unitarity*, *JHEP* **11** (2018) 116 [1809.09067].

[23] S. Badger, C. Brønnum-Hansen, H. B. Hartanto and T. Peraro, *Analytic helicity amplitudes for two-loop five-gluon scattering: the single-minus case*, *JHEP* **01** (2019) 186 [1811.11699].

[24] S. Badger, C. Brønnum-Hansen, T. Gehrmann, H. B. Hartanto, J. Henn, N. A. Lo Presti et al., *Applications of integrand reduction to two-loop five-point scattering amplitudes in QCD*, *PoS* **LL2018** (2018) 006 [1807.09709].

[25] S. Abreu, J. Dormans, F. Febres Cordero, H. Ita and B. Page, *Analytic Form of the Planar Two-Loop Five-Gluon Scattering Amplitudes in QCD*, 1812.04586.

[26] S. Abreu, L. J. Dixon, E. Herrmann, B. Page and M. Zeng, *The two-loop five-point amplitude in $\mathcal{N} = 4$ super-Yang-Mills theory*, 1812.08941.

[27] S. Abreu, J. Dormans, F. Febres Cordero, H. Ita, B. Page and V. Sotnikov, *Analytic Form of the Planar Two-Loop Five-Parton Scattering Amplitudes in QCD*, 1904.00945.

[28] D. Chicherin, T. Gehrmann, J. M. Henn, P. Wasser, Y. Zhang and S. Zoia, *The two-loop five-particle amplitude in $\mathcal{N} = 8$ supergravity*, 1901.05932.

[29] S. Abreu, L. J. Dixon, E. Herrmann, B. Page and M. Zeng, *The two-loop five-point amplitude in $\mathcal{N} = 8$ supergravity*, 1901.08563.

[30] J. M. Henn, T. Peraro, M. Stahlhofen and P. Wasser, *Matter dependence of the four-loop cusp anomalous dimension*, 1901.03693.

[31] A. von Manteuffel and R. M. Schabinger, *Quark and gluon form factors to four-loop order in QCD: the N_f^3 contributions*, *Phys. Rev.* **D95** (2017) 034030 [1611.00795].

[32] G. Mahlon, *Multi - gluon helicity amplitudes involving a quark loop*, *Phys. Rev.* **D49** (1994) 4438 [hep-ph/9312276].

[33] Z. Bern, G. Chalmers, L. J. Dixon and D. A. Kosower, *One loop N gluon amplitudes with maximal helicity violation via collinear limits*, *Phys. Rev. Lett.* **72** (1994) 2134 [hep-ph/9312333].

[34] Z. Bern, L. J. Dixon, D. C. Dunbar and D. A. Kosower, *One loop n point gauge theory amplitudes, unitarity and collinear limits*, *Nucl. Phys.* **B425** (1994) 217 [hep-ph/9403226].

[35] Z. Bern, L. J. Dixon, D. C. Dunbar and D. A. Kosower, *Fusing gauge theory tree amplitudes into loop amplitudes*, *Nucl. Phys.* **B435** (1995) 59 [`hep-ph/9409265`].

[36] S. J. Bidder, N. E. J. Bjerrum-Bohr, L. J. Dixon and D. C. Dunbar, *N=1 supersymmetric one-loop amplitudes and the holomorphic anomaly of unitarity cuts*, *Phys. Lett.* **B606** (2005) 189 [`hep-th/0410296`].

[37] J. Bedford, A. Brandhuber, B. J. Spence and G. Travaglini, *Non-supersymmetric loop amplitudes and MHV vertices*, *Nucl. Phys.* **B712** (2005) 59 [`hep-th/0412108`].

[38] R. Britto, E. Buchbinder, F. Cachazo and B. Feng, *One-loop amplitudes of gluons in SQCD*, *Phys. Rev.* **D72** (2005) 065012 [`hep-ph/0503132`].

[39] Z. Bern, L. J. Dixon and D. A. Kosower, *Bootstrapping multi-parton loop amplitudes in QCD*, *Phys. Rev.* **D73** (2006) 065013 [`hep-ph/0507005`].

[40] Z. Bern, N. E. J. Bjerrum-Bohr, D. C. Dunbar and H. Ita, *Recursive calculation of one-loop QCD integral coefficients*, *JHEP* **11** (2005) 027 [`hep-ph/0507019`].

[41] R. Britto, B. Feng and P. Mastrolia, *The Cut-constructible part of QCD amplitudes*, *Phys. Rev.* **D73** (2006) 105004 [`hep-ph/0602178`].

[42] C. F. Berger, Z. Bern, L. J. Dixon, D. Forde and D. A. Kosower, *Bootstrapping One-Loop QCD Amplitudes with General Helicities*, *Phys. Rev.* **D74** (2006) 036009 [`hep-ph/0604195`].

[43] C. F. Berger, Z. Bern, L. J. Dixon, D. Forde and D. A. Kosower, *All One-loop Maximally Helicity Violating Gluonic Amplitudes in QCD*, *Phys. Rev.* **D75** (2007) 016006 [`hep-ph/0607014`].

[44] Z. Xiao, G. Yang and C.-J. Zhu, *The Rational Part of QCD Amplitude. III. The Six-Gluon*, *Nucl. Phys.* **B758** (2006) 53 [`hep-ph/0607017`].

[45] D. C. Dunbar, *One-Loop Six Gluon Amplitude*, `0901.1202`.

[46] R. K. Ellis and S. Seth, *On Higgs boson plus gluon amplitudes at one loop*, *JHEP* **11** (2018) 006 [`1808.09292`].

[47] T. Neumann and C. Williams, *The Higgs boson at high p_T*, *Phys. Rev.* **D95** (2017) 014004 [`1609.00367`].

[48] N. Greiner, S. Höche, G. Luisoni, M. Schönherr and J.-C. Winter, *Full mass dependence in Higgs boson production in association with jets at the LHC and FCC*, *JHEP* **01** (2017) 091 [1608.01195].

[49] V. Del Duca, W. Kilgore, C. Oleari, C. Schmidt and D. Zeppenfeld, *Gluon fusion contributions to H + 2 jet production*, *Nucl. Phys.* **B616** (2001) 367 [hep-ph/0108030].

[50] H. Kawai, D. Lewellen and S.-H. Tye, *A relation between tree amplitudes of closed and open strings*, *Nuclear Physics B* **269** (1986) 1 .

[51] D. Fairlie and D. Roberts, *Dual Models without Tachyons - a New Approach*, *unpublished Durham preprint PRINT-72-2440* (1972) .

[52] D. Roberts, *Mathematical Structure of Dual Amplitudes*, *Durham PhD thesis* (1972) .

[53] D. B. Fairlie, *A Coding of Real Null Four-Momenta into World-Sheet Coordinates*, *Adv. Math. Phys.* **2009** (2009) 284689 [0805.2263].

[54] D. J. Gross and P. F. Mende, *String Theory Beyond the Planck Scale*, *Nucl. Phys.* **B303** (1988) 407.

[55] F. Cachazo, S. He and E. Y. Yuan, *Scattering in Three Dimensions from Rational Maps*, *JHEP* **10** (2013) 141 [1306.2962].

[56] F. Cachazo, S. He and E. Y. Yuan, *Scattering of Massless Particles in Arbitrary Dimensions*, *Phys. Rev. Lett.* **113** (2014) 171601 [1307.2199].

[57] F. Cachazo, S. He and E. Y. Yuan, *Scattering of Massless Particles: Scalars, Gluons and Gravitons*, *JHEP* **07** (2014) 033 [1309.0885].

[58] L. Dolan and P. Goddard, *Proof of the Formula of Cachazo, He and Yuan for Yang-Mills Tree Amplitudes in Arbitrary Dimension*, *JHEP* **05** (2014) 010 [1311.5200].

[59] T. Adamo, E. Casali and D. Skinner, *Ambitwistor strings and the scattering equations at one loop*, *JHEP* **04** (2014) 104 [1312.3828].

[60] Y. Geyer, L. Mason, R. Monteiro and P. Tourkine, *Loop Integrands for Scattering Amplitudes from the Riemann Sphere*, *Phys. Rev. Lett.* **115** (2015) 121603 [1507.00321].

[61] L. Mason and D. Skinner, *Ambitwistor strings and the scattering equations*, *JHEP* **07** (2014) 048 [`1311.2564`].

[62] F. Cachazo, S. He and E. Y. Yuan, *Scattering equations and Kawai-Lewellen-Tye orthogonality*, *Phys. Rev.* **D90** (2014) 065001 [`1306.6575`].

[63] S. Weinzierl, *On the solutions of the scattering equations*, *JHEP* **04** (2014) 092 [`1402.2516`].

[64] R. Huang, J. Rao, B. Feng and Y.-H. He, *An Algebraic Approach to the Scattering Equations*, *JHEP* **12** (2015) 056 [`1509.04483`].

[65] M. Søgaard and Y. Zhang, *Scattering Equations and Global Duality of Residues*, *Phys. Rev.* **D93** (2016) 105009 [`1509.08897`].

[66] J. A. Farrow, *A Monte Carlo Approach to the 4D Scattering Equations*, *JHEP* **08** (2018) 085 [`1806.02732`].

[67] Z. Bern, J. J. M. Carrasco and H. Johansson, *New Relations for Gauge-Theory Amplitudes*, *Phys. Rev.* **D78** (2008) 085011 [`0805.3993`].

[68] Z. Bern, J. J. M. Carrasco and H. Johansson, *Perturbative Quantum Gravity as a Double Copy of Gauge Theory*, *Phys. Rev. Lett.* **105** (2010) 061602 [`1004.0476`].

[69] Z. Bern, J. J. Carrasco, M. Chiodaroli, H. Johansson and R. Roiban, *The Duality Between Color and Kinematics and its Applications*, `1909.01358`.

[70] R. Kleiss and H. Kuijf, *Multi - Gluon Cross-sections and Five Jet Production at Hadron Colliders*, *Nucl. Phys.* **B312** (1989) 616.

[71] V. Del Duca, L. J. Dixon and F. Maltoni, *New color decompositions for gauge amplitudes at tree and loop level*, *Nucl. Phys. B* **571** (2000) 51 [`hep-ph/9910563`].

[72] Z. Bern and D. A. Kosower, *The computation of loop amplitudes in gauge theories*, *Nuclear Physics B* **379** (1992) 451 .

[73] G. Passarino and M. Veltman, *One Loop Corrections for e+ e- Annihilation Into mu+ mu- in the Weinberg Model*, *Nucl. Phys. B* **160** (1979) 151.

[74] E. Wigner, *On unitary representations of the inhomogeneous lorentz group*, 1939.

[75] L. J. Dixon, *A brief introduction to modern amplitude methods*, in *Proceedings, 2012 European School of High-Energy Physics (ESHEP 2012): La Pommeraye, Anjou, France, June 06-19, 2012*, pp. 31–67, 2014, 1310.5353, DOI.

[76] D. Maitre and P. Mastrolia, *S@M, a Mathematica Implementation of the Spinor-Helicity Formalism*, *Comput. Phys. Commun.* **179** (2008) 501 [0710.5559].

[77] M. E. Peskin, *Simplifying Multi-Jet QCD Computation*, in *Proceedings, 13th Mexican School of Particles and Fields (MSPF 2008): San Carlos, Sonora, Mexico, October 2-11, 2008*.

[78] H. Elvang and Y.-t. Huang, *Scattering Amplitudes*, 1308.1697.

[79] H. K. Dreiner, H. E. Haber and S. P. Martin, *Two-component spinor techniques and Feynman rules for quantum field theory and supersymmetry*, *Phys. Rept.* **494** (2010) 1 [0812.1594].

[80] R. Britto, F. Cachazo and B. Feng, *Generalized unitarity and one-loop amplitudes in N=4 super-Yang-Mills*, *Nucl. Phys.* **B725** (2005) 275 [hep-th/0412103].

[81] N. E. J. Bjerrum-Bohr, D. C. Dunbar and W. B. Perkins, *Analytic structure of three-mass triangle coefficients*, *JHEP* **04** (2008) 038 [0709.2086].

[82] D. Forde, *Direct extraction of one-loop integral coefficients*, *Phys. Rev.* **D75** (2007) 125019 [0704.1835].

[83] P. Mastrolia, *On Triple-cut of scattering amplitudes*, *Phys. Lett.* **B644** (2007) 272 [hep-th/0611091].

[84] W. B. Kilgore, *One-loop Integral Coefficients from Generalized Unitarity*, 0711.5015.

[85] A. Brandhuber, S. McNamara, B. J. Spence and G. Travaglini, *Loop amplitudes in pure Yang-Mills from generalised unitarity*, *JHEP* **10** (2005) 011 [hep-th/0506068].

[86] C. Anastasiou, R. Britto, B. Feng, Z. Kunszt and P. Mastrolia, *Unitarity cuts and Reduction to master integrals in d dimensions for one-loop amplitudes*, *JHEP* **03** (2007) 111 [hep-ph/0612277].

[87] C. Anastasiou, R. Britto, B. Feng, Z. Kunszt and P. Mastrolia, *D-dimensional unitarity cut method*, *Phys. Lett.* **B645** (2007) 213 [hep-ph/0609191].

[88] S. D. Badger, *Direct Extraction Of One Loop Rational Terms*, *JHEP* **01** (2009) 049 [`0806.4600`].

[89] W. Torres Bobadilla, A. Fazio, P. Mastrolia and E. Mirabella, *Generalised Unitarity for Dimensionally Regulated Amplitudes*, *Nucl. Part. Phys. Proc.* **267-269** (2015) 150 [`1505.05890`].

[90] P. Mastrolia, *Double-Cut of Scattering Amplitudes and Stokes' Theorem*, *Phys. Lett.* **B678** (2009) 246 [`0905.2909`].

[91] R. Britto, F. Cachazo and B. Feng, *New recursion relations for tree amplitudes of gluons*, *Nucl. Phys.* **B715** (2005) 499 [`hep-th/0412308`].

[92] R. Britto, F. Cachazo, B. Feng and E. Witten, *Direct proof of tree-level recursion relation in Yang-Mills theory*, *Phys. Rev. Lett.* **94** (2005) 181602 [`hep-th/0501052`].

[93] F. Berends and W. Giele, *Recursive calculations for processes with n gluons*, *Nuclear Physics B* **306** (1988) 759 .

[94] R. Roiban, M. Spradlin and A. Volovich, *Dissolving N=4 loop amplitudes into QCD tree amplitudes*, *Phys. Rev. Lett.* **94** (2005) 102002 [`hep-th/0412265`].

[95] R. E. Cutkosky, *Singularities and discontinuities of feynman amplitudes*, *Journal of Mathematical Physics* **1** (1960) 429 [`https://doi.org/10.1063/1.1703676`].

[96] G. Ossola, C. G. Papadopoulos and R. Pittau, *Reducing full one-loop amplitudes to scalar integrals at the integrand level*, *Nucl. Phys.* **B763** (2007) 147 [`hep-ph/0609007`].

[97] F. del Aguila and R. Pittau, *Recursive numerical calculus of one-loop tensor integrals*, *JHEP* **07** (2004) 017 [`hep-ph/0404120`].

[98] C. F. Berger, Z. Bern, L. J. Dixon, F. Febres Cordero, D. Forde, H. Ita et al., *An Automated Implementation of On-Shell Methods for One-Loop Amplitudes*, *Phys. Rev.* **D78** (2008) 036003 [`0803.4180`].

[99] G. Ossola, C. G. Papadopoulos and R. Pittau, *On the Rational Terms of the one-loop amplitudes*, *JHEP* **05** (2008) 004 [`0802.1876`].

[100] Z.-G. Xiao, G. Yang and C.-J. Zhu, *The rational parts of one-loop QCD amplitudes I: The general formalism*, *Nucl. Phys. B* **758** (2006) 1 [`hep-ph/0607015`].

[101] X. Su, Z. Xiao, G. Yang and C.-J. Zhu, *The Rational Part of QCD Amplitude. II. The Five-Gluon*, *Nucl. Phys. B* **758** (2006) 35 [`hep-ph/0607016`].

[102] Z. Bern, L. J. Dixon and D. A. Kosower, *One loop corrections to five gluon amplitudes*, *Phys. Rev. Lett.* **70** (1993) 2677 [`hep-ph/9302280`].

[103] G. De Laurentis, *The CHY formalism for massless scattering (master thesis)*, *Oxford MPhys thesis* (2016) .

[104] L. Dolan and P. Goddard, *The Polynomial Form of the Scattering Equations*, *JHEP* **07** (2014) 029 [`1402.7374`].

[105] L. Dolan and P. Goddard, *General Solution of the Scattering Equations*, *JHEP* **10** (2016) 149 [`1511.09441`].

[106] C. Cardona and C. Kalousios, *Elimination and recursions in the scattering equations*, *Phys. Lett.* **B756** (2016) 180 [`1511.05915`].

[107] F. Cachazo, S. He and E. Y. Yuan, *Scattering Equations and Matrices: From Einstein To Yang-Mills, DBI and NLSM*, *JHEP* **07** (2015) 149 [`1412.3479`].

[108] T. Azevedo and O. T. Engelund, *Ambitwistor formulations of R^2 gravity and $(DF)^2$ gauge theories*, *JHEP* **11** (2017) 052 [`1707.02192`].

[109] J. A. Farrow and A. E. Lipstein, *New Worldsheet Formulae for Conformal Supergravity Amplitudes*, *JHEP* **07** (2018) 074 [`1805.04504`].

[110] M. Mangano, S. Parke and Z. Xu, *Duality and multi-gluon scattering*, *Nuclear Physics B* **298** (1988) 653 .

[111] T. G. et al., *GNU multiple precision arithmetic library 4.1.2*, December, 2002.

[112] R. K. Ellis, W. T. Giele and G. Zanderighi, *The One-loop amplitude for six-gluon scattering*, *JHEP* **05** (2006) 027 [`hep-ph/0602185`].

[113] Z. Bern, G. Diana, L. J. Dixon, F. Febres Cordero, S. Hoeche, D. A. Kosower et al., *Four-Jet Production at the Large Hadron Collider at Next-to-Leading Order in QCD*, *Phys. Rev. Lett.* **109** (2012) 042001 [`1112.3940`].

[114] S. Badger, B. Biedermann, P. Uwer and V. Yundin, *NLO QCD corrections to multi-jet production at the LHC with a centre-of-mass energy of $\sqrt{s} = 8$ TeV*, *Phys. Lett.* **B718** (2013) 965 [`1209.0098`].

[115] D. Forde and D. A. Kosower, *All-multiplicity one-loop corrections to MHV amplitudes in QCD*, *Phys. Rev. D* **73** (2006) 061701 [`hep-ph/0509358`].

[116] C. Anastasiou, C. Duhr, F. Dulat, F. Herzog and B. Mistlberger, *Higgs Boson Gluon-Fusion Production in QCD at Three Loops*, *Phys. Rev. Lett.* **114** (2015) 212001 [`1503.06056`].

[117] B. Mistlberger, *Higgs boson production at hadron colliders at N^3LO in QCD*, *JHEP* **05** (2018) 028 [`1802.00833`].

[118] J. M. Campbell, R. K. Ellis and G. Zanderighi, *Next-to-Leading order Higgs + 2 jet production via gluon fusion*, *JHEP* **10** (2006) 028 [`hep-ph/0608194`].

[119] G. Cullen, H. van Deurzen, N. Greiner, G. Luisoni, P. Mastrolia, E. Mirabella et al., *Next-to-Leading-Order QCD Corrections to Higgs Boson Production Plus Three Jets in Gluon Fusion*, *Phys. Rev. Lett.* **111** (2013) 131801 [`1307.4737`].

[120] S. P. Jones, M. Kerner and G. Luisoni, *Next-to-Leading-Order QCD Corrections to Higgs Boson Plus Jet Production with Full Top-Quark Mass Dependence*, *Phys. Rev. Lett.* **120** (2018) 162001 [`1802.00349`].

[121] CMS collaboration, *Inclusive search for a highly boosted Higgs boson decaying to a bottom quark-antiquark pair*, *Phys. Rev. Lett.* **120** (2018) 071802 [`1709.05543`].

[122] R. K. Ellis, I. Hinchliffe, M. Soldate and J. J. van der Bij, *Higgs Decay to $\tau^+\tau^-$: A Possible Signature of Intermediate Mass Higgs Bosons at high energy hadron colliders*, *Nucl. Phys.* **B297** (1988) 221.

[123] U. Baur and E. W. N. Glover, *Higgs Boson Production at Large Transverse Momentum in Hadronic Collisions*, *Nucl. Phys.* **B339** (1990) 38.

[124] G. Cullen et al., *GOSAM-2.0: a tool for automated one-loop calculations within the Standard Model and beyond*, *Eur. Phys. J.* **C74** (2014) 3001 [`1404.7096`].

[125] V. Hirschi and O. Mattelaer, *Automated event generation for loop-induced processes*, *JHEP* **10** (2015) 146 [`1507.00020`].

[126] F. Buccioni, J.-N. Lang, J. M. Lindert, P. Maierhöfer, S. Pozzorini, H. Zhang et al., *OpenLoops 2*, *Eur. Phys. J.* **C79** (2019) 866 [`1907.13071`].

[127] R. K. Ellis, W. T. Giele, Z. Kunszt and K. Melnikov, *Masses, fermions and generalized D-dimensional unitarity*, *Nucl. Phys.* **B822** (2009) 270 [`0806.3467`].

[128] J. M. Campbell, R. K. Ellis and C. Williams, *Vector boson pair production at the LHC*, *JHEP* **07** (2011) 018 [`1105.0020`].

[129] J. M. Campbell, R. K. Ellis and W. T. Giele, *A Multi-Threaded Version of MCFM*, *Eur. Phys. J.* **C75** (2015) 246 [`1503.06182`].

[130] J. Campbell and T. Neumann, *Precision Phenomenology with MCFM*, *JHEP* **12** (2019) 034 [`1909.09117`].

[131] J. M. Lindert, K. Kudashkin, K. Melnikov and C. Wever, *Higgs bosons with large transverse momentum at the LHC*, *Phys. Lett.* **B782** (2018) 210 [`1801.08226`].

[132] T. Neumann, *NLO Higgs+jet production at large transverse momenta including top quark mass effects*, *J. Phys. Comm.* **2** (2018) 095017 [`1802.02981`].

[133] S. Davies, *One-Loop QCD and Higgs to Partons Processes Using Six-Dimensional Helicity and Generalized Unitarity*, *Phys. Rev.* **D84** (2011) 094016 [`1108.0398`].

[134] N. Berkovits and E. Witten, *Conformal supergravity in twistor-string theory*, *JHEP* **08** (2004) 009 [`hep-th/0406051`].

[135] H. Johansson, G. Mogull and F. Teng, *Unraveling conformal gravity amplitudes*, *JHEP* **09** (2018) 080 [`1806.05124`].

[136] J. Maldacena, *Einstein Gravity from Conformal Gravity*, `1105.5632`.

[137] G. Anastasiou and R. Olea, *From conformal to Einstein Gravity*, *Phys. Rev.* **D94** (2016) 086008 [`1608.07826`].

[138] H. Johansson and J. Nohle, *Conformal Gravity from Gauge Theory*, `1707.02965`.

[139] C. F. Berger, Z. Bern, L. J. Dixon, F. Febres Cordero, D. Forde, H. Ita et al., *One-Loop Calculations with BlackHat*, *Nucl. Phys. Proc. Suppl.* **183** (2008) 313 [`0807.3705`].